Dissertation zur Erlangung des Doktorgrades

der Fakultät für Chemie und Pharmazie

der Ludwig-Maximilians-Universität München

Identification of Novel Deubiquitinases in Stabilizing Integrins

Kaikai Yu

Aus Hangzhou, Zhejiang, China

2024

Erklärung

Diese Dissertation wurde im Sinne von § 7 der Promotionsordnung vom 28. November 2011 von Herrn Prof. Dr. Reinhard Fässler betreut.

Eidesstattliche Versicherung

Diese Dissertation wurde selbstständig, ohne unerlaubte Hilfe erarbeitet.

München, den 05.08.2024

_____

(Kaikai Yu)

Dissertation eingereicht am 09.08.2024
1. Gutachter: Prof. Dr. Reinhard Fässler
2. Gutachter: Prof. Dr. Arnoud Sonnenberg
Mündliche Prüfung am 02.10.2024

Table of Contents

Abbreviations

AAA	ATPase associated with various cellular activities
ADAM9	ADAM metallopeptidase domain 9
Alix	ALG-2 interacting protein X
AMPA	Alpha-amino-3-hydroxy-5-methyl-4-isoxazolepropionic acid
AMSH	associated molecule with the SH3 domain of STAM
AMSH-LP	AMSH-like protein
APC/C	anaphase-promoting complex/cyclosome
APPL1	adaptor protein, phosphotyrosine interacting with PH domain and leucine zipper 1
AR	androgen receptor
ATP	adenosine triphosphate
BioID	proximity-dependent biotin identification
BL	blocking loop
BRCA1	breast cancer gene 1
BRCC	BRCA1-BRCA2-containing complex
CCC	complex COMMDs, CCDC22 and CCDC93
CCL	catalytic cleft loop
CDK	cyclin-dependent kinase
CG	CLIC/GEEC
CHIP	carboxy terminus of Hsp70-interacting protein
CHMP6	charged multi-vesicular body protein 6
CIE	clathrin-independent endocytosis
CLIC	clathrin-independent carriers
CLIC3	chloride intracellular channel protein 3
CME	clathrin-mediated endocytosis
CRLs	cullin-RING ligases
DMWD	Dystrophia myotonica WD repeat-containing protein
Doa10	degradation of alpha 10
DUB	deubiquitinase
E6AP	homologous to E6AP C terminus
Eap45	ELL-associated protein of 45 kDa
ECM	extracellular matrix
EEA1	early endosome antigen 1
EGF	epidermal growth factor
EGFR	epidermal growth factor receptor
ER	endoplasmic reticulum
ERAD	ER-associated degradation
ERC	endocytic recycling compartment
ESCRT	endosomal sorting complex required for transport
FA	Fanconi anemia

FAK	focal adhesion kinase
FANCD2	Fanconi anemia group D2
FANCI	Fanconi anemia complementation group I
FANCL	Fanconi anemia complementation group L
FERM	4.1R, ezrin, radixin, moesin
FN	fibronectin
FYVE	Fab-1, YGL023, Vps27, and EEA1
GAP	GTPase activating proteins
GAT	GGAs and Tom
GEEC	GPI-AP enriched compartments
GEF	guanine nucleotide exchange factors
GLR-1	glutamate receptor-1
GPI-AP	glycosylphosphotidylinositol- anchored protein
GRAF1	GTPase regulator associated with FAK
HECT	homologous to E6AP carboxyl terminus
HHARI	human homolog of Ariadne
HOPS	homotypic fusion and protein sorting
Hrd1	HMG-CoA reductase degradation 1
Hrs	hepatocyte growth factor-regulated tyrosine kinase substrate
IBR	in-between-RINGs
ILV	intraluminal vesicles
Ist1	increased sodium tolerance 1 homolog
JAMM	JAB1/MPN/Mov34 metalloenzyme
LBPA	lysobisphosphatidic acid
LUBAC	linear ubiquitin chain assembly complex
Mdm2	murine double minute 2
MINDY	motif interacting with Ub-containing novel DUB
MJD	Machado–Josephin domain
MPN	Mpr1p Pad1p N-terminal
MVB	multivesicular body
Mvb12	multivesicular body 12
Nedd4	neural precursor cell expressed developmentally down-regulated protein 4
NLS	nuclear localization signal
OTU	ovarian tumor containing proteases
PCNA	proliferating cell nuclear antigen
PDGF	platelet-derived growth factor
PF	pinky finger
PHLPP1	PH domain leucine-rich repeat protein phosphatase 1
PI3P	phosphatidylinositol 3-phosphate
PM	plasma membrane
PNRC	perinuclear recycling compartment
PTEN	phosphatase and Tensin homolog
PTM	post-translational modifications

RBR	RING-between-RING
RCP	Rab coupling protein
RING	really interesting new gene
RNF4	RING finger protein 4
RPN11	regulatory particle non-ATPase 11
SCF	Skp1-Cul1-F-box protein
SLD	sumo-like domain
Snf7	sucrose non-fermenting protein 7
SNP	single nucleotide polymorphism
SNX17	sorting nexin 17
STAM	signal transducing adaptor molecule
TMD	transmembrane domain
TRAF6	tumor necrosis factor receptor associated factor 6
Tsg101	tumor susceptibility gene 101
UAF-1	USP1-associated factor 1
Ub	ubiquitin
UBAP1	ubiquitin-associated protein 1
UBZ	ubiquitin-binding zinc finger
UCH	ubiquitin C-terminal hydrolase
UEV	Ubiquitin E2 variant
UFM1	ubiquitin fold modifier 1
UIM	ubiquitin interaction motif
USP	ubiquitin-specific protease
VHS	VPS-27, Hrs and STAM
VPS	vacuolar protein sorting
Vta1	vesicle trafficking 1
WASH	Wiskott–Aldrich syndrome protein and SCAR homologue
YAP1	yes-associated protein 1
ZUFSP	zinc finger with UFM1-specific peptidase domain protein

1. Summary

The extracellular matrix (ECM) serves as a structural framework for tissues and organs. Numerous matrix-adhesion molecules bind to the ECM, initiating a cascade of biochemical and mechanical signals which govern diverse cellular functions such as survival, polarity, proliferation, and differentiation. Integrins, heterodimeric transmembrane proteins with α and β subunits, are key adhesion molecules linking the ECM and the intracellular actin-cytoskeleton and transducing biochemical and mechanical signals.

To dynamically modulate interactions between cells and the extracellular matrix (ECM), the spatial and temporal presence of receptors on the cell membrane and signaling transduction, integrins depend on the endosomal trafficking system. Integrins undergo internalization, enter the endosomal system which either recycles them back to the plasma membrane or routes them into the lysosomes for degradation. The ubiquitin system plays a central role in determining the fate of transmembrane proteins by orchestrating the delicate balance between their recycling and degradation. During my PhD thesis, I searched for the players in the ubiquitin system that regulates Itgb1-class integrins. I validated the novel deubiquitinase USP12 (and its paralog USP46) identified in genetic and biochemical screens.

First, in collaboration with Prof. Bassermann from the Technical University of Munich, we established a CRISPR/Cas9-based genetic screen using gRNAs targeting human deubiquitinases in human haploid cell line HAP1. Using the surface Itgb1 level as a readout measured by flow cytometry, several deubiquintinases including USP46 was identified as Itgb1 stabilizer. Second, I found that the deubiquitinase complexes consisting of USP12/USP46-WDR48-WDR20 associate in proximity to Itga5 using mouse kidney fibroblasts expressing Itga5-TurboID using the proximity-dependent biotin identification (BioID) assay. Based on these results, I decided to determine how the USP12/USP46-WDR48-WDR20 deubiquitinase complex stabilizes Itgb1 at the cellular and molecular level. Third, I generated CRISPR/Cas9 knockouts of each component of the USP12/USP46-WDR48-WDR20 complex. USP12 and USP46 shared around 90% of protein homology and compensate each other's function in regulating the surface level of Itgb1, whereas the double KO (dKO) of USP12/46 reduced both surface and total Itgb1 levels. A similar loss-of-function phenotype was observed when the adaptor proteins WDR20 and WDR48 were deleted in cells. Importantly, reconstituting the deleted components revealed that an active ternary

USP12/USP46-WDR48-WDR20 complex was required for maintaining Itgb1 levels. The findings were observed in fibroblasts and confirmed in the MDA-MB-231 human breast cancer cell line.

I also investigated the mechanism of how the DUB complex regulating integrin stability in cells. I found that the instability of Itgb1 caused by USP12/46 dKO was due to increased lysosomal degradation and reduced recycling, while transcription was unaffected. This regulation occurred independently of SNX17, a key regulator of Itgb1 trafficking. USP12 facilitated the removal of polyubiquitin chains from the cytosolic tail of Itgb1 in cells and *in vitro*. Consequently, this deubiquitination process impeded the recognition of Itgb1 by the ESCRT (endosomal sorting complex required for transport)-mediated sorting machinery, thereby mitigating degradation. A non-ubiquitinable α5β1 integrin with all cytosolic lysines being mutated to arginine, escaped the regulation of USP12/46 with resistance to ESCRT-mediated degradation. *In silico* data revealed that breast cancer patients with high USP12/46 expression levels have a poor prognosis and my experimental data also confirmed that loss of USP12/46 not only affected cell adhesion and spreading capacity of fibroblasts, but also impeded cell migration and invasion ability of breast cancer cells.

Altogether, my PhD study identified that the USP12/USP46-WDR48-WDR20 deubiquitinase complex is a novel regulator of integrin stability by counteracting the ESCRT-ubiquitin degradation pathway and that this regulation facilitates cancer cell migration and invasion.

2.Introduction

2.1 Integrins

Multicellular life depends on cell-cell and cell-extracellular matrix (ECM) adhesion. Cell-cell adhesion is mediated by specialized cell adhesion molecules such as cadherins, while cell-ECM interactions are predominantly facilitated by integrins (Hynes & Zhao, 2000). These adhesive interactions not only serve as a glue but also receive and respond to biochemical and mechanical signals, which in turn regulate cellular activities such as migration, proliferation, survival and differentiation (Campbell & Humphries, 2011; Sun *et al*, 2019).

Integrins constitute a large family of type I transmembrane receptors, consisting of non-covalently associated α and one β subunits. Their designation as 'integrins' denotes their integral function that 'integrate' the extracellular cytoskeleton, i.e. ECM, with the intracellular cytoskeleton, .i.e. actomyosin (Hynes, 2004; Tamkun *et al*, 1986). Integrins are exclusively expressed in metazoan organisms and have evolved over time, leading to a larger and more diverse integrin family. This evolution has contributed to the increased complexity of cellular organization (Johnson *et al*, 2009; Takada *et al*, 2007). This evolutionary trajectory equipped integrins with the adaptability required for varying demands in development, tissue regeneration and homeostasis (Johnson *et al.*, 2009).

2.1.1 Integrin structure

The mammalian integrin family consists of 24 integrins that are composed by 18 α and 8 β subunits. The combinatorial associations of these subunits result in the assembly of integrin receptors in the endoplasmic reticulum (ER). Integrins are characterized by specific binding properties and distinct tissue distribution patterns (Barczyk *et al*, 2010; Hynes, 2002). Integrins can be classified into leukocyte-specific integrins and integrins that interact with RGD motifs in proteins, collagens and laminins (Figure 1). The β1 integrin subfamily can associate with 12 α subunits and hence, generates the largest group of integrins.

Structurally, the α and β subunits consist of multiple domains that form a large ectodomain, a single-span transmembrane domain, and a short cytoplasmic domain (except for β4, which has a large cytoplasmic domain).

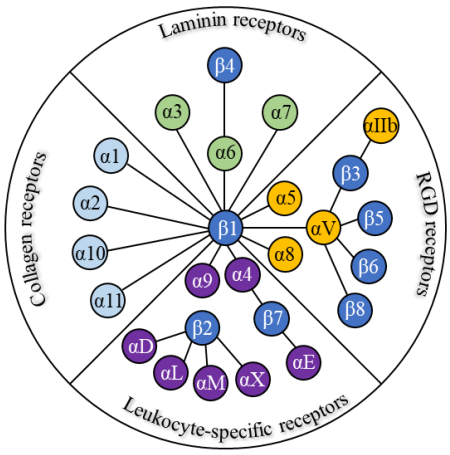

Figure 1. Mammalian integrin α subunit and β subunit pairings, along with their corresponding ligand binding specificity, are illustrated.

Ectodomain

The α subunit ectodomain contains an N-terminal β-propeller, followed by a thigh and two calf domains that adopt IgG-like and β-sandwich folds (Figure 2). Additionally, half of the 18 α subunits possess an extra α-I (α-inserted domain) domain that has similarity with von Willebrand factor A domain and hence, is also termed α-A domain. The α-I domain comprises approximately 200 amino acids and is inserted into a specific loop of the β propeller domain (Campbell & Humphries, 2011). Together with β head domain, the α-I domain directly interacts with ligands, via its metal ion-dependent adhesion site (MIDAS).

The β subunit ectodomain has a much more complex composition (Figure 2) and consists of a β-I domain, structurally akin to the I-domain of the α subunits, a plexin/semaphorin/integrin (PSI) domain, a hybrid domain, four cysteine-rich epidermal growth factor (EGF) repeats, and a membrane-proximal β tail domain (βTD) (Luo & Springer, 2006). Notably, the β-I domain is inserted into the hybrid domain. In integrins without α-I domains, the β-I domain, through its MIDAS motif, directly interacts with charged residues in ligands, along with the α head domain. This interaction is dependent on divalent cations.

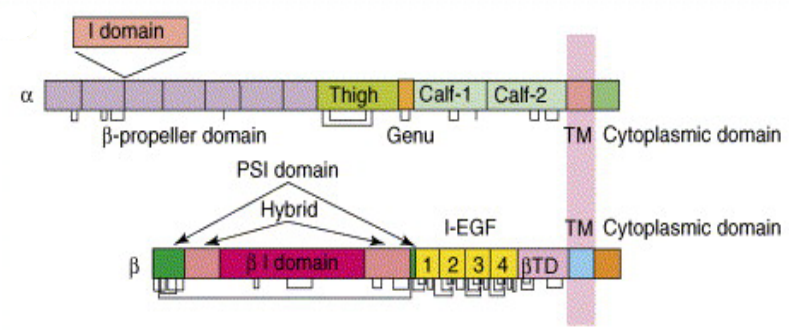

Figure 2. Arrangement of domains in the primary structures of integrins: α subunits feature an I domain inserted at the location indicated by dashed lines. Lines connecting cysteines at corresponding positions lines beneath the stick figures illustrate the presence of disulfide bonds. Adapted from (Luo & Springer, 2006).

A key characteristic of integrin ectodomains lies in their ability to converse into various conformations with distinct affinities for ligands (Kadry & Calderwood, 2020). This is accompanied by structural transformations, shifting between low-affinity and high-affinity conformations, a process referred to as integrin activation, which is tightly regulated and will be discussed in later sections.

Transmembrane domain

The TMD in integrins consists of approximately 25 to 29 amino acid residues which are conserved across different species (Kim *et al*, 2011). The single-pass TMDs, denoted as α-TMD and β-TMD engage in a non-covalent association within the plasma membrane, which is required for integrin folding and heterodimer formation in the endoplasmic reticulum (Reber et al., submitted), maintaining the inactive, low affinity state for ligand (see below) and bidirectional signaling to and from cytoplasm (Li *et al*, 2024; Sun *et al*, 2020; Sun *et al*, 2018).

Cytoplasmic domain

The cytoplasmic domains or tails of integrins serve as platforms for recruiting a plethora of ancillary proteins, which assemble into adhesion complexes such as nascent adhesions NAs), focal adhesions (FAs) and fibrillar adhesions (FBs) (Iwamoto & Calderwood, 2015; Mishra & Manavathi, 2021; Morse *et al*, 2014),

The intracellular domains of β subunits are short and largely unstructured, ranging from 40 to 70 amino acids (Wegener & Campbell, 2008). A singular exception is the cytoplasmic domain of integrin β4, which contains around 1000 amino acids (Alonso-Garcia *et al*, 2009; de Pereda *et al*, 2009; Manso *et al*, 2019; Suzuki & Naitoh, 1990). The β integrin tails exhibit highly conserved sequence motifs (Calderwood *et al*, 2003; Morse *et al.*, 2014; Moser *et al*, 2009) including a juxtamembrane HDRR/K motif and two NPxY (x represents any amino acid) motifs which serve as binding sites for talins (membrane proximal NPxY motif) and kindlins (membrane distal NPxY motif) which are essential to induce and/or maintain integrin activation (Calderwood *et al*, 1999; Horwitz *et al*, 1986; Moser *et al.*, 2009). Proximal to the talin-binding NPxY motif is a tryptophan residue and proximal to the kindlin-binding NPxY motif a serine/threonine (S/T)-rich motif, which also contribute to the recruitment of talin and kindlin, respectively (Figure 3).

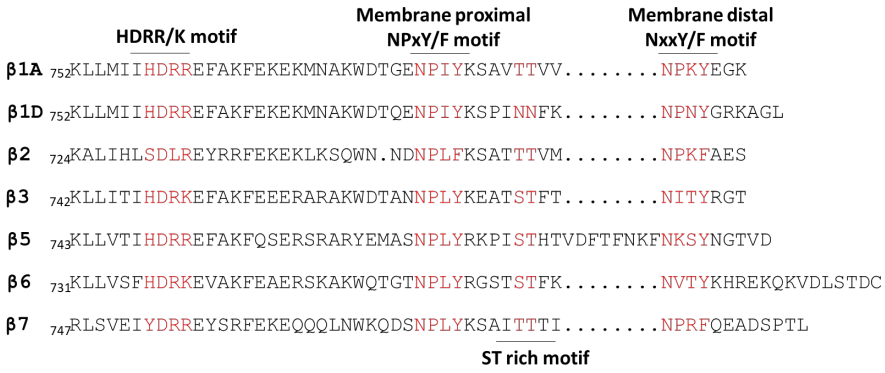

Figure 3. Sequence alignment of cytoplasmic tail sequences from human β-integrins reveals the presence of conserved motifs such as juxtamembrane HDRR/K motif (HDRR motif in β1), NP(I/L)(Y/F) and Nxx(Y/F) motifs (NPxY motifs in β1), and regions rich in Serine/Threonine (TT motif in β1). The exclusion of β4 from this alignment is due to its exceptionally large length, while β8 is omitted due to its limited conservation with the other β subunits in the alignment.

The cytoplasmic tails of α subunits are shorter than those of the β integrins subunits. While the binding associates of α-tails were less studied compared to those of β-tails, the interactions involving α-tails are gaining recognition. For example, Ginsberg and colleagues found that α4 tail binds directly and specifically to the focal adhesion adaptor paxillin, regulating cell spreading on fibrinogen (Liu *et al*, 1999). A more recent discovery has unveiled that binding of α1 tail is required to lift the autoinhibitory conformation of T-cell protein tyrosine phosphatase (TCPTP), leading to the dephosphorylation of EGFR. Additionally, an association between the α4 tail and Hsp90 was

indispensable for fever-induced T cell trafficking, highlighting its significance in modulating the thermal sensory reaction of T cells to fever (Lin *et al*, 2019), which implies that interactions involving α-tails might play a crucial role in regulating integrin function within the context of the immune response.

2.1.2 Integrin activation

Conformational changes

A hallmark of integrins is that they require an activation step prior to ligand binding. This activation step is characterized by a reversible conformational change of the entire integrin molecule. In the inactive conformation with low affinity for ligand the integrin is bent, the TMDs are associated and the ligand binding pocket masked/closed. This integrin conformation is referred to as 'bent-closed (BC)' conformation. To reach the active conformation, the ectodomain extends but still keeps the binding pocket closed. This conformation is referred to as 'extended-closed (EC)' conformation. Finally, in the active state the interaction between the α- and β-TMD separate and the hybrid domain swings away from the α subunit, which results in an opening of the ligand binding pocket and high affinity for ligand. This conformation is referred to as 'extended-open (EO)' conformation with much higher affinities for ligands-binding, a critical process for integrin activation (Li *et al.*, 2024; Luo *et al*, 2007; Sun *et al.*, 2019) (Figure 4). A very recent study by Springer and colleagues showed that while conformational transitions for unliganded integrins take around 30s, ligand binding induces the leg extension and headpiece opening of the bent closed integrin within miliseconds (Li *et al.*, 2024). In the bent-closed conformation, the αVβ3 integrin was bent in a V-shaped topology with the head domain facing the plasma membrane (Xiong *et al*, 2001; Xiong *et al*, 2002). It was hypothesized that this topology blocks the access to ligand and hence, renders the integrin inactive. However, in contrast to a completely bent conformation in resting states of αVβ3 integrin, α5β1 integrin adopts an incompletely bent form that did not cause steric hinderance for ligand (FN) binding (Schumacher *et al*, 2021), a scenario also observed for αIIbβ3 integrins (Adair *et al*, 2023). While both, the lower legs and transmembrane domains of the α and β subunits stay in close contact in bent-closed form (Luo *et al.*, 2007), they induce a partial opening for the binding of ligand (Adair *et al.*, 2023). Integrin activation can be triggered inside the cell, known as 'inside-out' signaling, and outside the cells, upon ligand binding, known as 'outside-in' signaling. 'Inside-out' signaling postulates that binding of the adaptor proteins

talins and kindlins to the β cytoplasmic tail shifts the BC to the EO conformation, whereas 'outside-in' signaling commences with ligand binding followed by the recruitment of talin and kindlin, association with actomyosin and force transduction to the integrin-ligand bond (Legate *et al*, 2009; Luo *et al.*, 2007; Sun *et al.*, 2019). A recent study, however, impressively demonstrated that talin binding (and probably the same is true for kindlin binding) is not required to induce integrin activation, which is solely accomplished by ligand binding (Li *et al.*, 2024).

Springer and colleagues also measured the energy required to switch between conformations. The measurements revealed that high energy is required to switch from BC to EC and small energy is released from EC to the EO conformation. Due to the high energy input required to achieve the extension of the ectodomain, the number of EC- and EO-integrins on the cell surface is low. The low number of EO-integrins, however, becomes stabilized when the EO-integrins bind ligand, recruit talin and kindlin and experience force (Li *et al.*, 2024).

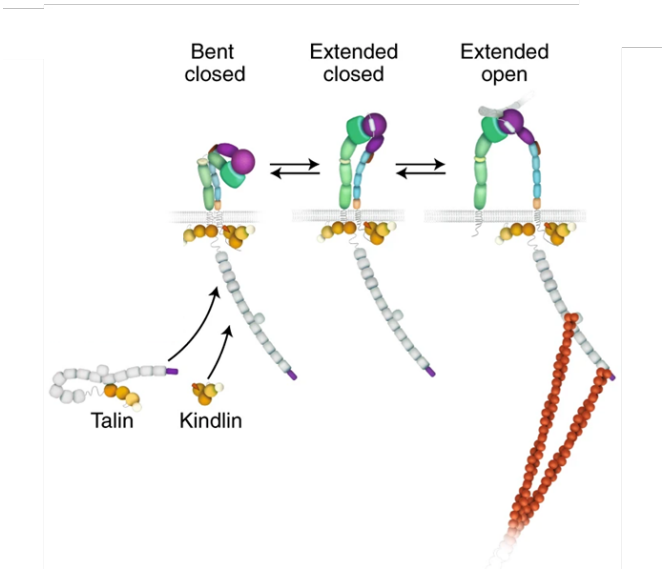

Figure 4. Models of integrin activation. Inactive integrins rest in a bent-closed conformation with associated transmembrane domains and leg pieces. 'Inside-out' activation such as adaptors binding to the tail primes integrins for ligand binding or 'outside-in' activation including ligand binding to extracellular domain shifts integrins from bent-closed/extended-closed forms to extended-open conformation. Adapted from (Sun et al., 2019).

Of note, integrins that reside in the BC conformation or EO conformations can be identified and measured with a set of antibodies that specifically recognize conformation-dependent epitopes in

α- and β-subunits, respectively (Byron *et al*, 2009). Numerous important findings have been deduced with the help of this important tool box that has been generated and generously made available by several laboratories.

Talin and kindlin cooperativity

Integrin function is intimately linked to integrin activation. The first essential protein required to induce/maintain the active state of integrins was talin (Ginsberg, 2014; Horwitz *et al.*, 1986) , which contains a 4.1, ezrin, radixin, moesin (FERM) domain at the N-terminus and a C-terminal rod domain (Calderwood *et al*, 2013). Talin resides in the cytoplasm in an autoinhibitory form in which the talin head is masked by the rod domain (Dedden *et al*, 2019; Goksoy *et al*, 2008; Goult *et al*, 2018). Once activated, the talin head binds to the membrane proximal NPxY motif of β-integrin cytoplasmic tails and the talin rod domain to actomyosin filaments, which leads to the transduction of the actomyosin-mediated pulling forces along the TMD to the integrin ligand bond and final bond re-enforcement (Dedden *et al.*, 2019; Zhang *et al*, 2008).

With kindlin, a second adaptor protein was identified that binds to β-integrin tails and plays an essential role in inducing/maintaining the active state of integrins (Ma *et al*, 2008; Moser *et al.*, 2009; Moser *et al*, 2008). In addition to β-integrin tail binding, kindlins also serve as a binding platform for branched actin (Bledzka *et al*, 2016) and focal adhesion proteins such as paxillin and the Arp2/3 complex to facilitate cell adhesion and spreading (Boettcher *et al*, 2017; Theodosiou *et al*, 2016; Zhu *et al*, 2019b; Zhu *et al*, 2021). Since the talin and kindlin binding sites partly overlap in β-integrin tails, it was enigmatic how two proteins cooperate instead of competing for tail binding (Calderwood *et al.*, 2013; Moser *et al.*, 2009; Moser *et al.*, 2008). Structural studies and affinity measurements of talin and kindlin to β-integrin tails revealed that in a minor number of ternary particles kindlin induces a conformational change in the β-integrin tail resulting in an increased talin affinity that in turn, decreases the affinity of kindlin, abrogates the conformational change in the β-integrin tail, decreases talin affinity and allows the cycle of binding and unbinding to commence again. To allow fast rebinding of kindlin at the end of the ternary complex binding cycle, talin and kindlin bind each other with low (Aretz *et al*, 2023).

Role of mechanobiology in integrin activation

The preeminent roles of intracellular and extracellular forces and matrix rigidity and elasticity for integrin functions are undisputed (Engler *et al*, 2006). A key study by the Springer lab reported that the transition of integrins from the inactive, BC to the active, ligand-bound EO conformation needs to overcome a high energy barrier and the stabilization of the integrin-ligand bond requires forces across the integrin-ligand complex (between 1-3 pN for FN-bound α5β1 integrin) exerted by the actin cytoskeleton and transduced via the ternary β-integrin tail/kindlin/talin complex (Li *et al.*, 2024; Li & Springer, 2017). The conclusions that can be drawn from this report are that the reversible integrin activation underlies a thermodynamic equilibrium principle that adjusts the distribution of the different integrin conformations on the cell surface, that the thermodynamic energy is obtained independent of talin and kindlin, and that the integrin ligand bond stabilization requires force transduced via talin and/or kindlin. The force dependence of integrin-ligand bonds points to a catch bond behavior, which counterintuitively implies that forces do not separate but rather strengthen and stabilize integrin-ligand complexes. Increasing the force will even further increase the integrin-ligand binding strength. Indeed, integrin-ligand complexes that do not experience force are unable support adhesion (Theodosiou et al., 2016). The catch bond strength, which - in the case of α5β1 integrin - can raise up to 30-40 pN (Bodescu *et al*, 2023; Kong *et al*, 2009), can be regulated extracellularly or intracellularly. Extracellularly for example, by the synergy site in FN which serves as an additional α5β1 integrin binding motif adjacent to the canonical RGD binding site (Benito-Jardon *et al*, 2017; Strohmeyer *et al*, 2017), and/or intracellularly for example, by tuning the myosin II activity or by blocking the actomyosin attachment to the talin rod as shown for the KANK proteins (Sun *et al*, 2016b).

Integrin clustering serves as another mechanism to secure integrin-mediated adhesions (Sun *et al*, 2016a), a scenario where integrins concentrate at a defined spot to rebind ligand, strengthen the adhesion and extend adhesion lifetime (Sun *et al.*, 2019; Sun *et al.*, 2016a). Depending on the strength of force applied, integrins cluster in difference sizes and inter-distance (Sun *et al.*, 2019), which in turn regulates adhesion dynamics, cell spreading and spatial sensing (Cavalcanti-Adam *et al*, 2007; Liu *et al*, 2015; Oria *et al*, 2017).

The studies on how mechanical forces regulate integrins extended our views on integrin activation. Forces converge with the biochemical and biophysical properties of ECM proteins and intracellular signaling and cytoskeletal on integrins to regulate their conformations.

Integrin phase separation

Phase separation is a basic physical process where a single mixture separates into distinct phases with different compositions (Nic M, 1997). This separation is driven by the interactions between molecules within the system. In biological systems, phase separation underscores the formation of the membrane-less assemblies or condensates without surrounding lipid bilayers, which plays a vital role for organizing cellular components and facilitating biochemical reactions (Banani *et al*, 2017; Hyman *et al*, 2014; Shin & Brangwynne, 2017).

For the cytoplasmic phase separation, the nucleolus stands out as a prominent structure formed by phase separation (Lafontaine *et al*, 2021; Pederson, 2011). It forms through the liquid-liquid phase separation of nucleolar proteins and nucleic acids, creating a highly concentrated environment that enhances the efficiency of ribosomal RNA synthesis and ribosome assembly.

Transmembrane proteins, such as integrins, can also undergo phase separation, influencing cellular organization and signaling. Bausch and colleagues have demonstrated a membrane-associated phase separation of integrin adhesion complex in a more physiological way where lipid membranes containing phosphoinositides were applied to induce the integrin adhesion condensates, comprising β1 integrin cytoplasmic tails, talin, kindlin, paxillin, and FAK, under high ionic strength and nanomolar protein concentrations (Hsu *et al*, 2023). This is in accordance with what was observed in cells, where phosphoinositides binding motifs are necessary for kindlin and talin to form focal adhesion sites. An *in vitro* study also showed that kindlin, paxillin, and FAK can undergo spontaneous phase separation in physiological buffer and bind to integrin tails on phosphoinositides-free membranes (Case *et al*, 2022), and a later study pointed out that phase separation of paxillin can drive the assembly of focal adhesions and integrin signaling (Liang *et al*, 2024), underscoring phase separation as an intracellular trigger for assembling integrin adhesion complexes. Thus, understanding the principles and mechanisms of integrin phase separation offers new insights into cell adhesion, signaling, and the dynamic nature of cellular membranes.

2.1.3 Endocytic trafficking of integrins

Protein trafficking is a fundamental cellular process that involves the transport of proteins within and between cellular compartments. It includes two major pathways, the exocytic or secretory

pathway, which carries proteins from the ER to the Golgi apparatus and later the cell surface, and the endocytic pathway, which routes proteins from the cell surface to endosomes where they are further sorted to late endosomes and lysosomes or recycled to the plasma membrane (Derby & Gleeson, 2007; Enns, 2001).

Endocytic trafficking of integrins was first observed in the late 1980s by showing that β1 integrin did not stay stationary at the PM but instead, enters the endocytic pathway within minutes (Bretscher, 1989). A subsequent paper showed that several other types of integrins are also routed into the endocytic cycle with different recycling speed, and that integrin endocytosis allows a moving cell to bring integrins to the leading edge (Bretscher, 1992). Together with conformational changes of integrins and interactions between integrin and ligands and intracellular adaptor proteins, respectively, integrin trafficking has been well recognized as a crucial mechanism to regulate the integrin function including adhesion and ECM-remodelling (De Franceschi *et al*, 2015; Moreno-Layseca *et al*, 2019; Yue *et al*, 2012).

The appliance of surface labelling methods advanced the understanding of integrin trafficking into a new era, in which the role and dynamics of integrin trafficking was dissected (Farage & Caswell, 2021; Roberts *et al*, 2001). Literature about integrin trafficking revealed that endocytosed β1 integrins are recycled back to the PM within 20 minutes, whereas their lysosomal degradation takes several hours (Boettcher *et al*, 2012; Lobert *et al*, 2010; Steinberg *et al*, 2012). This indicates that the a majority of integrins are primarily recycled back to the PM and hence, can undergo numerous endocytic cycles. Thus, a dynamic endocytic system is crucial to timely recognize and prevent integrins from degradation fate to maintain its proper cell surface level.

Integrin endocytosis

Endocytic trafficking of integrins starts with endocytosis. A well-studied route is the clathrin-mediated endocytosis (CME) which orchestrates the membrane invagination with clathrin-coated pits formation and subsequent vesicle scission (Kaksonen & Roux, 2018). Integrins undergo the CME endocytosis with the assistance of adaptor proteins including Dab2 (Teckchandani *et al*, 2009) and Numb (Nishimura & Kaibuchi, 2007). In polarized cells, Numb phosphorylation facilitate integrin endocytosis in the leading edge of cell migration (Nishimura & Kaibuchi, 2007) whereas in focal adhesion disassembly, binding of Dab2 to integrin is required for CME (Eskova *et al*, 2014; Ezratty *et al*, 2009; Teckchandani *et al.*, 2009) .

Clathrin-independent endocytosis (CIE) including caveolar endocytosis, clathrin-independent carriers (CLIC) and macropinocytosis also serve as passages for integrin uptake (Moreno-Layseca *et al.*, 2019). For example, caveolae formation, which is assisted by caveolins and cavins, mediates integrin uptake with the engagement of Syndecan-4 (Bass *et al*, 2011; Rennick *et al*, 2021). Galectin-3-mediated CLIC biogenesis induces integrin internalization by recruiting GRAF1, the GTPase regulator associated with FAK in complex with phosphorylated FAK (Doherty *et al*, 2011; Lakshminarayan *et al*, 2014). During platelet-derived growth factor (PDGF)-stimulated cell migration, integrins can be internalized through circular dorsal ruffles via macropinocytosis (Gu *et al*, 2011). The actin binding protein Swiprosin-1 has been recently reported to serve as an adaptor for clathrin- and dynamin-independent endocytic pathway (CLIC/GEEC, CG pathway) to promote the endocytosis of Rab21-associated integrins (Moreno-Layseca *et al*, 2021).

In addition, similar to epidermal growth factor receptor (EGFR) that undergoes ligand-induced internalization and degradation (Tomas *et al*, 2014), the endocytosis of integrins can also be regulated by ligands and other transmembrane proteins. For example, fibronectin binding was shown to promote α5β1 integrin internalization and ubiquitination with subsequent lysosomal degradation (Kharitidi *et al*, 2015; Lobert *et al.*, 2010). The transmembrane protease ADAM9 interacts with β1 integrin to promote its endocytosis and degradation independently of its protease activity, which eventually promotes prostate cancer cell migration. However, whether a specific motif in ADAM9 is required for such interaction is not disclosed (Mygind *et al*, 2018). Possessing a YRSL sequence which serves as endocytosis/sorting motif, Tetraspanin CD151 associates with laminin-binding integrins including α3β1 and α6β1 to promote their endocytosis and cell migration (Berditchevski *et al*, 2001; Liu *et al*, 2007; Yauch *et al*, 2000).

Thus, integrins choose between the numerous choices for endocytosis. Hence, understanding how the choices are regulated could provide crucial insights into cellular dynamics and enhance our understanding of how vesicular trafficking regulates integrin functions.

Integrin recycling

Endocytosed integrins can be routed to the late endosomes/lysosomes for degradation or be recycled back to plasma membrane. Importantly, the recycling of integrins allows cells to dynamically adjust the distribution, quantities and types of integrins on cell surface, thereby fine-tuning their abilities to adhere, spread as well as responding to extracellular cues (De Franceschi

et al., 2015; Moreno-Layseca *et al.*, 2019). Moreover, integrin recycling plays essential roles in maintaining various cellular processes, including cell polarization, tissue morphogenesis, and axon growth while dysregulation of integrin recycling has been implicated in many pathological conditions, including developmental disorders, inflammatory diseases, and cancer, etc (Moreno-Layseca *et al.*, 2019; Wickstrom & Faessler, 2011).

Integrins are constantly endocytosed and recycled, which is regulated by Rab GTPases (Paul *et al*, 2015; Subramani & Alahari, 2010; Zhen & Stenmark, 2015). Like all GTPases, also Rab GTPases act as molecular switches. They cycle between an inactive GDP-bound state and an active GTP-bound state. This cycle is controlled by effector proteins like guanine nucleotide exchange factors (GEFs) and GTPase-activating proteins (GAPs). These proteins help Rab GTPases to manage the different stages of membrane trafficking within the cell. (Kummel *et al*, 2023).

Endocytosed β1 integrin is routed to Rab5-positive early endosomes where endosomal maturation and the subsequent trafficking of β1 integrin continues (Moreno-Layseca *et al.*, 2019; Pellinen *et al*, 2006). While Rab5 defines early endosomes, the conversion from Rab5 to Rab7 leads to endosomal maturation (Kummel *et al.*, 2023; Rink *et al*, 2005). This conversion is orchestrated by the Mon1-Ccz1 complex, which can be recruited by PI(3)P and Rab5-GTP on the early endosomes (Kummel *et al.*, 2023; Poteryaev *et al*, 2010). Mon1-Ccz1 inactivates Rab5 by displacing its GEF Rabex-5 and activates Rab7 to facilitate its endosomal membrane association (Kiontke *et al*, 2017; Poteryaev *et al.*, 2010; Stroupe, 2018). Together with its effector proteins including the homotypic fusion and protein sorting (HOPS) complex, Rab7 marks sites for vesicles from early endosomes or other late endosomes to fuse, regulating membrane trafficking (Kummel *et al.*, 2023; van der Beek *et al*, 2019). While integrins can traffic from the early endosome to the late endosome/lysosome, two distinct recycling pathways facilitated by either Rab4 or Rab11 recycle a large proportion of integrins to the plasma membrane, leading to their remarkably long half-life time.

Rab4 plays a critical role in the budding and fission of 'recycling domains' from early endosomes by interacting with the early endosomes and microtubules (Caviston & Holzbaur, 2006), facilitating the fission of the early endosomes formed by Rab5. This process is required for recycling of molecules including transferrin receptors to PM (Chavrier *et al*, 1997; Mohrmann & van der Sluijs, 1999). Under PDGF (platelet-derived growth factor) stimulation, αVβ3 integrin, in

contrast to α5β1, undergoes a swift and 'short-loop' (without traversing the perinuclear region) recycling to the plasma membrane from early endosomes through a Rab4-dependent mechanism, independent of Rab11 participation (Jones *et al*, 2006; Roberts *et al.*, 2001). Similar to PDGF stimulation, VEGFR1 activation also promotes Rab4 mediated recycling of αVβ3 integrin (Jones *et al*, 2009).

Rab11, on the other hand, is commonly found on a subset of recycling endosomes known as the perinuclear recycling compartment (PNRC) or endocytic recycling compartment (ERC) to regulate 'long-loop' recycling of proteins (Hunt & Stephens, 2011; Jones *et al.*, 2006; Urbe *et al*, 1993). Together with the effector protein Rab coupling protein (RCP), Rab11 promotes the α9β1 integrin recycling in neurons (Eva *et al*, 2010; Jones *et al.*, 2009). Under hypoxia condition, Rab11 is also involved in α6β4 integrin recycling (Yoon *et al*, 2005).

The regulation of integrin trafficking by Rab proteins is more complex than previously described, involving numerous additional members of the Rab family. For example, Rab25, a member of Rab11 subfamily, regulates β1 integrin recycling in a chloride intracellular channel protein 3 (CLIC3)-dependent manner (Caswell *et al*, 2007; Dozynkiewicz *et al*, 2012) and silencing of Rab13 accumulates β1 integrin intracellularly (Sahgal *et al*, 2019). Other GTPases such as Arf GTPases also regulate integrin trafficking. Both, Arf-4 and Arf-6 facilitate integrin endocytosis (Dunphy *et al*, 2006; Rainero *et al*, 2015) and Arf-6 mediated tubulovesicular recycling promotes β1 integrin recycling, bypassing the early endosomal compartment (Chen *et al*, 2014; Morgan *et al*, 2013). Thus, various GTPases contribute to the spatial and temporal regulation of integrin dynamics and systematic investigations are necessary for a comprehensive understanding on these regulations.

Besides the involvement of GTPases, the recycling of cargos also heavily depends on multi-protein complexes like the retromer and retriever complexes (Lucas *et al*, 2016). The most well-studied and essential recycling multi-complex for β1 integrin is the sorting nexin 17 (SNX17)-retriever-CCC-WASH complex (Chen *et al*, 2019; McNally *et al*, 2017). SNX17 binds to the membrane distal NPxY motif in β1 integrin cytoplasmic tail via its FERM domain and recycles β1 integrin to PM (Boettcher *et al.*, 2012; Steinberg *et al.*, 2012). This is facilitated by the retriever complex consisting of DSCR3, C16orf62 and VPS29 (Rabouille, 2017). The recruitment of retriever to endosomes need the COMMDs, CCDC22 and CCDC93 (CCC) complex (Phillips-Krawczak *et al*,

2015), which is recruited via FAM21 in the Wiskott–Aldrich syndrome protein and SCAR homologue (WASH) complex localized on endosomes (Derivery *et al*, 2009; Gomez & Billadeau, 2009). Cells depleted with SNX17 suffered a dramatic loss of surface integrins and impaired cell adhesion, migration and spreading (Boettcher *et al.*, 2012; Steinberg *et al.*, 2012).

Of note, the depletion of SNX17 only caused a loss of around 50% of β1 integrins on the cell surface (Boettcher *et al.*, 2012; Steinberg *et al.*, 2012), suggesting that other recycling pathways exist that operate independent of SNX17. Indeed, α5β1 integrin mutant, which carries lysine to arginine substitutions in the cytoplasmic tails, is resistant to ubiquitination (detailed introduction below) and escapes degradation, even in the absence of SNX17, suggesting an interplay between SNX17 and the ubiquitin system (Boettcher *et al.*, 2012). Moreover, studies have shown that several endocytic adaptor proteins including APPL1 (adaptor protein, phosphotyrosine interacting with PH domain and leucine zipper 1) and subunits of the CORVET (class C core vacuole/endosome tethering) complex are involved in recycling of β1 integrins (Diggins *et al*, 2018; Jonker *et al*, 2018).

Collectively, various sorting complexes and endocytic adaptors contribute to the intricate network of endocytic pathways for spatiotemporal regulation of integrins. Further investigation into identifying potential pathways, novel regulatory factors, and their specific roles in diverse cellular contexts would enhance our comprehension of integrin recycling. This exploration is crucial for elucidating its physiological importance and implications in health and disease.

2.1.5 Integrins in diseases

In addition to their essential roles in regulating normal physiological cellular processes, integrins have been associated with numerous pathological conditions, including cancer, fibrosis and infectious diseases, etc.

Cancer often hijacks the integrin-mediated cell adhesion, migration and proliferation capacities during the progressions including cancer initiation, metastasis and multiple therapy resistance (Jiang *et al*, 2022; Krenn *et al*, 2020). Although debatable, most integrins are considered as tumor promoters (Ma *et al*, 2020; Yousefi *et al*, 2021). For example, α1β1 integrin promotes the tumorigenicity of colorectal cancer (Li *et al*, 2020) and β1 integrin was accountable for promoting the cancer metastasis and drug resistance in breast, liver, and lung cancer (Govaere *et al*, 2017;

Yousefi *et al.*, 2021; Zhao *et al*, 2019). However, conflicting roles (both promoting and suppressive) of laminin-binding integrins (α3β1 and α6β4) have been observed in cancer studies. Loss of integrin α3β1 impedes the formation of skin cancer (Sachs *et al*, 2012), whereas in patients with node-negative lobular breast carcinoma, low levels of α3β1 integrin expression is correlated with poor prognosis (Romanska *et al*, 2015). In the initiation and early proliferation stages, signaling events mediated by a functional α3β1 are required (Cagnet *et al*, 2014; Sachs *et al.*, 2012), while in late stages of carcinogenesis where adhesion-mediated proliferation is less important, α3β1 integrins may sustain the E-cadherin-mediated cell–cell adhesion, prevent epithelial to mesenchymal transition (EMT) events and consequently, keep tumor from further progression and metastatic growth (Baldwin *et al*, 2014; Yoon *et al*, 2013). Thus, the conflicting views of α3β1 integrin might depend on the cancer type and progression stages of cancer. Besides, the ability of α6β4 integrin to promote or suppress cancer progression also relies on the p53 status of the cells. In cells bearing mutant p53, α6β4 integrin promotes cell survival and adhesion abilities while in wild-type cell, α6β4 stimulates p53-dependent apoptosis (Bon *et al*, 2009; Lee *et al*, 2015).

In addition to influencing cancer cell behavior, integrins also regulate the immune system in the tumor micro-environment (Nolte & Margadant, 2020). For example, α4β7 serves as a key player in the recruitment of natural killer cells and cytotoxic CD8 +T cells to the colorectal cancer tissue where an effective anti-tumor response can be elicited (Zhang *et al*, 2021). Indeed, higher levels of β7 expression correlates with longer survival of patients bearing lung cancer with better immune response to anti-PD-1 treatment (Zhang *et al.*, 2021).

Apart from their regulatory functions in cancer development, integrins contribute tremendously to the progression of fibrotic diseases, in which TGF-β1 plays a critical role (Meng *et al*, 2016; Stewart *et al*, 2018). αV integrins have been well-known to bind and activate TGF-β1 to increase ECM production and fibrosis progression in skin, liver and lung (Asano *et al*, 2005; Reed *et al*, 2015; Zhang *et al*, 2020b), while β1 integrin, the most abundant β integrin subunit expressed in kidney (Kreidberg & Symons, 2000), promotes renal fibrosis by regulating the expression of α-smooth muscle actin (α-SMA), fibronectin, and collagen (Shi *et al*, 2012; Subramanian *et al*, 2012).

Recent studies on integrins have also shed light into the understanding of SARS-CoV-2 infection. *In vitro* studies indicated cognate binding interactions between the spike protein of SARS-CoV-2 and β1 (Beddingfield *et al*, 2021; Park *et al*, 2021) as well as β3 integrins (Kliche *et al*, 2021;

Nader *et al*, 2021). Inhibition of the interaction between spike proteins and β1 integrins, and the interaction of angiotensin converting enzyme II (ACE2) receptors with β1 integrins could serve as a novel therapy to treat SARS-CoV-2 infection (Beddingfield *et al.*, 2021).

Besides, integrins are involved in other infectious diseases, such as the infection of human immunodeficiency virus (HIV), of which the envelope protein GP120 binds and executes signal transductions by α4β7 (Arthos *et al*, 2018) and West Nile virus, which hijacks αVβ1 and αVβ3 to infect cells (Chu & Ng, 2004; Schmidt *et al*, 2013).

Despite the vast amount of studies on integrins and validations of integrins as drug targets in human diseases, the unmet clinical needs are still high. There are only seven FDA-approved drugs targeting integrins, with dozens of potential inhibitors under clinical trials (Pang *et al*, 2023). Majority of the drugs targeting integrins failed due to a lack of efficacy and side effects (Alday-Parejo *et al*, 2019; Pang *et al.*, 2023). Thus, a comprehensive understanding of integrins including its activation, recycling process and their implications in human diseases are of importance to develop integrin-targeting therapies.

2.2 The ubiquitin system

The ubiquitin system is a highly complex and finely regulated cellular signaling system for maintaining the homeostasis and functionality of living cells. Discovered in 1975 by Aaron Ciechanover, Avram Hershko, and Irwin Rose (Goldstein *et al*, 1975), this system revolves around a core regulatory module known as ubiquitin. Ubiquitin is a 76-amino acid protein that is ubiquitously expressed across eukaryotes and highly conserved among species with only three amino acid variations between yeast and human ubiquitin (Wilkinson, 2000), which underscores the evolutionary pressure to maintain the structural integrity of ubiquitin. Ubiquitin is structurally stable, adopting a compact β-grasp fold, complemented by a flexible six-residue C-terminal tail (Vijay-Kumar *et al*, 1987). While the majority of its core residues exhibit rigidity, the β1/β2 loop, housing Leu8, displays flexibility crucial for recognition by ubiquitin-binding proteins (Lange *et al*, 2008), which is facilitated by other hydrophobic residues Ile44 and Val70 (Dikic *et al*, 2009) (Figure 5). The most notable features of ubiquitin are its N-terminal methionine (M1) and the seven lysine residues (K6, K11, K27, K29, K33, K48, and K63), which serve the attachment sites for ubiquitin chain assembly (Figure 5).

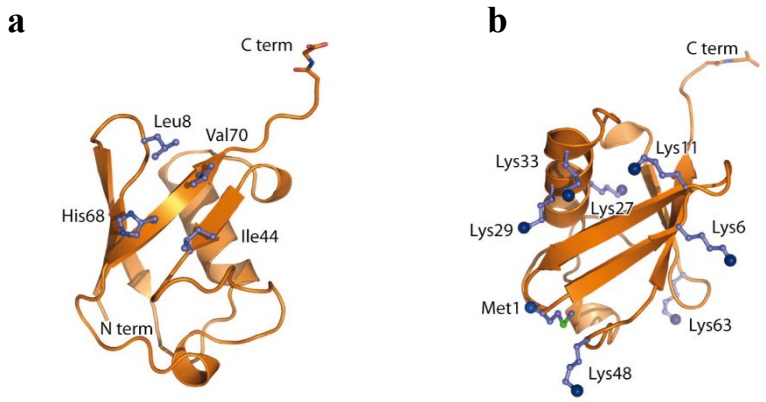

Figure 5. Structural features of the Ubiquitin. (a) The structure of ubiquitin with 3 hydrophobic residues Leu8, Ile44, and Val70 collectively providing a platform for numerous interactions with ubiquitin-binding domains (UBDs). (b) The structure of ubiquitin showing Met1 and the seven lysine residues. Blue spheres represent amino groups utilized in the formation of ubiquitin chains. Adapted from (Komander & Rape, 2012).

Ubiquitin serves as a molecular tag that can be covalently attached to proteins in cells, a process called ubiquitination. This process is reversible due to a subset of enzymes called deubiquitinases (DUBs), which cleave and release ubiquitins from target proteins (Wilkinson, 2000). The initial findings about the function of the ubiquitin system focused on how it regulates protein turnover by marking specific proteins for degradation. When a protein is tagged with a distinct ubiquitin chain, it is recognized and recruited to the proteasome, a cellular organelle responsible for protein breakdown. (Amm *et al*, 2014). This controlled degradation process is crucial for eliminating damaged, misfolded, or unnecessary proteins, thereby ensuring the proper functioning of cellular processes (Amm *et al.*, 2014; Kriegenburg *et al*, 2012).

Beyond protein degradation mediated by the ubiquitin-proteasome-system (UBS), the ubiquitin plays a crucial role in additional, diverse cellular functions, encompassing regulation of membrane trafficking, cell cycle, signal transduction, cellular stress, DNA damage, etc. (Deng *et al*, 2000; Jin *et al*, 2008; Shang & Taylor, 2011). Conversely, dysregulation of the ubiquitin system has been

implicated in numerous diseases, including neurodegenerative disorders (Atkin & Paulson, 2014), cancer (Dewson *et al*, 2023), disorders of immune system (Zinngrebe *et al*, 2014).

The discovery of the ubiquitin system tremendously contributed to our understanding of cellular homeostasis and has opened avenues for research in medicine and drug development (Huang & Dixit, 2016; Zhang *et al*, 2020a). The intricate interplay of the ubiquitin system and its targeted proteins continues to be a subject of extensive scientific investigation, revealing new insights into cellular function and potential therapeutic targets.

2.2.1 Ubiquitination

Ubiquitination is a dynamic and reversible process which requires ATP, tightly controlled by a cascade of enzymes including ubiquitin-activating (E1), ubiquitin-conjugating (E2), and ubiquitin ligase (E3) enzymes (Dove & Klevit, 2017; Middleton *et al*, 2017; Schulman & Harper, 2009). In the first step, the E1 ubiquitin-activating enzyme catalyzes the thioester bond formation between its catalytic cysteine and Gly76 in ubiquitin, utilizing ATP. Subsequently, the ubiquitin is transferred to the E2 ubiquitin-conjugating enzyme, where it forms another thioester bond with the cysteine residue of E2. Then the ubiquitin is transferred to a lysine residue on the substrate with the assistance of the E3 ubiquitin ligase. In the human proteome, approximately 8 E1 enzymes, more than 40 E2 enzymes, and over 600 E3 enzymes are known. The E3 ligases play a significant role in determining substrate specificity in the ubiquitination process (Clague *et al*, 2015; Stewart *et al*, 2016).

The formation of an isopeptide bond between the ubiquitin C terminus and typically a lysine residue on the substrate results in the monoubiquitylation of the substrate (Yau & Rape, 2016) (Figure 6). Subsequent conjugation to either the N-terminus methionine or one of the seven lysine residues on ubiquitin attached to a substrate result in the generation of polymeric chains, a process called polyubiquitylation. These chains may present in short forms, involving merely two ubiquitin molecules, or show more complicate structures, encompassing over ten moieties. Ubiquitin chains can be homogenous when the same residue within the ubiquitin undergoes modification during the elongation process, as observed in M1- (or linear), K11-, K48-, or K63-linked chains (Komander & Rape, 2012). The chains can also adopt a mixed topology in which different linkages alternate at successive positions along the chain (Boname *et al*, 2010), or a branched topology like a K48-K63 branched ubiquitin chain that mediates the NF-κB signalling (Ohtake *et al*, 2016).

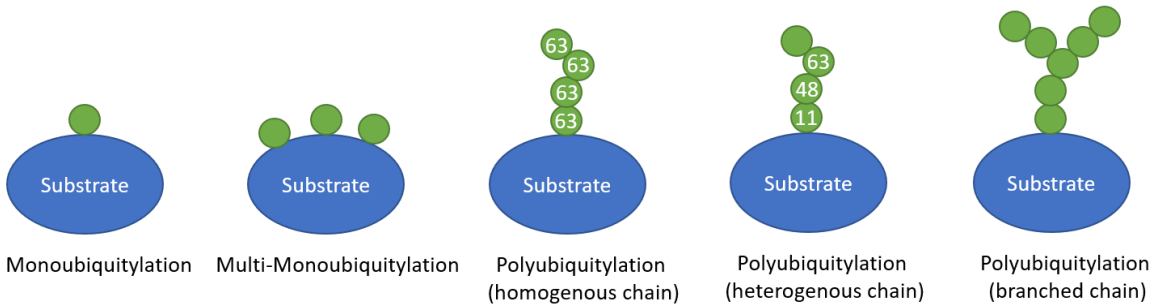

Figure 6. Ubiquitin chain topology. According to the number of ubiquitin attached and conjugation sites used, the substrate can be mono-, multimono- and polyubiquitylated.

All possible linkages have been discovered in cells (Peng *et al*, 2003; Xu *et al*, 2009). A robust body of evidence established that the monoubiquitylation and polyubiquitylation chain types elicit distinct cellular outcomes, implying that ubiquitylation functions as a coding mechanism for storing and transmitting information within the cell (Komander & Rape, 2012).

Monoubiquitination occurs when the ubiquitin system only attaches a single ubiquitin on the substrate, and is widely acknowledged as a molecular recognition signal pivotal in processes such as signal transduction and membrane trafficking (Chen *et al*, 2022b; Staub & Rotin, 2006). This modification requires that the enzymes responsible for catalyzing monoubiquitination must possess the ability to distinguish substrate lysine residues while avoiding modification of lysines on ubiquitin itself. This specificity in substrate selection can be modulated by various factors, including the E2 enzymes and the E3 ligases (Komander & Rape, 2012). Despite the unknown specificity, the E2 enzymes Ube2W and Ube2T, in concert with the E3 ligase Fanconi anemia complementation group L (FANCL), collaboratively engage in the modification process directed at the DNA repair protein Fanconi anemia group D2 (FANCD2) with attachment of a single ubiquitin molecule, an event that regulates the Fanconi anemia pathway (Alpi *et al*, 2008; Machida *et al*, 2006). While in some cases, E3 enzymes are capable of hindering the catalytic potential of E2 enzymes, thereby impeding their ability to initiate chain formation. For example, Rad6 exhibits the capacity to synthesize either mixed or K48-linked chains but in collaboration with Rad18 (Hibbert *et al*, 2011; Hwang *et al*, 2010a), Rad6 facilitates the process of monoubiquitylation of proliferating cell nuclear antigen (PCNA) (Hoege *et al*, 2002).

Polyubiquitination occurs when multiple ubiquitin molecules are covalently attached to the substrate forming ubiquitin chains in a way that ubiquitin molecules are linked together through specific lysine residues or the N-terminus of ubiquitin leading to linear or branched patterns. While still little is known about the functional significance of ubiquitinated chains linked through K6, K27, K29, or K33, a number of studies indicate that K48-linked polyubiquitin chains function as the recruitment signal for the proteasome, leading to the targeted degradation of proteins within the proteasomal system (Chen *et al*, 2022a; Du *et al*, 2022). Conversely, K63-linked ubiquitin chains do not direct proteins to the proteasome for degradation. Instead, they are pivotal in mediating interactions of proteins engaged in various cellular processes, including endocytic trafficking, DNA repair and protein translation (Pickart & Fushman, 2004). For example, K63-linked polyubiquitin chain is required for endolysosomal degradation of MHC type 1 (Duncan *et al*, 2006) and it also preferentially bind to free ends of double-stranded DNA directly to facilitate DNA repair (Liu *et al*, 2018), or regulates the nuclear translocation of proteins such as Bcl3 by CYLD (Massoumi et al., 2006).

The assembly of polyubiquitin chain is facilitated by E3 ligases. E3 ligases can be categorized into four groups based on distinctions in their structure and function: really interesting new gene (RING)-finger, U-box, homologous to E6AP carboxyl terminus (HECT) and RING-between-RING (RBR) (Figure 7). Remarkably, the different E3 ligase types exhibit little sequence homology (Rotin & Kumar, 2009).

RING-finger E3 ligases

RING E3 ligases constitute the major type among E3 ligases, and their distinguishing feature lies in the RING domain which is required to bind to E2-Ub (Freemont *et al*, 1991; Zheng & Shabek, 2017). More than 600 RING E3 ligases were found in human cells (Deshaies & Joazeiro, 2009). They transfer the ubiquitin from E2 enzymes directly to the substrate, facilitating the ubiquitin chain assembly (Nguyen *et al*, 2017). RING E3 ligases are categorized into two families: monomeric RING finger ligases and multi-subunit E3 ligases. Monomeric RING E3 ligases including murine double minute 2 (Mdm2) and tumor necrosis factor receptor associated factor 6 (TRAF6) not only bind and ubiquitinate the substrates, but can also undergo autoubiquitination, which regulates signal transduction and protein stability (Fang *et al*, 2000; Lamothe *et al*, 2007). Multi-subunit E3 ligases, exemplified by the cullin-RING ligases (CRLs), constitute a highly

diverse class of ubiquitin ligases. CRLs, numbering over 200 and accounting for about 20% of cellular ubiquitination (Petroski & Deshaies, 2005; Soucy *et al*, 2009), comprise a cullin protein scaffold, a RING E3 ligase binding to E2 enzymes, a substrate receptor mediating target binding, and an adaptor protein linking the substrate receptor to the cullin. (Nguyen *et al.*, 2017).

U-box E3 ligases

With around 60 members in Arabidopsis, U-box E3 ubiquitin ligases constitute a small family of E3 ligases (Andersen *et al*, 2004; Ryu *et al*, 2019; Wiborg *et al*, 2008; Yee & Goring, 2009). U-box E3 ligases such as carboxy terminus of Hsp70-interacting protein (CHIP) possess a conserved U-box domain which is around 70 amino acids in length at the C-terminal. Similar to the RING finger domain, the U-box domain is crucial for the enzyme activity and mediates the binding to E2 enzymes, facilitating the direct transfer of ubiquitin molecules to target proteins (Hatakeyama *et al*, 2001; Hu *et al*, 2018).

HECT E3 ligases

Around 28 HECT E3s have been found in human (Scheffner & Staub, 2007). Ranged in size from ~80 kDa to over 500 kDa, HECT E3 ligases are featured by the HECT domain, spanning around 350 amino acids in the C-terminal region which is similar to the C terminus of Homologous to E6AP C Terminus (E6AP) (Huibregtse *et al*, 1995; Rotin & Kumar, 2009; Scheffner & Staub, 2007). Contrary to RING-finger and U-box E3 ligases, the Ub from the E2s is transferred first to HECT domains via a catalytic cysteine, forming an E3-Ub intermediate, before the Ub is directed to the substrate (Weber *et al*, 2019). The first characterized HECT domain E3 ligase was E6-associated protein (E6-AP) which was discovered due to its role in the degradation of the p53 in the presence of the human papillomavirus (HPV) E6 protein (Scheffner *et al*, 1993).

RBR E3 ligases

The RBR E3 ligases have been identified as a unique family of E3 ligases that exhibit hybrid characteristics of both RING and HECT types (Yang *et al*, 2021a). They are featured by a conserved catalytic region, comprising a RING1 domain, followed by an in-between-RINGs (IBR) domain and a RING2 domain (Aguilera *et al*, 2000; Wang *et al*, 2020). Similar to the mechanism observed in HECT E3 ligases, RBR E3 ligases like the human homolog of Ariadne (HHARI) and Parkin, execute their function via a two-step reaction. They recruit E2 enzymes via the RING1

domain, which subsequently transfers the ubiquitin to a catalytic cysteine in the RING2 domain, forming a thioester intermediate before transferring the Ub to the substrates (Smit & Sixma, 2014; Wenzel *et al*, 2011).

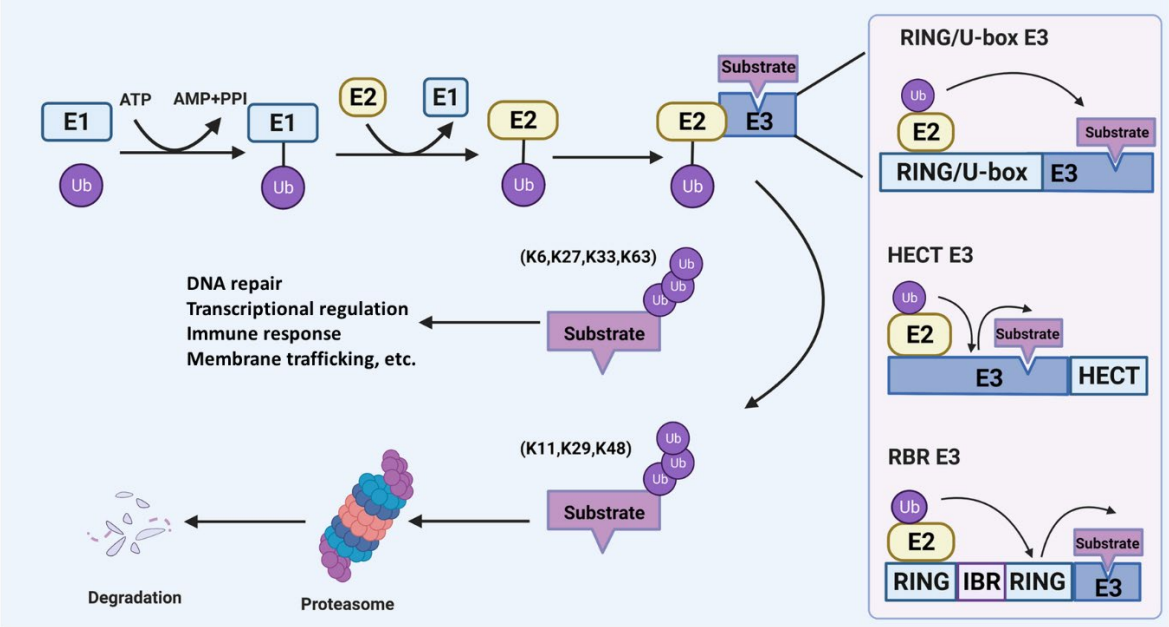

Figure 7. The ubiquitination process and mechanisms adopted by E3 ubiquitin ligases for transferring ubiquitin to target proteins. The ubiquitination process starts with the activation of E1 enzymes to form E1-Ub intermediate by consuming ATP. The E1-Ub later transfers the activated Ub to the E2 enzyme before the Ub is conjugated to the substrates via various E3 ubiquitin ligases. For RING and U-box E3 ubiquitin ligases, the RING and U-box domains function as scaffolds, facilitating the direct transfer of ubiquitin from the E2 enzyme to the substrate. For HECT E3 ligase, the HECT domain interacts with E2 enzyme to form a Ub-E3 intermediate before transferring the Ub to the substrate. For RBR E3 ubiquitin ligases, RING1 binds the E2 enzyme carrying ubiquitin, and RING2 forms a Ub-E3 intermediate by its active cysteine before transferring the Ub to the substrate. The ubiquitin linkage chain type routes substrates for various destinations: K11, K29, and K48 chains are mainly responsible for the ubiquitin-proteasome degradation pathway, while K6, K27, K33, and K63 chains are involved in DNA repair, transcriptional regulation, immune response and membrane trafficking, etc. Adapted from (Zhao et al, 2022).

2.2.2 Deubiquitination

Deubiquitination is a process leading to the elimination of ubiquitin moieties from proteins and is orchestrated by the DUBs (Komander *et al*, 2009a). The human genome encodes approximately 100 distinct DUBs. These enzymes function by removing ubiquitin molecules, preventing a constitutive conjugation of ubiquitin and leading to the disassembly of ubiquitin chains. In ubiquitin recycling, DUBs like USP14 and UCHL5 play a crucial role by removing ubiquitin chains and releasing free ubiquitin from substrates, which is essential for subsequent conjugation events. (Park & Ryu, 2014; Ventii & Wilkinson, 2008).

DUBs are generally categorized into two major classes: cysteine proteases and metalloproteases (Amerik & Hochstrasser, 2004). The cysteine proteases can be further subdivided into six families, based on domain architectures and sequence conservation (Li & Reverter, 2021). All cysteine protease family DUBs employ a catalytic triad consisting of an active-site cysteine residue, along with a histidine, and typically, an aspartate or asparagine, to hydrolyze the ubiquitin linkages (Amerik & Hochstrasser, 2004). In contrast to a catalytic cysteine, metalloprotease DUBs facilitate isopeptide hydrolysis through a catalytic serine accompanied by a zinc ion cofactor (Ambroggio *et al*, 2004; Shrestha *et al*, 2014).

The six families within the cysteine protease DUBs comprises the ubiquitin-specific protease (USP), ubiquitin C-terminal hydrolase (UCH), ovarian tumor containing proteases (OTU), motif interacting with Ub-containing novel DUB (MINDY), Machado–Josephin domain (MJD or Josephins), and the most recently identified DUB family known as Zn-finger and UFM1-specific peptidase (UFSP) domain protein (ZUFSP) (Li & Reverter, 2021).

USP family

The USP family of DUBs, characterized by three subdomains featuring a right hand: the thumb, palm, and fingers, is the largest DUB family consisting of at least 58 members (Hu *et al*, 2002; Hu *et al*, 2005). The catalytic region is positioned amid the thumb and palm subdomains, while the fingers stabilized the interaction with the ubiquitin on substrates (Hu *et al.*, 2002). An analysis of human and yeast USP DUBs disclosed 6 conserved sequence boxes with 5 common insertion points (Ye *et al*, 2009). These boxes harbor interaction domains, such as the B-box domain in CYLD (Komander *et al.*, 2009a; Komander *et al*, 2008), and ubiquitin binding domains, like UIM motifs in USP37 (Ye *et al.*, 2009). These domains facilitate the recruitment of many USP DUBs and ubiquitin-like domains that may regulate DUB activity (Sowa *et al*, 2009; Zhu *et al*, 2007).

Further regulations of USP DUBs are mediated by their interacting partners (Sowa *et al.*, 2009). Many USPs bind WDR40 repeat containing proteins for proper functions. For example, WDR48 interacts with and activates USP1, USP12, USP46 while further activation of USP12 and USP46 requires an additional binding of WDR20 (Cohn *et al*, 2009; Cohn *et al*, 2007; Kee *et al*, 2010; Li *et al*, 2016). Another common regulation for USPs and other DUB families are the bindings between DUBs and E3 ligases (Komander *et al.*, 2009a; Sowa *et al.*, 2009). It is suggested that DUBs exert a broad influence on specific E3 ligases, contributing to their stability or activity, as shown for the MDM2-USP7 (Qi *et al*, 2020) and KPC1-USP19 interaction (Lu *et al*, 2009). These observations highlight a reciprocal interaction between ubiquitination and deubiquitination processes.

It is reported that the majority of USPs exhibit activity against all types of ubiquitin linkages (Komander *et al*, 2009b; Virdee *et al*, 2010; Ye *et al*, 2011), with some members as exceptions. For example, USP14 has a preference for K48-linked chain (Hu *et al.*, 2005) while CYLD specifically cleaves the K63-linked ubiquitin chain (Komander *et al.*, 2009b).

UCH family

The UCH family of DUBs includes four mammalian members (UCHL1, UCHL3, UCHL5, and BAP1). Both UCHL1 and UCHL3 are related to brain functions (Setsuie & Wada, 2007; Wood *et al*, 2005) and UHCL5 can serve as a proteasome bound DUB which frees and recycles ubiquitin (Deol *et al*, 2020). BAP1 (BRCA1-associated protein-1) is a tumor suppressor involving in DNA repair and cell cycle (Artegiani *et al*, 2019; Masoomian *et al*, 2018; Yu *et al*, 2010). A common feature of UCH family DUBs is a cross-loop structure covering their active sites, which limits the size of substrates they can interact with, typically restricting their activity to small peptides generated from proteasomal or lysosomal degradation (Johnston *et al*, 1997; Johnston *et al*, 1999). UCH DUBs showed minimal activities towards ubiquitin polymers with various linkage types *in vitro* (Komander *et al.*, 2009b; Popp *et al*, 2009). However, proteasome-bound UCHL5 possess the ability to process polyubiquitin chains, which could be reasoned that binding to the proteasome induces a conformational change to remodel the crosscover loop or ubiquitin polymers are unfolded before being processed via the crosscover loop in UCHL5.

OTU family

The OTU family of DUBs comprises 17 members. Like USP-DUBs, they often possess additional domains including ubiquitin interaction motif (UIM), ubiquitin associated (UBA) and ubiquitin like (UBL) domains (Komander *et al.*, 2009a). The core of the OTU domain consists of approximately 150-200 residues (Nanao *et al*, 2004). However, a subgroup of enzymes, including tumor necrosis factor alpha–induced protein 3 (A20), Cezanne, OTUD1, and Valosin Containing Protein Interacting Protein 1 (VCIP1), features an extended catalytic core spanning approximately 360 residues (Komander, 2010; Komander & Barford, 2008). An intriguing characteristic of the OTU family is that certain members lack the asparagine or aspartate residue in the catalytic triad, which is commonly found in DUBs (Nijman *et al*, 2005b). Certain members of the OTU family including OTUB2, are expected to be inactive due to the absence of the negatively charged residue in the catalytic triad necessary for polarizing the histidine. In contrast, A20 has been shown to maintain activity even after its catalytic aspartate residue was mutated (Lin *et al*, 2008; Nanao *et al.*, 2004). On the other hand, OTU domains in OTUD1 remain inactive before binding to the ubiquitin and a conformational change is required prior to the enzyme activation. This mechanism is suggested to prevent catalytic cysteine residues from being oxidized by the reactive oxygen species (ROS) (Enesa *et al*, 2008).

A majority of OTU DUBs exhibit specificity for ubiquitin substrates with distinct linkages (Mevissen *et al*, 2013). For example, OTUB1 is K48-chain specific while Cezanne works on K11 chains and OTUD2 displays specificity for K11, K27, and K33 chains (Bremm *et al*, 2010; Edelmann *et al*, 2009; Mevissen *et al.*, 2013). The specificity of OTU DUBs is facilitated by additional ubiquitin interaction sites, which enable them to bind Ub chains with specific linkages. This characteristic has established OTU DUBs as key regulators in various signaling pathways. (Mevissen *et al.*, 2013).

MINDY family

The MINDY DUB family, comprising five members (MINDY1–4 and MINDY4B), features an exclusive catalytic triad consisting of cysteine, histidine, and glutamine. Notably, these DUBs exhibit a high specificity for K48 chains. similar to members of OTU family. MINDY DUBs are autoinhibited before substrate binding, triggering a conformational change that activates the enzyme (Abdul Rehman *et al*, 2016).

MJD family

This family received its name from the Machado–Josephin disease, a neurological condition originating from an elongation of the CAG repeat motif in ataxin 3 (ATXN3). This expansion gives rise to polyglutamine, inducing protein misfolding and aggregation (Kawaguchi *et al*, 1994). All four members of the MJD family (Josephin domain-containing 1, Josephin domain-containing 2, ATXN3 and ATXN3L) share a remarkably conserved catalytic Josephin domain. This domain features a catalytic cysteine residue, two conserved histidines and two ubiquitin binding sites which are essential for the DUB function (Albrecht *et al*, 2004; Li & Reverter, 2021). It is noteworthy that MDJ DUBs are absent in yeast, suggesting they fulfill specific functions in higher eukaryotes which evolved during evolution. The specificity of MJD DUBs towards linkage types is unclear. Although the UIM domains in ATXN3 were reported to preferentially bind to K48 chains (Sims & Cohen, 2009; Winborn *et al*, 2008), ATXN3 also edits K63-linked chains (Winborn *et al.*, 2008).

ZUFSP

With little homology to already discovered DUBs, Zinc finger with UFM1 (ubiquitin fold modifier 1)-specific peptidase domain protein (ZUFSP) represents a new member within the realm of DUBs (Kwasna *et al*, 2018). ZUFSP possesses two ubiquitin binding domains: a ZUFSP helical arm (ZHA) and a ubiquitin-binding zinc finger (UBZ) domain that binds to the distal ubiquitin and polyubiquitin, respectively. Of note, both domains are crucial for the K63-linked chain specificity of ZUFSP (Kwasna *et al.*, 2018).

The activation of cysteine proteases depends on whether the cysteine contains an inactive thiol (-SH) or an active thiolate ($-S^-$) group (Ronau *et al*, 2016). The transition between those two groups are typically mediated by conformational changes induced by the binding of substrate or interacting partners, or post-translational modifications (PTMs) on the DUBs (Boudreaux *et al*, 2010; Hu *et al.*, 2002; Komander *et al.*, 2009a; Maiti *et al*, 2011). Conformational change results in the polarization of the active histidine residue, accompanied by an aspartate or an asparagine residue (Eletr & Wilkinson, 2014; Nijman *et al.*, 2005b), which decreases the pKa of the cysteine, leading to thiol deprotonation while stabilizing the thiolate (Komander, 2010; Suresh *et al*, 2020). The active thiolate in the cysteine then undergoes a nucleophilic attack on the isopeptide bond between ubiquitin and the substrate, resulting in a thioester intermediate involving the DUB and the substrate with ubiquitin (Komander, 2010; Snyder & Silva, 2021; Zhang *et al*, 2011b). The

release of ubiquitin and substrate occurs when a water molecule hydrolyzes the bonds between the ubiquitin and the DUB, which resets the DUB with a thiolate, ready for a new cycle of enzymatic reaction (Komander, 2010; Zhang *et al.*, 2011b).

Metalloproteases

The JAMM (JAB1/MPN/Mov34 metalloenzyme)/MPN (Mpr1p Pad1p N-terminal) metalloprotease class of DUBs comprises zinc-dependent enzymes and is encoded by 14 genes with this domain in human genome. The active sites of the metalloprotease class of DUBs consist of a serine, an aspartate, and two histidine residues, along with a zinc ion and a water molecule (Ambroggio *et al.*, 2004; Shrestha *et al.*, 2014). The mechanism for JAMM/MPN+ domain DUBs involves a zinc ion generating a hydroxide ion from water to cleave the isopeptide bond (Ambroggio *et al.*, 2004). Due to this mechanism, DUBs in this class do not establish a covalent intermediate consisting of the enzyme and its substrate. This property makes them resistant to classical DUB inhibitors and redox reactions, which typically target the catalytic cysteine in other DUB families (Mevissen & Komander, 2017).

Regulatory particle non-ATPase 11 (RPN11), one of the proteasome-bounds DUBs, is one of the best studied metalloprotease DUBs (Verma *et al*, 2002). It removes the whole polyubiquitin chain at once by cleaving the proximal ubiquitin of the ubiquitin chain from the substrate (Yao & Cohen, 2002). Failure of this function causes steric hindrance for substrates to be further processed by 20S core particle of the proteasome, subsequently preventing protein degradation (Worden *et al*, 2017).

Another well-known metalloprotease DUB, associated molecule with the SH3 domain of STAM (AMSH), participates in the regulation of endosomal membrane trafficking via its DUB activity towards ubiquitinated cargos (McCullough *et al*, 2004). The function of AMSH influences the sorting destination of cargos to be degraded or recycled (McCullough *et al.*, 2004; McCullough *et al*, 2006). JAMM/MPN+ DUBs can cleave K63-linked chains while AMSH, AMSH-like protein (AMSH-LP) and BRCA1-BRCA2-containing complex (BRCC) 3 have a particular preference for such chain type (Cooper *et al*, 2009; McCullough *et al.*, 2004).

2.2.3 Specificity of the ubiquitin system

Specificity of the ubiquitin system is essential for protein degradation or cellular activities such as the endocytic trafficking and DNA repair. Several factors contribute to the specificity of the ubiquitin system.

E3 ligases

E3 ligases play a crucial role in determining the specificity of substrate recognition. With the help of their structural motifs, adaptor proteins, or other distinctive features, they specifically recognize substrates. Structural motifs including the F box motif in Skp1-Cul1-F-box protein (SCF) E3 ligases (Jin *et al*, 2005) and WDR40 repeat domain in Cullin-RING E3 ligases (Harper & Schulman, 2021) are responsible for substrate recognition. Adaptor proteins like Cdc20 and Cdh1 serve as activator subunits of the Anaphase-Promoting Complex/Cyclosome (APC/C), recognizing specific substrates during different phases of the cell cycle (Li & Zhang, 2009). Interestingly, a recent study showed that the autoinhibition of the E3 ligase CRL2 protects itself from processing non-substrates, raising the theory that a polymer formation facilitates the autoinhibition and selectivity of E3 ligases towards substrates (Scott *et al*, 2023).

Motifs or status of the substrate

Specific sequences or structural motifs within substrate proteins can serve as recognition signals for the ubiquitin system. Examples include degrons, PEST sequences and destruction boxes.

Degrons were introduced as signals for hydrolysis of peptide bonds (Varshavsky, 1991). N-degron, also referred by the term ‘N-end rule’, was the first degradation signal discovered for proteins with short lifespan (Varshavsky, 1991, 2019). The primary characteristic defining an N-degron is that a protein contains a destabilizing N-terminal residue. In eukaryotes, it has been suggested to designate the proteolytic systems that specifically target N-degrons as the Arg/N-degron (N-terminal arginine) pathway, the Pro/N-degron (N-terminal proline) pathway, and the Ac/N-degron (N-terminal acetylated) pathway (Hwang *et al*, 2010b). Later studies also discovered C-terminal degron, or internal degron which can be recognized by different E3 ligases (Hwang *et al.*, 2010a; Keiler *et al*, 1996; Varshavsky, 2019). A thoroughly investigated instance of an E3 ligase-degron pairing can be found in the degron present in p53 and the E3 ligase MDM2 where three hydrophobic amino acids Phe19, Trp23, and Leu26 from p53 strengthen its binding to MDM2 (Meszaros *et al*, 2017; Wade *et al*, 2010).

Proteins with regions that contain a high concentration of proline (P), glutamic acid (E), serine (S), and threonine (T) residues (PEST) are often characterized by a short half-life within cells with rapid degradation by the UPS (Rechsteiner & Rogers, 1996; Rogers *et al*, 1986). Cell cycle proteins including G1 cyclin (Salama *et al*, 1994) and cyclin F (Bai *et al*, 1994) contain PEST sequences, ensuring their timely degradation during specific phases of the cell cycle. In contrast to PEST sequences in G1 cyclin, cyclin B contains a destruction box (Glotzer *et al*, 1991) with conserved sequence RxxLxyzxN for the recognition by E3 ligase complex APC/C (Lehner & O'Farrell, 1990; Minshull *et al*, 1990; Rechsteiner & Rogers, 1996).

The conformational state or folding status of a substrate can also affect its susceptibility to ubiquitination (Garg *et al*, 2020; Hansen *et al*, 1996). Misfolded proteins with improper disulfide bonds (Niwa *et al*, 2007; Wakabayashi *et al*, 2007) or the exposure of hydrophobic residues on the surface are often targeted for ubiquitin-mediated degradation as part of cellular quality control mechanisms (Ciechanover & Kwon, 2015; Connell *et al*, 2001; Ravid & Hochstrasser, 2008). For example, the E3 ligase CHIP is known to interact with heat shock protein Hsp70 to determine the degradation fate of misfolded cytosolic proteins (Connell *et al.*, 2001; VanPelt & Page, 2017).

Post-translational modifications

The ubiquitin system is highly responsive to various post-translational modifications on E3 ligases, substrate proteins, and ubiquitin itself. Phosphorylation, methylation, acetylation, and other modifications serve as specific signals within the ubiquitin system, leading to diverse cellular outcomes. (Feldman *et al*, 1997; Ohtake *et al*, 2015; Swatek & Komander, 2016; Zhang *et al*, 2011a). For example, modifications including phosphorylation (Feldman *et al.*, 1997; Liu *et al*, 2010) or glycosylation (Yoshida *et al*, 2002) on substrates promotes the recognition by F-box proteins. Phosphorylation of the E3 ligase complex APC/C and its coactivator proteins, including CDC20, by cyclin-dependent kinases (CDKs) is a critical step in determining the substrate specificity of the complex during cell cycle (Fujimitsu *et al*, 2016). Ubiquitin Ser65 phosphorylation on mitochondria serves as an allosteric regulator to lift the auto-inhibition status of the E3 ligase Parkin and facilitates its recruitment to mitochondria and triggers subsequent ubiquitination process (Koyano *et al*, 2014; Ordureau *et al*, 2014)

Ubiquitin chain topology

Ubiquitin chain topology includes the ubiquitination chain type (mono- or poly-) and ubiquitin linkage specificity. For ubiquitination chain type, monoubiquitination is important in DNA repair. For example, monoubiquitination of FANCD2 is necessary for recruiting the E3 ligase breast cancer gene 1 (BRCA1) in DNA repair process (Garcia-Higuera *et al*, 2001). Polyubiquitin chains, on the other hand, are crucial for substrate recognition by the proteasome (Li & Ye, 2008). An *in vitro* study revealed that a polyubiquitin chain carrying minimal 4 Ubs is required for efficient processing by the 19S proteasome complex (Thrower *et al*, 2000). The yeast transcription factor Met4 used its UIM domain to shield attached ubiquitin chain via inter- or intramolecular interaction, thus restricting the chain length and preventing its recognition by the proteasome (Flick *et al*, 2006).

Diverse ubiquitin linkage types, exemplified by the distinctive characteristics of K48-linked chain, one of the most abundant linkage types (Jacobson *et al*, 2009; Xu *et al.*, 2009), is pivotal in marking proteins for degradation within the proteasome (Figure 7). In addition, K11/K48 heterotypic polyubiquitin chains and K29 linked polyubiquitin chains are also involved in proteasome degradation during cell cycle or proteotoxic stress response (Davis *et al*, 2021; Yu *et al*, 2021). Although the levels of K6, K27, K29, and K33 ubiquitin linkages are low within cells, their abundance significantly rises to varying degrees upon proteasome inhibition (Xu *et al.*, 2009). Moreover, K6 and K27 linkages play crucial roles in DNA replication repair (Gatti *et al*, 2015; Morris & Solomon, 2004).

The ubiquitin chain variant represented by K63-linked chains, another abundant linkage in cells (Jacobson *et al.*, 2009; Xu *et al.*, 2009) are implicated in numerous cellular functions, including DNA repair (Lee *et al*, 2017), signal transduction (Kuchitsu *et al*, 2023), and endosomal trafficking (Duncan *et al.*, 2006). The K63-linked chain preferentially accumulates at DNA double strand break sites, which is important for DNA repair (Liu *et al.*, 2018). It also facilitates the substrate binding to tumor susceptibility gene 101 (Tsg101) from the ESCRT machinery (detailed introduction below), regulating protein trafficking (Strickland *et al*, 2022).

Thus, the diversity of ubiquitin chain linkages act as distinct molecular signals that convey specific instructions to the cellular machinery, which significantly contributes to the specificity of the ubiquitin system (Komander & Rape, 2012).

DUBs

DUBs can act on particular substrates via their interaction domains or on specific ubiquitin chain linkages, contributing to the overall specificity of the system. With few exceptions, USP DUBs possess extra domains for interacting with other proteins, either externally or notably as insertions within the catalytic domains (Clague *et al*, 2013; Ye *et al.*, 2009). These domains can bind to substrates for deubiquitination, and the majority of USPs cleave ubiquitin chains irrespectively of the linkage type or structural arrangement (Faesen *et al*, 2011; Ritorto *et al*, 2014), while CYLD and USP30 prefer K63- and K6- polyubiquitin chains, respectively (Bingol *et al*, 2014; Cunningham *et al*, 2015; Komander *et al.*, 2008). One interesting example for a DUB with specificity for a particular linkage is OTULIN (OTU DUB), which selectively focuses on Met1-linked ubiquitin chains (Keusekotten *et al*, 2013; Rivkin *et al*, 2013).

In addition to interaction domains within the DUBs, interacting partners of DUBs add another layer of their specificity towards target proteins. UCHL5 binds to Rpn13 to process polyubiquitinated substrates sent for proteasomal degradation, however, by interacting the human chromatin complex INO80 it may regulate transcriptional activity and DNA repair (Husnjak *et al*, 2008; Yao *et al*, 2008; Yao *et al*, 2006). Another intriguing example is the interaction between USP46 with its adaptor/activator protein WDR48. The C-term sumo-like domain of WDR48 is supposed to facilitate the substrate recognition (Yin *et al*, 2015) while a point mutation in WDR48 prevents USP46-WDR48 complex from recognizing and deubiquitinating the substrate PH Domain Leucine-rich Repeat Protein Phosphatase 1 (PHLPP 1) (Gangula & Maddika, 2013). Structurally, the crossover loop in the active site of UCH DUBs is a key element that influences substrate selection, typically favoring substrates of restricted sizes. (Das *et al*, 2006; Reyes-Turcu *et al*, 2009).

Subcellular localization

Subcellular localization critically influences the specificity of the ubiquitin system. Protein organization within cellular compartments dictates accessibility to ubiquitin ligases, DUBs, and the system as a whole.

Several organelles and cellular structures harbor specific ubiquitin ligases. Nuclear residential E3 ligase RING Finger Protein 4 (RNF4) regulates nucleocytoplasmic proteins transport and turnover, controlling the transcriptional activity (Moilanen *et al*, 1998; Nishida & Yamada, 2020). Endoplasmic reticulum (ER) harbors a set of membrane embedded E3 ligases including HMG-

CoA reductase degradation 1 (Hrd1) and degradation of alpha 10 (Doa10) which are responsible for the ubiquitination and degradation of misfolded proteins in the ER, a process known as ERAD (ER-associated degradation) (Braakman & Hebert, 2013; Lopata *et al*, 2020). The plasma membrane also possesses several E3 ligases. For example, neural precursor cell expressed developmentally down-regulated protein 4 (Nedd4) regulates the ubiquitination of cell surface proteins with subsequent alternations in endocytosis and lysosomal degradation (Kabra *et al*, 2008; Rotin *et al*, 2000; Sun *et al*, 2021). E3 ligases residing on other subcellular compartment including mitochondria (Phu *et al*, 2020), Golgi apparatus (Yamada *et al*, 2013) and cytoskeleton (Ikeda & Inoue, 2012) also contribute to the precise regulation of protein turnover, cellular signaling, and organelle homeostasis by the ubiquitin system.

Similarly, some DUBs process specific substrates within their subcellular compartments. For example, USP1 translocates into the nucleus with its nuclear localization signals (NLSs) (Garcia-Santisteban *et al*, 2012) where it meets substrates including PCNA (Huang *et al*, 2006) and Fanconi anemia (FA) proteins FANCD2 (Nijman *et al*, 2005a) and FA complementation group I (FANCI) (Sims *et al*, 2007) to regulate DNA repair process. Another predominantly nuclear DUB USP7 (Kim & Sixma, 2017) cleave monoubiquitination on substrates Phosphatase and Tensin Homolog (PTEN) (Morotti *et al*, 2014) and FOXO4 (van der Horst *et al*, 2006) to exclude them from the nucleus with subsequent signaling alterations. The ER-resident DUB USP19 rescues ERAD substrates from proteasomal degradation (Hassink *et al*, 2009) while USP8 can localize to endosomes to deubiquitinate EGFR and prevent its lysosomal degradation (Berlin *et al*, 2010).

Subcellular localization influences the availability of substrates and the proximity between substrates and the ubiquitin system to regulate distinct cellular processes, highlighting the dynamic and context-dependent nature of the ubiquitin system within the cell.

In summary, the specificity of the ubiquitin system is a result of the interplay between various factors listed above and beyond. These factors collectively ensure the precise regulation of protein degradation or other cellular processes mediated by the ubiquitin system.

2.2.4 Ubiquitin system in membrane protein trafficking

Ubiquitin system is a key regulator in membrane protein trafficking including its quality control, endocytosis, vesicular transport and endosomal sorting for recycling or degradation (Figure 8) (Hicke & Dunn, 2003; Migliano & Teis, 2018; Millard & Wood, 2006).

Endocytosis can be regulated by direct ubiquitination on membrane proteins or on endocytic adaptor proteins (Savio *et al*, 2016; Weinberg & Drubin, 2014). While ubiquitination is dispensable for the clathrin-mediated internalization of EGFR (Huang *et al*, 2007), it serves as a crucial factor for its clathrin-independent endocytosis (CIE) (Sigismund *et al*, 2013). On other hand, a monoubiquitination of the endocytic adaptor protein Eps15 is necessary for EGFR internalization in a USP9X-dependent manner (Savio *et al.*, 2016). However, depletion of USP9X increased ubiquitination of α5β1 integrins while leaving the internalization rate undisturbed (Kharitidi *et al.*, 2015), suggesting α5β1 integrins can be endocytosed without ubiquitination.

Another crucial role of the ubiquitin lies in the regulation of endosomal sorting and vesicle transport (Ageta & Tsuchida, 2019; Shields & Piper, 2011). Ubiquitination of membrane proteins recruit sorting adaptors such as hepatocyte growth factor-regulated tyrosine kinase substrate (Hrs) and Tsg101 from the ESCRT machinery, initiating ESCRT-mediated lysosomal degradation or exosome secretion to regulate cellular membrane protein levels. (Ageta & Tsuchida, 2019; Migliano & Teis, 2018). During those processes, DUBs have dual functions, to free and recycle ubiquitin on the substrate for maintaining the ubiquitin pool and to recycle the substrates back to the PM. This is exemplified by USP8 protecting EGFR from lysosomal degradation (Berlin *et al.*, 2010) and USP12 stabilizing T-cell receptor adaptor proteins LAT and Trat1 during TCR signaling (Jahan *et al*, 2016).

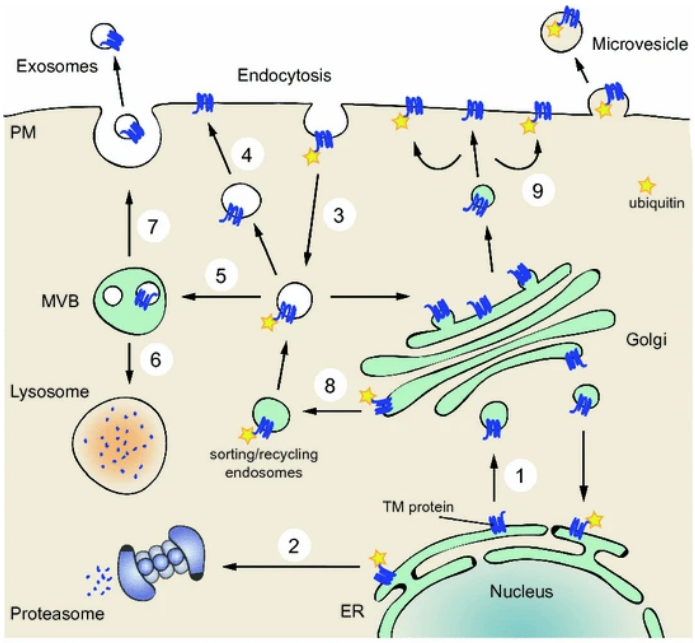

Figure 8. Ubiquitination in membrane protein trafficking. Membrane protein synthesized at ER and transported to Golgi undergo quality control (1) and misfolded proteins are ubiquitinated and degraded in the proteasome (2). Endocytosis of membrane proteins on the PM can be triggered by ubiquitination (3). Once internalized, membrane proteins can be recycled back to cell surface (4) or further sorted into endolysosomal system in the ESCRT-ubiquitin pathway (5) and degraded in the lysosomes (6) or released via exosomes (7). Membrane proteins ubiquitinated at Golgi are directed to endosomal sorting (8). Correctly folded membrane proteins are transported from the Golgi to the PM (9). Adapted from (Migliano & Teis, 2018).

The ubiquitin system dynamically regulates trafficking of membrane proteins, which contributes to cellular homeostasis, signaling, and adaptation to changing environmental conditions (Kennedy & Marchese, 2015; Marchese & Trejo, 2013). Dysregulation of membrane protein ubiquitination is associated with various diseases, including neurodegenerative disorders and cancer (Gireud-Goss *et al*, 2020; Neefjes & van der Kant, 2014; Zhou & Sun, 2021). Thus, precise and timely regulation of ubiquitinated membrane proteins is essential for proper cellular function.

2.3 The ESCRT machinery

The ESCRT machinery, initially identified via genetic and biochemical analysis of a subset of vacuolar protein sorting (vps) mutants in budding yeast (Katzmann *et al*, 2001; Schoneberg *et al*,

2017), is an evolutionarily conserved apparatus responsible for the scission of membrane necks from their interior. In mammalian cells, five distinct subunit complexes (ESCRT-0, -I, -II, -III and the Vps4 complex) were discovered. In addition to mediating multivesicular body (MVB) biogenesis, the ESCRT machinery plays crucial roles in retroviral budding and cytokinetic abscission (Figure 9).

In the MVB pathway, ubiquitinated membrane proteins and lipids were sorted to lysosomes for degradation. In this sorting process, a complete ESCRT machinery assembles sequentially on endosomes. This orchestrated process entails the generation of MVB, initiated by the recognition and sequestration of ubiquitin-tagged transmembrane proteins into microdomains (Katzmann *et al.*, 2001). This recognition is facilitated by the interaction of ubiquitin-binding domains, which promotes the invagination of the endosomal limiting membrane and the budding of intraluminal vesicles (ILVs). These ILVs encapsulate specific cargos intended for degradation into the lumen of the MVB. (Katzmann *et al*, 2002). Given its crucial role in membrane protein turnover, this process is vital for regulating cell surface receptor signaling within cells and throughout development.

The initial appearance of ESCRTs occurred in Archaea, where their primary role was in facilitating cell division (Lindas *et al*, 2008; Samson *et al*, 2008). During the final stages of cytokinesis, ESCRT complexes facilitate membrane abscission by disassembling microtubules at the midbody, leading to the physical separation of the two daughter cells.

In a third scenario, viruses engage in intricate interactions with the host's ESCRT machinery to propagate the infection. In this context, the ESCRT machinery is hijacked in membrane shaping, neck stabilization or the scission of the membrane stalk, mediating the viral replication and budding (Scourfield & Martin-Serrano, 2017; Votteler & Sundquist, 2013).

Despite the different biological outcomes, all three processes demand the presence of ESCRT in membrane shaping and remodeling. This intricate process is orchestrated by the coordinated efforts of the ESCRT complexes, as depicted in Figure 10. Notably, the MVB pathway necessitates the involvement of all five ESCRT complexes.

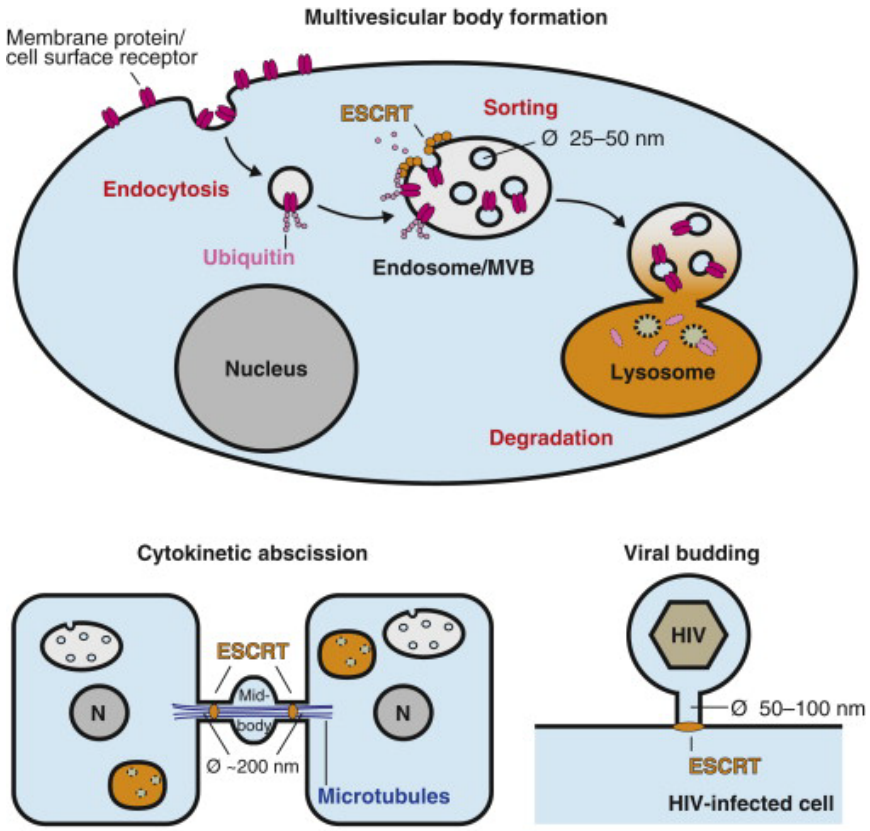

Figure 9. ESCRT-mediated cellular processes. ESCRT complexes orchestrate a unique membrane-remodelling process: the formation and separation of membranes distanced from the cytosol. In the sorting of MVB pathway, the ESCRT machinery generates intraluminal vesicles (with dimensions of approximately 25 nm to 50 nm in human cells) within MVBs, facilitating the transport of ubiquitinated cargos to lysosomes for degradation. In cytokinesis, ESCRT complexes conduct membrane abscission at the midbody. Furthermore, the ESCRT machinery is essential for liberating specific enveloped viruses (such as the human immunodeficiency virus, HIV) from the host cells. Adapted from (Schmidt & Teis, 2012).

2.5.1 ESCRT complexes

Five distinct ESCRT subunit complexes (ESCRT-0, -I, -II, -III and the Vps4 complex), along with associated proteins, are sequentially recruited to endosomal membranes and involved in the recognition, sorting, and eventual degradation of ubiquitinated membrane proteins (Figure 10).

ESCRT-0

ESCRT-0 is composed of two components, namely Hrs and signal transducing adaptor molecule (STAM) in mammals, or Vps27 and Hse1 in yeast. These subunits engage in a 1:1 interaction facilitated by coiled-coil GGAs and Tom (GAT) domains (Asao *et al*, 1997; Prag *et al*, 2007)**.** While both subunits exhibit structural similarities, a distinguishing feature is the presence of a Fab-1, YGL023, Vps27, and EEA1 (FYVE) zinc finger domain exclusively found on Hrs (Mao *et al*, 2000). The Hrs FYVE domain's capability to associate with phosphatidylinositol 3-phosphate (PI3P) contributes to the recruitment of membranes and ensures endosomal specificity within the ESCRT-0 complex (Raiborg *et al*, 2001). Each subunit possesses several ubiquitin-binding domains: Vps27/Hrs comprises a VHS domain along with either a double-sided UIM (Hrs) or two distinct UIMs (Vps27), while Hse1/STAM includes a VHS (Vps27, Hrs and STAM) domain and a UIM. Consequently, one ESCRT-0 complex has the capacity to bind up to five diverse ubiquitinated membrane proteins or multiple ubiquitin molecules from the polyubiquitinated cargo. This feature serves as an extra targeting module, enhancing their attachment to endosomes enriched with cargos (Schmidt & Teis, 2012). Due to its capability to bind both PI3P and ubiquitin, ESCRT-0 acts as a detection module, initiating the MVB pathway on endosomes. Furthermore, ESCRT-0 also recruits ESCRT-I complex to membrane in both yeast and metazoans (Bache *et al*, 2003; Katzmann *et al*, 2003; Lu *et al*, 2003). Vps27/Hrs directly associates with the amino terminus of the Tsg101 (Vps23 in yeast) subunit of ESCRT-I through its carboxy-terminal P(T/S)AP motif. Intriguingly, ESCRT-0 is exclusive to fungi and animals. In contrast, plants, despite lacking ESCRT-0, use the ESCRT-mediated MVB pathway for membrane protein degradation. Recent studies reveal that TOM1-like (TOL) proteins serve as upstream ESCRT factors in plants, partially corresponds to the function of ESCRT-0, suggesting that plants employ a distinct adaptor complex to recruit ESCRT-I to endosomes (Gao *et al*, 2017). Thus, the ability of ESCRT-0 to connect PI3P and ubiquitin and recruit ESCRT-I complex paves the way of MVB-dependent cargo sorting.

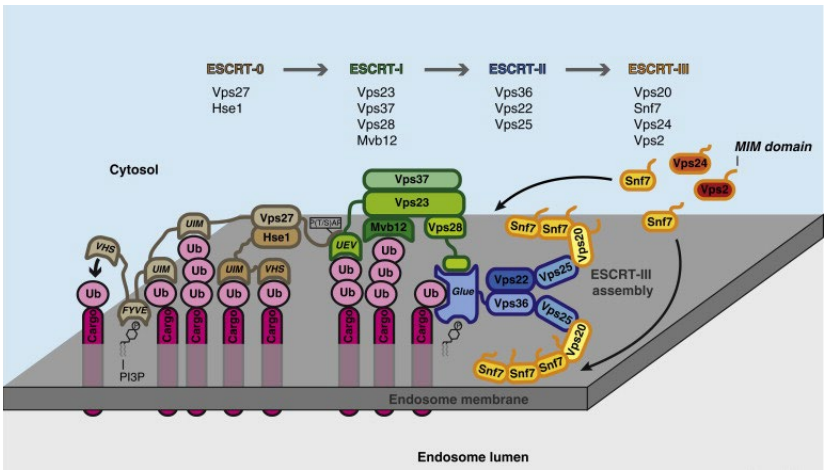

Figure 10. Conceptual framework for the clustering of cargo and assembly of ESCRT complexes in the MVB pathway. The initiation of the MVB pathway involves ESCRT-0 (depicted in brown), which clusters ubiquitinated membrane proteins and binds to PI3P. ESCRT-I (illustrated in green) is recruited by ESCRT-0 (Vps27) and also engages with ubiquitinated cargo. ESCRT-II (depicted in blue) interacts, via the Glue domain of Vps36, with ESCRT-I, PI3P, and cargo. The ESCRT-II component Vps25 acts as a nucleation site, initiating the sequential assembly of ESCRT-III complex (depicted in yellow–orange). This complex both captures cargo and facilitates the inward budding of the vesicle. Adapted from (Schmidt & Teis, 2012).

ESCRT-I

The initial description of an ESCRT complex focused on ESCRT-I, originally recognized in yeast as a heteromeric assembly comprising Vps23, along with Vps28 and Vps37 (Katzmann *et al.*, 2001). Subsequently, multivesicular body 12 (Mvb12) was recognized as an additional component of the ESCRT-I complex (Chu *et al*, 2006; Curtiss *et al*, 2007). ESCRT-I is a soluble hetero-tetramer, comprising Vps23/TSG101, Vps28, Vps37, and either Mvb12 (isoforms Mvb12A or Mvb12B) or UBAP1 (ubiquitin-associated protein 1) (Migliano & Teis, 2018). Its effective translocation from the cytoplasm to endosomes need interactions with the ESCRT-0 complex. UBAP1 possesses a greater specificity for MVB sorting, while Mvb12 plays a role in HIV budding (Morita *et al*, 2007; Wunderley *et al*, 2014). Given the affinity of Vps23/TSG101 and UBAP1/Mvb12 for ubiquitin, ESCRT-I has the potential to attach to two ubiquitin moieties on endosomes. Structurally**,** the ESCRT-I complex adopts a firm rod-shaped structure around 25 nm in length (Kostelansky *et al*, 2007). At one end, the Ubiquitin E2 variant (UEV) domain of

Vps23/TSG101 engages with both ESCRT-0 and ubiquitinated membrane proteins (Katzmann *et al.*, 2003; Kostelansky *et al*, 2006). At another end of the ESCRT-I rod, Vps28 connects with the GLUE domain of the ESCRT-II protein Vps36 (ELL-associated protein of 45 kDa, Eap45 in mammals), establishing interactions with the ESCRT-II complex (Gill *et al*, 2007; Teo *et al*, 2006). Apart from facilitating cargo sorting, the concerted action of ESCRT-I and ESCRT-II results in the deformation of the membrane into buds, encapsulating the cargo within them (Wollert & Hurley, 2010).

ESCRT-II

ESCRT-II is a Y-shaped hetero-tetrameric protein complex comprising Vps36/Eap45, Vps22/Eap22, and two Vps25/Eap20 molecules (Babst *et al*, 2002b; Langelier *et al*, 2006). Vps36/Eap45 and Vps22/Eap22 tightly interact with two Vps25/Eap20 molecules. This creates the ESCRT-II complex's Y-shape, with two separate arms. (Hierro *et al*, 2004; Teo *et al*, 2004). At the base of the Y-shaped structure, the GLUE domain of Vps36/Eap45 serves as a central hub, establishing a connection with Vps28 of ESCRT-I and exhibiting a high-affinity binding to PI3P as well as ubiquitin (Slagsvold *et al*, 2005).

Therefore, together with their capacity to engage with ubiquitinated cargo and PI3P, the three ESCRT (ESCRT-0, -I, and -II) complexes can orchestrate the specific sorting of ubiquitinated membrane proteins and localization to endosomal membrane along the MVB pathway. The transfer of cargo molecules between different ESCRT complexes is similar to a conveyor belt mechanism (Schmidt & Teis, 2012). Alternatively, ESCRT-0, -I, and -II could interact simultaneously with different membrane proteins on endosomal surfaces, gradually forming a sorting domain that evolves into a site facilitating MVB formation. (Henne *et al*, 2011).

While ESCRT-II together with ESCRT-I could initiate endosomal membrane budding with cargo accumulation (Wollert & Hurley, 2010), both arms of ESCRT-II (Vps25/Eap20) exhibit the ability to interact with one of the initial ESCRT-III subunits, Vps20 (charged multi-vesicular body protein 6, CHMP6 in mammals). This interaction results in the conversion of Vps20/CHMP6 into an active nucleator, thereby facilitating the assembly of ESCRT-III on endosomes (Teo *et al.*, 2004).

ESCRT-III

Unlike the early ESCRT (ESCRT-0, -I, and -II) complexes which establish stable cytoplasmic protein complexes, the assembly of the ESCRT-III complex on endosomes is transient in nature. The ESCRT-III complex comprises four fundamental subunits, namely Vps20/CHMP6, Snf7/CHMP4 (A-C), Vps24/CHMP3, and Vps2/CHMP2 (A,B) (Babst *et al*, 2002a) and several other accessory components including increased sodium tolerance 1 homolog (Ist1), Doa4-independent degradation-2 (Did2) and Vps60 which exist as cytosolic monomers (Dimaano *et al*, 2008; Henne *et al.*, 2011; Nickerson *et al*, 2006). The structural analysis of human Vps24 revealed a configuration of approximately 7 nm hairpin structure formed by first 2 α helices which mediates membrane binding and dimerization (Bajorek *et al*, 2009; Muziol *et al*, 2006). The carboxyl termini of the ESCRT-III subunits exhibit less ordered structure comprising α5 helix and the microtubule-interacting and transport (MIT) interacting motifs (MIM), which facilitate the interaction with Vps4 (Obita *et al*, 2007; Scott *et al*, 2005b; Stuchell-Brereton *et al*, 2007). Within the cytoplasm, the negatively charged carboxyl terminus of the ESCRT-III has the capacity to fold back towards the positively charged N terminus, existing in an 'closed' but stable auto-inhibition state. The binding of ESCRT-II subunit Vps25 to the α1 helix of Vps20 leads to the displacement of auto-inhibitory loops, thus alleviating the auto-inhibition. Meanwhile, the alleviation of auto-inhibition also strengthens the affinities of ESCRT-III proteins for both membranes and mutual interactions (Shim *et al*, 2007; Zamborlini *et al*, 2006). Consequently, the recruitment of Vps20 initiates a stepwise homo-oligomerization process of sucrose non-fermenting protein 7 (Snf7). The oligomerization of Snf7 is capped with Vps24 binding to the last Snf7 protomer. Upon translocation to the endosome, Vps24 further recruits Vps2, thereby completing the assembly of ESCRT-III complex (Im *et al*, 2009; Teis *et al*, 2010).

The accessory components of ESCRT-III serves four major functions: bridging the interaction between Vps4 complex and ESCRT-III subunits (Azmi *et al*, 2008; Shiflett *et al*, 2004), promoting ATP hydrolysis of Vps4 (Azmi *et al*, 2006), enhancing the stability of Snf7 oligomers and recruiting deubiquitinase Doa4 (Bowers *et al*, 2004). The latter play a crucial role in mediating the deubiquitination of cargo, thereby recycling ubiquitin prior to the initiation of ILV formation.

Vps4 complex

Vps4 complex and the ESCRT-III complex constitute the most evolutionarily conserved structural elements of the ESCRT machinery. Vps4, composed of the type I AAA-ATPase (ATPase

associated with various cellular activities) and its co-factor Vta1, is the only factor within the ESCRT machinery that consumes adenosine triphosphate (ATP). ATP hydrolysis is essential for breaking down ESCRT-III polymers, thereby enabling the release of individual ESCRT-III subunits back into the cytoplasm. (Babst *et al*, 1998).

Each protomer within the Vps4 complex features a crucial N-terminal MIT domain, playing a pivotal role in binding to the MIMs of the ESCRT-III subunits (Scott *et al.*, 2005b). When engaged with their ESCRT-III substrates, Vps4 protomers assemble into either hexamers (Monroe *et al*, 2014) or dodecamers (Babst *et al.*, 1998), characterized by two superimposed hexametric rings that collectively form a central pore. The co-factor vesicle trafficking 1 (Vta1) significantly enhances the ATPase activity of Vps4 by stabilizing Vps4 oligomers (Scott *et al*, 2005a; Yu *et al*, 2008). The activated Vps4 complex subsequently threads ESCRT-III subunits through its central pore by turning the energy from ATP hydrolysis into mechanical power, consequently driving the neck constriction while generating the indispensable force essential for the scission event at the ILV neck (Adell *et al*, 2014; Adell *et al*, 2017; Henne *et al.*, 2011). Upon the complete disassembly of ESCRT-III complex, the Vps4 complex undergoes dissociation into its protomers. This process marks the termination of each cycle of the cargo sorting and subsequent formation of vesicles in the MVB pathway.

2.3.2 ESCRT in cargo trafficking

The intricate orchestration of cargo trafficking within cells involves a dynamic interplay among membranes, ESCRT complexes, and the cargos they transport (Figure 11). Membranes provide the structural foundation, offering a platform for ESCRT complexes to spatiotemporally mediate cargo trafficking.

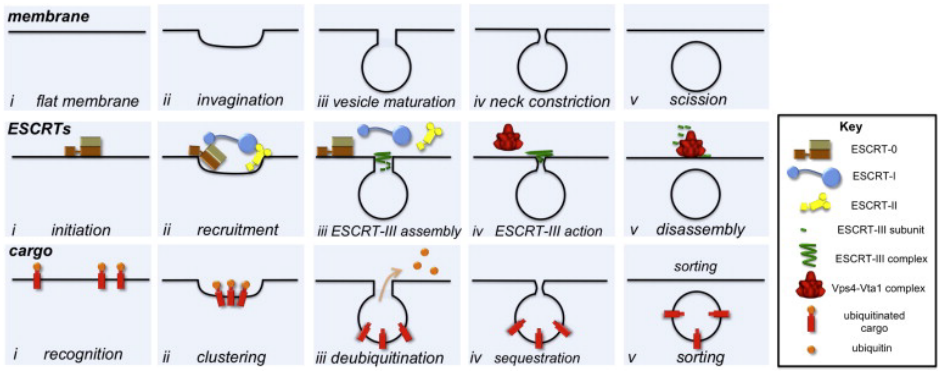

Figure 11. ESCRT-Mediated Vesicle Budding from three perspectives. From the standpoint of the membrane, the top view elucidates five stages in ILV budding. An initially flat membrane (i) undergoes invagination (ii) and maturation into a vesicle, which remains tethered to the limiting membrane via a 'neck' region (iii). The neck further experience constriction (iv) and a subsequent scission event (v) for the final budding of vesicles. From the ESCRTs' perspective, depicted in the middle view, ESCRT-0 initiates the cargo sorting by interacting with ubiquitinated cargo and the membrane (i) with a stepwise recruitment of ESCRT-I and ESCRT-II complexes, forming an ESCRT-cargo-enriched region (ii). ESCRT-II subsequently recruits ESCRT-III subunits and promotes their assembly (iii), nucleation of ESCRT-III complex drives neck constriction and vesicle budding, which is facilitated by the Vps4-Vta1 complex (iv). Afterwards, the Vps4-Vta1 complex disassembles ESCRT-III polymers (v). The bottom view, from the cargo standpoint, highlights the initial recognition of ubiquitinated cargo by the ESCRT-0 (i), followed by clustering through the collaboration of ESCRT-0, -I, and -II complexes (ii). ESCRT-III complex recruits deubiquitinases which deubiquitinate cargos and recycle ubiquitin (iii), further sequester cargos (iv) and eventually completes the sorting by budding the vesicles (v). Adapted from (Henne et al., 2011).

ESCRT adopts several mechanisms including binding to the ubiquitin and endosomal membrane for sorting cargos.

ESCRT binds to the ubiquitin

As described above, ESCRT 0, I and II complexes possess several unique ubiquitin-binding motifs, providing them advantages in binding to ubiquitinated cargos. While ubiquitination of cargo effectively recruits the ESCRT machinery, questions arise regarding its specificity and sufficiency for cargo trafficking. Cytosolic proteins can also undergo ubiquitination, and *in vitro* studies show that both K48- and K63-ubiquitinated proteins bind ESCRT and proteasomes with comparable affinities, leading to substrate degradation at similar rates. (Kim *et al*, 2007; Peth *et al*, 2010). Biochemical analysis has shown that ESCRT-0 components Hrs and STAM preferentially bind to K63-linked chains of ubiquitinated substrates. This binding outcompetes proteasomes for substrate binding in cells, thereby impeding substrate capture by proteasomes. (Nathan *et al*, 2013). Additionally, recombinant Hrs exhibits enhanced binding property to K63-polyubiquitin chains in comparison to monoubiquitin (Barriere *et al*, 2007). A recent structural analysis further resolved

the configuration of the K63-linked di-ubiquitin engaging with the UEV domain of ESCRT I component TSG101, revealing its preference for K63-linked ubiquitin chains. (Strickland *et al.*, 2022). Thus, given the enhanced affinity of K63 chains for ESCRT subunits, it is plausible to propose that the formation of K63 chains enhances the specificity and efficiency of cargo sorting.

ESCRT binds to the endosomal membrane

Another major factor for recruiting the ESCRT machinery in cargo sorting is the ability of ESCRT components to bind endosomal membrane. The crucial role of PI3P in the endosomal localization of ESCRT components is evident, as both ESCRT-0 components and ESCRT-II subunit VPS36 interact with PI3P on endosomes. However, the role of lipids in ILV formation is still illusive. Research has shown that MVB biogenesis relies on phospholipid lysobisphosphatidic acid (LBPA), a lipid species absent in yeast (Matsuo *et al*, 2004). LBPA induces membrane invagination in acidic liposomes and ALG-2 Interacting Protein X (Alix), a component necessary for the recruitment of TSG101 and the ESCRT-III machinery (Bissig *et al*, 2013), regulates this invagination process and organizes LBPA-containing endosomes in cells (Matsuo *et al.*, 2004). Crenarchaea, despite possessing lipid compositions distinct from mammals, utilize the ESCRT for cell division (Henne *et al.*, 2011). Thus, further exploration is needed to comprehend the influence of lipid composition on the budding and scission events.

Furthermore, the ESCRT-0 component Hrs can also bind to the clathrin heavy chain through its clathrin box motif, establishing a connection with flat clathrin coats situated on endosomal membranes. This interaction potentially augments the sequestering of ubiquitinated cargo (Bilodeau *et al*, 2002; Clague, 2002; Raiborg *et al.*, 2001). STAM, another ESCRT-0 component, possess a canonical clathrin-binding motif, which mediates the direct interaction with the terminal domain of clathrin heavy chain (Dell'Angelica, 2001; McCullough *et al.*, 2006). The engagement between ESCRT-0 and clathrin gives rise to microdomains characterized by ESCRT-0, flat clathrin lattices together with ubiquitinated cargo. And these microdomains are of significant importance for cargo sorting (Raiborg *et al*, 2006; Sachse *et al*, 2002).

Interplay of cargos, ESCRTs and DUBs

Cargoes such as growth factor receptors, integrins, and tight junction proteins undergo degradation via the MVB pathway within lysosomes, with minimal impact on their internalization

rates. (Kharitidi *et al.*, 2015; Lobert *et al.*, 2010; Raiborg *et al*, 2008; Tu *et al*, 2010). The epidermal growth factor receptor (EGFR) is typically used as a representative model for investigating the impact of ESCRT depletion on the degradation of transmembrane proteins and cell signaling. (Mattissek & Teis, 2014). The function of the ESCRT machinery in EGFR trafficking is broadly studied, yet the conclusions of the studies are surprisingly contradictory. For example, transient depletions of ESCRT-I and -III complexes, but not ESCRT-0 or -II complex, impeded amphiregulin-induced EGFR recycling (Baldys & Raymond, 2009). However, depletion of Hrs and Tsg101, components of ESCRT-0 and ESCRT-I respectively, increased the recycling rate of internalized EGF to the plasma membrane (Babst *et al*, 2000; Raiborg *et al.*, 2008). A proper functioning of the ESCRT seems to be also important for the continual recycling of tight junction protein claudin-1 and the preservation of polarity in vertebrate epithelial cells since interfering ESCRT function results in accumulated ubiquitination signal colocalized with claudin-1 and transferrin receptor within the cells (Dukes *et al*, 2011). Conversely, although interfering ESCRT early components results in accumulation of ubiquitinated integrins, recycling of integrins surface levels elevated (Kharitidi *et al.*, 2015; Lobert *et al.*, 2010).

The varying outcomes described above indicate discrepancies among different ESCRT complexes, suggesting they may have distinct roles in various trafficking pathways, despite collectively participating in protein sorting for degradation. This likely signifies their involvement at specific stages within the endocytic pathway.

However, those contradictories might be explained by the fact that different ligands induce various trafficking routes of EGFR (Roepstorff *et al*, 2009) as well as the cell models used and time-scale which was applied to monitor the effect caused by perturbations of ESCRT. DUBs like USP8 and AMSH, which associate with ESCRT, should be considered as they cleave ubiquitin and facilitate cargo recycling. (Berlin *et al.*, 2010; Sierra *et al*, 2010).

Within the central region of USP8, there are three extended Arg-X-X-Lys (RXXK) motifs that determine direct, low-affinity interactions with the SH3 domain(s) of ESCRT-0 proteins, specifically STAM1/2 (Berlin *et al.*, 2010). The USP8-STAM complex is pivotal in influencing the ubiquitination status of receptors and regulating the dynamics of ubiquitin on endosomes positive for EGFR. As a result, the USP8-STAM complex serves as a protective role in the precise orchestration of early endosomal sorting of EGFR, determining its fate between pathways leading

to lysosomal degradation and recycling. Similarly, the RXXK motif within AMSH exhibits a high-affinity interaction with the SH3 domains found in STAM1/2 and Grb2. Reduced catalytic activity of AMSH or depletion through RNA interference leads to hyperubiquitination of both STAM1 and Hrs, which also leads to elevated steady-state levels of CXCR4 under basal conditions (Sierra *et al.*, 2010).

On the other hand, the deubiquitination process of cargos, facilitated by USP8 and AMSH, may happen at a later stage. This is due to both deubiquitinases being recruited by ESCRT-III to deubiquitinate cargos before they are sorted into ILVs, thereby facilitating the recycling of ubiquitin. In addition, USP8 and AMSH also deubiquitinate ESCRT-III subunits. For example, USP8 mediates the deubiquitination of ESCRT-III proteins Shrub and CHMP2B, thereby inhibiting complete abscission and allowing cytoplasmic bridges to persist, connecting sister cells (Mathieu *et al*, 2022).

In conclusion, the precise coordination of cargo trafficking depends significantly on the interplay between ESCRT and the ubiquitin system. However, DUB(s) that remove ubiquitin modifications from the β1 integrin cytoplasmic tail while facilitating its recycling remain unknown.

2.4 The USP12/46-WDR48-WDR20 complex

Numerous USPs exhibit modular structures comprising not just catalytic domains but also additional domains or interacting partners dedicated to protein-protein interactions and localization (Sowa *et al.*, 2009; Ye *et al.*, 2009). USP1, USP12 and USP46 belong to a same subfamily of USP DUBs which share a common binding partner WD40-repeat protein WDR48 (also termed UAF-1, USP1-associated factor 1). The binding of WDR48 activates all three USPs, while a full activation of USP12 and USP46 requires the additional binding of another WDR protein, WDR20, which specifically regulates the DUB activity of USP12 and USP46, not USP1 (Li *et al.*, 2016; Zhu *et al*, 2019a).

USP12 and USP46, derived from whole-genome duplication and highly conserved from yeast to human, share approximately 90% protein sequence similarity (Dehal & Boore, 2005; Hodul *et al*, 2017; Vlasschaert *et al*, 2017). They both interact with at least five partners, including WDR48, WDR20, PH domain leucine-rich repeat protein phosphatase 1 (PHLPP1), PHLPP2, and Dystrophia myotonica WD repeat-containing protein (DMWD) (Sowa *et al.*, 2009). Similarly,

homologs of WDR48 and WDR20 can also be found in fission yeast *S. pombe*, suggesting the conservation of the DUB complex across different species. A variety of functions of USP12 and USP46 have been disclosed in recent years. For example, USP12 regulates the cell cycle progression via upregulation of c-Myc and cyclin D2 levels (Tang *et al*, 2016) while USP46 inhibits cell proliferation via stabilizing mammalian Ste20-like kinases (MST1) with causative degradation of yes-associated protein 1 (YAP1) (Qiu *et al*, 2021). Both USP12 and USP46 are involved in human papillomavirus DNA replication via their interaction with WDR48 (Lehoux *et al*, 2014) and in deubiquitinating histones H2A and H2B *in vitro* and in cells (Joo *et al*, 2011). However, whether there is a functional redundancy between USP12 and USP46 is not properly evaluated.

2.4.1 Structure of the USP12/46-WDR48-WDR20 complex

The overall structure of USP12-WDR48-WDR20 complex highly resembles to the structure of USP46-WDR48-WDR20 complex (Figure 12). USP12 and USP46 share the same binding sites to WDR48 and WDR20. Similar to other USPs, core structures of USP12 and USP46 feature a right hand with the finger, palm, and thumb domains. Both USP12 and USP46 contain a catalytic triad comprising cysteine-histine-aspartic acid located within the palm and thumb domains (Villamil *et al*, 2013). The palm and thumb domains provide a binding pocket for ubiquitin to interact with the catalytic cysteine (Yin *et al.*, 2015). The finger domain of USP12 exhibits a high structural plasticity, with the outer edge forming a distinct coiled structure termed ‘Pinky Finger’ (Li *et al.*, 2016). Inactive free USP12 also contains two surface loops called ‘Blocking Loops’ with high flexibility on the palm domain (Li *et al.*, 2016). Upon binding to the ubiquitin, a small catalytic cleft loop (CCL) undergoes conformational changes which is required for the DUB activity (Li *et al.*, 2016).

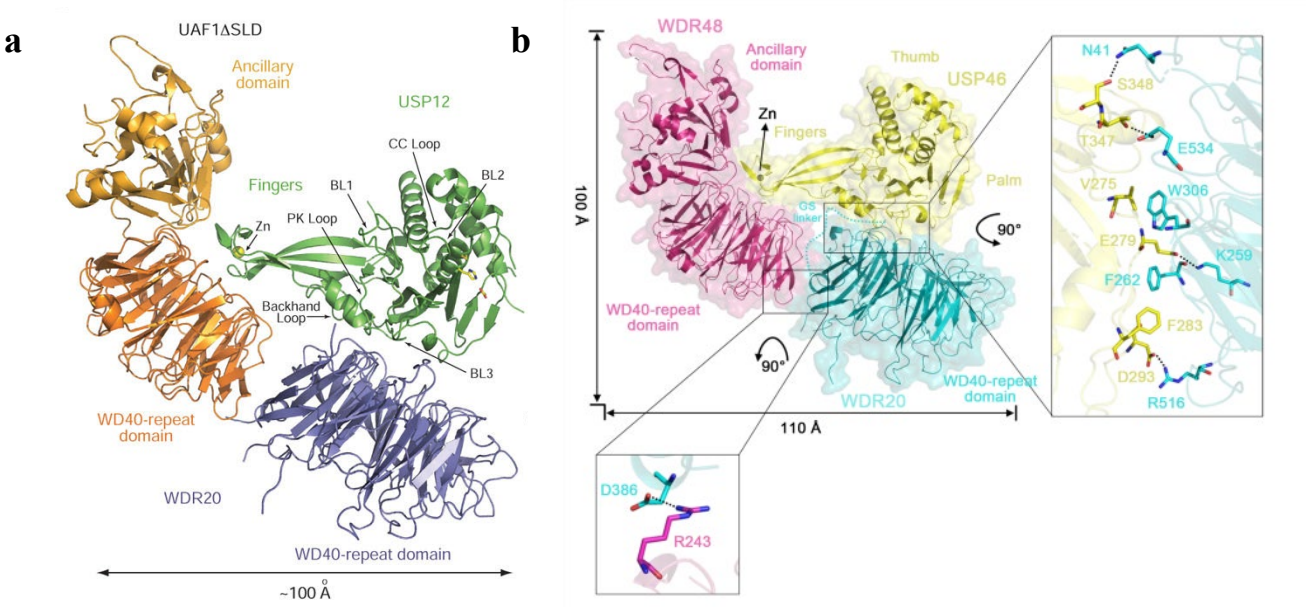

***Figure 12**. The structure of USP12/46-WDR48-WDR20 complex. (**a**) The ribbon diagram illustrates the USP12-WDR48-WDR20 complex, showing USP12, WDR48 and WDR20 (without the sumo-like domain) in green, gold and slate color, respectively. The catalytic triad is represented in sticks. Adapted from (Li et al., 2016) (**b**) The overall architecture of the USP46-WDR48-WDR20 complex with a transparent envelope surface is depicted in a ribbon model with USP46, WDR20 and WDR48 (without the sumo-like domain) color-coded in yellow, cyan and pink, respectively. Interaction interfaces between USP46 and WDR20 (depicted in the zoom box below) and between WDR48 and WDR20 (shown in zoom box right) are depicted. Key residues participating in these interactions are illustrated with their side chains represented in stick models. Hydrogen-bonds and salt-bridges are highlighted using dashed lines. Adapted from (Zhu et al., 2019a).*

WDR48 possess a β-Propeller with seven WD-repeat, a curved ancillary domain (AD) and a sumo-like domain (SLD). The β-Propeller binds to the distal finger domain of the USP46 (Yin *et al.*, 2015). While AD does not directly contact with Ub, its concave structure creates a chaperone-like environment that sterically shields Ub. This may bring the SLD closer to USP46 (Yin *et al.*, 2015). Additionally, the C-terminal SLD of WDR48 is reported to mediate the recognition of substrates such as PHLPP1. (Gangula & Maddika, 2013). Three residues from the WDR48 side (K214/W256/R272) and one residue from USP12 side (E190) in the binding interface are critical for the USP12-WDR48 complex assembly and activation (Dharadhar *et al*, 2016; Yin *et al.*, 2015).

Of note, the binding of WDR48 to USP12 is not stoichiometrically fixed to 1:1 ratio. WDR48:USP12 binding ratios can vary from 1:1 to 2:1. USP12 contains two interfaces which bind to WDR48 with different affinities: the first one in the finger domain comes into interaction with high affinity (Kd = 4 nM) and the second one behind the ubiquitin-binding cleft interacts with WDR48 at higher concentration (Kd = 325 nM) (Dharadhar *et al.*, 2016). Although the second binding of WDR48 to USP12 did not alter its DUB activity *in vitro*, the activity towards natural substrates of USP12 has not been tested yet. Given the second binding interface partially overlaps with WDR20 binding site on USP12 and the high affinity between WDR20 and USP12 (Kd = 7 nM) (Li *et al.*, 2016), WDR20 binding can compete with or prevent the second WDR48 from binding. This provides an additional regulatory mechanism for the formation of the DUB complex. In addition, protein stability of USP46 is regulated by the binding of WDR48, as the loss of WDR48 leads to ubiquitination and degradation of USP46 (Hodul *et al*, 2020).

Similar to the structure of WDR48, WDR20 possesses a seven-bladed-β-Propeller which mediates its interaction of its 'top' surface area with the palm domain of USP12/46 (Li *et al.*, 2016). Interestingly, WDR20 contains two uncharacterized loops with a nuclear export sequence (NES) signal and a C-term fragment that folds back to its N-term region which may stabilize the structural integrity (Li *et al.*, 2016). The NES in WDR20 is suggested to play a role in dynamically shuttling USP12 among the nucleus, cytoplasm and plasma membrane while a short amino acid motif 'MEIL' within the N-term of USP12, not USP46, contributes to its PM localisation (Olazabal-Herrero *et al*, 2019). Two residues from the WDR20 side (F262/W306) and two residues from USP12 side (F287/V279) in the binding interface are critical for the complex assembly and activation (Li *et al.*, 2016).

2.4.2 Activation of the USP12/46-WDR48-WDR20 complex

The activation of US12/46 requires two individual bindings of WD48 and WDR20, which facilitates the catalytical turnover (K_{cat}) instead of increasing the affinity between USP12/46 and substrate-Ub (K_M). Although several biochemical studies have shown that the activity of USP12/46 is upregulated to different extents upon single WDR48 or WDR20 binding, the binding of single WDR20 or WDR48 only induces minimal activation of USP12/46 compared to the full activation achieved when both WDR proteins bind. Thus, WDR20 and WDR48 independently yet synergistically activate USP12/46. (Li *et al.*, 2016; Yin *et al.*, 2015; Zhu *et al.*, 2019a).

Mechanistically, the binding of WDR48 and WDR20 allosterically changes the topology of structural modules in USP12 into a productive conformation which can process substrate-Ub with high turnovers (Figure 13) (Li *et al.*, 2016). The free USP12 is fully capable of binding to the substrate-Ub. However the enzyme is inactive to process the substrate-Ub with two possible reasons. First, the Blocking Loop (BL) 1 adopts a non-productive conformation, leaving the Ub-tail distorted for catalysis in free USP12. Second, the flexible BL2 and CCL are not in an optimal form for catalytical reaction. WDR48 activates USP12 by binding to Pinky Finger (PF) and transmits the allosteric signal to BL1, rendering it to a productive form upon the substrate-Ub binding. A further binding of WDR20, located at the base of BL1, allosterically regulates the topology of BL2 and CCL, resulting in full activation of USP12. In conclusion, the activation of USP12/46 requires the binding of three elements: WDR48, WDR20 and substrate-Ub.

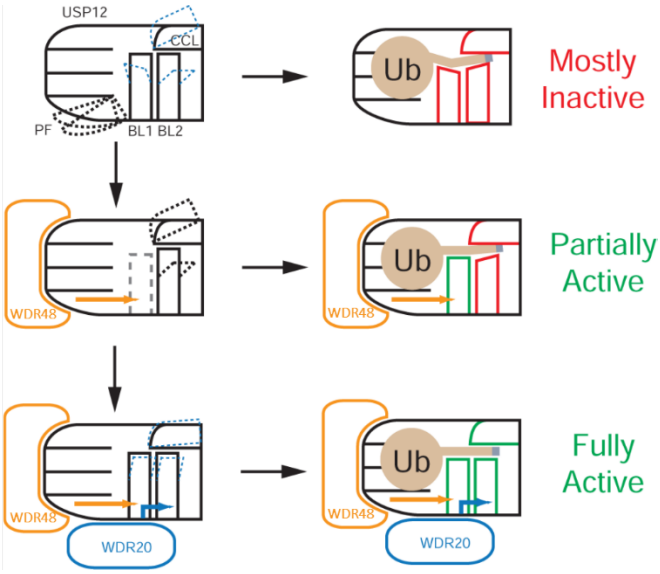

Figure 13. *A schematic view of the activation of the USP12/46-WDR20-WDR48 complex. Thick dotted black lines show flexible conformations. Thin dotted blue lines depict expected alternations in conformational changes. Solid red lines represent sub-optimal structural conformations for catalysis. Solid green lines show optimal structural conformations for catalysis. Arrowed lines point the propagation of allosteric effects triggered by the binding of an activator. A gray block located at the Ub tail represents the isopeptide bond linkage. The unbound USP12 exhibits structural flexibility in its PF, BL1 and BL2, and potentially CCL, allowing the access of a Ub-conjugate substrate the catalytic cleft. However, enzyme inactivity is probably due to non-*

productive conformations of BLs and CCL. WDR48 binds to the PF and regulate the BL1 allosterically and together with the binding of WDR20 which is also remote from the catalytic center, BLs and CCL are stabilized in an optimal form upon substrate-Ub interaction, which allows the highest activity of the DUB complex. Adapted from (Li et al., 2016).

2.4.3 The USP12/46-WDR20-WDR48 complex in transmembrane protein trafficking

Beside its role in deubiquitinating cytoplasmic or nuclear proteins, USP12/46-WDR20-WDR48 complex is also involved in the trafficking of transmembrane proteins.

In the nervous system, the USP46-WDR20-WDR48 complex controls the level of the glutamate receptor GLR-1 in *Caenorhabditis elegans* (Dahlberg & Juo, 2014; Kowalski *et al*, 2011). USP46 facilitates the recycling of GLR-1 to cell surface while preventing its lysosomal degradation by deubiquitinating GLR-1 (Kowalski *et al.*, 2011). Interestingly, a later study in mammalian cells showed that the deubiquitination of Alpha-amino-3-hydroxy-5-methyl-4-isoxazolepropionic acid receptor (AMPA receptor) is also mediated by USP46, not USP12, despite both DUBs being present in the mammalian brain. This suggests some specificity of USP46 towards this substrate (Huo *et al*, 2015).

In contrast to the protective role of USP46 on glutamate receptors, USP12 negatively regulates the surface Notch receptors. USP12 deubiquitinates nonactivated Notch receptors in cells and *in vitro* while unaffecting the degradation of EGF-labelled EGFR receptor (Moretti *et al*, 2012). However, USP46 barely deubiquitinates Notch receptors *in vitro*, indicating a distinct substrate preference compared to USP12 (Moretti *et al.*, 2012). In addition, USP12 positively stabilizes T-cell receptor adaptor proteins LAT and Trat1 during TCR signaling. There was no compensatory effect from USP46 suggested by the authors, as the protein level of USP46 decreased after USP12 was depleted. (Jahan *et al.*, 2016). On the other hand, functional redundancy of USP12 and USP46 has been observed since they both deubiquitinate the nuclear androgen receptor (AR), resulting in enhanced transcriptional activity (Burska *et al*, 2013; McClurg *et al*, 2018). In addition, both USP12 and USP46 have been shown to deubiquitinate histone H2A and H2B, regulating *Xenopus* Development (Joo *et al.*, 2011).

A multifaced role of USP12 and USP46 has been revealed in protein trafficking. The molecular mechanisms underlying how the DUB complex influences protein trafficking and the factors determining its specificity remain elusive, presenting an intriguing area for further investigation.

2.4.4 The USP12/46-WDR20-WDR48 complex in diseases

Beyond its fundamental contributions to normal cellular functions, the USP12/46-WDR20-WDR48 complex has been implicated in various pathological conditions including cancer and nervous system dysfunction.

While a majority of research work suggest that USP12 and USP46 are positively involved in cancer progression, contradictory findings also exist. Overexpression of exogenous USP12 promotes $Kras^{G12D/+}$-induced lung tumour growth while depletion of endogenous USP12 increases higher proliferation capacity in Lewis lung carcinoma cells (Yang *et al*, 2021b). A more recent work shows that USP12 depletion inhibits lung cancer cell growth and tumor growth in lung-cancer xenograft mice model (Chen *et al*, 2023). In addition, USP12 promotes the lung metastasis ability of breast cancer cells *in vivo* by stabilizing midkine expression (Sheng *et al*, 2021). USP12 is also suggested as a positive regulator in prostate cancer (McClurg *et al*, 2015), hepatocellular carcinoma and multiple myeloma *in vitro* (Li *et al*, 2022). UP46, on the other hand, is suggested as a tumor suppressor in the progression of hepatocellular carcinoma (Qiu *et al.*, 2021), renal cell carcinoma (Gui *et al*, 2019) and colon cancer (Li *et al*, 2013). However, USP46 is essential for HPV-transformed tumor growth (Kiran *et al*, 2018) and the proliferation and migration of triple negative breast cancer cells (Ke *et al*, 2023). Moreover, USP46 enhances the invasion and lung metastasis of esophageal squamous cell (Tian *et al*, 2020). Similar to USP12, USP46 also positively correlates with prostate cancer (McClurg *et al.*, 2018). Those discrepancies can be explained by the different cancer cell type or tumor microenvironment involved.

In the nervous system, mice with USP46 depletion mutants or USP46 knockout show abnormal behavior in tail suspension tests and reduced preference for sucrose, indicative of a depression-like phenotype. This observation may have implications for human mental disorders. (Imai *et al*, 2013; Imai *et al*, 2012; Tomida *et al*, 2009). Consistent with this, a sequence-based large scale screening study in a Caucasian population revealed that one SNP (single nucleotide polymorphism) within the USP46 coding sequence is associated with schizophrenia (Need *et al*, 2009). A more recent study showed that loss of WDR20 and WDR48 in *Caenorhabditis elegans* downregulated

glutamate receptor GLR-1, affecting normal locomotion behavior (Dahlberg & Juo, 2014), a similar phenotype found in the USP46 depletion model in *Caenorhabditis elegans* (Kowalski *et al.*, 2011). The stabilization of AMPA receptor in mammals or GLR-1 in *Caenorhabditis elegans* by USP46 could contribute to the observed loss-of-function phenotypes.

Of note, USP12 also plays a role in Huntington's disease by inducing neuronal autophagy, independent of its enzymatic activity, suggesting a scaffold protein function for USP12 (Aron *et al*, 2018).

Collectively, these findings underscore the intricate involvement of the DUB complex in disease progression, offering potential avenues for therapeutic strategies. They also underscore the importance of unraveling the molecular mechanisms that underlie its diverse functions in pathological conditions.

3. Aim of the thesis

As introduced above, the ubiquitin-ESCRT machinery has been well recognized for endosomal trafficking and regulation of the stability of many transmembrane proteins including integrins. However, key players within the ubiquitin system and mechanisms underlying their regulation in integrin trafficking and stability remain elusive.

The 1st aim of my PhD study is to identify and validate DUB candidates in stabilizing integrin surface levels. Based on the Crispr screen and biotin-based proximity screen, we have identified the USP12/46-WDR48-WDR20 complexes. By conducting a comprehensive validation, we can report their regulatory roles in integrin stability.

The 2nd pivotal aim of my PhD study is to unravel the intricate molecular mechanisms that underlie the protective function exerted by the DUB complex on integrin stability. Combining cell biology and biochemistry techniques, I seeked to delineate the specific pathways and molecular machinery that orchestrate the fine-tuned regulation of integrin stability by DUBs. This aspect of the study motivated me to establish a reliable detection method for gaining insights into the ubiquitin modification patterns of β1 integrin, thereby discerning the specific ubiquitination sites, subcellular compartments, ubiquitin chains involved and their functional implications for integrin trafficking, and provides an understanding of the interplay between DUBs and integrins at the molecular level.

A 3rd key objective of my PhD study is to investigate the biological function of the DUBs in regulating integrin stability. By performing cell functional analysis evaluating the capacity of cell adhesion, spreading, migration and invasion, I characterized the biological and pathological relevance of the regulation of DUBs on integrin stability and thereby, shedding light on potential regulatory axis, particularly USP12-intergin axis in maintaining cell adhesion and spreading, promoting cancer cell migration and invasion. The findings may suggest potential therapeutic strategies linking integrin stability and DUB function. The results are presented in the Manuscript I.

Finally, I was also involved in investigating the role of Rab7 proteins in stabilizing integrins. By providing detailed examinations on how Rab7 depletion affects integrin stability, trafficking and biological functions including adhesion and spreading capacities, I deepened our understanding of

the intricate interplay between Rab GTPases and integrins. The results are presented in the Manuscript II.

4. Short summary of the manuscripts

4.1 The USP12/46 deubiquitinases protect integrins from ESCRT-mediated lysosomal degradation

Kaikai Yu, Shiny Shengzhen Guo, Florian Bassermann, Reinhard Fässler, Guan Wang (Manuscript in revision in EMBO Reports)

In this manuscript, we developed a CRISPR screen and proximity-dependent biotin identification (BioID), and identified that a ternary complex, comprised of USP12 (or its paralog USP46), WDR20 and WDR48, is a novel DUB complex for maintaining the stability of β1 integrin (Itgb1). We found that loss of the complex results in reduced Itgb1 surface and protein levels due to increased lysosomal degradation and decreased recycling. Mechanistically, we showed that this complex stabilizes Itgb1 via its deubiquitinating activity by removing polyubiquitin chain(s) from the cytosolic tail of Itgb1, thus preventing its recognition by the ESCRT (endosomal sorting complex required for transport)-mediated sorting and protein degradation. Consequently, the loss-of-function of this DUB complex impaired integrin-mediated cell adhesion, spreading and migration as well cancer cell migration and invasion.

4.2 Rab7 deficiency induces lysosome formation from recycling endosomes leading to an increased degradation of cell surface proteins

Guan Wang, Peng Xu, Kaikai Yu, Shiny Shengzhen Guo, Reinhard Fässler
(Manuscript in revision in The EMBO Journal)

In this manuscript, we developed a whole genome screen using Itgb1 surface level as a readout. We identified the Rab7 small GTPase, believed to be required for lysosome biogenesis, as integrin stabilizer. We showed that cells with Rab7 deficiency contain late endosomes and lysosomes that are functional in protein degradation and organelle fusion, and the Rab7-deficient lysosomes can be formed from Rab4- and transferrin receptor-positive recycling endosomes. Finally, we found that overexpression of Rab4 can drive lysosome formation from recycling endosomes in absence as well as presence of Rab7, however, the latter to a much lesser extent. Our findings illustrated a lysosome biogenesis and lysosomal protein degradation pathway that becomes dominant in absence of Rab7 or when Rab4 is highly abundant.

5. Discussion

As introduced above, USP12 and USP46 are structurally very similar with low tissue specificity in terms of expression pattern. Interestingly, only few published work pointsthe compensatory effect between these two proteins. One fact is that the USP12 and USP46 do possess several sequence discrepancies especially in the flexible N-term, which possibly facilitates the selective binding towards their substrates. Another explanation might be that the cells heavily rely on both DUBs that single USP12 or USP46 depletion is sufficient to induce loss-of-function phenotypes. Furthermore, conclusions made from negative data with no phenotypic changes in single USP12 or USP46 depleted cells should be reconsidered especially if the compensatory function between USP12 and USP46 is not thoroughly evaluated. In our study, we found no phenotypic changes on Itgb1 surface levels in single USP12 or USP46 knockout cells unless both USP12 and USP46 were depleted, demonstrating their functional redundancy in regulating integrins. Further studies are required to address the overlapping function and distinct properties between USP12 and USP46 in complex with WDR48 and WDR20.

Although our data demonstrate the functional link between the DUB complex and integrins, we did not observe strong and direct interactions between the DUB complex and in vitro synthesized and non-ubiquitinated Itgb1 tail using *in vitro* microscale thermophoresis (MST) analysis or in cells to co-IP the DUB complex and integrins with crosslinking. One explanation could be that the DUB complex recognizes ubiquitinated Itgb1, which is a very minor population in cells. On the other hand, the *in vitro* deubiquitination assay showing a direct activity of the DUB complex towards ubiquitinated Itgb1 strongly suggests that the direct interaction between them may exist, at least in a transient manner. Alternatively, a third protein can act as an intermediate for recruiting the DUB complex to Itgb1. USP12 and USP46 share a common interactor, PHLPP1, which can bind to the lipids with the PH domain. In our cell model, both PHLPP1 and its paralog, PHLPP2 interact with the DUB complex. Individual and double depletion of both PHLPPs in the genome should be considered to evaluate their involvement in regulating the DUB function in cells. While the PHLPPs are supposed to be substrates of USP12 and USP46, we did not see protein loss in MS analysis comparing WT and USP12/46 dKO cells, which contradicts published observations in colon cancer cell HCT116 (Li *et al.*, 2013) but agrees with a PhD thesis which used the same colon cancer cell line but failed to see protein loss of PHLPP1 upon USP46 knockdown Inspired by

studies on CRL2 and GID E3 ligases, where substrate specificity is mediated through supramolecular assembly (Scott *et al.*, 2023; Sherpa *et al*, 2021), it is pertinent to investigate whether DUBs such as USP12 and USP46 require the formation of a supramolecular machinery or utilize ESCRTs to achieve selective substrate cleavage.

One question raised from the study is that why USP12/46/SNX17 triple KO does still not remove all integrins. To address this question, one need to distinguish integrins on the cell surface and integrins in the recycling pool intracellularly. We observed a more decrease in total protein levels of integrins detected by WB compared to surface levels of integrins detected by flow cytometry in various KO cells. This indicates that the primary reduction in integrin levels occurs from the recycling pool, with the depletion of surface integrins being a consequence thereof. Initially, integrins undergo endocytosis before exiting to either the plasma membrane (PM) or lysosomes. While our study did not address this directly, delayed or slower endocytosis of integrins in general could compromise subsequent degradation processes. Moreover, it is plausible that alternative recycling pathways, whether passive or active through other trafficking adaptors, operate independently of SNX17 and the USP12/46-WDR48-WDR20 complex to protect integrins from degradation.

In addition, whether surface integrins can also be degraded in a ubiquitin-independent pathway is not known. We observed a minor increase in surface and total protein levels of non-ubiquitinable integrins when cells are treated with Bafilomycin A1, which indicates non-ubiquitinable integrins might still be degraded, though to a lesser extent. One explanation is that the non-canonical ubiquitination process can occur on serine and threonine residues instead of lysine resdieus (McDowell & Philpott, 2013). Secondly, together with other transmembrane proteins including tetraspanin CD151 on the PM (Liu *et al.*, 2007), integrins are co-trafficked into microdomains where they can enter the endolysosomal system (Baron *et al*, 2003; Martin *et al*, 2012). Thirdly, ILV formation is not always ubiquitin-ESCRT dependent, ESCRT-independent pathway also contributes the formation of ILV, thus leading to a subsequent degradation of transmembrane proteins (McNally & Brett, 2018).

Inhibitors against USP1 and USP14 have been discovered and are used in clinical trials for anti-cancer therapy (Ge *et al*, 2022; Rowinsky *et al*, 2020). However, inhibitors tailored specifically targeting USP12 and USP46 are still missing. In light of previous studies and our current work,

developing inhibitors blocking the interaction between WDR48/20 and USP12(46) or the USP12(46) activity would be novel strategies for addressing diseases associated with the DUB complex, particularly for cancer.

6. References

Abdul Rehman SA, Kristariyanto YA, Choi SY, Nkosi PJ, Weidlich S, Labib K, Hofmann K, Kulathu Y (2016) MINDY-1 Is a Member of an Evolutionarily Conserved and Structurally Distinct New Family of Deubiquitinating Enzymes. *Mol Cell* 63: 146-155

Adair BD, Xiong JP, Yeager M, Arnaout MA (2023) Cryo-EM structures of full-length integrin alphaIIbbeta3 in native lipids. *Nat Commun* 14: 4168

Adell MA, Vogel GF, Pakdel M, Muller M, Lindner H, Hess MW, Teis D (2014) Coordinated binding of Vps4 to ESCRT-III drives membrane neck constriction during MVB vesicle formation. *J Cell Biol* 205: 33-49

Adell MAY, Migliano SM, Upadhyayula S, Bykov YS, Sprenger S, Pakdel M, Vogel GF, Jih G, Skillern W, Behrouzi R *et al* (2017) Recruitment dynamics of ESCRT-III and Vps4 to endosomes and implications for reverse membrane budding. *Elife* 6

Ageta H, Tsuchida K (2019) Post-translational modification and protein sorting to small extracellular vesicles including exosomes by ubiquitin and UBLs. *Cell Mol Life Sci* 76: 4829-4848

Aguilera M, Oliveros M, Martinez-Padron M, Barbas JA, Ferrus A (2000) Ariadne-1: a vital Drosophila gene is required in development and defines a new conserved family of ring-finger proteins. *Genetics* 155: 1231-1244

Albrecht M, Golatta M, Wullner U, Lengauer T (2004) Structural and functional analysis of ataxin-2 and ataxin-3. *Eur J Biochem* 271: 3155-3170

Alday-Parejo B, Stupp R, Ruegg C (2019) Are Integrins Still Practicable Targets for Anti-Cancer Therapy? *Cancers (Basel)* 11

Alonso-Garcia N, Ingles-Prieto A, Sonnenberg A, de Pereda JM (2009) Structure of the Calx-beta domain of the integrin beta4 subunit: insights into function and cation-independent stability. *Acta Crystallogr D Biol Crystallogr* 65: 858-871

Alpi AF, Pace PE, Babu MM, Patel KJ (2008) Mechanistic insight into site-restricted monoubiquitination of FANCD2 by Ube2t, FANCL, and FANCI. *Mol Cell* 32: 767-777

Ambroggio XI, Rees DC, Deshaies RJ (2004) JAMM: a metalloprotease-like zinc site in the proteasome and signalosome. *PLoS Biol* 2: E2

Amerik AY, Hochstrasser M (2004) Mechanism and function of deubiquitinating enzymes. *Biochim Biophys Acta* 1695: 189-207

Amm I, Sommer T, Wolf DH (2014) Protein quality control and elimination of protein waste: the role of the ubiquitin-proteasome system. *Biochim Biophys Acta* 1843: 182-196

Andersen P, Kragelund BB, Olsen AN, Larsen FH, Chua NH, Poulsen FM, Skriver K (2004) Structure and biochemical function of a prototypical Arabidopsis U-box domain. *J Biol Chem* 279: 40053-40061

Aretz J, Aziz M, Strohmeyer N, Sattler M, Fassler R (2023) Talin and kindlin use integrin tail allostery and direct binding to activate integrins. *Nat Struct Mol Biol* 30: 1913-1924

Aron R, Pellegrini P, Green EW, Maddison DC, Opoku-Nsiah K, Oliveira AO, Wong JS, Daub AC, Giorgini F, Muchowski P, Finkbeiner S (2018) Deubiquitinase Usp12 functions noncatalytically to induce autophagy and confer neuroprotection in models of Huntington's disease. *Nat Commun* 9: 3191

Artegiani B, van Voorthuijsen L, Lindeboom RGH, Seinstra D, Heo I, Tapia P, Lopez-Iglesias C, Postrach D, Dayton T, Oka R *et al* (2019) Probing the Tumor Suppressor Function of BAP1 in CRISPR-Engineered Human Liver Organoids. *Cell Stem Cell* 24: 927-943 e926

Arthos J, Cicala C, Nawaz F, Byrareddy SN, Villinger F, Santangelo PJ, Ansari AA, Fauci AS (2018) The Role of Integrin alpha(4)beta(7) in HIV Pathogenesis and Treatment. *Curr HIV/AIDS Rep* 15: 127-135

Asano Y, Ihn H, Yamane K, Jinnin M, Mimura Y, Tamaki K (2005) Increased expression of integrin alpha(v)beta3 contributes to the establishment of autocrine TGF-beta signaling in scleroderma fibroblasts. *J Immunol* 175: 7708-7718

Asao H, Sasaki Y, Arita T, Tanaka N, Endo K, Kasai H, Takeshita T, Endo Y, Fujita T, Sugamura K (1997) Hrs is associated with STAM, a signal-transducing adaptor molecule. Its suppressive effect on cytokine-induced cell growth. *J Biol Chem* 272: 32785-32791

Atkin G, Paulson H (2014) Ubiquitin pathways in neurodegenerative disease. *Front Mol Neurosci* 7: 63

Azmi I, Davies B, Dimaano C, Payne J, Eckert D, Babst M, Katzmann DJ (2006) Recycling of ESCRTs by the AAA-ATPase Vps4 is regulated by a conserved VSL region in Vta1. *J Cell Biol* 172: 705-717

Azmi IF, Davies BA, Xiao J, Babst M, Xu Z, Katzmann DJ (2008) ESCRT-III family members stimulate Vps4 ATPase activity directly or via Vta1. *Dev Cell* 14: 50-61

Babst M, Katzmann DJ, Estepa-Sabal EJ, Meerloo T, Emr SD (2002a) Escrt-III: an endosome-associated heterooligomeric protein complex required for mvb sorting. *Dev Cell* 3: 271-282

Babst M, Katzmann DJ, Snyder WB, Wendland B, Emr SD (2002b) Endosome-associated complex, ESCRT-II, recruits transport machinery for protein sorting at the multivesicular body. *Dev Cell* 3: 283-289

Babst M, Odorizzi G, Estepa EJ, Emr SD (2000) Mammalian tumor susceptibility gene 101 (TSG101) and the yeast homologue, Vps23p, both function in late endosomal trafficking. *Traffic* 1: 248-258

Babst M, Wendland B, Estepa EJ, Emr SD (1998) The Vps4p AAA ATPase regulates membrane association of a Vps protein complex required for normal endosome function. *EMBO J* 17: 2982-2993

Bache KG, Raiborg C, Mehlum A, Stenmark H (2003) STAM and Hrs are subunits of a multivalent ubiquitin-binding complex on early endosomes. *J Biol Chem* 278: 12513-12521

Bai C, Richman R, Elledge SJ (1994) Human cyclin F. *EMBO J* 13: 6087-6098

Bajorek M, Schubert HL, McCullough J, Langelier C, Eckert DM, Stubblefield WM, Uter NT, Myszka DG, Hill CP, Sundquist WI (2009) Structural basis for ESCRT-III protein autoinhibition. *Nat Struct Mol Biol* 16: 754-762

Baldwin LA, Hoff JT, Lefringhouse J, Zhang M, Jia C, Liu Z, Erfani S, Jin H, Xu M, She QB *et al* (2014) CD151-alpha3beta1 integrin complexes suppress ovarian tumor growth by repressing slug-mediated EMT and canonical Wnt signaling. *Oncotarget* 5: 12203-12217

Baldys A, Raymond JR (2009) Critical role of ESCRT machinery in EGFR recycling. *Biochemistry* 48: 9321-9323

Banani SF, Lee HO, Hyman AA, Rosen MK (2017) Biomolecular condensates: organizers of cellular biochemistry. *Nat Rev Mol Cell Biol* 18: 285-298

Barczyk M, Carracedo S, Gullberg D (2010) Integrins. *Cell Tissue Res* 339: 269-280

Baron W, Decker L, Colognato H, ffrench-Constant C (2003) Regulation of integrin growth factor interactions in oligodendrocytes by lipid raft microdomains. *Curr Biol* 13: 151-155

Barriere H, Nemes C, Du K, Lukacs GL (2007) Plasticity of polyubiquitin recognition as lysosomal targeting signals by the endosomal sorting machinery. *Mol Biol Cell* 18: 3952-3965

Bass MD, Williamson RC, Nunan RD, Humphries JD, Byron A, Morgan MR, Martin P, Humphries MJ (2011) A syndecan-4 hair trigger initiates wound healing through caveolin- and RhoG-regulated integrin endocytosis. *Dev Cell* 21: 681-693

Beddingfield BJ, Iwanaga N, Chapagain PP, Zheng W, Roy CJ, Hu TY, Kolls JK, Bix GJ (2021) The Integrin Binding Peptide, ATN-161, as a Novel Therapy for SARS-CoV-2 Infection. *JACC Basic Transl Sci* 6: 1-8

Benito-Jardon M, Klapproth S, Gimeno LI, Petzold T, Bharadwaj M, Muller DJ, Zuchtriegel G, Reichel CA, Costell M (2017) The fibronectin synergy site re-enforces cell adhesion and mediates a crosstalk between integrin classes. *Elife* 6

Berditchevski F, Gilbert E, Griffiths MR, Fitter S, Ashman L, Jenner SJ (2001) Analysis of the CD151-alpha3beta1 integrin and CD151-tetraspanin interactions by mutagenesis. *J Biol Chem* 276: 41165-41174

Berlin I, Schwartz H, Nash PD (2010) Regulation of epidermal growth factor receptor ubiquitination and trafficking by the USP8.STAM complex. *J Biol Chem* 285: 34909-34921

Bilodeau PS, Urbanowski JL, Winistorfer SC, Piper RC (2002) The Vps27p Hse1p complex binds ubiquitin and mediates endosomal protein sorting. *Nat Cell Biol* 4: 534-539

Bingol B, Tea JS, Phu L, Reichelt M, Bakalarski CE, Song Q, Foreman O, Kirkpatrick DS, Sheng M (2014) The mitochondrial deubiquitinase USP30 opposes parkin-mediated mitophagy. *Nature* 510: 370-375

Bissig C, Lenoir M, Velluz MC, Kufareva I, Abagyan R, Overduin M, Gruenberg J (2013) Viral infection controlled by a calcium-dependent lipid-binding module in ALIX. *Dev Cell* 25: 364-373

Bledzka K, Bialkowska K, Sossey-Alaoui K, Vaynberg J, Pluskota E, Qin J, Plow EF (2016) Kindlin-2 directly binds actin and regulates integrin outside-in signaling. *J Cell Biol* 213: 97-108

Bodescu MA, Aretz J, Grison M, Rief M, Fassler R (2023) Kindlin stabilizes the talin.integrin bond under mechanical load by generating an ideal bond. *Proc Natl Acad Sci U S A* 120: e2218116120

Boettcher RT, Stremmel C, Meves A, Meyer H, Widmaier M, Tseng HY, Fassler R (2012) Sorting nexin 17 prevents lysosomal degradation of beta1 integrins by binding to the beta1-integrin tail. *Nat Cell Biol* 14: 584-592

Boettcher RT, Veelders M, Rombaut P, Faix J, Theodosiou M, Stradal TE, Rottner K, Zent R, Herzog F, Fassler R (2017) Kindlin-2 recruits paxillin and Arp2/3 to promote membrane protrusions during initial cell spreading. *J Cell Biol* 216: 3785-3798

Bon G, Di Carlo SE, Folgiero V, Avetrani P, Lazzari C, D'Orazi G, Brizzi MF, Sacchi A, Soddu S, Blandino G *et al* (2009) Negative regulation of beta4 integrin transcription by homeodomain-interacting protein kinase 2 and p53 impairs tumor progression. *Cancer Res* 69: 5978-5986

Boname JM, Thomas M, Stagg HR, Xu P, Peng J, Lehner PJ (2010) Efficient internalization of MHC I requires lysine-11 and lysine-63 mixed linkage polyubiquitin chains. *Traffic* 11: 210-220

Boudreaux DA, Maiti TK, Davies CW, Das C (2010) Ubiquitin vinyl methyl ester binding orients the misaligned active site of the ubiquitin hydrolase UCHL1 into productive conformation. *Proc Natl Acad Sci U S A* 107: 9117-9122

Bowers K, Lottridge J, Helliwell SB, Goldthwaite LM, Luzio JP, Stevens TH (2004) Protein-protein interactions of ESCRT complexes in the yeast Saccharomyces cerevisiae. *Traffic* 5: 194-210

Braakman I, Hebert DN (2013) Protein folding in the endoplasmic reticulum. *Cold Spring Harb Perspect Biol* 5: a013201

Bremm A, Freund SM, Komander D (2010) Lys11-linked ubiquitin chains adopt compact conformations and are preferentially hydrolyzed by the deubiquitinase Cezanne. *Nat Struct Mol Biol* 17: 939-947

Bretscher MS (1989) Endocytosis and recycling of the fibronectin receptor in CHO cells. *EMBO J* 8: 1341-1348

Bretscher MS (1992) Circulating integrins: alpha 5 beta 1, alpha 6 beta 4 and Mac-1, but not alpha 3 beta 1, alpha 4 beta 1 or LFA-1. *EMBO J* 11: 405-410

Burska UL, Harle VJ, Coffey K, Darby S, Ramsey H, O'Neill D, Logan IR, Gaughan L, Robson CN (2013) Deubiquitinating enzyme Usp12 is a novel co-activator of the androgen receptor. *J Biol Chem* 288: 32641-32650

Byron A, Humphries JD, Askari JA, Craig SE, Mould AP, Humphries MJ (2009) Anti-integrin monoclonal antibodies. *J Cell Sci* 122: 4009-4011

Cagnet S, Faraldo MM, Kreft M, Sonnenberg A, Raymond K, Glukhova MA (2014) Signaling events mediated by alpha3beta1 integrin are essential for mammary tumorigenesis. *Oncogene* 33: 4286-4295

Calderwood DA, Campbell ID, Critchley DR (2013) Talins and kindlins: partners in integrin-mediated adhesion. *Nat Rev Mol Cell Biol* 14: 503-517

Calderwood DA, Fujioka Y, de Pereda JM, Garcia-Alvarez B, Nakamoto T, Margolis B, McGlade CJ, Liddington RC, Ginsberg MH (2003) Integrin beta cytoplasmic domain interactions with phosphotyrosine-binding domains: a structural prototype for diversity in integrin signaling. *Proc Natl Acad Sci U S A* 100: 2272-2277

Calderwood DA, Zent R, Grant R, Rees DJ, Hynes RO, Ginsberg MH (1999) The Talin head domain binds to integrin beta subunit cytoplasmic tails and regulates integrin activation. *J Biol Chem* 274: 28071-28074

Campbell ID, Humphries MJ (2011) Integrin structure, activation, and interactions. *Cold Spring Harb Perspect Biol* 3

Case LB, De Pasquale M, Henry L, Rosen MK (2022) Synergistic phase separation of two pathways promotes integrin clustering and nascent adhesion formation. *Elife* 11

Caswell PT, Spence HJ, Parsons M, White DP, Clark K, Cheng KW, Mills GB, Humphries MJ, Messent AJ, Anderson KI *et al* (2007) Rab25 associates with alpha5beta1 integrin to promote invasive migration in 3D microenvironments. *Dev Cell* 13: 496-510

Cavalcanti-Adam EA, Volberg T, Micoulet A, Kessler H, Geiger B, Spatz JP (2007) Cell spreading and focal adhesion dynamics are regulated by spacing of integrin ligands. *Biophys J* 92: 2964-2974

Caviston JP, Holzbaur EL (2006) Microtubule motors at the intersection of trafficking and transport. *Trends Cell Biol* 16: 530-537

Chavrier P, van der Sluijs P, Mishal Z, Nagelkerken B, Gorvel JP (1997) Early endosome membrane dynamics characterized by flow cytometry. *Cytometry* 29: 41-49

Chen C, Xue N, Liu K, He Q, Wang C, Guo Y, Tian J, Liu X, Pan Y, Chen G (2023) USP12 promotes nonsmall cell lung cancer progression through deubiquitinating and stabilizing RRM2. *Mol Carcinog* 62: 1518-1530

Chen KE, Healy MD, Collins BM (2019) Towards a molecular understanding of endosomal trafficking by Retromer and Retriever. *Traffic* 20: 465-478

Chen NP, Aretz J, Fassler R (2022a) CDK1-cyclin-B1-induced kindlin degradation drives focal adhesion disassembly at mitotic entry. *Nat Cell Biol* 24: 723-736

Chen PW, Luo R, Jian X, Randazzo PA (2014) The Arf6 GTPase-activating proteins ARAP2 and ACAP1 define distinct endosomal compartments that regulate integrin alpha5beta1 traffic. *J Biol Chem* 289: 30237-30248

Chen Y, Zhou D, Yao Y, Sun Y, Yao F, Ma L (2022b) Monoubiquitination in Homeostasis and Cancer. *Int J Mol Sci* 23

Chu JJ, Ng ML (2004) Interaction of West Nile virus with alpha v beta 3 integrin mediates virus entry into cells. *J Biol Chem* 279: 54533-54541

Chu T, Sun J, Saksena S, Emr SD (2006) New component of ESCRT-I regulates endosomal sorting complex assembly. *J Cell Biol* 175: 815-823

Ciechanover A, Kwon YT (2015) Degradation of misfolded proteins in neurodegenerative diseases: therapeutic targets and strategies. *Exp Mol Med* 47: e147

Clague MJ (2002) Membrane transport: a coat for ubiquitin. *Curr Biol* 12: R529-531

Clague MJ, Barsukov I, Coulson JM, Liu H, Rigden DJ, Urbe S (2013) Deubiquitylases from genes to organism. *Physiol Rev* 93: 1289-1315

Clague MJ, Heride C, Urbe S (2015) The demographics of the ubiquitin system. *Trends Cell Biol* 25: 417-426

Cohn MA, Kee Y, Haas W, Gygi SP, D'Andrea AD (2009) UAF1 is a subunit of multiple deubiquitinating enzyme complexes. *J Biol Chem* 284: 5343-5351

Cohn MA, Kowal P, Yang K, Haas W, Huang TT, Gygi SP, D'Andrea AD (2007) A UAF1-containing multisubunit protein complex regulates the Fanconi anemia pathway. *Mol Cell* 28: 786-797

Connell CM, Shaw BA, Holmes SB, Foster NL (2001) Caregivers' attitudes toward their family members' participation in Alzheimer disease research: implications for recruitment and retention. *Alzheimer Dis Assoc Disord* 15: 137-145

Cooper EM, Cutcliffe C, Kristiansen TZ, Pandey A, Pickart CM, Cohen RE (2009) K63-specific deubiquitination by two JAMM/MPN+ complexes: BRISC-associated Brcc36 and proteasomal Poh1. *EMBO J* 28: 621-631

Cunningham CN, Baughman JM, Phu L, Tea JS, Yu C, Coons M, Kirkpatrick DS, Bingol B, Corn JE (2015) USP30 and parkin homeostatically regulate atypical ubiquitin chains on mitochondria. *Nat Cell Biol* 17: 160-169

Curtiss M, Jones C, Babst M (2007) Efficient cargo sorting by ESCRT-I and the subsequent release of ESCRT-I from multivesicular bodies requires the subunit Mvb12. *Mol Biol Cell* 18: 636-645

Dahlberg CL, Juo P (2014) The WD40-repeat proteins WDR-20 and WDR-48 bind and activate the deubiquitinating enzyme USP-46 to promote the abundance of the glutamate receptor GLR-1 in the ventral nerve cord of Caenorhabditis elegans. *J Biol Chem* 289: 3444-3456

Das C, Hoang QQ, Kreinbring CA, Luchansky SJ, Meray RK, Ray SS, Lansbury PT, Ringe D, Petsko GA (2006) Structural basis for conformational plasticity of the Parkinson's disease-associated ubiquitin hydrolase UCH-L1. *Proc Natl Acad Sci U S A* 103: 4675-4680

Davis C, Spaller BL, Matouschek A (2021) Mechanisms of substrate recognition by the 26S proteasome. *Curr Opin Struct Biol* 67: 161-169

De Franceschi N, Hamidi H, Alanko J, Sahgal P, Ivaska J (2015) Integrin traffic - the update. *J Cell Sci* 128: 839-852

de Pereda JM, Lillo MP, Sonnenberg A (2009) Structural basis of the interaction between integrin alpha6beta4 and plectin at the hemidesmosomes. *EMBO J* 28: 1180-1190

Dedden D, Schumacher S, Kelley CF, Zacharias M, Biertumpfel C, Fassler R, Mizuno N (2019) The Architecture of Talin1 Reveals an Autoinhibition Mechanism. *Cell* 179: 120-131 e113

Dehal P, Boore JL (2005) Two rounds of whole genome duplication in the ancestral vertebrate. *PLoS Biol* 3: e314

Dell'Angelica EC (2001) Clathrin-binding proteins: got a motif? Join the network! *Trends Cell Biol* 11: 315-318

Deng L, Wang C, Spencer E, Yang L, Braun A, You J, Slaughter C, Pickart C, Chen ZJ (2000) Activation of the IkappaB kinase complex by TRAF6 requires a dimeric ubiquitin-conjugating enzyme complex and a unique polyubiquitin chain. *Cell* 103: 351-361

Deol KK, Crowe SO, Du J, Bisbee HA, Guenette RG, Strieter ER (2020) Proteasome-Bound UCH37/UCHL5 Debranches Ubiquitin Chains to Promote Degradation. *Mol Cell* 80: 796-809 e799

Derby MC, Gleeson PA (2007) New insights into membrane trafficking and protein sorting. *Int Rev Cytol* 261: 47-116

Derivery E, Sousa C, Gautier JJ, Lombard B, Loew D, Gautreau A (2009) The Arp2/3 activator WASH controls the fission of endosomes through a large multiprotein complex. *Dev Cell* 17: 712-723

Deshaies RJ, Joazeiro CA (2009) RING domain E3 ubiquitin ligases. *Annu Rev Biochem* 78: 399-434

Dewson G, Eichhorn PJA, Komander D (2023) Deubiquitinases in cancer. *Nat Rev Cancer* 23: 842-862

Dharadhar S, Clerici M, van Dijk WJ, Fish A, Sixma TK (2016) A conserved two-step binding for the UAF1 regulator to the USP12 deubiquitinating enzyme. *J Struct Biol* 196: 437-447

Diggins NL, Kang H, Weaver A, Webb DJ (2018) alpha5beta1 integrin trafficking and Rac activation are regulated by APPL1 in a Rab5-dependent manner to inhibit cell migration. *J Cell Sci* 131

Dikic I, Wakatsuki S, Walters KJ (2009) Ubiquitin-binding domains - from structures to functions. *Nat Rev Mol Cell Biol* 10: 659-671

Dimaano C, Jones CB, Hanono A, Curtiss M, Babst M (2008) Ist1 regulates Vps4 localization and assembly. *Mol Biol Cell* 19: 465-474

Doherty GJ, Ahlund MK, Howes MT, Moren B, Parton RG, McMahon HT, Lundmark R (2011) The endocytic protein GRAF1 is directed to cell-matrix adhesion sites and regulates cell spreading. *Mol Biol Cell* 22: 4380-4389

Dove KK, Klevit RE (2017) RING-Between-RING E3 Ligases: Emerging Themes amid the Variations. *J Mol Biol* 429: 3363-3375

Dozynkiewicz MA, Jamieson NB, Macpherson I, Grindlay J, van den Berghe PV, von Thun A, Morton JP, Gourley C, Timpson P, Nixon C *et al* (2012) Rab25 and CLIC3 collaborate to promote integrin recycling from late endosomes/lysosomes and drive cancer progression. *Dev Cell* 22: 131-145

Du J, Babik S, Li Y, Deol KK, Eyles SJ, Fejzo J, Tonelli M, Strieter E (2022) A cryptic K48 ubiquitin chain binding site on UCH37 is required for its role in proteasomal degradation. *Elife* 11

Dukes JD, Fish L, Richardson JD, Blaikley E, Burns S, Caunt CJ, Chalmers AD, Whitley P (2011) Functional ESCRT machinery is required for constitutive recycling of claudin-1 and maintenance of polarity in vertebrate epithelial cells. *Mol Biol Cell* 22: 3192-3205

Duncan LM, Piper S, Dodd RB, Saville MK, Sanderson CM, Luzio JP, Lehner PJ (2006) Lysine-63-linked ubiquitination is required for endolysosomal degradation of class I molecules. *EMBO J* 25: 1635-1645

Dunphy JL, Moravec R, Ly K, Lasell TK, Melancon P, Casanova JE (2006) The Arf6 GEF GEP100/BRAG2 regulates cell adhesion by controlling endocytosis of beta1 integrins. *Curr Biol* 16: 315-320

Edelmann MJ, Iphofer A, Akutsu M, Altun M, di Gleria K, Kramer HB, Fiebiger E, Dhe-Paganon S, Kessler BM (2009) Structural basis and specificity of human otubain 1-mediated deubiquitination. *Biochem J* 418: 379-390

Eletr ZM, Wilkinson KD (2014) Regulation of proteolysis by human deubiquitinating enzymes. *Biochim Biophys Acta* 1843: 114-128

Enesa K, Ito K, Luong le A, Thorbjornsen I, Phua C, To Y, Dean J, Haskard DO, Boyle J, Adcock I, Evans PC (2008) Hydrogen peroxide prolongs nuclear localization of NF-kappaB in activated cells by suppressing negative regulatory mechanisms. *J Biol Chem* 283: 18582-18590

Engler AJ, Sen S, Sweeney HL, Discher DE (2006) Matrix elasticity directs stem cell lineage specification. *Cell* 126: 677-689

Enns C (2001) Overview of protein trafficking in the secretory and endocytic pathways. *Curr Protoc Cell Biol* Chapter 15: Unit 15 11

Eskova A, Knapp B, Matelska D, Reusing S, Arjonen A, Lisauskas T, Pepperkok R, Russell R, Eils R, Ivaska J *et al* (2014) An RNAi screen identifies KIF15 as a novel regulator of the endocytic trafficking of integrin. *J Cell Sci* 127: 2433-2447

Eva R, Dassie E, Caswell PT, Dick G, ffrench-Constant C, Norman JC, Fawcett JW (2010) Rab11 and its effector Rab coupling protein contribute to the trafficking of beta 1 integrins during axon growth in adult dorsal root ganglion neurons and PC12 cells. *J Neurosci* 30: 11654-11669

Ezratty EJ, Bertaux C, Marcantonio EE, Gundersen GG (2009) Clathrin mediates integrin endocytosis for focal adhesion disassembly in migrating cells. *J Cell Biol* 187: 733-747

Faesen AC, Luna-Vargas MP, Geurink PP, Clerici M, Merkx R, van Dijk WJ, Hameed DS, El Oualid F, Ovaa H, Sixma TK (2011) The differential modulation of USP activity by internal regulatory domains, interactors and eight ubiquitin chain types. *Chem Biol* 18: 1550-1561

Fang S, Jensen JP, Ludwig RL, Vousden KH, Weissman AM (2000) Mdm2 is a RING finger-dependent ubiquitin protein ligase for itself and p53. *J Biol Chem* 275: 8945-8951

Farage E, Caswell PT (2021) Quantitative Analysis of Integrin Trafficking. *Methods Mol Biol* 2217: 251-263

Feldman RM, Correll CC, Kaplan KB, Deshaies RJ (1997) A complex of Cdc4p, Skp1p, and Cdc53p/cullin catalyzes ubiquitination of the phosphorylated CDK inhibitor Sic1p. *Cell* 91: 221-230

Flick K, Raasi S, Zhang H, Yen JL, Kaiser P (2006) A ubiquitin-interacting motif protects polyubiquitinated Met4 from degradation by the 26S proteasome. *Nat Cell Biol* 8: 509-515

Freemont PS, Hanson IM, Trowsdale J (1991) A novel cysteine-rich sequence motif. *Cell* 64: 483-484

Fujimitsu K, Grimaldi M, Yamano H (2016) Cyclin-dependent kinase 1-dependent activation of APC/C ubiquitin ligase. *Science* 352: 1121-1124

Gangula NR, Maddika S (2013) WD repeat protein WDR48 in complex with deubiquitinase USP12 suppresses Akt-dependent cell survival signaling by stabilizing PH domain leucine-rich repeat protein phosphatase 1 (PHLPP1). *J Biol Chem* 288: 34545-34554

Gao C, Zhuang X, Shen J, Jiang L (2017) Plant ESCRT Complexes: Moving Beyond Endosomal Sorting. *Trends Plant Sci* 22: 986-998

Garcia-Higuera I, Taniguchi T, Ganesan S, Meyn MS, Timmers C, Hejna J, Grompe M, D'Andrea AD (2001) Interaction of the Fanconi anemia proteins and BRCA1 in a common pathway. *Mol Cell* 7: 249-262

Garcia-Santisteban I, Zorroza K, Rodriguez JA (2012) Two nuclear localization signals in USP1 mediate nuclear import of the USP1/UAF1 complex. *PLoS One* 7: e38570

Garg A, Hazra JP, Sannigrahi MK, Rakshit S, Sinha S (2020) Variable Mutations at the p53-R273 Oncogenic Hotspot Position Leads to Altered Properties. *Biophys J* 118: 720-728

Gatti M, Pinato S, Maiolica A, Rocchio F, Prato MG, Aebersold R, Penengo L (2015) RNF168 promotes noncanonical K27 ubiquitination to signal DNA damage. *Cell Rep* 10: 226-238

Ge F, Li Y, Yuan T, Wu Y, He Q, Yang B, Zhu H (2022) Deubiquitinating enzymes: Promising targets for drug resistance. *Drug Discov Today* 27: 2603-2613
Gill DJ, Teo H, Sun J, Perisic O, Veprintsev DB, Emr SD, Williams RL (2007) Structural insight into the ESCRT-I/-II link and its role in MVB trafficking. *EMBO J* 26: 600-612
Ginsberg MH (2014) Integrin activation. *BMB Rep* 47: 655-659
Gireud-Goss M, Reyes S, Tewari R, Patrizz A, Howe MD, Kofler J, Waxham MN, McCullough LD, Bean AJ (2020) The ubiquitin ligase UBE4B regulates amyloid precursor protein ubiquitination, endosomal trafficking, and amyloid beta42 generation and secretion. *Mol Cell Neurosci* 108: 103542
Glotzer M, Murray AW, Kirschner MW (1991) Cyclin is degraded by the ubiquitin pathway. *Nature* 349: 132-138
Goksoy E, Ma YQ, Wang X, Kong X, Perera D, Plow EF, Qin J (2008) Structural basis for the autoinhibition of talin in regulating integrin activation. *Mol Cell* 31: 124-133
Goldstein G, Scheid M, Hammerling U, Schlesinger DH, Niall HD, Boyse EA (1975) Isolation of a polypeptide that has lymphocyte-differentiating properties and is probably represented universally in living cells. *Proc Natl Acad Sci U S A* 72: 11-15
Gomez TS, Billadeau DD (2009) A FAM21-containing WASH complex regulates retromer-dependent sorting. *Dev Cell* 17: 699-711
Goult BT, Yan J, Schwartz MA (2018) Talin as a mechanosensitive signaling hub. *J Cell Biol* 217: 3776-3784
Govaere O, Petz M, Wouters J, Vandewynckel YP, Scott EJ, Topal B, Nevens F, Verslype C, Anstee QM, Van Vlierberghe H *et al* (2017) The PDGFRalpha-laminin B1-keratin 19 cascade drives tumor progression at the invasive front of human hepatocellular carcinoma. *Oncogene* 36: 6605-6616
Gu Z, Noss EH, Hsu VW, Brenner MB (2011) Integrins traffic rapidly via circular dorsal ruffles and macropinocytosis during stimulated cell migration. *J Cell Biol* 193: 61-70
Gui D, Peng W, Jiang W, Huang G, Liu G, Ye Z, Wang Y, Xu Z, Fu J, Luo S, Zhao Y (2019) Ubiquitin-specific peptidase 46 (USP46) suppresses renal cell carcinoma tumorigenesis through AKT pathway inactivation. *Biochem Biophys Res Commun* 519: 689-696
Hansen S, Hupp TR, Lane DP (1996) Allosteric regulation of the thermostability and DNA binding activity of human p53 by specific interacting proteins. CRC Cell Transformation Group. *J Biol Chem* 271: 3917-3924
Harper JW, Schulman BA (2021) Cullin-RING Ubiquitin Ligase Regulatory Circuits: A Quarter Century Beyond the F-Box Hypothesis. *Annu Rev Biochem* 90: 403-429
Hassink GC, Zhao B, Sompallae R, Altun M, Gastaldello S, Zinin NV, Masucci MG, Lindsten K (2009) The ER-resident ubiquitin-specific protease 19 participates in the UPR and rescues ERAD substrates. *EMBO Rep* 10: 755-761
Hatakeyama S, Yada M, Matsumoto M, Ishida N, Nakayama KI (2001) U box proteins as a new family of ubiquitin-protein ligases. *J Biol Chem* 276: 33111-33120
Henne WM, Buchkovich NJ, Emr SD (2011) The ESCRT pathway. *Dev Cell* 21: 77-91
Hibbert RG, Huang A, Boelens R, Sixma TK (2011) E3 ligase Rad18 promotes monoubiquitination rather than ubiquitin chain formation by E2 enzyme Rad6. *Proc Natl Acad Sci U S A* 108: 5590-5595
Hicke L, Dunn R (2003) Regulation of membrane protein transport by ubiquitin and ubiquitin-binding proteins. *Annu Rev Cell Dev Biol* 19: 141-172
Hierro A, Sun J, Rusnak AS, Kim J, Prag G, Emr SD, Hurley JH (2004) Structure of the ESCRT-II endosomal trafficking complex. *Nature* 431: 221-225
Hodul M, Dahlberg CL, Juo P (2017) Function of the Deubiquitinating Enzyme USP46 in the Nervous System and Its Regulation by WD40-Repeat Proteins. *Front Synaptic Neurosci* 9: 16
Hodul M, Ganji R, Dahlberg CL, Raman M, Juo P (2020) The WD40-repeat protein WDR-48 promotes the stability of the deubiquitinating enzyme USP-46 by inhibiting its ubiquitination and degradation. *J Biol Chem* 295: 11776-11788
Hoege C, Pfander B, Moldovan GL, Pyrowolakis G, Jentsch S (2002) RAD6-dependent DNA repair is linked to modification of PCNA by ubiquitin and SUMO. *Nature* 419: 135-141

Horwitz A, Duggan K, Buck C, Beckerle MC, Burridge K (1986) Interaction of plasma membrane fibronectin receptor with talin--a transmembrane linkage. *Nature* 320: 531-533
Hsu CP, Aretz J, Hordeichyk A, Fassler R, Bausch AR (2023) Surface-induced phase separation of reconstituted nascent integrin clusters on lipid membranes. *Proc Natl Acad Sci U S A* 120: e2301881120
Hu H, Dong C, Sun D, Hu Y, Xie J (2018) Genome-Wide Identification and Analysis of U-Box E3 Ubiquitin(-)Protein Ligase Gene Family in Banana. *Int J Mol Sci* 19
Hu M, Li P, Li M, Li W, Yao T, Wu JW, Gu W, Cohen RE, Shi Y (2002) Crystal structure of a UBP-family deubiquitinating enzyme in isolation and in complex with ubiquitin aldehyde. *Cell* 111: 1041-1054
Hu M, Li P, Song L, Jeffrey PD, Chenova TA, Wilkinson KD, Cohen RE, Shi Y (2005) Structure and mechanisms of the proteasome-associated deubiquitinating enzyme USP14. *EMBO J* 24: 3747-3756
Huang F, Goh LK, Sorkin A (2007) EGF receptor ubiquitination is not necessary for its internalization. *Proc Natl Acad Sci U S A* 104: 16904-16909
Huang TT, Nijman SM, Mirchandani KD, Galardy PJ, Cohn MA, Haas W, Gygi SP, Ploegh HL, Bernards R, D'Andrea AD (2006) Regulation of monoubiquitinated PCNA by DUB autocleavage. *Nat Cell Biol* 8: 339-347
Huang X, Dixit VM (2016) Drugging the undruggables: exploring the ubiquitin system for drug development. *Cell Res* 26: 484-498
Huibregtse JM, Scheffner M, Beaudenon S, Howley PM (1995) A family of proteins structurally and functionally related to the E6-AP ubiquitin-protein ligase. *Proc Natl Acad Sci U S A* 92: 2563-2567
Hunt SD, Stephens DJ (2011) The role of motor proteins in endosomal sorting. *Biochem Soc Trans* 39: 1179-1184
Huo Y, Khatri N, Hou Q, Gilbert J, Wang G, Man HY (2015) The deubiquitinating enzyme USP46 regulates AMPA receptor ubiquitination and trafficking. *J Neurochem* 134: 1067-1080
Husnjak K, Elsasser S, Zhang N, Chen X, Randles L, Shi Y, Hofmann K, Walters KJ, Finley D, Dikic I (2008) Proteasome subunit Rpn13 is a novel ubiquitin receptor. *Nature* 453: 481-488
Hwang CS, Shemorry A, Auerbach D, Varshavsky A (2010a) The N-end rule pathway is mediated by a complex of the RING-type Ubr1 and HECT-type Ufd4 ubiquitin ligases. *Nat Cell Biol* 12: 1177-1185
Hwang CS, Shemorry A, Varshavsky A (2010b) N-terminal acetylation of cellular proteins creates specific degradation signals. *Science* 327: 973-977
Hyman AA, Weber CA, Julicher F (2014) Liquid-liquid phase separation in biology. *Annu Rev Cell Dev Biol* 30: 39-58
Hynes RO (2002) Integrins: bidirectional, allosteric signaling machines. *Cell* 110: 673-687
Hynes RO (2004) The emergence of integrins: a personal and historical perspective. *Matrix Biol* 23: 333-340
Hynes RO, Zhao Q (2000) The evolution of cell adhesion. *J Cell Biol* 150: F89-96
Ikeda K, Inoue S (2012) TRIM proteins as RING finger E3 ubiquitin ligases. *Adv Exp Med Biol* 770: 27-37
Im YJ, Wollert T, Boura E, Hurley JH (2009) Structure and function of the ESCRT-II-III interface in multivesicular body biogenesis. *Dev Cell* 17: 234-243
Imai S, Kano M, Nonoyama K, Ebihara S (2013) Behavioral characteristics of ubiquitin-specific peptidase 46-deficient mice. *PLoS One* 8: e58566
Imai S, Mamiya T, Tsukada A, Sakai Y, Mouri A, Nabeshima T, Ebihara S (2012) Ubiquitin-specific peptidase 46 (Usp46) regulates mouse immobile behavior in the tail suspension test through the GABAergic system. *PLoS One* 7: e39084
Iwamoto DV, Calderwood DA (2015) Regulation of integrin-mediated adhesions. *Curr Opin Cell Biol* 36: 41-47
Jacobson AD, Zhang NY, Xu P, Han KJ, Noone S, Peng J, Liu CW (2009) The lysine 48 and lysine 63 ubiquitin conjugates are processed differently by the 26 s proteasome. *J Biol Chem* 284: 35485-35494
Jahan AS, Lestra M, Swee LK, Fan Y, Lamers MM, Tafesse FG, Theile CS, Spooner E, Bruzzone R, Ploegh HL, Sanyal S (2016) Usp12 stabilizes the T-cell receptor complex at the cell surface during signaling. *Proc Natl Acad Sci U S A* 113: E705-714

Jiang Y, Zhang H, Wang J, Liu Y, Luo T, Hua H (2022) Targeting extracellular matrix stiffness and mechanotransducers to improve cancer therapy. *J Hematol Oncol* 15: 34

Jin J, Ang XL, Shirogane T, Wade Harper J (2005) Identification of substrates for F-box proteins. *Methods Enzymol* 399: 287-309

Jin L, Williamson A, Banerjee S, Philipp I, Rape M (2008) Mechanism of ubiquitin-chain formation by the human anaphase-promoting complex. *Cell* 133: 653-665

Johnson MS, Lu N, Denessiouk K, Heino J, Gullberg D (2009) Integrins during evolution: evolutionary trees and model organisms. *Biochim Biophys Acta* 1788: 779-789

Johnston SC, Larsen CN, Cook WJ, Wilkinson KD, Hill CP (1997) Crystal structure of a deubiquitinating enzyme (human UCH-L3) at 1.8 A resolution. *EMBO J* 16: 3787-3796

Johnston SC, Riddle SM, Cohen RE, Hill CP (1999) Structural basis for the specificity of ubiquitin C-terminal hydrolases. *EMBO J* 18: 3877-3887

Jones MC, Caswell PT, Moran-Jones K, Roberts M, Barry ST, Gampel A, Mellor H, Norman JC (2009) VEGFR1 (Flt1) regulates Rab4 recycling to control fibronectin polymerization and endothelial vessel branching. *Traffic* 10: 754-766

Jones MC, Caswell PT, Norman JC (2006) Endocytic recycling pathways: emerging regulators of cell migration. *Curr Opin Cell Biol* 18: 549-557

Jonker CTH, Galmes R, Veenendaal T, Ten Brink C, van der Welle REN, Liv N, de Rooij J, Peden AA, van der Sluijs P, Margadant C, Klumperman J (2018) Vps3 and Vps8 control integrin trafficking from early to recycling endosomes and regulate integrin-dependent functions. *Nat Commun* 9: 792

Joo HY, Jones A, Yang C, Zhai L, Smith ADt, Zhang Z, Chandrasekharan MB, Sun ZW, Renfrow MB, Wang Y *et al* (2011) Regulation of histone H2A and H2B deubiquitination and Xenopus development by USP12 and USP46. *J Biol Chem* 286: 7190-7201

Kabra R, Knight KK, Zhou R, Snyder PM (2008) Nedd4-2 induces endocytosis and degradation of proteolytically cleaved epithelial Na+ channels. *J Biol Chem* 283: 6033-6039

Kadry YA, Calderwood DA (2020) Chapter 22: Structural and signaling functions of integrins. *Biochim Biophys Acta Biomembr* 1862: 183206

Kaksonen M, Roux A (2018) Mechanisms of clathrin-mediated endocytosis. *Nat Rev Mol Cell Biol* 19: 313-326

Katzmann DJ, Babst M, Emr SD (2001) Ubiquitin-dependent sorting into the multivesicular body pathway requires the function of a conserved endosomal protein sorting complex, ESCRT-I. *Cell* 106: 145-155

Katzmann DJ, Odorizzi G, Emr SD (2002) Receptor downregulation and multivesicular-body sorting. *Nat Rev Mol Cell Biol* 3: 893-905

Katzmann DJ, Stefan CJ, Babst M, Emr SD (2003) Vps27 recruits ESCRT machinery to endosomes during MVB sorting. *J Cell Biol* 162: 413-423

Kawaguchi Y, Okamoto T, Taniwaki M, Aizawa M, Inoue M, Katayama S, Kawakami H, Nakamura S, Nishimura M, Akiguchi I, et al. (1994) CAG expansions in a novel gene for Machado-Joseph disease at chromosome 14q32.1. *Nat Genet* 8: 221-228

Ke L, Jia Z, Gao W, Luo L (2023) Ubiquitin specific protease 46 potentiates triple negative breast cancer development by stabilizing PGAM1-mediated glycolysis. *Cell Biol Int* 47: 41-51

Kee Y, Yang K, Cohn MA, Haas W, Gygi SP, D'Andrea AD (2010) WDR20 regulates activity of the USP12 x UAF1 deubiquitinating enzyme complex. *J Biol Chem* 285: 11252-11257

Keiler KC, Waller PR, Sauer RT (1996) Role of a peptide tagging system in degradation of proteins synthesized from damaged messenger RNA. *Science* 271: 990-993

Kennedy JE, Marchese A (2015) Regulation of GPCR Trafficking by Ubiquitin. *Prog Mol Biol Transl Sci* 132: 15-38

Keusekotten K, Elliott PR, Glockner L, Fiil BK, Damgaard RB, Kulathu Y, Wauer T, Hospenthal MK, Gyrd-Hansen M, Krappmann D *et al* (2013) OTULIN antagonizes LUBAC signaling by specifically hydrolyzing Met1-linked polyubiquitin. *Cell* 153: 1312-1326

Kharitidi D, Apaja PM, Manteghi S, Suzuki K, Malitskaya E, Roldan A, Gingras MC, Takagi J, Lukacs GL, Pause A (2015) Interplay of Endosomal pH and Ligand Occupancy in Integrin alpha5beta1 Ubiquitination, Endocytic Sorting, and Cell Migration. *Cell Rep* 13: 599-609

Kim C, Ye F, Ginsberg MH (2011) Regulation of integrin activation. *Annu Rev Cell Dev Biol* 27: 321-345

Kim HT, Kim KP, Lledias F, Kisselev AF, Scaglione KM, Skowyra D, Gygi SP, Goldberg AL (2007) Certain pairs of ubiquitin-conjugating enzymes (E2s) and ubiquitin-protein ligases (E3s) synthesize nondegradable forked ubiquitin chains containing all possible isopeptide linkages. *J Biol Chem* 282: 17375-17386

Kim RQ, Sixma TK (2017) Regulation of USP7: A High Incidence of E3 Complexes. *J Mol Biol* 429: 3395-3408

Kiontke S, Langemeyer L, Kuhlee A, Schuback S, Raunser S, Ungermann C, Kummel D (2017) Architecture and mechanism of the late endosomal Rab7-like Ypt7 guanine nucleotide exchange factor complex Mon1-Ccz1. *Nat Commun* 8: 14034

Kiran S, Dar A, Singh SK, Lee KY, Dutta A (2018) The Deubiquitinase USP46 Is Essential for Proliferation and Tumor Growth of HPV-Transformed Cancers. *Mol Cell* 72: 823-835 e825

Kliche J, Kuss H, Ali M, Ivarsson Y (2021) Cytoplasmic short linear motifs in ACE2 and integrin beta(3) link SARS-CoV-2 host cell receptors to mediators of endocytosis and autophagy. *Sci Signal* 14

Komander D (2010) Mechanism, specificity and structure of the deubiquitinases. *Subcell Biochem* 54: 69-87

Komander D, Barford D (2008) Structure of the A20 OTU domain and mechanistic insights into deubiquitination. *Biochem J* 409: 77-85

Komander D, Clague MJ, Urbe S (2009a) Breaking the chains: structure and function of the deubiquitinases. *Nat Rev Mol Cell Biol* 10: 550-563

Komander D, Lord CJ, Scheel H, Swift S, Hofmann K, Ashworth A, Barford D (2008) The structure of the CYLD USP domain explains its specificity for Lys63-linked polyubiquitin and reveals a B box module. *Mol Cell* 29: 451-464

Komander D, Rape M (2012) The ubiquitin code. *Annu Rev Biochem* 81: 203-229

Komander D, Reyes-Turcu F, Licchesi JD, Odenwaelder P, Wilkinson KD, Barford D (2009b) Molecular discrimination of structurally equivalent Lys 63-linked and linear polyubiquitin chains. *EMBO Rep* 10: 466-473

Kong F, Garcia AJ, Mould AP, Humphries MJ, Zhu C (2009) Demonstration of catch bonds between an integrin and its ligand. *J Cell Biol* 185: 1275-1284

Kostelansky MS, Schluter C, Tam YY, Lee S, Ghirlando R, Beach B, Conibear E, Hurley JH (2007) Molecular architecture and functional model of the complete yeast ESCRT-I heterotetramer. *Cell* 129: 485-498

Kostelansky MS, Sun J, Lee S, Kim J, Ghirlando R, Hierro A, Emr SD, Hurley JH (2006) Structural and functional organization of the ESCRT-I trafficking complex. *Cell* 125: 113-126

Kowalski JR, Dahlberg CL, Juo P (2011) The deubiquitinating enzyme USP-46 negatively regulates the degradation of glutamate receptors to control their abundance in the ventral nerve cord of Caenorhabditis elegans. *J Neurosci* 31: 1341-1354

Koyano F, Okatsu K, Kosako H, Tamura Y, Go E, Kimura M, Kimura Y, Tsuchiya H, Yoshihara H, Hirokawa T *et al* (2014) Ubiquitin is phosphorylated by PINK1 to activate parkin. *Nature* 510: 162-166

Kreidberg JA, Symons JM (2000) Integrins in kidney development, function, and disease. *Am J Physiol Renal Physiol* 279: F233-242

Krenn PW, Koschmieder S, Fassler R (2020) Kindlin-3 loss curbs chronic myeloid leukemia in mice by mobilizing leukemic stem cells from protective bone marrow niches. *Proc Natl Acad Sci U S A* 117: 24326-24335

Kriegenburg F, Ellgaard L, Hartmann-Petersen R (2012) Molecular chaperones in targeting misfolded proteins for ubiquitin-dependent degradation. *FEBS J* 279: 532-542

Kuchitsu Y, Mukai K, Uematsu R, Takaada Y, Shinojima A, Shindo R, Shoji T, Hamano S, Ogawa E, Sato R *et al* (2023) STING signalling is terminated through ESCRT-dependent microautophagy of vesicles originating from recycling endosomes. *Nat Cell Biol* 25: 453-466

Kummel D, Herrmann E, Langemeyer L, Ungermann C (2023) Molecular insights into endolysosomal microcompartment formation and maintenance. *Biol Chem* 404: 441-454

Kwasna D, Abdul Rehman SA, Natarajan J, Matthews S, Madden R, De Cesare V, Weidlich S, Virdee S, Ahel I, Gibbs-Seymour I, Kulathu Y (2018) Discovery and Characterization of ZUFSP/ZUP1, a Distinct Deubiquitinase Class Important for Genome Stability. *Mol Cell* 70: 150-164 e156

Lafontaine DLJ, Riback JA, Bascetin R, Brangwynne CP (2021) The nucleolus as a multiphase liquid condensate. *Nat Rev Mol Cell Biol* 22: 165-182

Lakshminarayan R, Wunder C, Becken U, Howes MT, Benzing C, Arumugam S, Sales S, Ariotti N, Chambon V, Lamaze C *et al* (2014) Galectin-3 drives glycosphingolipid-dependent biogenesis of clathrin-independent carriers. *Nat Cell Biol* 16: 595-606

Lamothe B, Besse A, Campos AD, Webster WK, Wu H, Darnay BG (2007) Site-specific Lys-63-linked tumor necrosis factor receptor-associated factor 6 auto-ubiquitination is a critical determinant of I kappa B kinase activation. *J Biol Chem* 282: 4102-4112

Lange OF, Lakomek NA, Fares C, Schroder GF, Walter KF, Becker S, Meiler J, Grubmuller H, Griesinger C, de Groot BL (2008) Recognition dynamics up to microseconds revealed from an RDC-derived ubiquitin ensemble in solution. *Science* 320: 1471-1475

Langelier C, von Schwedler UK, Fisher RD, De Domenico I, White PL, Hill CP, Kaplan J, Ward D, Sundquist WI (2006) Human ESCRT-II complex and its role in human immunodeficiency virus type 1 release. *J Virol* 80: 9465-9480

Lee BL, Singh A, Mark Glover JN, Hendzel MJ, Spyracopoulos L (2017) Molecular Basis for K63-Linked Ubiquitination Processes in Double-Strand DNA Break Repair: A Focus on Kinetics and Dynamics. *J Mol Biol* 429: 3409-3429

Lee JG, Ahn JH, Jin Kim T, Ho Lee J, Choi JH (2015) Mutant p53 promotes ovarian cancer cell adhesion to mesothelial cells via integrin beta4 and Akt signals. *Sci Rep* 5: 12642

Legate KR, Wickstrom SA, Fassler R (2009) Genetic and cell biological analysis of integrin outside-in signaling. *Genes Dev* 23: 397-418

Lehner CF, O'Farrell PH (1990) The roles of Drosophila cyclins A and B in mitotic control. *Cell* 61: 535-547

Lehoux M, Gagnon D, Archambault J (2014) E1-mediated recruitment of a UAF1-USP deubiquitinase complex facilitates human papillomavirus DNA replication. *J Virol* 88: 8545-8555

Li H, Lim KS, Kim H, Hinds TR, Jo U, Mao H, Weller CE, Sun J, Chatterjee C, D'Andrea AD, Zheng N (2016) Allosteric Activation of Ubiquitin-Specific Proteases by beta-Propeller Proteins UAF1 and WDR20. *Mol Cell* 63: 249-260

Li H, Roy M, Liang L, Cao W, Hu B, Li Y, Xiao X, Wang H, Ye M, Sun S *et al* (2022) Deubiquitylase USP12 induces pro-survival autophagy and bortezomib resistance in multiple myeloma by stabilizing HMGB1. *Oncogene* 41: 1298-1308

Li H, Wang Y, Rong SK, Li L, Chen T, Fan YY, Wang YF, Yang CR, Yang C, Cho WC, Yang J (2020) Integrin alpha1 promotes tumorigenicity and progressive capacity of colorectal cancer. *Int J Biol Sci* 16: 815-826

Li J, Jo MH, Yan J, Hall T, Lee J, Lopez-Sanchez U, Yan S, Ha T, Springer TA (2024) Ligand binding initiates single-molecule integrin conformational activation. *Cell* 187: 2990-3005 e2917

Li J, Springer TA (2017) Integrin extension enables ultrasensitive regulation by cytoskeletal force. *Proc Natl Acad Sci U S A* 114: 4685-4690

Li M, Zhang P (2009) The function of APC/CCdh1 in cell cycle and beyond. *Cell Div* 4: 2

Li W, Ye Y (2008) Polyubiquitin chains: functions, structures, and mechanisms. *Cell Mol Life Sci* 65: 2397-2406

Li X, Stevens PD, Yang H, Gulhati P, Wang W, Evers BM, Gao T (2013) The deubiquitination enzyme USP46 functions as a tumor suppressor by controlling PHLPP-dependent attenuation of Akt signaling in colon cancer. *Oncogene* 32: 471-478
Li Y, Reverter D (2021) Molecular Mechanisms of DUBs Regulation in Signaling and Disease. *Int J Mol Sci* 22
Liang P, Wu Y, Zheng S, Zhang J, Yang S, Wang J, Ma S, Zhang M, Gu Z, Liu Q *et al* (2024) Paxillin phase separation promotes focal adhesion assembly and integrin signaling. *J Cell Biol* 223
Lin C, Zhang Y, Zhang K, Zheng Y, Lu L, Chang H, Yang H, Yang Y, Wan Y, Wang S *et al* (2019) Fever Promotes T Lymphocyte Trafficking via a Thermal Sensory Pathway Involving Heat Shock Protein 90 and alpha4 Integrins. *Immunity* 50: 137-151 e136
Lin SC, Chung JY, Lamothe B, Rajashankar K, Lu M, Lo YC, Lam AY, Darnay BG, Wu H (2008) Molecular basis for the unique deubiquitinating activity of the NF-kappaB inhibitor A20. *J Mol Biol* 376: 526-540
Lindas AC, Karlsson EA, Lindgren MT, Ettema TJ, Bernander R (2008) A unique cell division machinery in the Archaea. *Proc Natl Acad Sci U S A* 105: 18942-18946
Liu CY, Zha ZY, Zhou X, Zhang H, Huang W, Zhao D, Li T, Chan SW, Lim CJ, Hong W *et al* (2010) The hippo tumor pathway promotes TAZ degradation by phosphorylating a phosphodegron and recruiting the SCFbeta-TrCP E3 ligase. *J Biol Chem* 285: 37159-37169
Liu J, Wang Y, Goh WI, Goh H, Baird MA, Ruehland S, Teo S, Bate N, Critchley DR, Davidson MW, Kanchanawong P (2015) Talin determines the nanoscale architecture of focal adhesions. *Proc Natl Acad Sci U S A* 112: E4864-4873
Liu L, He B, Liu WM, Zhou D, Cox JV, Zhang XA (2007) Tetraspanin CD151 promotes cell migration by regulating integrin trafficking. *J Biol Chem* 282: 31631-31642
Liu P, Gan W, Su S, Hauenstein AV, Fu TM, Brasher B, Schwerdtfeger C, Liang AC, Xu M, Wei W (2018) K63-linked polyubiquitin chains bind to DNA to facilitate DNA damage repair. *Sci Signal* 11
Liu S, Thomas SM, Woodside DG, Rose DM, Kiosses WB, Pfaff M, Ginsberg MH (1999) Binding of paxillin to alpha4 integrins modifies integrin-dependent biological responses. *Nature* 402: 676-681
Lobert VH, Brech A, Pedersen NM, Wesche J, Oppelt A, Malerod L, Stenmark H (2010) Ubiquitination of alpha 5 beta 1 integrin controls fibroblast migration through lysosomal degradation of fibronectin-integrin complexes. *Dev Cell* 19: 148-159
Lopata A, Kniss A, Lohr F, Rogov VV, Dotsch V (2020) Ubiquitination in the ERAD Process. *Int J Mol Sci* 21
Lu Q, Hope LW, Brasch M, Reinhard C, Cohen SN (2003) TSG101 interaction with HRS mediates endosomal trafficking and receptor down-regulation. *Proc Natl Acad Sci U S A* 100: 7626-7631
Lu Y, Adegoke OA, Nepveu A, Nakayama KI, Bedard N, Cheng D, Peng J, Wing SS (2009) USP19 deubiquitinating enzyme supports cell proliferation by stabilizing KPC1, a ubiquitin ligase for p27Kip1. *Mol Cell Biol* 29: 547-558
Lucas M, Gershlick DC, Vidaurrazaga A, Rojas AL, Bonifacino JS, Hierro A (2016) Structural Mechanism for Cargo Recognition by the Retromer Complex. *Cell* 167: 1623-1635 e1614
Luo BH, Carman CV, Springer TA (2007) Structural basis of integrin regulation and signaling. *Annu Rev Immunol* 25: 619-647
Luo BH, Springer TA (2006) Integrin structures and conformational signaling. *Curr Opin Cell Biol* 18: 579-586
Ma H, Wang J, Zhao X, Wu T, Huang Z, Chen D, Liu Y, Ouyang G (2020) Periostin Promotes Colorectal Tumorigenesis through Integrin-FAK-Src Pathway-Mediated YAP/TAZ Activation. *Cell Rep* 30: 793-806 e796
Ma YQ, Qin J, Wu C, Plow EF (2008) Kindlin-2 (Mig-2): a co-activator of beta3 integrins. *J Cell Biol* 181: 439-446
Machida YJ, Machida Y, Chen Y, Gurtan AM, Kupfer GM, D'Andrea AD, Dutta A (2006) UBE2T is the E2 in the Fanconi anemia pathway and undergoes negative autoregulation. *Mol Cell* 23: 589-596

Maiti TK, Permaul M, Boudreaux DA, Mahanic C, Mauney S, Das C (2011) Crystal structure of the catalytic domain of UCHL5, a proteasome-associated human deubiquitinating enzyme, reveals an unproductive form of the enzyme. *FEBS J* 278: 4917-4926

Manso JA, Gomez-Hernandez M, Carabias A, Alonso-Garcia N, Garcia-Rubio I, Kreft M, Sonnenberg A, de Pereda JM (2019) Integrin alpha6beta4 Recognition of a Linear Motif of Bullous Pemphigoid Antigen BP230 Controls Its Recruitment to Hemidesmosomes. *Structure* 27: 952-964 e956

Mao Y, Nickitenko A, Duan X, Lloyd TE, Wu MN, Bellen H, Quiocho FA (2000) Crystal structure of the VHS and FYVE tandem domains of Hrs, a protein involved in membrane trafficking and signal transduction. *Cell* 100: 447-456

Marchese A, Trejo J (2013) Ubiquitin-dependent regulation of G protein-coupled receptor trafficking and signaling. *Cell Signal* 25: 707-716

Martin TD, Mitin N, Cox AD, Yeh JJ, Der CJ (2012) Phosphorylation by protein kinase Calpha regulates RalB small GTPase protein activation, subcellular localization, and effector utilization. *J Biol Chem* 287: 14827-14836

Masoomian B, Shields JA, Shields CL (2018) Overview of BAP1 cancer predisposition syndrome and the relationship to uveal melanoma. *J Curr Ophthalmol* 30: 102-109

Mathieu J, Michel-Hissier P, Boucherit V, Huynh JR (2022) The deubiquitinase USP8 targets ESCRT-III to promote incomplete cell division. *Science* 376: 818-823

Matsuo H, Chevallier J, Mayran N, Le Blanc I, Ferguson C, Faure J, Blanc NS, Matile S, Dubochet J, Sadoul R *et al* (2004) Role of LBPA and Alix in multivesicular liposome formation and endosome organization. *Science* 303: 531-534

Mattissek C, Teis D (2014) The role of the endosomal sorting complexes required for transport (ESCRT) in tumorigenesis. *Mol Membr Biol* 31: 111-119

McClurg UL, Azizyan M, Dransfield DT, Namdev N, Chit N, Nakjang S, Robson CN (2018) The novel anti-androgen candidate galeterone targets deubiquitinating enzymes, USP12 and USP46, to control prostate cancer growth and survival. *Oncotarget* 9: 24992-25007

McClurg UL, Harle VJ, Nabbi A, Batalha-Pereira A, Walker S, Coffey K, Gaughan L, McCracken SR, Robson CN (2015) Ubiquitin-specific protease 12 interacting partners Uaf-1 and WDR20 are potential therapeutic targets in prostate cancer. *Oncotarget* 6: 37724-37736

McCullough J, Clague MJ, Urbe S (2004) AMSH is an endosome-associated ubiquitin isopeptidase. *J Cell Biol* 166: 487-492

McCullough J, Row PE, Lorenzo O, Doherty M, Beynon R, Clague MJ, Urbe S (2006) Activation of the endosome-associated ubiquitin isopeptidase AMSH by STAM, a component of the multivesicular body-sorting machinery. *Curr Biol* 16: 160-165

McDowell GS, Philpott A (2013) Non-canonical ubiquitylation: mechanisms and consequences. *Int J Biochem Cell Biol* 45: 1833-1842

McNally EK, Brett CL (2018) The intralumenal fragment pathway mediates ESCRT-independent surface transporter down-regulation. *Nat Commun* 9: 5358

McNally KE, Faulkner R, Steinberg F, Gallon M, Ghai R, Pim D, Langton P, Pearson N, Danson CM, Nagele H *et al* (2017) Retriever is a multiprotein complex for retromer-independent endosomal cargo recycling. *Nat Cell Biol* 19: 1214-1225

Meng XM, Nikolic-Paterson DJ, Lan HY (2016) TGF-beta: the master regulator of fibrosis. *Nat Rev Nephrol* 12: 325-338

Meszaros B, Kumar M, Gibson TJ, Uyar B, Dosztanyi Z (2017) Degrons in cancer. *Sci Signal* 10

Mevissen TE, Hospenthal MK, Geurink PP, Elliott PR, Akutsu M, Arnaudo N, Ekkebus R, Kulathu Y, Wauer T, El Oualid F *et al* (2013) OTU deubiquitinases reveal mechanisms of linkage specificity and enable ubiquitin chain restriction analysis. *Cell* 154: 169-184

Mevissen TET, Komander D (2017) Mechanisms of Deubiquitinase Specificity and Regulation. *Annu Rev Biochem* 86: 159-192

Middleton AJ, Wright JD, Day CL (2017) Regulation of E2s: A Role for Additional Ubiquitin Binding Sites? *J Mol Biol* 429: 3430-3440

Migliano SM, Teis D (2018) ESCRT and Membrane Protein Ubiquitination. *Prog Mol Subcell Biol* 57: 107-135

Millard SM, Wood SA (2006) Riding the DUBway: regulation of protein trafficking by deubiquitylating enzymes. *J Cell Biol* 173: 463-468

Minshull J, Golsteyn R, Hill CS, Hunt T (1990) The A- and B-type cyclin associated cdc2 kinases in Xenopus turn on and off at different times in the cell cycle. *EMBO J* 9: 2865-2875

Mishra YG, Manavathi B (2021) Focal adhesion dynamics in cellular function and disease. *Cell Signal* 85: 110046

Mohrmann K, van der Sluijs P (1999) Regulation of membrane transport through the endocytic pathway by rabGTPases. *Mol Membr Biol* 16: 81-87

Moilanen AM, Poukka H, Karvonen U, Hakli M, Janne OA, Palvimo JJ (1998) Identification of a novel RING finger protein as a coregulator in steroid receptor-mediated gene transcription. *Mol Cell Biol* 18: 5128-5139

Monroe N, Han H, Gonciarz MD, Eckert DM, Karren MA, Whitby FG, Sundquist WI, Hill CP (2014) The oligomeric state of the active Vps4 AAA ATPase. *J Mol Biol* 426: 510-525

Moreno-Layseca P, Icha J, Hamidi H, Ivaska J (2019) Integrin trafficking in cells and tissues. *Nat Cell Biol* 21: 122-132

Moreno-Layseca P, Jantti NZ, Godbole R, Sommer C, Jacquemet G, Al-Akhrass H, Conway JRW, Kronqvist P, Kallionpaa RE, Oliveira-Ferrer L *et al* (2021) Cargo-specific recruitment in clathrin- and dynamin-independent endocytosis. *Nat Cell Biol* 23: 1073-1084

Moretti J, Chastagner P, Liang CC, Cohn MA, Israel A, Brou C (2012) The ubiquitin-specific protease 12 (USP12) is a negative regulator of notch signaling acting on notch receptor trafficking toward degradation. *J Biol Chem* 287: 29429-29441

Morgan MR, Hamidi H, Bass MD, Warwood S, Ballestrem C, Humphries MJ (2013) Syndecan-4 phosphorylation is a control point for integrin recycling. *Dev Cell* 24: 472-485

Morita E, Sandrin V, Alam SL, Eckert DM, Gygi SP, Sundquist WI (2007) Identification of human MVB12 proteins as ESCRT-I subunits that function in HIV budding. *Cell Host Microbe* 2: 41-53

Morotti A, Panuzzo C, Crivellaro S, Pergolizzi B, Familiari U, Berger AH, Saglio G, Pandolfi PP (2014) BCR-ABL disrupts PTEN nuclear-cytoplasmic shuttling through phosphorylation-dependent activation of HAUSP. *Leukemia* 28: 1326-1333

Morris JR, Solomon E (2004) BRCA1 : BARD1 induces the formation of conjugated ubiquitin structures, dependent on K6 of ubiquitin, in cells during DNA replication and repair. *Hum Mol Genet* 13: 807-817

Morse EM, Brahme NN, Calderwood DA (2014) Integrin cytoplasmic tail interactions. *Biochemistry* 53: 810-820

Moser M, Legate KR, Zent R, Fassler R (2009) The tail of integrins, talin, and kindlins. *Science* 324: 895-899

Moser M, Nieswandt B, Ussar S, Pozgajova M, Fassler R (2008) Kindlin-3 is essential for integrin activation and platelet aggregation. *Nat Med* 14: 325-330

Muziol T, Pineda-Molina E, Ravelli RB, Zamborlini A, Usami Y, Gottlinger H, Weissenhorn W (2006) Structural basis for budding by the ESCRT-III factor CHMP3. *Dev Cell* 10: 821-830

Mygind KJ, Schwarz J, Sahgal P, Ivaska J, Kveiborg M (2018) Loss of ADAM9 expression impairs beta1 integrin endocytosis, focal adhesion formation and cancer cell migration. *J Cell Sci* 131

Nader D, Fletcher N, Curley GF, Kerrigan SW (2021) SARS-CoV-2 uses major endothelial integrin alphavbeta3 to cause vascular dysregulation in-vitro during COVID-19. *PLoS One* 16: e0253347

Nanao MH, Tcherniuk SO, Chroboczek J, Dideberg O, Dessen A, Balakirev MY (2004) Crystal structure of human otubain 2. *EMBO Rep* 5: 783-788

Nathan JA, Kim HT, Ting L, Gygi SP, Goldberg AL (2013) Why do cellular proteins linked to K63-polyubiquitin chains not associate with proteasomes? *EMBO J* 32: 552-565

Need AC, Ge D, Weale ME, Maia J, Feng S, Heinzen EL, Shianna KV, Yoon W, Kasperaviciute D, Gennarelli M *et al* (2009) A genome-wide investigation of SNPs and CNVs in schizophrenia. *PLoS Genet* 5: e1000373

Neefjes J, van der Kant R (2014) Stuck in traffic: an emerging theme in diseases of the nervous system. *Trends Neurosci* 37: 66-76
Nguyen HC, Wang W, Xiong Y (2017) Cullin-RING E3 Ubiquitin Ligases: Bridges to Destruction. *Subcell Biochem* 83: 323-347
Nic M JJ, Kosata B (1997) *Phase separation*. Oxford: Blackwell Scientific Publications
Nickerson DP, West M, Odorizzi G (2006) Did2 coordinates Vps4-mediated dissociation of ESCRT-III from endosomes. *J Cell Biol* 175: 715-720
Nijman SM, Huang TT, Dirac AM, Brummelkamp TR, Kerkhoven RM, D'Andrea AD, Bernards R (2005a) The deubiquitinating enzyme USP1 regulates the Fanconi anemia pathway. *Mol Cell* 17: 331-339
Nijman SM, Luna-Vargas MP, Velds A, Brummelkamp TR, Dirac AM, Sixma TK, Bernards R (2005b) A genomic and functional inventory of deubiquitinating enzymes. *Cell* 123: 773-786
Nishida T, Yamada Y (2020) RNF4-mediated SUMO-targeted ubiquitination relieves PARIS/ZNF746-mediated transcriptional repression. *Biochem Biophys Res Commun* 526: 110-116
Nishimura T, Kaibuchi K (2007) Numb controls integrin endocytosis for directional cell migration with aPKC and PAR-3. *Dev Cell* 13: 15-28
Niwa J, Yamada S, Ishigaki S, Sone J, Takahashi M, Katsuno M, Tanaka F, Doyu M, Sobue G (2007) Disulfide bond mediates aggregation, toxicity, and ubiquitylation of familial amyotrophic lateral sclerosis-linked mutant SOD1. *J Biol Chem* 282: 28087-28095
Nolte M, Margadant C (2020) Controlling Immunity and Inflammation through Integrin-Dependent Regulation of TGF-beta. *Trends Cell Biol* 30: 49-59
Obita T, Saksena S, Ghazi-Tabatabai S, Gill DJ, Perisic O, Emr SD, Williams RL (2007) Structural basis for selective recognition of ESCRT-III by the AAA ATPase Vps4. *Nature* 449: 735-739
Ohtake F, Saeki Y, Ishido S, Kanno J, Tanaka K (2016) The K48-K63 Branched Ubiquitin Chain Regulates NF-kappaB Signaling. *Mol Cell* 64: 251-266
Ohtake F, Saeki Y, Sakamoto K, Ohtake K, Nishikawa H, Tsuchiya H, Ohta T, Tanaka K, Kanno J (2015) Ubiquitin acetylation inhibits polyubiquitin chain elongation. *EMBO Rep* 16: 192-201
Olazabal-Herrero A, Sendino M, Arganda-Carreras I, Rodriguez JA (2019) WDR20 regulates shuttling of the USP12 deubiquitinase complex between the plasma membrane, cytoplasm and nucleus. *Eur J Cell Biol* 98: 12-26
Ordureau A, Sarraf SA, Duda DM, Heo JM, Jedrychowski MP, Sviderskiy VO, Olszewski JL, Koerber JT, Xie T, Beausoleil SA *et al* (2014) Quantitative proteomics reveal a feedforward mechanism for mitochondrial PARKIN translocation and ubiquitin chain synthesis. *Mol Cell* 56: 360-375
Oria R, Wiegand T, Escribano J, Elosegui-Artola A, Uriarte JJ, Moreno-Pulido C, Platzman I, Delcanale P, Albertazzi L, Navajas D *et al* (2017) Force loading explains spatial sensing of ligands by cells. *Nature* 552: 219-224
Pang X, He X, Qiu Z, Zhang H, Xie R, Liu Z, Gu Y, Zhao N, Xiang Q, Cui Y (2023) Targeting integrin pathways: mechanisms and advances in therapy. *Signal Transduct Target Ther* 8: 1
Park CW, Ryu KY (2014) Cellular ubiquitin pool dynamics and homeostasis. *BMB Rep* 47: 475-482
Park EJ, Myint PK, Appiah MG, Darkwah S, Caidengbate S, Ito A, Matsuo E, Kawamoto E, Gaowa A, Shimaoka M (2021) The Spike Glycoprotein of SARS-CoV-2 Binds to beta1 Integrins Expressed on the Surface of Lung Epithelial Cells. *Viruses* 13
Paul NR, Jacquemet G, Caswell PT (2015) Endocytic Trafficking of Integrins in Cell Migration. *Curr Biol* 25: R1092-1105
Pederson T (2011) The nucleolus. *Cold Spring Harb Perspect Biol* 3
Pellinen T, Arjonen A, Vuoriluoto K, Kallio K, Fransen JA, Ivaska J (2006) Small GTPase Rab21 regulates cell adhesion and controls endosomal traffic of beta1-integrins. *J Cell Biol* 173: 767-780
Peng J, Schwartz D, Elias JE, Thoreen CC, Cheng D, Marsischky G, Roelofs J, Finley D, Gygi SP (2003) A proteomics approach to understanding protein ubiquitination. *Nat Biotechnol* 21: 921-926
Peth A, Uchiki T, Goldberg AL (2010) ATP-dependent steps in the binding of ubiquitin conjugates to the 26S proteasome that commit to degradation. *Mol Cell* 40: 671-681

Petroski MD, Deshaies RJ (2005) Function and regulation of cullin-RING ubiquitin ligases. *Nat Rev Mol Cell Biol* 6: 9-20

Phillips-Krawczak CA, Singla A, Starokadomskyy P, Deng Z, Osborne DG, Li H, Dick CJ, Gomez TS, Koenecke M, Zhang JS *et al* (2015) COMMD1 is linked to the WASH complex and regulates endosomal trafficking of the copper transporter ATP7A. *Mol Biol Cell* 26: 91-103

Phu L, Rose CM, Tea JS, Wall CE, Verschueren E, Cheung TK, Kirkpatrick DS, Bingol B (2020) Dynamic Regulation of Mitochondrial Import by the Ubiquitin System. *Mol Cell* 77: 1107-1123 e1110

Pickart CM, Fushman D (2004) Polyubiquitin chains: polymeric protein signals. *Curr Opin Chem Biol* 8: 610-616

Popp MW, Artavanis-Tsakonas K, Ploegh HL (2009) Substrate filtering by the active site crossover loop in UCHL3 revealed by sortagging and gain-of-function mutations. *J Biol Chem* 284: 3593-3602

Poteryaev D, Datta S, Ackema K, Zerial M, Spang A (2010) Identification of the switch in early-to-late endosome transition. *Cell* 141: 497-508

Prag G, Watson H, Kim YC, Beach BM, Ghirlando R, Hummer G, Bonifacino JS, Hurley JH (2007) The Vps27/Hse1 complex is a GAT domain-based scaffold for ubiquitin-dependent sorting. *Dev Cell* 12: 973-986

Qi SM, Cheng G, Cheng XD, Xu Z, Xu B, Zhang WD, Qin JJ (2020) Targeting USP7-Mediated Deubiquitination of MDM2/MDMX-p53 Pathway for Cancer Therapy: Are We There Yet? *Front Cell Dev Biol* 8: 233

Qiu Y, Huang D, Sheng Y, Huang J, Li N, Zhang S, Hong Z, Yin X, Yan J (2021) Deubiquitinating enzyme USP46 suppresses the progression of hepatocellular carcinoma by stabilizing MST1. *Exp Cell Res* 405: 112646

Rabouille C (2017) Retriever fetches integrins from endosomes. *Nat Cell Biol* 19: 1144-1146

Raiborg C, Bremnes B, Mehlum A, Gillooly DJ, D'Arrigo A, Stang E, Stenmark H (2001) FYVE and coiled-coil domains determine the specific localisation of Hrs to early endosomes. *J Cell Sci* 114: 2255-2263

Raiborg C, Malerod L, Pedersen NM, Stenmark H (2008) Differential functions of Hrs and ESCRT proteins in endocytic membrane trafficking. *Exp Cell Res* 314: 801-813

Raiborg C, Wesche J, Malerod L, Stenmark H (2006) Flat clathrin coats on endosomes mediate degradative protein sorting by scaffolding Hrs in dynamic microdomains. *J Cell Sci* 119: 2414-2424

Rainero E, Howe JD, Caswell PT, Jamieson NB, Anderson K, Critchley DR, Machesky L, Norman JC (2015) Ligand-Occupied Integrin Internalization Links Nutrient Signaling to Invasive Migration. *Cell Rep* 10: 398-413

Ravid T, Hochstrasser M (2008) Diversity of degradation signals in the ubiquitin-proteasome system. *Nat Rev Mol Cell Biol* 9: 679-690

Rechsteiner M, Rogers SW (1996) PEST sequences and regulation by proteolysis. *Trends Biochem Sci* 21: 267-271

Reed NI, Jo H, Chen C, Tsujino K, Arnold TD, DeGrado WF, Sheppard D (2015) The alphavbeta1 integrin plays a critical in vivo role in tissue fibrosis. *Sci Transl Med* 7: 288ra279

Rennick JJ, Johnston APR, Parton RG (2021) Key principles and methods for studying the endocytosis of biological and nanoparticle therapeutics. *Nat Nanotechnol* 16: 266-276

Reyes-Turcu FE, Ventii KH, Wilkinson KD (2009) Regulation and cellular roles of ubiquitin-specific deubiquitinating enzymes. *Annu Rev Biochem* 78: 363-397

Rink J, Ghigo E, Kalaidzidis Y, Zerial M (2005) Rab conversion as a mechanism of progression from early to late endosomes. *Cell* 122: 735-749

Ritorto MS, Ewan R, Perez-Oliva AB, Knebel A, Buhrlage SJ, Wightman M, Kelly SM, Wood NT, Virdee S, Gray NS *et al* (2014) Screening of DUB activity and specificity by MALDI-TOF mass spectrometry. *Nat Commun* 5: 4763

Rivkin E, Almeida SM, Ceccarelli DF, Juang YC, MacLean TA, Srikumar T, Huang H, Dunham WH, Fukumura R, Xie G *et al* (2013) The linear ubiquitin-specific deubiquitinase gumby regulates angiogenesis. *Nature* 498: 318-324

Roberts M, Barry S, Woods A, van der Sluijs P, Norman J (2001) PDGF-regulated rab4-dependent recycling of alphavbeta3 integrin from early endosomes is necessary for cell adhesion and spreading. *Curr Biol* 11: 1392-1402

Roepstorff K, Grandal MV, Henriksen L, Knudsen SL, Lerdrup M, Grovdal L, Willumsen BM, van Deurs B (2009) Differential effects of EGFR ligands on endocytic sorting of the receptor. *Traffic* 10: 1115-1127

Rogers S, Wells R, Rechsteiner M (1986) Amino acid sequences common to rapidly degraded proteins: the PEST hypothesis. *Science* 234: 364-368

Romanska HM, Potemski P, Krakowska M, Mieszkowska M, Chaudhri S, Kordek R, Kubiak R, Speirs V, Hanby AM, Sadej R, Berditchevski F (2015) Lack of CD151/integrin alpha3beta1 complex is predictive of poor outcome in node-negative lobular breast carcinoma: opposing roles of CD151 in invasive lobular and ductal breast cancers. *Br J Cancer* 113: 1350-1357

Ronau JA, Beckmann JF, Hochstrasser M (2016) Substrate specificity of the ubiquitin and Ubl proteases. *Cell Res* 26: 441-456

Rotin D, Kumar S (2009) Physiological functions of the HECT family of ubiquitin ligases. *Nat Rev Mol Cell Biol* 10: 398-409

Rotin D, Staub O, Haguenauer-Tsapis R (2000) Ubiquitination and endocytosis of plasma membrane proteins: role of Nedd4/Rsp5p family of ubiquitin-protein ligases. *J Membr Biol* 176: 1-17

Rowinsky EK, Paner A, Berdeja JG, Paba-Prada C, Venugopal P, Porkka K, Gullbo J, Linder S, Loskog A, Richardson PG, Landgren O (2020) Phase 1 study of the protein deubiquitinase inhibitor VLX1570 in patients with relapsed and/or refractory multiple myeloma. *Invest New Drugs* 38: 1448-1453

Ryu MY, Cho SK, Hong Y, Kim J, Kim JH, Kim GM, Chen YJ, Knoch E, Moller BL, Kim WT *et al* (2019) Classification of barley U-box E3 ligases and their expression patterns in response to drought and pathogen stresses. *BMC Genomics* 20: 326

Sachs N, Secades P, van Hulst L, Kreft M, Song JY, Sonnenberg A (2012) Loss of integrin alpha3 prevents skin tumor formation by promoting epidermal turnover and depletion of slow-cycling cells. *Proc Natl Acad Sci U S A* 109: 21468-21473

Sachse M, Urbe S, Oorschot V, Strous GJ, Klumperman J (2002) Bilayered clathrin coats on endosomal vacuoles are involved in protein sorting toward lysosomes. *Mol Biol Cell* 13: 1313-1328

Sahgal P, Alanko J, Icha J, Paatero I, Hamidi H, Arjonen A, Pietila M, Rokka A, Ivaska J (2019) GGA2 and RAB13 promote activity-dependent beta1-integrin recycling. *J Cell Sci* 132

Salama SR, Hendricks KB, Thorner J (1994) G1 cyclin degradation: the PEST motif of yeast Cln2 is necessary, but not sufficient, for rapid protein turnover. *Mol Cell Biol* 14: 7953-7966

Samson RY, Obita T, Freund SM, Williams RL, Bell SD (2008) A role for the ESCRT system in cell division in archaea. *Science* 322: 1710-1713

Savio MG, Wollscheid N, Cavallaro E, Algisi V, Di Fiore PP, Sigismund S, Maspero E, Polo S (2016) USP9X Controls EGFR Fate by Deubiquitinating the Endocytic Adaptor Eps15. *Curr Biol* 26: 173-183

Scheffner M, Huibregtse JM, Vierstra RD, Howley PM (1993) The HPV-16 E6 and E6-AP complex functions as a ubiquitin-protein ligase in the ubiquitination of p53. *Cell* 75: 495-505

Scheffner M, Staub O (2007) HECT E3s and human disease. *BMC Biochem* 8 Suppl 1: S6

Schmidt K, Keller M, Bader BL, Korytar T, Finke S, Ziegler U, Groschup MH (2013) Integrins modulate the infection efficiency of West Nile virus into cells. *J Gen Virol* 94: 1723-1733

Schmidt O, Teis D (2012) The ESCRT machinery. *Curr Biol* 22: R116-120

Schoneberg J, Lee IH, Iwasa JH, Hurley JH (2017) Reverse-topology membrane scission by the ESCRT proteins. *Nat Rev Mol Cell Biol* 18: 5-17

Schulman BA, Harper JW (2009) Ubiquitin-like protein activation by E1 enzymes: the apex for downstream signalling pathways. *Nat Rev Mol Cell Biol* 10: 319-331

Schumacher S, Dedden D, Nunez RV, Matoba K, Takagi J, Biertumpfel C, Mizuno N (2021) Structural insights into integrin alpha(5)beta(1) opening by fibronectin ligand. *Sci Adv* 7

Scott A, Chung HY, Gonciarz-Swiatek M, Hill GC, Whitby FG, Gaspar J, Holton JM, Viswanathan R, Ghaffarian S, Hill CP, Sundquist WI (2005a) Structural and mechanistic studies of VPS4 proteins. *EMBO J* 24: 3658-3669

Scott A, Gaspar J, Stuchell-Brereton MD, Alam SL, Skalicky JJ, Sundquist WI (2005b) Structure and ESCRT-III protein interactions of the MIT domain of human VPS4A. *Proc Natl Acad Sci U S A* 102: 13813-13818

Scott DC, King MT, Baek K, Gee CT, Kalathur R, Li J, Purser N, Nourse A, Chai SC, Vaithiyalingam S *et al* (2023) E3 ligase autoinhibition by C-degron mimicry maintains C-degron substrate fidelity. *Mol Cell* 83: 770-786 e779

Scourfield EJ, Martin-Serrano J (2017) Growing functions of the ESCRT machinery in cell biology and viral replication. *Biochem Soc Trans* 45: 613-634

Setsuie R, Wada K (2007) The functions of UCH-L1 and its relation to neurodegenerative diseases. *Neurochem Int* 51: 105-111

Shang F, Taylor A (2011) Ubiquitin-proteasome pathway and cellular responses to oxidative stress. *Free Radic Biol Med* 51: 5-16

Sheng B, Wei Z, Wu X, Li Y, Liu Z (2021) USP12 promotes breast cancer angiogenesis by maintaining midkine stability. *Cell Death Dis* 12: 1074

Sherpa D, Chrustowicz J, Qiao S, Langlois CR, Hehl LA, Gottemukkala KV, Hansen FM, Karayel O, von Gronau S, Prabu JR *et al* (2021) GID E3 ligase supramolecular chelate assembly configures multipronged ubiquitin targeting of an oligomeric metabolic enzyme. *Mol Cell* 81: 2445-2459 e2413

Shi M, Pedchenko V, Greer BH, Van Horn WD, Santoro SA, Sanders CR, Hudson BG, Eichman BF, Zent R, Pozzi A (2012) Enhancing integrin alpha1 inserted (I) domain affinity to ligand potentiates integrin alpha1beta1-mediated down-regulation of collagen synthesis. *J Biol Chem* 287: 35139-35152

Shields SB, Piper RC (2011) How ubiquitin functions with ESCRTs. *Traffic* 12: 1306-1317

Shiflett SL, Ward DM, Huynh D, Vaughn MB, Simmons JC, Kaplan J (2004) Characterization of Vta1p, a class E Vps protein in Saccharomyces cerevisiae. *J Biol Chem* 279: 10982-10990

Shim S, Kimpler LA, Hanson PI (2007) Structure/function analysis of four core ESCRT-III proteins reveals common regulatory role for extreme C-terminal domain. *Traffic* 8: 1068-1079

Shin Y, Brangwynne CP (2017) Liquid phase condensation in cell physiology and disease. *Science* 357

Shrestha RK, Ronau JA, Davies CW, Guenette RG, Strieter ER, Paul LN, Das C (2014) Insights into the mechanism of deubiquitination by JAMM deubiquitinases from cocrystal structures of the enzyme with the substrate and product. *Biochemistry* 53: 3199-3217

Sierra MI, Wright MH, Nash PD (2010) AMSH interacts with ESCRT-0 to regulate the stability and trafficking of CXCR4. *J Biol Chem* 285: 13990-14004

Sigismund S, Algisi V, Nappo G, Conte A, Pascolutti R, Cuomo A, Bonaldi T, Argenzio E, Verhoef LG, Maspero E *et al* (2013) Threshold-controlled ubiquitination of the EGFR directs receptor fate. *EMBO J* 32: 2140-2157

Sims AE, Spiteri E, Sims RJ, 3rd, Arita AG, Lach FP, Landers T, Wurm M, Freund M, Neveling K, Hanenberg H *et al* (2007) FANCI is a second monoubiquitinated member of the Fanconi anemia pathway. *Nat Struct Mol Biol* 14: 564-567

Sims JJ, Cohen RE (2009) Linkage-specific avidity defines the lysine 63-linked polyubiquitin-binding preference of rap80. *Mol Cell* 33: 775-783

Slagsvold T, Aasland R, Hirano S, Bache KG, Raiborg C, Trambaiolo D, Wakatsuki S, Stenmark H (2005) Eap45 in mammalian ESCRT-II binds ubiquitin via a phosphoinositide-interacting GLUE domain. *J Biol Chem* 280: 19600-19606

Smit JJ, Sixma TK (2014) RBR E3-ligases at work. *EMBO Rep* 15: 142-154

Snyder NA, Silva GM (2021) Deubiquitinating enzymes (DUBs): Regulation, homeostasis, and oxidative stress response. *J Biol Chem* 297: 101077

Soucy TA, Smith PG, Milhollen MA, Berger AJ, Gavin JM, Adhikari S, Brownell JE, Burke KE, Cardin DP, Critchley S *et al* (2009) An inhibitor of NEDD8-activating enzyme as a new approach to treat cancer. *Nature* 458: 732-736

Sowa ME, Bennett EJ, Gygi SP, Harper JW (2009) Defining the human deubiquitinating enzyme interaction landscape. *Cell* 138: 389-403

Staub O, Rotin D (2006) Role of ubiquitylation in cellular membrane transport. *Physiol Rev* 86: 669-707

Steinberg F, Heesom KJ, Bass MD, Cullen PJ (2012) SNX17 protects integrins from degradation by sorting between lysosomal and recycling pathways. *J Cell Biol* 197: 219-230
Stewart AG, Thomas B, Koff J (2018) TGF-beta: Master regulator of inflammation and fibrosis. *Respirology* 23: 1096-1097
Stewart MD, Ritterhoff T, Klevit RE, Brzovic PS (2016) E2 enzymes: more than just middle men. *Cell Res* 26: 423-440
Strickland M, Watanabe S, Bonn SM, Camara CM, Starich MR, Fushman D, Carter CA, Tjandra N (2022) Tsg101/ESCRT-I recruitment regulated by the dual binding modes of K63-linked diubiquitin. *Structure* 30: 289-299 e286
Strohmeyer N, Bharadwaj M, Costell M, Fassler R, Muller DJ (2017) Fibronectin-bound alpha5beta1 integrins sense load and signal to reinforce adhesion in less than a second. *Nat Mater* 16: 1262-1270
Stroupe C (2018) This Is the End: Regulation of Rab7 Nucleotide Binding in Endolysosomal Trafficking and Autophagy. *Front Cell Dev Biol* 6: 129
Stuchell-Brereton MD, Skalicky JJ, Kieffer C, Karren MA, Ghaffarian S, Sundquist WI (2007) ESCRT-III recognition by VPS4 ATPases. *Nature* 449: 740-744
Subramani D, Alahari SK (2010) Integrin-mediated function of Rab GTPases in cancer progression. *Mol Cancer* 9: 312
Subramanian B, Ko WC, Yadav V, DesRochers TM, Perrone RD, Zhou J, Kaplan DL (2012) The regulation of cystogenesis in a tissue engineered kidney disease system by abnormal matrix interactions. *Biomaterials* 33: 8383-8394
Sun H, Fan Z, Gingras AR, Lopez-Ramirez MA, Ginsberg MH, Ley K (2020) Frontline Science: A flexible kink in the transmembrane domain impairs beta2 integrin extension and cell arrest from rolling. *J Leukoc Biol* 107: 175-183
Sun H, Lagarrigue F, Gingras AR, Fan Z, Ley K, Ginsberg MH (2018) Transmission of integrin beta7 transmembrane domain topology enables gut lymphoid tissue development. *J Cell Biol* 217: 1453-1465
Sun L, Amraei R, Rahimi N (2021) NEDD4 regulates ubiquitination and stability of the cell adhesion molecule IGPR-1 via lysosomal pathway. *J Biomed Sci* 28: 35
Sun Z, Costell M, Fassler R (2019) Integrin activation by talin, kindlin and mechanical forces. *Nat Cell Biol* 21: 25-31
Sun Z, Guo SS, Fassler R (2016a) Integrin-mediated mechanotransduction. *J Cell Biol* 215: 445-456
Sun Z, Tseng HY, Tan S, Senger F, Kurzawa L, Dedden D, Mizuno N, Wasik AA, Thery M, Dunn AR, Fassler R (2016b) Kank2 activates talin, reduces force transduction across integrins and induces central adhesion formation. *Nat Cell Biol* 18: 941-953
Suresh HG, Pascoe N, Andrews B (2020) The structure and function of deubiquitinases: lessons from budding yeast. *Open Biol* 10: 200279
Suzuki S, Naitoh Y (1990) Amino acid sequence of a novel integrin beta 4 subunit and primary expression of the mRNA in epithelial cells. *EMBO J* 9: 757-763
Swatek KN, Komander D (2016) Ubiquitin modifications. *Cell Res* 26: 399-422
Takada Y, Ye X, Simon S (2007) The integrins. *Genome Biol* 8: 215
Tamkun JW, DeSimone DW, Fonda D, Patel RS, Buck C, Horwitz AF, Hynes RO (1986) Structure of integrin, a glycoprotein involved in the transmembrane linkage between fibronectin and actin. *Cell* 46: 271-282
Tang LJ, Li Y, Liu YL, Wang JM, Liu DW, Tian QB (2016) USP12 regulates cell cycle progression by involving c-Myc, cyclin D2 and BMI-1. *Gene* 578: 92-99
Teckchandani A, Toida N, Goodchild J, Henderson C, Watts J, Wollscheid B, Cooper JA (2009) Quantitative proteomics identifies a Dab2/integrin module regulating cell migration. *J Cell Biol* 186: 99-111
Teis D, Saksena S, Judson BL, Emr SD (2010) ESCRT-II coordinates the assembly of ESCRT-III filaments for cargo sorting and multivesicular body vesicle formation. *EMBO J* 29: 871-883

Teo H, Gill DJ, Sun J, Perisic O, Veprintsev DB, Vallis Y, Emr SD, Williams RL (2006) ESCRT-I core and ESCRT-II GLUE domain structures reveal role for GLUE in linking to ESCRT-I and membranes. *Cell* 125: 99-111

Teo H, Perisic O, Gonzalez B, Williams RL (2004) ESCRT-II, an endosome-associated complex required for protein sorting: crystal structure and interactions with ESCRT-III and membranes. *Dev Cell* 7: 559-569

Theodosiou M, Widmaier M, Bottcher RT, Rognoni E, Veelders M, Bharadwaj M, Lambacher A, Austen K, Muller DJ, Zent R, Fassler R (2016) Kindlin-2 cooperates with talin to activate integrins and induces cell spreading by directly binding paxillin. *eLife* 5: e10130

Thrower JS, Hoffman L, Rechsteiner M, Pickart CM (2000) Recognition of the polyubiquitin proteolytic signal. *EMBO J* 19: 94-102

Tian M, Zhu R, Ding F, Liu Z (2020) Ubiquitin-specific peptidase 46 promotes tumor metastasis through stabilizing ENO1 in human esophageal squamous cell carcinoma. *Exp Cell Res* 395: 112188

Tomas A, Futter CE, Eden ER (2014) EGF receptor trafficking: consequences for signaling and cancer. *Trends Cell Biol* 24: 26-34

Tomida S, Mamiya T, Sakamaki H, Miura M, Aosaki T, Masuda M, Niwa M, Kameyama T, Kobayashi J, Iwaki Y *et al* (2009) Usp46 is a quantitative trait gene regulating mouse immobile behavior in the tail suspension and forced swimming tests. *Nat Genet* 41: 688-695

Tu C, Ortega-Cava CF, Winograd P, Stanton MJ, Reddi AL, Dodge I, Arya R, Dimri M, Clubb RJ, Naramura M *et al* (2010) Endosomal-sorting complexes required for transport (ESCRT) pathway-dependent endosomal traffic regulates the localization of active Src at focal adhesions. *Proc Natl Acad Sci U S A* 107: 16107-16112

Urbe S, Huber LA, Zerial M, Tooze SA, Parton RG (1993) Rab11, a small GTPase associated with both constitutive and regulated secretory pathways in PC12 cells. *FEBS Lett* 334: 175-182

van der Beek J, Jonker C, van der Welle R, Liv N, Klumperman J (2019) CORVET, CHEVI and HOPS - multisubunit tethers of the endo-lysosomal system in health and disease. *J Cell Sci* 132

van der Horst A, de Vries-Smits AM, Brenkman AB, van Triest MH, van den Broek N, Colland F, Maurice MM, Burgering BM (2006) FOXO4 transcriptional activity is regulated by monoubiquitination and USP7/HAUSP. *Nat Cell Biol* 8: 1064-1073

VanPelt J, Page RC (2017) Unraveling the CHIP:Hsp70 complex as an information processor for protein quality control. *Biochim Biophys Acta Proteins Proteom* 1865: 133-141

Varshavsky A (1991) Naming a targeting signal. *Cell* 64: 13-15

Varshavsky A (2019) N-degron and C-degron pathways of protein degradation. *Proc Natl Acad Sci U S A* 116: 358-366

Ventii KH, Wilkinson KD (2008) Protein partners of deubiquitinating enzymes. *Biochem J* 414: 161-175

Verma R, Aravind L, Oania R, McDonald WH, Yates JR, 3rd, Koonin EV, Deshaies RJ (2002) Role of Rpn11 metalloprotease in deubiquitination and degradation by the 26S proteasome. *Science* 298: 611-615

Vijay-Kumar S, Bugg CE, Cook WJ (1987) Structure of ubiquitin refined at 1.8 A resolution. *J Mol Biol* 194: 531-544

Villamil MA, Liang Q, Zhuang Z (2013) The WD40-repeat protein-containing deubiquitinase complex: catalysis, regulation, and potential for therapeutic intervention. *Cell Biochem Biophys* 67: 111-126

Virdee S, Ye Y, Nguyen DP, Komander D, Chin JW (2010) Engineered diubiquitin synthesis reveals Lys29-isopeptide specificity of an OTU deubiquitinase. *Nat Chem Biol* 6: 750-757

Vlasschaert C, Cook D, Xia X, Gray DA (2017) The evolution and functional diversification of the deubiquitinating enzyme superfamily. *Genome Biol Evol* 9: 558-573

Votteler J, Sundquist WI (2013) Virus budding and the ESCRT pathway. *Cell Host Microbe* 14: 232-241

Wade M, Wang YV, Wahl GM (2010) The p53 orchestra: Mdm2 and Mdmx set the tone. *Trends Cell Biol* 20: 299-309

Wakabayashi K, Nakagawa H, Tamura A, Koshiba S, Hoshijima K, Komada M, Ishikawa T (2007) Intramolecular disulfide bond is a critical check point determining degradative fates of ATP-binding cassette (ABC) transporter ABCG2 protein. *J Biol Chem* 282: 27841-27846

Wang P, Dai X, Jiang W, Li Y, Wei W (2020) RBR E3 ubiquitin ligases in tumorigenesis. *Semin Cancer Biol* 67: 131-144

Weber J, Polo S, Maspero E (2019) HECT E3 Ligases: A Tale With Multiple Facets. *Front Physiol* 10: 370

Wegener KL, Campbell ID (2008) Transmembrane and cytoplasmic domains in integrin activation and protein-protein interactions (review). *Mol Membr Biol* 25: 376-387

Weinberg JS, Drubin DG (2014) Regulation of clathrin-mediated endocytosis by dynamic ubiquitination and deubiquitination. *Curr Biol* 24: 951-959

Wenzel DM, Lissounov A, Brzovic PS, Klevit RE (2011) UBCH7 reactivity profile reveals parkin and HHARI to be RING/HECT hybrids. *Nature* 474: 105-108

Wiborg J, O'Shea C, Skriver K (2008) Biochemical function of typical and variant Arabidopsis thaliana U-box E3 ubiquitin-protein ligases. *Biochem J* 413: 447-457

Wickstrom SA, Faessler R (2011) Regulation of membrane traffic by integrin signaling. *Trends Cell Biol* 21: 266-273

Wilkinson KD (2000) Ubiquitination and deubiquitination: targeting of proteins for degradation by the proteasome. *Semin Cell Dev Biol* 11: 141-148

Winborn BJ, Travis SM, Todi SV, Scaglione KM, Xu P, Williams AJ, Cohen RE, Peng J, Paulson HL (2008) The deubiquitinating enzyme ataxin-3, a polyglutamine disease protein, edits Lys63 linkages in mixed linkage ubiquitin chains. *J Biol Chem* 283: 26436-26443

Wollert T, Hurley JH (2010) Molecular mechanism of multivesicular body biogenesis by ESCRT complexes. *Nature* 464: 864-869

Wood MA, Kaplan MP, Brensinger CM, Guo W, Abel T (2005) Ubiquitin C-terminal hydrolase L3 (Uchl3) is involved in working memory. *Hippocampus* 15: 610-621

Worden EJ, Dong KC, Martin A (2017) An AAA Motor-Driven Mechanical Switch in Rpn11 Controls Deubiquitination at the 26S Proteasome. *Mol Cell* 67: 799-811 e798

Wunderley L, Brownhill K, Stefani F, Tabernero L, Woodman P (2014) The molecular basis for selective assembly of the UBAP1-containing endosome-specific ESCRT-I complex. *J Cell Sci* 127: 663-672

Xiong JP, Stehle T, Diefenbach B, Zhang R, Dunker R, Scott DL, Joachimiak A, Goodman SL, Arnaout MA (2001) Crystal structure of the extracellular segment of integrin alpha Vbeta3. *Science* 294: 339-345

Xiong JP, Stehle T, Zhang R, Joachimiak A, Frech M, Goodman SL, Arnaout MA (2002) Crystal structure of the extracellular segment of integrin alpha Vbeta3 in complex with an Arg-Gly-Asp ligand. *Science* 296: 151-155

Xu P, Duong DM, Seyfried NT, Cheng D, Xie Y, Robert J, Rush J, Hochstrasser M, Finley D, Peng J (2009) Quantitative proteomics reveals the function of unconventional ubiquitin chains in proteasomal degradation. *Cell* 137: 133-145

Yamada T, Yang Y, Bonni A (2013) Spatial organization of ubiquitin ligase pathways orchestrates neuronal connectivity. *Trends Neurosci* 36: 218-226

Yang Q, Zhao J, Chen D, Wang Y (2021a) E3 ubiquitin ligases: styles, structures and functions. *Mol Biomed* 2: 23

Yang Z, Xu G, Wang B, Liu Y, Zhang L, Jing T, Tang M, Xu X, Jiao K, Xiang L *et al* (2021b) USP12 downregulation orchestrates a protumourigenic microenvironment and enhances lung tumour resistance to PD-1 blockade. *Nat Commun* 12: 4852

Yao T, Cohen RE (2002) A cryptic protease couples deubiquitination and degradation by the proteasome. *Nature* 419: 403-407

Yao T, Song L, Jin J, Cai Y, Takahashi H, Swanson SK, Washburn MP, Florens L, Conaway RC, Cohen RE, Conaway JW (2008) Distinct modes of regulation of the Uch37 deubiquitinating enzyme in the proteasome and in the Ino80 chromatin-remodeling complex. *Mol Cell* 31: 909-917

Yao T, Song L, Xu W, DeMartino GN, Florens L, Swanson SK, Washburn MP, Conaway RC, Conaway JW, Cohen RE (2006) Proteasome recruitment and activation of the Uch37 deubiquitinating enzyme by Adrm1. *Nat Cell Biol* 8: 994-1002

Yau R, Rape M (2016) The increasing complexity of the ubiquitin code. *Nat Cell Biol* 18: 579-586

Yauch RL, Kazarov AR, Desai B, Lee RT, Hemler ME (2000) Direct extracellular contact between integrin alpha(3)beta(1) and TM4SF protein CD151. *J Biol Chem* 275: 9230-9238
Ye Y, Akutsu M, Reyes-Turcu F, Enchev RI, Wilkinson KD, Komander D (2011) Polyubiquitin binding and cross-reactivity in the USP domain deubiquitinase USP21. *EMBO Rep* 12: 350-357
Ye Y, Scheel H, Hofmann K, Komander D (2009) Dissection of USP catalytic domains reveals five common insertion points. *Mol Biosyst* 5: 1797-1808
Yee D, Goring DR (2009) The diversity of plant U-box E3 ubiquitin ligases: from upstream activators to downstream target substrates. *J Exp Bot* 60: 1109-1121
Yin J, Schoeffler AJ, Wickliffe K, Newton K, Starovasnik MA, Dueber EC, Harris SF (2015) Structural Insights into WD-Repeat 48 Activation of Ubiquitin-Specific Protease 46. *Structure* 23: 2043-2054
Yoon HJ, Cho YR, Joo JH, Seo DW (2013) Knockdown of integrin alpha3beta1 expression induces proliferation and migration of non-small cell lung cancer cells. *Oncol Rep* 29: 662-668
Yoon SO, Shin S, Mercurio AM (2005) Hypoxia stimulates carcinoma invasion by stabilizing microtubules and promoting the Rab11 trafficking of the alpha6beta4 integrin. *Cancer Res* 65: 2761-2769
Yoshida Y, Chiba T, Tokunaga F, Kawasaki H, Iwai K, Suzuki T, Ito Y, Matsuoka K, Yoshida M, Tanaka K, Tai T (2002) E3 ubiquitin ligase that recognizes sugar chains. *Nature* 418: 438-442
Yousefi H, Vatanmakanian M, Mahdiannasser M, Mashouri L, Alahari NV, Monjezi MR, Ilbeigi S, Alahari SK (2021) Understanding the role of integrins in breast cancer invasion, metastasis, angiogenesis, and drug resistance. *Oncogene* 40: 1043-1063
Yu H, Mashtalir N, Daou S, Hammond-Martel I, Ross J, Sui G, Hart GW, Rauscher FJ, 3rd, Drobetsky E, Milot E *et al* (2010) The ubiquitin carboxyl hydrolase BAP1 forms a ternary complex with YY1 and HCF-1 and is a critical regulator of gene expression. *Mol Cell Biol* 30: 5071-5085
Yu Y, Zheng Q, Erramilli SK, Pan M, Park S, Xie Y, Li J, Fei J, Kossiakoff AA, Liu L, Zhao M (2021) K29-linked ubiquitin signaling regulates proteotoxic stress response and cell cycle. *Nat Chem Biol* 17: 896-905
Yu Z, Gonciarz MD, Sundquist WI, Hill CP, Jensen GJ (2008) Cryo-EM structure of dodecameric Vps4p and its 2:1 complex with Vta1p. *J Mol Biol* 377: 364-377
Yue J, Zhang K, Chen J (2012) Role of integrins in regulating proteases to mediate extracellular matrix remodeling. *Cancer Microenviron* 5: 275-283
Zamborlini A, Usami Y, Radoshitzky SR, Popova E, Palu G, Gottlinger H (2006) Release of autoinhibition converts ESCRT-III components into potent inhibitors of HIV-1 budding. *Proc Natl Acad Sci U S A* 103: 19140-19145
Zhang L, Ding X, Cui J, Xu H, Chen J, Gong YN, Hu L, Zhou Y, Ge J, Lu Q *et al* (2011a) Cysteine methylation disrupts ubiquitin-chain sensing in NF-kappaB activation. *Nature* 481: 204-208
Zhang W, Sulea T, Tao L, Cui Q, Purisima EO, Vongsamphanh R, Lachance P, Lytvyn V, Qi H, Li Y, Menard R (2011b) Contribution of active site residues to substrate hydrolysis by USP2: insights into catalysis by ubiquitin specific proteases. *Biochemistry* 50: 4775-4785
Zhang X, Jiang G, Cai Y, Monkley SJ, Critchley DR, Sheetz MP (2008) Talin depletion reveals independence of initial cell spreading from integrin activation and traction. *Nat Cell Biol* 10: 1062-1068
Zhang X, Linder S, Bazzaro M (2020a) Drug Development Targeting the Ubiquitin-Proteasome System (UPS) for the Treatment of Human Cancers. *Cancers (Basel)* 12
Zhang Y, Reif G, Wallace DP (2020b) Extracellular matrix, integrins, and focal adhesion signaling in polycystic kidney disease. *Cell Signal* 72: 109646
Zhang Y, Xie R, Zhang H, Zheng Y, Lin C, Yang L, Huang M, Li M, Song F, Lu L *et al* (2021) Integrin beta7 Inhibits Colorectal Cancer Pathogenesis via Maintaining Antitumor Immunity. *Cancer Immunol Res* 9: 967-980
Zhao G, Gong L, Su D, Jin Y, Guo C, Yue M, Yao S, Qin Z, Ye Y, Tang Y *et al* (2019) Cullin5 deficiency promotes small-cell lung cancer metastasis by stabilizing integrin beta1. *J Clin Invest* 129: 972-987
Zhao Y, Li J, Chen J, Ye M, Jin X (2022) Functional roles of E3 ubiquitin ligases in prostate cancer. *J Mol Med (Berl)* 100: 1125-1144
Zhen Y, Stenmark H (2015) Cellular functions of Rab GTPases at a glance. *J Cell Sci* 128: 3171-3176

Zheng N, Shabek N (2017) Ubiquitin Ligases: Structure, Function, and Regulation. *Annu Rev Biochem* 86: 129-157
Zhou X, Sun SC (2021) Targeting ubiquitin signaling for cancer immunotherapy. *Signal Transduct Target Ther* 6: 16
Zhu H, Zhang T, Wang F, Yang J, Ding J (2019a) Structural insights into the activation of USP46 by WDR48 and WDR20. *Cell Discov* 5: 34
Zhu L, Liu H, Lu F, Yang J, Byzova TV, Qin J (2019b) Structural Basis of Paxillin Recruitment by Kindlin-2 in Regulating Cell Adhesion. *Structure* 27: 1686-1697 e1685
Zhu L, Plow EF, Qin J (2021) Initiation of focal adhesion assembly by talin and kindlin: A dynamic view. *Protein Sci* 30: 531-542
Zhu X, Menard R, Sulea T (2007) High incidence of ubiquitin-like domains in human ubiquitin-specific proteases. *Proteins* 69: 1-7
Zinngrebe J, Montinaro A, Peltzer N, Walczak H (2014) Ubiquitin in the immune system. *EMBO Rep* 15: 28-45

7. Acknowledgement

During the PhD thesis time, I met a lot of people who accompanied me through ups and downs. I would like to express my sincere gratitude to everyone who have contributed to the completion of my PhD thesis.

First and foremost, I would like to show my deepest appreciation to my project supervisor, my PhD god father, Prof. Dr. Reinhard Fässler, for giving me such a fantastic chance to study in Munich, for his unwavering support and such an amazing platform for research, for his mentorship throughout the PhD journey. His expertise, encouragement, and constructive feedback have been crucial for guiding the directions of my work. All the time spent with him will be invaluable experience for my future where I would like to become a critical and disciplined scientist like him.

Second, I would like to thank Dr. Guan Wang for his endless support to help me from WT to KO, from a simple WB to beautiful IF imaging, from scratch to a paper, from zero to hero; for his timely and detailed discussion with me about the project, what could be done and how could it be done, and also a proper interpretation of the results. His expertise and experience truly broadened my perspective. In many months of the manuscript preparation process, he helped me to review the manuscript word by word, comma by comma. I am so grateful for what he has done to help the PhD project doable and publishable.

Third, I greatly appreciate members of my thesis advisory board, Prof. Dr. Florian Bassermann from Technical University of Munich and Dr. Arno Alpi from the Max-Planck-Institute of Biochemistry, for their time spent on discussion with my project, which inspired me to focus on a correct direction for the project and also encouraged me to move forward. Prof. Dr. Florian Bassermann also provided us the sgRNA for Crispr screen, which is essential for my study.

I am also grateful to the members of my doctoral committee, Prof. Dr. Reinhard Fässler, Prof. Dr. Arnoud Sonnenberg, Prof. Dr. Martin Biel, Prof. Dr. Stephan Zahler, Prof. Dr. Mercedes Costell and Prof. Dr. Julian Stingele, for their time and effort spending on reading my thesis. Their collective expertise and diverse viewpoints will be valuable not only to my thesis but also my future work.

I am very thankful to my colleagues and fellow researchers for their inspiring discussions, shared experiences and techniques as well as their help in science and life in Munich. Many thanks to Jakob Reber, for the experimental materials and methods, discussions and coffee breaks. Together with Dr. Ralph Böttcher, they provided instructions with experiments. I also want to thank the imaging core facility, MS core facility and protein core facility for providing me excellent assistance. Special thanks to Drs. Zhiqi Sun, Shiny Shengzhen Guo, Nanpeng Chen, Andrea Seiwert, Sebastian Gruen, Jan Dominik Speidel and Alexandros Anastasakis for good company, which released a lot pressure from the work.

Last but not least, I want to express my appreciation to my family for their unwavering love, encouragement, and support, especially to my wife, for her continuous understanding and belief in me of finishing the PhD project, which is my ultimate strength and motivation.

8. Curriculum vitae

Full name: Kaikai Yu

Born: in Hangzhou, China, on Oct.23, 1993

Nationality: Chinese

Email: kyu@biochem.mpg.de

Education:

2019-08 to Present: PhD thesis at the Max-Planck-Institute of Biochemistry

2016-09 to 2019-06: Master thesis at School of Pharmacy, Shanghai Jiao Tong University

2012-09 to 2016-06: Bachelor thesis at School of Pharmacy, Shanghai University of Traditional Chinese Medicine

Selected Publications:

1. Hu, Y., **Yu, K.**, Wang, G., Zhang, D., Shi, C., Ding, Y., Hong, D., Zhang, D., He, H., Sun, L., Zheng, J. N., Sun, S., & Qian, F. (2018). Lanatoside C inhibits cell proliferation and induces apoptosis through attenuating Wnt/β-catenin/c-Myc signaling pathway in human gastric cancer cell. Biochemical pharmacology, 150, 280–292.

2. Nie, Y., **Yu, K.**, Li, B., Hu, Y., Zhang, H., Xin, R., Xiong, Y., Zhao, P., & Chai, G. (2019). S-allyl-l-cysteine attenuates bleomycin-induced pulmonary fibrosis and inflammation via AKT/NF-κB signaling pathway in mice. Journal of pharmacological sciences, 139(4), 377–384.

3. Wang, Z., **Yu, K.**, Hu, Y., Su, F., Gao, Z., Hu, T., Yang, Y., Cao, X., & Qian, F. (2020). Schisantherin A induces cell apoptosis through ROS/JNK signaling pathway in human gastric cancer cells. Biochemical pharmacology, 173, 113673.

9. Appendix

9.1 Manuscript I

The USP12/46 deubiquitinases protect integrins from ESCRT-mediated lysosomal degradation (Manuscript in revision in EMBO Reports, the decision letter from EMBO Reports is attached)

9.2 Manuscript II

Rab7 deficiency induces lysosome formation from recycling endosomes leading to an increased degradation of cell surface proteins (Manuscript in revision in The EMBO Journal, the decision letter from The EMBO Journal is attached)

The USP12/46 deubiquitinases protect integrins from ESCRT-mediated lysosomal degradation

Kaikai Yu[1], Shiny S. Guo[1], Florian Bassermann[2,3,4,5], Reinhard Fässler[1*] and Guan M. Wang[1*]

[1]Department of Molecular Medicine, Max Planck Institute of Biochemistry, Martinsried, Germany
[2]Department of Medicine III, Klinikum rechts der Isar, Technical University of Munich, Munich, Germany
[3]TranslaTUM, Center for Translational Cancer Research, Technical University of Munich, Munich, Germany
[4]Deutsches Konsortium fürr Translationale Krebsforschung (DKTK), Heidelberg, Germany
[5]Bavarian Cancer Research Center (BZKF), Munich, Germany

*Corresponding authors: faessler@biochem.mpg.de (R.F.), gwang@biochem.mpg.de (G.M.W.)

Keywords: ubiquitination, integrin, DUB, USP12/USP46, ESCRT

Abstract

The functions of integrins are tightly regulated via multiple mechanisms including trafficking and degradation. Integrins are repeatedly internalized, routed into the endosomal system and either degraded by the lysosome or recycled back to the plasma membrane. The ubiquitin system dictates whether internalized proteins are degraded or recycled. Here, we used a genetic screen and proximity-dependent biotin identification to identify deubiquitinase(s) that control integrin surface levels. We found that a ternary deubiquitinating complex, comprised of USP12 (or the homologous USP46), WDR48 and WDR20, stabilizes β1 integrin (Itgb1) by preventing ESCRT-mediated lysosomal degradation. Mechanistically, the USP12/46-WDR48-WDR20 complex removes ubiquitin from the cytoplasmic tail of internalized Itgb1 in early endosomes, which in turn prevents ESCRT-mediated sorting and Itgb1 degradation.

Introduction

Integrins are α/β heterodimers that mediate cell adhesion between cells and to the extracellular matrix (ECM) proteins (Hynes, 2002). The function of integrins is tightly regulated, on one hand by changing the conformational state that turns ligand binding on and off (Calderwood *et al*, 2013; Moser *et al*, 2009), and on the other hand by adjusting surface location and levels through an endosomal sorting process that dictates whether the integrins are recycled back to the cell surface or delivered to lysosomes for degradation (Moreno-Layseca *et al*, 2019). Considering that the approximate half-life of Itgb1-class integrins is 24-48 hours, their cell surface residence time 10 minutes and the recycling from and back to the plasma membrane around 20 minutes (Bottcher *et al*, 2012; Dozynkiewicz *et al*, 2012; Moreno-Layseca *et al.*, 2019), it can be assumed that Itgb1-class integrins undergo numerous cycles of endocytosis and recycling during their lifespan before they are degraded in lysosomes.

The ubiquitin system is a labelling system that marks proteins for different proteolytic fates, such as integrins that are determined for lysosomal degradation. Integrins and other cell surface proteins designated for internalization are ubiquitin-tagged at lysine residues in their cytoplasmic tail (Clague *et al*, 2012). The removal of the ubiquitin tags by specific deubiquitinases (DUBs) in early endosomes directs proteins into the recycling pathway and back to the cell surface (Clague *et al.*, 2012; Komander *et al*, 2009). Proteins, which retain the ubiquitin tag are recognized by the Endosomal Sorting Complex Required for Transport (ESCRT) complex, sequestered into microdomains and internalized as intraluminal vesicles (ILVs) leading to the formation of multivesicular bodies (MVBs), also known as late endosomes (Hanson & Cashikar, 2012). MVBs/late endosomes either mature into lysosomes in which transmembrane membrane proteins on ILVs are degraded by lysosomal proteases, or fuse with the plasma membrane which leads to the extracellular release of their cargo including the ILVs as exosomes (Huotari & Helenius, 2011; Saftig & Klumperman, 2009).

Previous studies have shown that the binding of α5β1 integrin to soluble fibronectin (FN) induces integrin cytoplasmic tail ubiquitination, internalization and the degradation of the integrin (Kharitidi *et al*, 2015; Lobert *et al*, 2010). It has also been demonstrated that internalized Itgb1 recruits the SNX17-retriever complex, which leads to the retrieval and recycling of integrins (Bottcher *et al.*, 2012; McNally *et al*, 2017; Steinberg *et al*, 2012). Indeed, SNX17-binding-deficient Itgb1 tail mutants fail to recycle and are degraded in the lysosome. They can be rescued from degradation upon additionally substituting the α5β1 integrin tails lysines for non-ubiquitinatable arginines, which led to the hypothesis that SNX17 fulfils two functions: on one hand it recruits DUB(s) to deubiquitinate the Itgb1 tail (Bottcher *et al.*, 2012),

and on the other hand it recruits the retriever complex to retrieve and recycle integrins. USP9X has been identified to bind SNX17 and deubiquitinate centriolar satellite proteins required for ciliogenesis (Wang et al., 2019). Although integrin deubiquitination has not been investigated in this report, Kharitidi and colleagues showed in an independent study that USP9X can deubiquitinate the α5-subunit (Itga5) in cells upon treatment with soluble FN (Kharitidi *et al.*, 2015). Importantly, however, tissues contain primarily FN that is crosslinked by the lysyl oxidase into an insoluble fibrillar network (Melamed *et al*, 2023) which, in contrast to soluble FN, cannot be internalized by integrins, raising the question whether USB9X also controls the steady state levels of unbound α5β1 integrins.

In the present paper, we designed unbiased genetic and biochemical screens aimed at identifying novel DUB(s) that stabilize Itgb1 levels at the cell surface at steady state. Our experiments revealed that the DUBs USP12 and USP46 complexed with WDR48 and WDR20 remove ubiquitin from the cytoplasmic tails of internalized Itgb1 and several other cells surface proteins including signalling proteins and solute transporters resulting in a decoupling from ESCRT-mediated degradation. The significance of our findings is discussed.

Results

The Itgb1 protein is stabilized by USP12 and USP46

As USP9X was shown to deubiquitinate Itga5 tails on endosomes following soluble FN stimulation (Kharitidi *et al.*, 2015), we first investigated whether USP9X also deubiquitinates and stabilizes Itgb1 in cells cultured under steady state conditions. To this end, we cultured USP9X-depleted mouse fibroblasts, Hela, RPE-1 and MDA-MB-231 cells, respectively, either continuously in the presence of fetal bovine serum (10%, high concentration of soluble serum FN) or in the presence of serum replacement medium (which lacks soluble FN). The experiments revealed that depletion of USP9X in all cells analysed was either without effect or slightly increased rather than decreased Itga5 and Itgb1 levels on the surface which was measured by flow cytometry, and in lysates which was determined by Western blot (WB), irrespective whether exposed to medium containing or lacking FBS (Fig. EV1). These findings indicate that USP9X does not control integrin turnover under steady state culture conditions and suggests that unknown DUB(s) ensure retrieval of integrins.

These results prompted us to design an unbiased Crispr/Cas9-based genetic screen aimed at identifying DUBs that regulate the surface stability of Itgb1 in cells cultured with 10% FBS-containing medium at steady state (Fig. 1A). Specifically, we targeted 98 human DUBs genes by transducing the human Cas9-expressing haploid HAP1 cell line with pooled lentiviral guide RNA (gRNA) libraries (Paulmann *et al*, 2022). The transduced HAP1 cells were then expanded, fixed, immunostained for Itgb1 and sorted by flow cytometry to obtain the 5% cells with the lowest and the 5% cells with the highest Itgb1 surface levels. Next, we used next-generation sequencing (NGS) to identify the gRNA-targeted genes in the Itgb1^{low} and Itgb1^{high} cell populations, respectively. We identified *BAP1*, *USP7*, *OTUD6B* and *USP46* genes in the Itgb1^{low}, and *PSMD14* and *USP14* in the Itgb1^{high} as potential regulators of Itgb1 cell surface levels (Fig. 1B).

To identify which of the DUBs identified in the Crispr/Cas9-based screen are present in the proximity of the Itgb1 tail in mouse fibroblasts, we determined the Itgb1 proximitome by combining the proximity-dependent biotin identification (BioID) assay in combination with mass spectrometry (MS)-based proteomics. First, we fused the miniTurbo (Branon *et al*, 2018) to the cytosolic tail of Itga5 which associates with Itgb1 whose tail integrity is required to bind interactors such as Kindlins and SNX17 (Bottcher *et al.*, 2012; Fitzpatrick *et al*, 2014; Li *et al*, 2017). The Itga5-miniTurbo was retrovirally transduced into wild-type (WT) and Itgb1-KO fibroblasts. The newly synthesized Itga5 cannot heterodimerize in the absence of Itgb1 and is degraded in the endoplasmatic reticulum, which makes Itgb1-KO cells a perfect negative

control. Next, we isolated biotinylated proteins from cell lysates with streptavidin-conjugated beads, performed MS and identified USP46, the paralog USP12, and the USP12- and USP46-binding and activating adaptor proteins WDR48 and WDR20 (Li *et al*, 2016; Zhu *et al*, 2019) (Fig. 1C). USP12 and USP46 share approximately 90% protein sequence similarity and conserved binding sites for WDR48 and WDR20 (Li *et al.*, 2016; Zhu *et al.*, 2019). The BAP1, USP7, OTUD6B and USP14 proteins were undetectable by MS. PSMD14 and USP9X were detected at comparably low levels in WT and Itgb1-KO fibroblasts, suggesting that these two proteins exhibit background binding, e.g. to the beads used in the experiment. Thus, the unbiased genetic screen as well as the proximitome point to the USP12/46-WDR48-WDR20 DUB complex (hereafter referred to as USP12/46-WDRs complex) as stabilizer of the Itgb1 surface levels.

To validate the results of our screens, we used Crispr/Cas9 technology to knockout (KO) the *USP12*, *USP46*, *WDR20*, and *WDR48* genes either individually or in combination in at least two different mouse fibroblast and human breast cancer MDA-MB-231 cell clones, respectively. Since antibodies against the USP12/46-WDRs complex are not available and several attempts to generate specific homemade polyclonal antisera were unsuccessful, we validated the KOs of the individual clones by genomic PCR followed by sequencing of the amplified genes (Fig. EV2). Flow cytometry analysis revealed that the expression levels of Itgb1 on fibroblasts carrying single KO of either USP12 or USP46 were comparable to those of wild-type fibroblasts (Fig. 1D), whereas the levels of Itgb1 on fibroblasts with the double knockout of USP12 and USP46 (USP12/46-dKO) were significantly reduced (Fig. 1D), suggesting that USP12 and USP46 compensate each other. WB of fibroblast lysates revealed that the levels of the 105 kDa Itgb1 band corresponding to the immature, ER-resident Itgb1 remained unaffected by the USP12/46-dKO, while the levels corresponding to the 125 kDa mature Itgb1 band were reduced in USP12/46-dKO cells (Fig. 1E, F), indicating that the destabilization occurs either in the secretory pathway, on the cell surface and/or in the endosomal system. Concomitantly with the decrease of the mature Itgb1 also the Itga5 levels were reduced in USP12/USP46-dKO lysates (Fig. 1E, F). In MDA-MB-231 cells, the dKO of USP12/46 also reduced the levels of Itgb1 at the cell surface and those of the 125 kDa mature Itgb1 in the whole cell lysate (Fig. EV3A-C).

The reduced Itgb1 levels in USP12/46-dKO fibroblasts were restored upon expression of either EGFP-tagged $USP12^{WT}$ or Flag-tagged $USP46^{WT}$ (Fig. 1G-I and Fig. EV3D-G). In contrast, re-expression of the catalytically inactive $USP12^{C48S}$ or $USP46^{C44S}$ mutants, in which the catalytic site cysteine was substituted for serine (Li *et al.*, 2016; Yin *et al*, 2015), were unable to restore

the Itgb1 levels indicating that USP12/46 require the DUB activity to stabilize the 125 kDa mature Itgb1 levels. Since USP12 and USP46 compensate each other, we used USP12 to delineate the DUB function in the following reconstitution experiments.

To assess whether USP12 regulates surface proteins other than Itgb1, we determined the cell surface proteome of USP12/46-dKO fibroblasts (Fig. 1J) and USP12/46-dKO MDA-MB-231 cells reconstituted with either $USP12^{WT}$ or $USP12^{C48S}$ (Fig. EV3H). To this end, we biotinylated cell surface proteins, precipitated the biotinylated proteins using streptavidin-conjugated beads and compared the abundance of the precipitated proteins by MS. We found that the levels of numerous surface receptors including integrins (Itgb3, Itgb5, Itga3 and Itgav), IL17rc, Pcdhb17, Acvr1, Ddr1, etc. were significantly decreased in $USP12^{C48S}$ expressing fibroblasts (Fig. 1J). Decreased surface levels of integrins, FAT4, STEAP3, PLXNB3, FZD6, etc. were identified in $USP12^{C48S}$ expressing MDA-MB-231 cells (Fig. EV3H). These results indicate that USP12 controls the levels of numerous surface proteins.

Binding of USP12 to WDR48-WDR20 is essential to maintain Itgb1 surface levels

Previous studies have shown that the deubiquitinase activity of USP12 and USP46 requires the association with the adaptor proteins WDR48 or WDR20 and is further increased upon binding to both, WDR48 and WDR20 (Li *et al.*, 2016; Zhu *et al.*, 2019). In line with these findings, we observed that Crispr/Cas9-mediated KO of either WDR48 or WDR20 moderately decreased Itgb1 surface levels on independently generated fibroblast clones, whereas the dKO of WDR48 as well as WDR20 decreased Itgb1 surface levels to the same extent as in USP12/46-dKO or $USP12^{C48S}$-expressing USP12/46-dKO fibroblasts (Fig. 2A). Furthermore, expression of either WDR48 or WDR20 alone in WDR48/20-dKO fibroblasts restored the levels of Itgb1 at the cell surface to a lesser extent than expression of the two WDR proteins together (Fig. 2B).

We also confirmed that the activity of USP12 depends on the direct interaction with WDR48 and WDR20 (Dharadhar *et al*, 2016; Li *et al.*, 2016) by mutating the binding site in EGFP-tagged USP12 for WDR48 ($USP12^{1XMUT}$, E190K) (Dharadhar *et al.*, 2016), for WDR20 ($USP12^{2XMUT}$, F287A, V279A) (Li *et al.*, 2016) or for both, WDR48 and WDR20 ($USP12^{3XMUT}$, E190K, F287A, V279A) (Fig. EV4A). Expression of $USP12^{WT}$ in USP12/46-dKO fibroblasts rescued Itgb1 surface levels, whereas expression of $USP12^{1XMUT}$ or $USP12^{2XMUT}$ only partially rescued Itgb1 surface levels and expression of $USP12^{3XMUT}$ did not increase Itgb1 levels beyond the levels of USP12/46-dKO fibroblasts expressing EGFP-only (Fig. 2C and Fig. EV4B). Also the expression of EGFP-tagged WDR48 mutant proteins ($WDR48^{MUT}$, K214E/W256A/R272D) in WDR48-KO fibroblasts, and WDR20 mutant proteins ($WDR20^{MUT}$, F262A/W306A) in WDR20-KO fibroblasts, both of which are unable to bind USP12/46 (Li *et al.*, 2016; Yin *et al.*,

2015), failed to normalize Itgb1 surface levels (Fig. 2D, E and Fig. EV4C-F). These findings indicate that the entire USP12/46-WDRs complex is required to stabilize Itgb1.

The WDR48 protein consists of an N-terminal β propeller domain followed by an ancillary domain (AD) and a C-terminal sumo-like domain (SLD), which is thought to recruit the substrate (in our case the ubiquitinated Itgb1 tail) to the USP-WDR48 complex (Li *et al.*, 2016; Yin *et al.*, 2015). However, expression of EGFP-tagged WDR48 protein lacking the SLD ($WDR48^{1-580}$) or the SLD as well as the AD ($WDR48^{1-359}$) domain in WDR48-KO fibroblasts restored Itgb1 surface levels to the same extent as expression of $WDR48^{WT}$, indicating that neither the SLD nor the AD domains are required to control DUB-mediated Itgb1 surface levels (Fig. EV4G-I).

SNX17 and the USP12/46-WDRs complex stabilize Itgb1 independently of each other

SNX17 binds Itgb1 on early endosomes and was shown to promote recycling of Itgb1 in an Itgb1-tail ubiquitination-dependent manner (Bottcher *et al.*, 2012; Steinberg *et al.*, 2012). Since dKO of USP12/46 reduced Itgb1 cell surface levels and total levels in cell lysates to a similar extent as loss of SNX17, we tested whether the deletion of the *Snx17* gene in USP12/46-dKO fibroblasts affects Itgb1 surface levels. The experiment revealed that the cell surface and total Itgb1 levels in USP12/46/SNX17-triple (t)KO fibroblast clones were further decreased compared to those in the USP12/46-dKO fibroblasts, suggesting that the DUB complex and SNX17 act independently of each other in maintaining Itgb1 levels (Fig. 3A-C). Re-expression of USP12 in USP12/46-dKO or SNX17 in SNX17-KO fully restored the surface levels of Itgb1 (Fig. 3D). Co-expression of USP12 and SNX17 fully restored the Itgb1 levels in tKO fibroblasts, whereas separate expression of USP12 or SNX17 in tKO fibroblasts failed to normalize Itgb1 surface levels (Fig. 3D).

The USP12/46-WDRs complex prevents lysosomal degradation of Itgb1

Next, we investigated the mechanism underlying the downregulation of Itgb1 expression in USP12/46-dKO cells. A role for *Itgb1* mRNA transcript stability in regulating Itgb1 protein levels could be excluded as no difference in *Itgb1* mRNA levels were found between USP12/46-dKO and WT fibroblasts (Fig. 4A). Cycloheximide (CHX) chase assays, which allow to compare the degradation kinetics of proteins, revealed accelerated Itgb1 protein degradation in USP12/46-dKO compared to WT fibroblasts (Fig. 4B, C). Furthermore, surface biotinylation followed by capture ELISA (Bottcher *et al.*, 2012) showed a significantly reduced Itgb1 surface stability in USP12/46-dKO fibroblasts compared to WT fibroblasts. The Itgb1 protein half-life was approximately 12 hours in USP12/46-dKO fibroblasts and more than 20 hours in WT fibroblasts (Fig. 4D). The reduced Itgb1 surface stability in USP12/46-dKO

fibroblasts was restored upon re-expression of $USP12^{WT}$ but not upon re-expression of the catalytically inactive $USP12^{C48S}$ (Fig. 4E). We also found that the internalization kinetics of Itgb1 was similar between $USP12^{WT}$ and $USP12^{C48S}$ re-expressing USP12/46-dKO fibroblasts (Fig. 4F), whereas the recycling rate of Itgb1 was reduced in $USP12^{C48S}$ expressing fibroblasts compared to $USP12^{WT}$ expressing fibroblasts (Fig. 4G). These data indicate that the catalytic activity of the USP12/46-WDRs complex stabilizes the surface as well as total Itgb1 protein levels by enabling the recycling of internalized Itgb1 to the cell surface.

To determine the pathway through which Itgb1 is degraded in the absence of USP12/46, we treated USP12/46-dKO fibroblasts with MG132 or Bafilomycin A1 (BafA1). Whereas inhibition of the proteasome with MG132 did not restore Itgb1 levels, inhibition of the lysosome with BafA1 restored total Itgb1 levels in cell lysates (Fig. 4H, I). Surprisingly, however, BafA1 treatment did not restore the surface levels of Itgb1 in USP12/46-dKO fibroblasts (Fig. 4J). To determine the subcellular localization of Itgb1 in WT and USP12/46-dKO fibroblasts, we immuno-stained fixed cells and found Itgb1 in FAs, ER, and a few intracellular puncta in both, WT and USP12/46-dKO fibroblasts. Following BafA1 treatment, we observed large Itgb1-positive puncta co-stained with the late endosome/lysosome marker Lamp1 in USP12/46-dKO fibroblasts, which were rarely observed in WT fibroblasts (Fig. 4K). An increased Pearson correlation coefficient (PCC) of Itgb1 with Lamp1 in USP12/46-dKO fibroblasts confirmed the increased endo/lysosomal localization of Itgb1 in USP12/46-dKO compared to WT fibroblasts (Fig. 4L). Collectively, these findings indicate that USP12/46 depletion leads to an increased lysosomal targeting of Itgb1, resulting in degradation, impaired recycling and reduced Itgb1 surface levels.

The USP12/46-WDRs complex prevents ESCRT-mediated degradation of Itgb1

Since BafA1 prevents the degradation of proteins in lysosomes by blocking the vacuolar-type ATPase and the lysosomal acidification (Wang *et al*, 2021), we hypothesized that the absent Itgb1 deubiquitination in USP12/46-dKO cells promotes ESCRT binding, internalization of Itgb1 via intraluminal vesicles (ILVs) and Itgb1 degradation. To test this hypothesis, we conjointly depleted ESCRT-0 component HGS and ESCRT-I component TSG101 by siRNAs (ESCRT-KD) in WT and USP12/46-dKO fibroblasts and found that Itgb1 levels and stability increased in both, $WT^{ESCRT\text{-}KD}$ and USP12/46-$dKO^{ESCRT\text{-}KD}$ fibroblasts (Fig. 5A and Fig. EV5A-C). Immunoprecipitation of endogenous Itgb1 followed by WB for ubiquitinated Itgb1 with anti-Ub antibody revealed elevated poly-ubiquitination of Itgb1 in USP12/46-$dKO^{ESCRT\text{-}KD}$ fibroblasts compared to $WT^{ESCRT\text{-}KD}$ fibroblasts (see smears between 130-200 kDa in Fig. 5B; Fig. EV5D). The increased Itgb1 ubiquitination in USP12/46-$dKO^{ESCRT\text{-}KD}$ fibroblasts was

confirmed by capturing ubiquitinated proteins using ubiquitin-trap beads and subsequently probing the gel separated proteins with a polyclonal anti-Itgb1 antibody (Fig. 5C and Fig. EV5E).

To identify the lysine residues in the Itgb1 tail that are ubiquitinated, we immunoprecipitated Itgb1, treated the precipitate with trypsin and used MS to identify peptides containing a Gly-Gly motif, which is a remaining signature of an Ub-conjugated site (Xu *et al*, 2010). The experiment identified lysine-774 (K774), K784 and K794 modified by ubiquitin (Fig. 5D, Supplementary table S1). Interestingly, K794 is located within the Kindlin- and SNX17-binding $NPK_{794}Y$ motif and K784 is adjacent to the Talin-binding $NPIY_{783}$ motif.

The ubiquitin (Ub) chain linkage specificity determines fate and function of polyubiquitinated proteins (Miranda & Sorkin, 2007; Swatek & Komander, 2016). Lysine-63 (K63)-linked polyUb chains are preferentially associated with ESCRT-mediated lysosomal degradation, while lysine-48 (K48)-linked chains lead to proteasomal degradation (Nathan *et al*, 2013; Strickland *et al*, 2022). To inhibit K48- or K63-mediated Ub conjugation we overexpressed ubiquitin mutants carrying K48R or K63R substitutions (Lim *et al*, 2005) and concomitantly depleted WT and USP12/46-dKO fibroblasts with ESCRT-KD siRNAs to enrich for ubiquitinated Itgb1 (Fig. 5E and Fig. EV5F). The experiment revealed an increase of ubiquitinated Itgb1 in cells expressing Ub^{WT} or Ub^{K48R}, but not Ub^{K63R}. The levels of Itgb1 ubiquitinated with Ub^{WT} and Ub^{K48R} were higher in USP12/46-$dKO^{ESCRT\text{-}KD}$ compared to $WT^{ESCRT\text{-}KD}$ fibroblasts, which indicates that K63-mediated polyUb chain modification destines Itgb1 for lysosomal degradation.

To further confirm the role of the USP12/46-WDRs complex in the deubiquitination of Itgb1, we performed an *in vitro* deubiquitination assay with recombinantly produced ternary wildtype $USP12^{WT}$-WDR48-WDR20 or catalytically inactive $USP12^{C48S}$-WDR48-WDR20 complexes (Fig. 5F). To enrich for ubiquitinated Itgb1, fibroblasts were first depleted with ESCRT-KD siRNAs and then Itgb1 was immunoprecipitated from cell lysates and incubated with the recombinant $USP12^{WT}$-WDRs or the recombinant $USP12^{C48S}$-WDRs complex (Fig. EV5G). Whereas $USP12^{WT}$-WDRs reduced Itgb1 ubiquitination, the catalytically inactive $USP12^{C48S}$-WDRs did not. Furthermore, neither recombinant UCHL5 nor USP7, which are integrin-unrelated DUBs and were used as controls, were able to reduce Itgb1 ubiquitination (Fig. 5F and Fig. EV5H). We also found that the EGFP-tagged USP12 expressed in USP12/46-$dKO^{ESCRT\text{-}KD}$ fibroblasts colocalized with Itgb1 and ubiquitin on the limiting membrane of enlarged endosomes and was absent from Itgb1-positive focal adhesions (FAs) (Fig. 5G-J). Enlarged endosomes were not observed in control siRNA transfected USP12/46-dKO

fibroblasts. Altogether, these data indicates that the USP12/46-WDRs complex colocalizes with Itgb1 on endosomes and deubiquitinates Itgb1, which in turn prevents ESCRT-mediated Itgb1 degradation.

Itgb1 crosslinking followed by IP and MS excluded a direct association between Itgb1 and the USP12/46-WDRs complex (Supplementary table S2). Since EGFP-USP12 was absent from FAs (Fig. 5G) and the members of the USP12/46-WDRs complex were also undetectable in the integrin adhesome (Horton *et al*, 2015; Kuo *et al*, 2011; Schiller *et al*, 2011), we conclude that the USP12/46-WDRs complex binds Itgb1 on endosomes and not in FAs.

If USP12/46-WDRs complex-mediated deubiquitination prevents Itgb1 degradation, non-ubiquitinable α5β1 integrins in which the lysine residues in the cytoplasmic tails of the α5 and β1 subunits were replaced with arginine residues should also escape ESCRT-mediated degradation and be recycled to the cell surface. To test this hypothesis, we generated Itgb1-KO fibroblasts expressing endogenous USP12/46 (Itgb1-KO^{WT}) or lacking USP12/46 (Itgb1-KO$^{USP12/46\text{-}dKO}$) and expressed $\alpha5^{WT}\beta1^{WT}$ or $\alpha5^{KR}\beta1^{KR}$, in which the 4 lysine residues in the Itga5 tail and the 8 lysine residues in the Itgb1 tail were substituted for arginine residues (Bottcher *et al.*, 2012) (Fig. 6A). BafA1 treatment to block lysosomal degradation followed by immunostaining revealed that $\alpha5^{WT}\beta1^{WT}$ accumulated in Lamp1^{+} endo/lysosomes in Itgb1-KO$^{USP12/46\text{-}dKO}$ fibroblasts, whereas $\alpha5^{KR}\beta1^{KR}$ did not accumulate (Fig. 6B). PCC confirmed the lower colocalization between Lamp1 and $\alpha5^{KR}\beta1^{KR}$ compared to Lamp1 and $\alpha5^{WT}\beta1^{WT}$ (Fig. 6C). Consistent with this observation, BafA1 treatment increased the surface levels of $\alpha5^{KR}\beta1^{KR}$ and to a much lower extent of $\alpha5^{WT}\beta1^{WT}$ in Itgb1-KO$^{USP12/46\text{-}dKO}$ fibroblasts (Fig. 6D). Moreover, treatment with ESCRT-KD siRNAs significantly increased the surface levels of $\alpha5^{WT}\beta1^{WT}$ but barely of $\alpha5^{KR}\beta1^{KR}$ in Itgb1-KO$^{USP12/46\text{-}dKO}$ fibroblasts, indicating that the ESCRT binds Ub^{K63} modified Itgb1 tails, which in turn leads to Itgb1 degradation and thereby prevents Itgb1 from being recycled to cell surface (Fig. 6E).

The stabilization of Itgb1 by USP12/46-WDRs promotes integrin functions

In line with the increased ubiquitination, elevated degradation and decreased levels of cell surface Itgb1 associated with loss of USP12/46 expression, we observed an impaired adhesion, spreading and *in vitro* wound healing-based migration of USP12/46-dKO fibroblasts and transwell migration of USP12/46-dKO MDA-MB-231 cells (Fig. 7A-E and Fig. EV6A). Furthermore, USP12/46-dKO MDA-MB-231 cells showed reduced invasion through Matrigel-coated transwell filters compared to WT MDA-MB-231 cells (Fig. 7F, G). In line with these findings, analysis of the TCGC BRCA database linked high expression of USP12 and USP46 with reduced overall survival and progression free intervals of breast cancer patients (Fig. 7H,

I and Fig. EV6B-E). These findings indicate that the Itgb1 deubiquitinating and stabilizing function of the USP12/46-WDRs complex is essential for basic integrin functions such as adhesion, spreading and migration. Furthermore, if their levels surpass a certain threshold such as in cancer Itgb1 levels rise, which is advantageous for invading cancer cells.

Discussion

The steady-state surface level of Itgb1 underlies a tightly regulated decision-making process, which routes internalized Itgb1 either to lysosomes for degradation or to recycling endosomes for their reuse on the cell surface. The decision depends on ubiquitin moieties that are attached to the Itgb1-tail upon internalization and are either retained and recognized by the ESCRT machinery or removed by DUBs. USP9X, a DUB best known for its role in mitosis and DNA repair (Meng *et al*, 2023), was shown to remove ubiquitin from α5-integrin tails and stabilize α5β1 integrins in starved cells treated with soluble FN (Kharitidi et al., 2015). Since we excluded an involvement of USP9X in controling α5β1 integrin in cells cultured under steady state conditions, we decided to perform a Crispr/Cas9-based genetic screen and a BioID-based proximitome screen to identify DUB(s) that stabilize the steady-state surface levels of Itgb1.

Our screens identified the ternary DUB complex consisting of the deubiquitinase USP12 (or its paralog USP46) and two accessory proteins, WDR48 and WDR20, which form a complex that facilitates the stabilization of Itgb1 in sub-confluent HAP1 cells, MDA-MB-231 cells and mouse fibroblasts. In search for a mechanistic explanation for the Itgb1 protein stabilization, we found that the activity of the USP12/46-WDRs complex removes ubiquitin from Itgb1 at early endosomal membranes and thereby, inhibits ESCRT-mediated sorting of Itgb1 into intraluminal vesicles (ILVs) and lysosomal degradation, and instead retrieves Itgb1 into recycling endosomes. Consistently, loss of the two DUBs, USP12 and USP46, which compensate each other, or of either WDR20 or WDR48, which facilitates the DUB activity, decreases the half-life of the Itgb1 protein from 24 to 12 hours. Importantly, our cell surface proteome analysis also revealed that the USP12/46-WDRs complex regulates not only the stabilization of Itgb1 but also of other surface proteins, including signaling receptors and solute transporters. This diverse group of surface proteins with very different cytoplasmic domains did not reveal a common domain or motif that may serve as direct or indirect binding site of the USP12/46-WDRs complex (Yu et al., unpublished), nor did our attempts to compare the sequences of the Itgb1 tail with those of the known nuclear and cytosolic substrates of USP12/46-WDRs (Niu *et al*, 2023). Immunostaining and proteomics analysis indicate that the USP12/46-WDRs complex-mediated Itgb1 deubiquitination occurs at endosomes, as neither our immunostainings nor previous studies on the adhesome composition found the complex in integrin adhesion sites.

Our findings also show that the three lysine residues, K774, K784 and K794 in the Itgb1-tail are ubiquitin-modified in the absence of USP12/46. The K784 is located adjacent to the membrane proximal NPIY motif that serves as binding site for Talins, and the K794 is located

in the distal NPKY motif that serves as binding site for Kindlin and SNX17. It is conceivable that the ubiquitination of K784 and K794 couples integrin inactivation by compromising Talin and Kindlin binding and blockade of endosomal retrieval and recycling by compromising SNX17 binding with ESCRT-mediated degradation. Hence, Itgb1-tail ubiquitination may have a dual function by coordinating activity and stability of integrins.

USP12 and USP46 can functionally compensate for each other *in vitro*. The two DUBs are ubiquitously expressed, however, display distinct expression levels in different tissues. USP12 is prominently expressed in bone marrow, whereas USP46 in muscle and brain tissues (proteinatlas.org) (Uhlen *et al*, 2015). Despite the different abundance of USP46 and USP12 in tissues, USP12- as well as USP46-KO mice are viable and lack obvious developmental and postnatal defects (mousephenotype.org) (Groza *et al*, 2023). However, increased levels of USP12 and USP46 have been associated with the progressions of several cancers, including breast cancer, liver cancer and multiple myeloma (Niu *et al.*, 2023). The diminished Itgb1 levels in USP12/46-dKO MDA-MB-231 cells severely impaired migration and invasion. Hence, the link between USP12/46 and Itgb1 stability may well have a contributory role for the course of different cancer entities, originating of both epithelial and blood origin, and call for the exploration of compounds that inhibit the activity of the DUB complex.

Methods

All methods can be found in the accompanying Supplementary Methods file.

Acknowledgment

We thank the sequencing, mass spectrometry and imaging facilities of the Max Planck Institute of Biochemistry for the invaluable support, and Dr. Arnoud Sonnenberg for critically reading the manuscript and discussions. This work was supported by the German Research Foundation (project numbers 452409123 and 537477296) to F.B. and the European Research Council (ERC) under the European Union's Horizon 2020 research and innovation program (grant agreement No. 810104 – Point) and the Max Planck Society to R.F.

Author contribution

Conceptualization: GW and RF; Investigation: KY, SG and GW; Resource: FB; Supervision: GW and RF; Funding Acquisition: RF; Writing: KY, GW and RF.

Declaration of interests

The authors declare no competing interests.

Reference

Bottcher RT, Stremmel C, Meves A, Meyer H, Widmaier M, Tseng HY, Fassler R (2012) Sorting nexin 17 prevents lysosomal degradation of beta1 integrins by binding to the beta1-integrin tail. *Nat Cell Biol* 14: 584-592

Branon TC, Bosch JA, Sanchez AD, Udeshi ND, Svinkina T, Carr SA, Feldman JL, Perrimon N, Ting AY (2018) Efficient proximity labeling in living cells and organisms with TurboID. *Nat Biotechnol* 36: 880-887

Calderwood DA, Campbell ID, Critchley DR (2013) Talins and kindlins: partners in integrin-mediated adhesion. *Nat Rev Mol Cell Biol* 14: 503-517

Clague MJ, Liu H, Urbe S (2012) Governance of endocytic trafficking and signaling by reversible ubiquitylation. *Dev Cell* 23: 457-467

Dharadhar S, Clerici M, van Dijk WJ, Fish A, Sixma TK (2016) A conserved two-step binding for the UAF1 regulator to the USP12 deubiquitinating enzyme. *J Struct Biol* 196: 437-447

Dozynkiewicz MA, Jamieson NB, Macpherson I, Grindlay J, van den Berghe PV, von Thun A, Morton JP, Gourley C, Timpson P, Nixon C *et al* (2012) Rab25 and CLIC3 collaborate to promote integrin recycling from late endosomes/lysosomes and drive cancer progression. *Dev Cell* 22: 131-145

Fitzpatrick P, Shattil SJ, Ablooglu AJ (2014) C-terminal COOH of integrin beta1 is necessary for beta1 association with the kindlin-2 adapter protein. *J Biol Chem* 289: 11183-11193

Goldman MJ, Craft B, Hastie M, Repecka K, McDade F, Kamath A, Banerjee A, Luo Y, Rogers D, Brooks AN *et al* (2020) Visualizing and interpreting cancer genomics data via the Xena platform. *Nat Biotechnol* 38: 675-678

Groza T, Gomez FL, Mashhadi HH, Munoz-Fuentes V, Gunes O, Wilson R, Cacheiro P, Frost A, Keskivali-Bond P, Vardal B *et al* (2023) The International Mouse Phenotyping Consortium:

comprehensive knockout phenotyping underpinning the study of human disease. *Nucleic Acids Res* 51: D1038-D1045
Hanson PI, Cashikar A (2012) Multivesicular Body Morphogenesis. *Annual Review of Cell and Developmental Biology* 28: 337-362
Horton ER, Byron A, Askari JA, Ng DHJ, Millon-Fremillon A, Robertson J, Koper EJ, Paul NR, Warwood S, Knight D *et al* (2015) Definition of a consensus integrin adhesome and its dynamics during adhesion complex assembly and disassembly. *Nat Cell Biol* 17: 1577-1587
Hsiau T, Conant D, Rossi N, Maures T, Waite K, Yang J, Joshi S, Kelso R, Holden K, Enzmann BL, Stoner R, 2018. Inference of CRISPR Edits from Sanger Trace Data. Cold Spring Harbor Laboratory.
Huotari J, Helenius A (2011) Endosome maturation. *EMBO J* 30: 3481-3500
Hynes RO (2002) Integrins: bidirectional, allosteric signaling machines. *Cell* 110: 673-687
Kharitidi D, Apaja PM, Manteghi S, Suzuki K, Malitskaya E, Roldan A, Gingras MC, Takagi J, Lukacs GL, Pause A (2015) Interplay of Endosomal pH and Ligand Occupancy in Integrin alpha5beta1 Ubiquitination, Endocytic Sorting, and Cell Migration. *Cell Rep* 13: 599-609
Komander D, Clague MJ, Urbé S (2009) Breaking the chains: structure and function of the deubiquitinases. *Nature Reviews Molecular Cell Biology* 10: 550-563
Kuo J-C, Han X, Hsiao C-T, Yates Iii JR, Waterman CM (2011) Analysis of the myosin-II-responsive focal adhesion proteome reveals a role for β-Pix in negative regulation of focal adhesion maturation. *Nature Cell Biology* 13: 383-393
Li H, Deng Y, Sun K, Yang H, Liu J, Wang M, Zhang Z, Lin J, Wu C, Wei Z, Yu C (2017) Structural basis of kindlin-mediated integrin recognition and activation. *Proc Natl Acad Sci U S A* 114: 9349-9354
Li H, Lim KS, Kim H, Hinds TR, Jo U, Mao H, Weller CE, Sun J, Chatterjee C, D'Andrea AD, Zheng N (2016) Allosteric Activation of Ubiquitin-Specific Proteases by beta-Propeller Proteins UAF1 and WDR20. *Mol Cell* 63: 249-260
Li W, Xu H, Xiao T, Cong L, Love MI, Zhang F, Irizarry RA, Liu JS, Brown M, Liu XS (2014) MAGeCK enables robust identification of essential genes from genome-scale CRISPR/Cas9 knockout screens. *Genome Biology* 15
Lim KL, Chew KC, Tan JM, Wang C, Chung KK, Zhang Y, Tanaka Y, Smith W, Engelender S, Ross CA *et al* (2005) Parkin mediates nonclassical, proteasomal-independent ubiquitination of synphilin-1: implications for Lewy body formation. *J Neurosci* 25: 2002-2009
Lobert VH, Brech A, Pedersen NM, Wesche J, Oppelt A, Malerod L, Stenmark H (2010) Ubiquitination of alpha 5 beta 1 integrin controls fibroblast migration through lysosomal degradation of fibronectin-integrin complexes. *Dev Cell* 19: 148-159
McNally KE, Faulkner R, Steinberg F, Gallon M, Ghai R, Pim D, Langton P, Pearson N, Danson CM, Nagele H *et al* (2017) Retriever is a multiprotein complex for retromer-independent endosomal cargo recycling. *Nat Cell Biol* 19: 1214-1225
Melamed S, Zaffryar-Eilot S, Nadjar-Boger E, Aviram R, Zhao H, Yaseen-Badarne W, Kalev-Altman R, Sela-Donenfeld D, Lewinson O, Astrof S *et al* (2023) Initiation of fibronectin fibrillogenesis is an enzyme-dependent process. *Cell Reports* 42: 112473
Meng Y, Hong C, Yang S, Qin Z, Yang L, Huang Y (2023) Roles of USP9X in cellular functions and tumorigenesis (Review). *Oncology Letters* 26
Miranda M, Sorkin A (2007) Regulation of receptors and transporters by ubiquitination: new insights into surprisingly similar mechanisms. *Mol Interv* 7: 157-167
Moreno-Layseca P, Icha J, Hamidi H, Ivaska J (2019) Integrin trafficking in cells and tissues. *Nat Cell Biol* 21: 122-132
Moser M, Legate KR, Zent R, Fassler R (2009) The tail of integrins, talin, and kindlins. *Science* 324: 895-899
Nathan JA, Kim HT, Ting L, Gygi SP, Goldberg AL (2013) Why do cellular proteins linked to K63-polyubiquitin chains not associate with proteasomes? *EMBO J* 32: 552-565
Niu K, Shi Y, Lv Q, Wang Y, Chen J, Zhang W, Feng K, Zhang Y (2023) Spotlights on ubiquitin-specific protease 12 (USP12) in diseases: from multifaceted roles to pathophysiological mechanisms. *J Transl Med* 21: 665
Paulmann C, Spallek R, Karpiuk O, Heider M, Schaffer I, Zecha J, Klaeger S, Walzik M, Ollinger R, Engleitner T *et al* (2022) The OTUD6B-LIN28B-MYC axis determines the proliferative state in multiple myeloma. *EMBO J* 41: e110871

Saftig P, Klumperman J (2009) Lysosome biogenesis and lysosomal membrane proteins: trafficking meets function. *Nat Rev Mol Cell Biol* 10: 623-635

Schiller HB, Friedel CC, Boulegue C, Fässler R (2011) Quantitative proteomics of the integrin adhesome show a myosin II-dependent recruitment of LIM domain proteins. *EMBO reports* 12: 259-266

Steinberg F, Heesom KJ, Bass MD, Cullen PJ (2012) SNX17 protects integrins from degradation by sorting between lysosomal and recycling pathways. *J Cell Biol* 197: 219-230

Strickland M, Watanabe S, Bonn SM, Camara CM, Starich MR, Fushman D, Carter CA, Tjandra N (2022) Tsg101/ESCRT-I recruitment regulated by the dual binding modes of K63-linked diubiquitin. *Structure* 30: 289-299 e286

Swatek KN, Komander D (2016) Ubiquitin modifications. *Cell Res* 26: 399-422

Uhlen M, Fagerberg L, Hallstrom BM, Lindskog C, Oksvold P, Mardinoglu A, Sivertsson A, Kampf C, Sjostedt E, Asplund A *et al* (2015) Proteomics. Tissue-based map of the human proteome. *Science* 347: 1260419

Wang R, Wang J, Hassan A, Lee CH, Xie XS, Li X (2021) Molecular basis of V-ATPase inhibition by bafilomycin A1. *Nat Commun* 12: 1782

Xu G, Paige JS, Jaffrey SR (2010) Global analysis of lysine ubiquitination by ubiquitin remnant immunoaffinity profiling. *Nat Biotechnol* 28: 868-873

Yin J, Schoeffler AJ, Wickliffe K, Newton K, Starovasnik MA, Dueber EC, Harris SF (2015) Structural Insights into WD-Repeat 48 Activation of Ubiquitin-Specific Protease 46. *Structure* 23: 2043-2054

Zhu H, Zhang T, Wang F, Yang J, Ding J (2019) Structural insights into the activation of USP46 by WDR48 and WDR20. *Cell Discov* 5: 34

Figure legends

Figure 1. The USP12/46-WDRs complex stabilizes Itgb1 protein levels.

(A) Schematic overview of the CRISPR screen for identifying DUBs regulating Itgb1 surface levels. Cas9-expressing HAP1 cells were transduced with pooled lentiviral guide RNA (gRNA) libraries targeting 98 DUBs from the human genome. After 2 weeks in culture, cells with the 5% lowest ($Itgb1^{Lo}$) and the 5% highest ($Itgb1^{Hi}$) Itgb1 surface levels were sorted by flow cytometry and gRNA-targeted genes were determined.

(B) Volcano plot of the results from the CRISPR screen. The x-axis represents the $\log_2$ fold change (lfc) in the frequency of genes targeted between the $Itgb1^{Lo}$ and $Itgb1^{Hi}$ populations. The y-axis indicates the Robust Rank Aggregation (RRA) score determined by the MAGeCK algorithm (MAGeCK-RRA) (Li *et al*, 2014). Dots represent individual targeted genes, and those meeting the criteria of $|lfc| > 0.33$ and $-\log_{10}(RRA) > 2$ were considered significant. Genes significantly enriched in $Itgb1^{Lo}$ cells are colored in blue and those enriched in $Itgb1^{Hi}$ in red.

(C) Volcano plot of the α5β1 integrin proximitome determined by label-free MS analysis in mouse kidney fibroblasts expressing miniTurbo-tagged Itag5 (TurboID) versus Itgb1-KO fibroblasts (Ctrl). *P*-values were determined using two-sided permuted *t*-test with 250 randomizations. The black dashed line indicates the significance cutoff (FDR:0.05, S0:0.1) estimated by the Perseus software. n=3 biological replicates. The red dots indicate the subunits of the α5β1 heterodimer and the components of the USP12/46-WDR48-WDR20 complex.

(D) Itgb1 surface levels in WT and two independent clones (cl1 and cl2) of USP12-KO, USP46-KO and USP12/46-dKO fibroblasts determined by flow cytometry. Statistical analysis was carried out by RM one-way ANOVA with Dunnett's multiple comparison test. Data are shown as Mean±SD, n=3 independent experiments.

(E, F) WB (**E**) and densitometric quantification (**F**) of Itgb1 and Itga5 protein levels in WT and USP12/46-dKO fibroblasts. Gapdh served as loading control. Statistical analysis was carried out by RM one-way ANOVA with Dunnett's multiple comparison test. Data are shown as Mean±SD, n=3 independent experiments.

(G-I) Itgb1 surface levels determined by flow cytometry (**G**), Itgb1 protein levels in cell lysates determined by WB (**H**) and densitometric quantification (**I**) in WT and USP12/46-dKO fibroblasts stably expressing EGFP, EGFP-$USP12^{WT}$ or EGFP-$USP12^{C48S}$. Gapdh served as a loading control. Statistical analysis was carried out by RM two-way ANOVA with Dunnett's multiple comparison test. Data are shown as Mean±SD, n=3 independent experiments.

(J) Volcano plot of the cell surface proteome of USP12/46-dKO fibroblasts stably expressing EGFP-$USP12^{C48S}$ versus EGFP-$USP12^{WT}$ identified by label-free MS. *P*-values were

525 determined using two-sided permuted *t*-test with 250 randomizations. The black dashed line
526 indicates the significance cutoff (FDR:0.05, S0:0.1) estimated by the Perseus software. n=4
527 biological replicates. Arbitrarily selected cell surface receptors were highlighted in red.
528

Figure EV1. The effect of USP9X-KD on integrin levels.

(A-H) WB and densitometric quantification of Itga5 and Itgb1 protein levels (**A**, **C**, **E**, **G**) and flow cytometry analysis of Itga5 and Itgb1 surface levels (**B**, **D**, **F**, **H**) in mouse fibroblasts (**A**, **B**), Hela (**C**, **D**), RPE-1 (**E**, **F**) and MDA-MB-231 cells (**G**, **H**) treated with control non-targeting siRNA (CTL) or siRNAs targeting USP9X (USP9X-KD). Cells were cultured overnight in DMEM with 10% serum or serum-replacement medium. Gapdh served as a loading control. Statistical analysis was carried out by paired t-test. Data are shown as Mean±SD, n=3 independent experiments.

Figure EV2. Validation of KO clones.

(A-G) Agarose gel electrophoresis images show PCR amplification products from the genomic region containing the indicated Cas9 targeting sites of the indicated genes in the parental WT and two independent mouse fibroblast clones (**A-F**) and MDA-MB-231 cell clones (**G**). PCR products were sequenced, analyzed with the Synthego Inference of CRISPR Edits (ICE) analysis tool (Hsiau *et al*, 2018) and the corresponding alignments are shown on the right panel.

Figure EV3. The USP12/46-WDRs complex stabilizes Itgb1 protein levels

(A-C) Itgb1 surface levels determined by flow cytometry (**A**) and Itgb1 protein levels in cell lysates determined by WB (**B**) with densitometric quantification (**C**) in WT and USP12/46-dKO MDA-MB-231 cells. Gapdh served as a loading control. Statistical analysis was carried out by RM one-way ANOVA with Dunnett's multiple comparison test comparing with WT. Data are shown as Mean±SD, n=3 independent experiments.

(D) EGFP fluorescence intensities in WT and USP12/46-dKO fibroblasts stably expressing EGFP, EGFP-USP12^{WT} or EGFP-USP12^{C48S} determined by flow cytometry. Statistical analysis was carried out by ordinary two-way ANOVA with Šidák's multiple comparison test. Data are shown as Mean±SD, n=3 independent experiments.

(E-G) Itgb1 surface levels determined by flow cytometry (**E**) and Itgb1 protein levels in cell lysates determined by WB (**F**) with densitometric quantification (**G**) in WT and USP12/46-dKO fibroblasts stably expressing FLAG-USP46^{WT} or FLAG-USP46^{C44S}. Mock transduced cells (Mock) served as control. Gapdh served as a loading control. Statistical analysis was carried out by RM two-way ANOVA with Dunnett's multiple comparison test. Data are shown as Mean±SD. **E**, n=3; **F, G** n=4 independent experiments.

(H) Volcano plot of the cell surface proteome of USP12/46-dKO MDA-MB-231 cells expressing EGFP-USP12^{C48S} versus EGFP-USP12^{WT} identified by label-free MS. *P*-values are determined using two-sided permuted t-test with 250 randomizations. The black dashed line indicates the significance cutoff (FDR:0.05, S0:0.1) estimated by the Perseus software. n=4 biological replicates. Arbitrarily selected cell surface receptors are highlighted in red.

Figure 2. The integrity of the USP12/48-WDR20-WDR48 complex is required to stabilize Itgb1 protein levels.

(A) Itgb1 surface levels in WT and WDR48-KO, WDR20-KO and WDR48/20-dKO fibroblasts determined by flow cytometry. Statistical analysis was carried out by RM one-way ANOVA with Dunnett's multiple comparison test comparing with WT. Data are shown as Mean±SD, n=3 independent experiments.

(B) Itgb1 surface levels in WT and WDR48/20-dKO fibroblasts transiently expressing EGFP, mScarlet, EGFP-WDR48 and/or WDR20-mScarlet determined by flow cytometry. Statistical analysis was carried out by RM two-way ANOVA with Dunnett's multiple comparison test. Data are shown as Mean±SD, n=3 independent experiments.

(C) Itgb1 surface levels in WT and USP12/46-dKO fibroblasts transiently expressing EGFP, EGFP-USP12^{WT}, EGFP-USP12^{1XMUT} (E190K, deficient in binding to WDR48), EGFP-USP12^{2XMUT} (F287A, V279A, deficient in binding to WDR20) or EGFP-USP12^{3XMUT} (E190K, F287A, V279A, deficient in binding to WDR48 as well as WDR20) determined by flow cytometry. Statistical analysis was carried out by ordinary one-way ANOVA with Dunnett's multiple comparison test. Data are shown as Mean±SD, n=3 independent experiments.

(D) Itgb1 surface levels in WT and WDR48-KO fibroblasts transiently expressing EGFP-WDR48^{WT} or EGFP-WDR48^{MUT} (deficient in binding to USP12 as well as USP46) determined by flow cytometry. Statistical analysis was carried out by RM two-way ANOVA with Dunnett's multiple comparison test. Data are shown as Mean±SD, n=3 independent experiments.

(E) Itgb1 surface levels in WT and WDR20-KO fibroblasts transiently expressing WDR20^{WT}-EGFP or WDR20^{MUT}-EGFP (deficient in binding to USP12 as well as USP46) determined by flow cytometry. Statistical analysis was carried out by RM two-way ANOVA with Dunnett's multiple comparison test. Data are shown as Mean±SD, n=3 independent experiments.

Figure EV4. Characterization of binding-deficient USP12, WDR48 and WDR20 mutants.

(A) GFP immunoprecipitation (GFP IP) from USP12/46-dKO fibroblasts transiently expressing EGFP, EGFP-USP12^{WT}, EGFP-USP12^{1XMUT}, EGFP-USP12^{2XMUT} or EGFP-USP12^{3XMUT} analyzed by WB for indicated proteins. Gapdh served as a loading control. Representative images from 3 independent experiments are shown.

(B) EGFP fluorescence in WT and USP12/46-dKO fibroblasts transiently expressing EGFP, EGFP-USP12^{WT}, EGFP-USP12^{1XMUT}, EGFP-USP12^{2XMUT} or EGFP-USP12^{3XMUT} determined by flow cytometry. Statistical analysis was carried out by ordinary one-way ANOVA with Dunnett's multiple comparison test. Data are shown as Mean±SD, n=3 independent experiments.

(C) GFP IP from USP12/46-dKO fibroblasts stably expressing mScarlet-USP12 and transiently expressing EGFP, EGFP-WDR48^{WT} or EGFP-WDR48^{MUT} analyzed by WB for indicated proteins. Gapdh served as a loading control. Representative images from 3 independent experiments are shown.

(D) GFP IP from USP12/46-dKO fibroblasts stably expressing mScarlet-USP12 and transiently expressing EGFP, WDR20^{WT}-EGFP or WDR20^{MUT}-EGFP analyzed by WB for indicated proteins. Gapdh served as a loading control. Representative images from 3 independent experiments are shown.

(E) EGFP fluorescence in WT and WDR48-KO fibroblasts transiently expressing EGFP, EGFP-WDR48^{WT} or EGFP-WDR48^{MUT} determined by flow cytometry. Statistical analysis was carried out by ordinary two-way ANOVA with Šidák's multiple comparison test. Data are shown as Mean±SD, n=3 independent experiments.

(F) EGFP fluorescence in WT and WDR20-KO fibroblasts transiently expressing EGFP, WDR20^{WT}-EGFP or WDR20^{MUT}-EGFP determined by flow cytometry. Statistical analysis was carried out by ordinary two-way ANOVA with Šidák's multiple comparison test. Data are shown as Mean±SD, n=3 independent experiments.

(G) Domain organization of the WT WDR48 and WDR48 domain-deletion mutants.

(H, I) Itgb1 surface levels (**H**) and EGFP fluorescence (**I**) in WDR48-KO fibroblasts stably expressing EGFP, EGFP-WDR48^{WT}, EGFP-WDR48$^{1-580}$ or EGFP-WDR48$^{1-359}$ determined by flow cytometry. Statistical analysis was carried out by RM one-way ANOVA with Dunnett's multiple comparison test. Data are shown as Mean±SD, n=3 independent experiments.

Figure 3. The USP12/46-WDRs complex stabilizes Itgb1 protein levels in a SNX17-independent manner.

(A-C) Itgb1 surface levels determined by flow cytometry (**A**) and Itgb1 and SNX17 protein levels in cell lysates determined by WB (**B**) with densitometric quantification (**C**) in WT, USP12/46-dKO, SNX17-KO, and USP12/46/SNX17-tKO fibroblasts. Gapdh served as a loading control. Statistical analysis was carried out by RM one-way ANOVA with Dunnett's multiple comparison test. Data are shown as Mean±SD, n=3 independent experiments.

(D) Itgb1 surface levels in WT, USP12/46-dKO, SNX17-KO, and USP12/46/SNX17-tKO fibroblasts transiently expressing indicated combinations of constructs determined by flow cytometry. Statistical analysis was carried out by RM two-way ANOVA with Dunnett's multiple comparison test. Data are shown as Mean±SD, n=3 independent experiments.

Figure 4. USP12/46-WDRs complex prevents lysosomal degradation of Itgb1.

(A) *Itgb1* mRNA levels in WT and USP12/46-dKO fibroblasts determined by qPCR. Statistical analysis was carried out by RM one-way ANOVA with Dunnett's multiple comparison test. Data are shown as Mean±SD, n=3 independent experiments.

(B, C) WB (**B**) and densitometric quantification (**C**) of Itgb1 protein levels in WT and USP12/46-dKO fibroblasts at indicated time points after cycloheximide (CHX) treatment (5 μg/ml). Gapdh served as a loading control. Statistical analysis was carried out by ordinary one-way ANOVA with Dunnett's multiple comparison test. Data are shown as Mean±SD, n=3 independent experiments.

(D) Quantification of surface Itgb1 degradation kinetics in WT and USP12/46-dKO fibroblasts. The amount of Itgb1 remaining over indicated times were measured by capture-ELISA. Statistical analysis was carried out by ordinary one-way ANOVA with Dunnett's multiple comparison test. Data are shown as Mean±SD, n=3 independent experiments.

(E) Quantification of surface Itgb1 degradation kinetics in WT fibroblasts stably expressing EGFP, and USP12/46-dKO fibroblasts stably expressing EGFP-USP12^{WT} or EGFP-USP12^{C48S} determined by capture-ELISA. Statistical analysis was carried out by ordinary one-way ANOVA with Dunnett's multiple comparison test. Data are shown as Mean±SD, n=3 independent experiments.

(F, G) The internalization rate (**F**) and the recycling rate (**G)** of Itgb1 in USP12/46-dKO fibroblasts stably expressing EGFP-USP12^{WT} or EGFP-USP12^{C48S} determined by capture-ELISA. Statistical analysis was carried out by two-sided Welch's *t*-test. Data are shown as Mean±SD, n=3 independent experiments.

(H, I) WB (**H**) with densitometric quantification (**I**) of Itgb1 protein levels in lysates of WT and USP12/46-dKO fibroblasts treated with DMSO, MG132 (0.5 uM) or BafA1 (40 nM) for 9 hours. Gapdh served as a loading control. Statistical analysis was carried out by RM two-way ANOVA with Dunnett's multiple comparison test. Data are shown as Mean±SD, n=3 independent experiments.

(J) Itgb1 surface levels in WT, USP12/46-dKO and SNX17-KO fibroblasts treated with DMSO or BafA1 (40 nM) for 9 hours determined by flow cytometry. Statistical analysis was carried out by RM two-way ANOVA with Šidák's multiple comparison test. Data are shown as Mean±SD, n=3 independent experiments.

(K) Representative immunofluorescence (IF) images of Itgb1 and Lamp1 in WT and USP12/46-dKO fibroblasts treated with DMSO or BafA1 (100 nM) for 3 hours. Arrowheads show the accumulation of Itgb1 in Lamp1-positive endo/lysosomes. Boxes indicate magnified

cell regions displayed in the Zoom panel. Sum intensity projections from confocal stacks are presented. Scale bar, 10 µm.

(L) Superplots showing the Pearson correlation coefficients (PCC) between Itgb1 and Lamp1 in WT and USP12/46-dKO fibroblasts. Statistical analysis was carried out by RM two-way ANOVA with Šidák's multiple comparison test. Data are shown as Mean±SD, n=3 independent experiments; 49 cells were analyzed in DMSO-treated WT cells, 43 in BafA1-treated WT cells, 52 in DMSO-treated USP12/46-dKO cells and 45 in BafA1-treated USP12/46-dKO cells.

Figure 5. The USP12/46-WDRs complex deubiquitinates Itgb1 and prevents Itgb1 degradation via the ESCRT pathway.

(A) WB of Itgb1 protein levels in WT and USP12/46-dKO fibroblasts transfected with control non-targeting siRNA (CTL) or siRNAs targeting jointly HGS and TSG101 (ESCRT-KD). Gapdh served as a loading control. Representative images from 3 independent experiments are shown.

(B) IP of denatured Itgb1 from WT, USP12/46-dKO and Itgb1-KO fibroblast lysates with or without ESCRT-KD and analyzed by WB for Ubiquitin (Ub) and Itgb1. Itgb1-KO served as a negative control. Gapdh served as a loading control. Representative images from 3 independent experiments are shown.

(C) IP of ubiquitinated proteins in WT and USP12/46-dKO fibroblasts with or without ESCRT-KD and analyzed by WB for Itgb1. Gapdh served as a loading control. Representative images from 3 independent experiments are shown.

(D) Amino acid sequence of Itgb1 cytoplasmic tail. The ubiquitin-conjugated lysines detected by MS are colored in red. The underlined regions indicate the NPxY motifs that bind to Talin, Kindlin and SNX17. See also supplementary table S1.

(E) IP of denatured Itgb1 from WT and USP12/46-dKO fibroblasts overexpressing HA-tagged Ub^{WT}, Ub^{K48R} or Ub^{K63R} treated with or without ESCRT-KD siRNAs and analyzed by WB for HA and Itgb1. Gapdh served as a loading control. Representative images from 3 independent experiments were shown.

(F) *In vitro* deubiquitination assay using recombinant WDR48-WDR20-USP12 (WT or C48S) complex, UCHL5 or USP7 and ubiquitinated Itgb1 enriched from USP12/46-dKO$^{ESCRT-KD}$ fibroblast cell lysate followed by WB for ubiquitin. BSA served as a negative control. Representative images from 3 independent experiments were shown.

(G) Representative Structured Illumination Microscopy (SIM) images of Itgb1 and Ub in USP12/46-dKO fibroblasts stably expressing EGFP-USP12 treated with or without ESCRT-KD siRNAs. Boxes indicate magnified cell regions displayed in the Zoom panel. Arrowheads show the Itgb1-labeled focal adhesion sites and arrows show the direction of line profiles. Scale bar, 10 µm.

(H-J) Superplots showing the PCC between Ub and EGFP-USP12 (**H**), Ub and Itgb1 (**I**), and Itgb1 and EGFP-USP12 (**J**) in USP12/46-dKO fibroblasts stably expressing EGFP-USP12 and treated with or without ESCRT-KD siRNAs. Statistical analysis was carried out by two-sided Welch's *t*-test. Data are shown as Mean±SD, n=3 independent experiments, in total 42 cells per condition.

Figure EV5. The ubiquitin-ESCRT pathway mediates Itgb1 degradation.

(A) Densitometric quantification of Itgb1 proteins levels in Fig. 5A. Statistical analysis was carried out by RM two-way ANOVA with Šidák's multiple comparison test. Data are shown as Mean±SD, n=3 independent experiments.

(B) Itgb1 surface levels in WT and USP12/46-dKO fibroblasts treated with or without ESCRT-KD siRNAs determined by flow cytometry. Statistical analysis was carried out by RM two-way ANOVA with Šidák's multiple comparison test. Data are shown as Mean±SD, n=3 independent experiments.

(C) Surface Itgb1 degradation kinetics in WT and USP12/46-dKO fibroblasts treated with or without ESCRT-KD siRNAs measured by capture-ELISA. Statistical analysis was carried out by RM two-way ANOVA with Šidák's multiple comparison test. Data are shown as Mean±SD, n=3 independent experiments.

(D) Quantification of Itgb1 ubiquitination levels in Fig. 5B. The intensity of the Ub signals was normalized to the intensity of the IP-ed Itgb1 signals. Statistical analysis was carried out by RM two-way ANOVA with Šidák's multiple comparison test. Data are shown as Mean±SD, n=3 independent experiments.

(E) Quantification of Itgb1 ubiquitination levels in Fig. 5C. The intensity of the IP-ed Itgb1 signals was normalized to the intensity of the input Itgb1 signals. Statistical analysis was carried out by RM two-way ANOVA with Šidák's multiple comparison test. Data are shown as Mean±SD, n=3 independent experiments.

(F) Quantification of Itgb1 ubiquitination levels in Fig. 5E. The intensity of the HA signals was normalized to the intensity of the IP-ed Itgb1 signals. Statistical analysis was carried out by RM two-way ANOVA with Dunnett's multiple comparison test. Data are shown as Mean±SD, n=3 independent experiments.

(G) Coomassie-blue staining of recombinant proteins used in the *in vitro* de-ubiquitination assay. MS was used to determine the identity of the protein bands indicated in the DUB complexes. Band1, WDR48; band2, WDR20; band3, a cleaved WDR20; band4, USP12.

(H) Quantification of Itgb1 ubiquitination levels in Fig. 5F. The intensity of the Ub signals was normalized to the intensity of the IP-ed Itgb1 signals. Statistical analysis was carried out by RM two-way ANOVA with Dunnett's multiple comparison test. Data are shown as Mean±SD, n=3 independent experiments.

Figure 6. Itgb1 ubiquitination is required for Itgb1 sorting into the endosomal lumen.

(A) Amino acid sequence alignments of the cytosolic tails of WT α5β1 integrin ($\alpha5^{WT}\beta1^{WT}$) and mutant $\alpha5^{KR}\beta1^{KR}$ where lysine residues were substituted for non-ubiquitinable arginine residues.

(B) Representative IF images of exogenous human Itga5 (h-Itga5) and Lamp1 in BafA1-treated Itgb1-KO^{WT} and Itgb1-$KO^{USP12/46\text{-}dKO}$ fibroblasts. Itgb1-KO cells were retrovirally transduced with human $\alpha5^{WT}\beta1^{WT}$ or $\alpha5^{KR}\beta1^{KR}$ integrins. A human specific Itga5 antibody was used for IF. Boxes indicate magnified cell regions displayed in the Zoom panel. Arrowheads indicates the colocalization of h-Itga5 with Lamp1. Sum intensity projections from confocal stacks are shown. Scale bar, 10 µm.

(C) Superplots showing the PCC between Itgb1 and Lamp1 in fibroblasts as described above. Statistical analysis was carried out by ordinary two-way ANOVA with Šidák's multiple comparison test. Data are shown as Mean±SD, n=3 independent experiments; 48 cells were analyzed in $\alpha5^{WT}\beta1^{WT}$-expressing Itgb1-KO^{WT} cells, 44 in $\alpha5^{KR}\beta1^{KR}$-expressing Itgb1-KO^{WT} cells, 52 in $\alpha5^{WT}\beta1^{WT}$-expressing Itgb1-$KO^{USP12/46\text{-}dKO}$ cells and 55 in $\alpha5^{KR}\beta1^{KR}$-expressing Itgb1-$KO^{USP12/46\text{-}dKO}$ cells .

(D) Human Itga5 surface levels in DMSO- or BafA1-treated cells as described above. Statistical analysis was carried out by RM two-way ANOVA with Šidák's multiple comparison test. Data are shown as Mean±SD, n=3 independent experiments.

(E) Human Itga5 surface levels in cells as described above treated with or without ESCRT-KD siRNAs. Statistical analysis was carried out by RM two-way ANOVA with Šidák's multiple comparison test. Data are shown as Mean±SD, n=3 independent experiments.

Figure 7. The USP12/46-WDRs complex promotes cancer cell migration and invasion.

(A) Quantification of cell adhesion of WT and USP12/46-dKO fibroblasts at indicated time points after seeding on FN-coated plates. Statistical analysis was carried out by RM one-way ANOVA with Dunnett's multiple comparison test at the 30-minute time point. Data are shown as Mean±SD, n=4 independent experiments.

(B) Cell spreading area of WT and USP12/46-dKO fibroblasts on FN-coated glass surface shown at indicated time points after seeding. Statistical analysis was carried out by RM one-way ANOVA with Dunnett's multiple comparison test at the 120-minute time point. Data are shown as Mean±SD, n=4 independent experiments.

(C) Normalized wound healing area of WT and USP12/46-dKO fibroblasts on FN-coated plates after 12 hours. Statistical analysis was carried out by RM one-way ANOVA with Dunnett's multiple comparison test. Data are shown as Mean±SD, n=4 independent experiments.

(D, E) Representative images (**D**) and quantification (**E**) of WT and USP12/46-dKO MDA-MB-231 cells upon migration through transwell inserts 16 hours after seeding. Scale bar, 200 µm. Statistical analysis was carried out by RM one-way ANOVA with Dunnett's multiple comparison test. Data are shown as Mean±SD, n=4 independent experiments.

(F, G) Representative images (**F**) and quantification (**G**) of WT and USP12/46-dKO MDA-MB-231 cells upon migration through Matrigel-coated transwell inserts 16 hours after seeding. Scale bar, 200 µm. Statistical analysis was carried out by RM one-way ANOVA with Dunnett's multiple comparison test. Data are shown as Mean±SD, n=4 independent experiments.

(H, I) Kaplan Meier-plot of overall survival (**H**) **a**nd progression free interval (**I**) of breast cancer patients with high (red line) or low (blue line) combined total *USP12* and *USP46* gene expression levels. The GDC TCGA dataset obtained from the UCSC Xena project (Goldman *et al*, 2020) was used. Two-group risk model with cut-off at the median was applied. *P*-values were calculated by Log-rank test.

Figure EV6. USP12 and USP46 are not favorable for prognosis in cancer patients.

(A) Representative images of the *in vitro* wound healing assay showing WT and USP12/46-dKO fibroblasts migrating on FN-coated 2D surfaces at 0 and 12 hours. Lines mark the leading edge of cell migration towards the wound. Scale bar, 200 µm.

(B-E) Kaplan Meier-plot of the overall survival (**B, D**) and progression free interval (**C, E**) of breast cancer patients with high (red line) or low (blue line) gene expression *USP12* (**B, C**) or *USP46* (**D, E**) levels. The GDC TCGA dataset obtained from the UCSC Xena project (Goldman *et al.*, 2020) was used. Two-group risk model with cut-off at the median was applied. *P*-values were calculated by Log-rank test.

Materials & Methods

Cell culture

HAP1 cells (C859, Horizon Discovery) were cultured in IMDM medium (#31980030, Gibco) supplemented with 10% FBS (#A5256701, Gibco). RPE1 cells (CRL-4000, ATCC), Hela cells (CCL-2, ATCC), MDA-MB-231 cells (HTB-26, ATCC) and mouse kidney fibroblasts (Böttcher *et al*, 2012) in DMEM (#61965059, Gibco) supplemented with 10% FBS (#A5256701, Gibco). All cells were cultured at 37 ºC with 5% CO_2 and routinely tested for mycoplasma.

CRISPR screen

The CRISPR screen for human DUBs was carried out as previously described (Paulmann *et al*, 2022) with slight modifications. Briefly, $3x10^6$ HAP1 cells lentivirally transduced (lentiCas9-blast) to stably express the Cas9 protein (Sanjana *et al*, 2014) and cultured in the presence of 8 ug/ml protamine sulfate were retrovirally transduced with pooled sgRNA library targeting 98 DUBs and 5 genes essential for cell survival with 3 sgRNAs per gene and contained 12 non-targeting sgRNAs (Paulmann *et al.*, 2022). Mutagenized HAP1 cells were cultured for one week, sorted for GFP expression by flow cytometry and expanded for another week. Subsequently, $40x10^6$ cells were harvested, resuspended in 0.4 ml FACS buffer (PBS containing 2% FBS and 2.5 mM EDTA), stained with PE-labeled anti-Itgb1antibody (#303004, Biolegend) for 45 minutes on ice, washed twice with ice-cold PBS, fixed with BD Cytofix™ Fixation Buffer (#554655, BD) for 10 minutes on ice and then for 10 minutes at room temperature (RT). The fixed cells were stored in FACS buffer supplemented with 0.01% sodium azide at 4 °C in the dark before cells were sorted with a FACSAriaIII flow cell sorter. Prior to loading onto the sorter, cells were stained with Hoechst 33343 (#H1399, Thermofisher) for 30 minutes on ice and haploid cells were gated based on the Hoechst signal followed by forward and sideward gating, and finally gating 5% high and 5% low PE-positive Itgb1 expressing cell populations.

Genomic DNA from the 5% high and 5% low populations was extracted followed by the amplification of the sgRNA cassettes by a two-step PCR approach and by adding adapters and sample barcodes for deep sequencing. PCR products were sequenced on an Illumina NextSeq 500 instrument and the fastq output files were analyzed on the Galaxy platform (Galaxy, 2022) using the instances at usegalaxy.eu. Reads were mapped into the sgRNA library and the count

table were analyzed with MAGeCK packages. Figure was generated using the R software with the packages tidyverse, ggplot and ggrepel.

Generation of cell lines

The Crispr-Cas9 technique was used to generate knockout (KO) clones of USP12, USP46, WDR48, WDR20 and SNX17 following published protocols (Ran *et al*, 2013). The vector pSpCas9(BB)-2A-Puro (PX459) V2.0 (a gift from Feng Zhang, Addgene plasmid # 62988) was used to express the gRNA and Cas9. The gRNA sequences and primers for genomic DNA amplification and sequencing are listed in Table 1.

The gene disruptions were confirmed by sequencing the genomic DNA regions which were targeted by the gRNAs or Western blot if specific antibodies were available. Itgb1-KO fibroblasts were generated by adding adenoviral Cre to Itgb1-floxed fibroblasts derived from the kidneys of adult Itgb1-floxed mice (Böttcher *et al.*, 2012).

To express ectopic integrin, Itgb1-null fibroblasts were retrovirally transduced with cDNAs encoding human Itgb1 and Itga5. WT or nullizygous USP12, USP46 and WDR48 cells were reconstituted by retrovirally transducing the cells with cDNA constructs tagged with EGFP, mScarlet or 3XFlag tags, respectively, as indicated in the Results section. To generate cells stably expressing miniTurbo-tagged Itga5, Itgb1-floxed fibroblasts were retrovirally transduced with the human Itga5 tagged with the miniTurbo DNA at the 3'-end.

Genes	**gRNA target sequence**	**Forward primer for genomic DNA amplification**	**Reverse primer for genomic DNA amplification**	**Sequencing primer**
human *USP12*	TCTTGTGATGAACTTCTTAG	GCAGTTTGGGAATACCTGCTAC	GTGCTGGAATTATGGCACACTA	GCAGTTTGGGAATACCTGCTAC
human *USP46*	TATTGCGGACATCCTTCAGG	TAACCACCTTCTCCTTTCCAGA	GTTTCACAGTTCAAGCATCGAG	TAACCACCTTCTCCTTTCCAGA
mouse *Usp12*	TTTACAGGGCGCCAATGCCT	TTTGCTGTAACTTGAGTGTGGC	TTTGCTGTGAGAATTCTGTTGC	TTTGCTGTGAGAATTCTGTTGC
mouse *Usp46*	GCCGTTCCGGGAGAATGTGT	ATTTTGAGGCTACACAGAACCG	GCAGTTTGGAAACACATGCTAC	ATTTTGAGGCTACACAGAACCG
mouse *Wdr20*	GACCGCCTCTGCTTCAATGT	CGAGATTAAGACCCAATTCACCA	GGCCCACTCAAAAGTACAAGTG	CGAGATTAAGACCCAATTCACCA

mouse *Wdr48*	ACATACCGAGT CCATGATGA	GCACCTCACCT TATTTCCTTTG	AGGGTCTTCTTG ACCCCATTAT	AGGGTCTTCTTGA CCCCATTAT
mouse *Snx17*	CTCCATGACAT CGTCGTCAT			

Table 1. gRNA targeting sequences and primers for genomic PCR and Sanger sequencing for specified genes.

Plasmids and siRNAs

The mouse USP12, USP46, WDR48 cDNAs were reverse transcribed from mouse kidney fibroblasts and cloned into pEGFP-C1 and pRetroQ-C1 vectors (Clontech). The mouse WDR20 cDNA was prepared as described above and cloned into pEGFP-N1 (Clontech). The cDNAs encoding catalytically inactive $USP12^{C48S}$ and $USP46^{C44S}$ and binding deficient $USP12^{E190K}$, $USP12^{V279A/F287A}$, $USP12^{E190K/V279A/F287A}$, $WDR48^{K214E/W256A/R272D}$ and $WDR20^{F262A/W306A}$ were generated by site-directed mutagenesis and cloned into pEGFP-C1 and pRetroQ-C1 vectors (Clontech). The cDNAs encoding $WDR48^{1-580}$ and $WDR48^{1-359}$ deletion mutants were amplified from the $WDR48^{WT}$ cDNA and cloned into the pRetroQ-C1 vector. The Itgb1 and Itga5 cDNAs carrying lysine for arginine substitutions in the cytoplasmic domain ($Itgb1^{8xKR}$ and $Itga5^{4xKR}$) were previously generated by site-directed mutagenesis (Böttcher *et al.*, 2012) and cloned into the HSC1 retroviral vector (a gift from James Ellis, Addgene plasmid # 58254). The cDNA encoding miniTurbo tagged Itga5 was generated by fusing the miniTurbo tag (a gift from Alice Ting, Addgene plasmid # 107168) in frame to the 3' end of the human Itag5 cDNA (a gift from Rick Horwitz, Addgene plasmid # 15238) and subsequently cloned into pRetroQ-N1 vector. The cDNAs encoding Ub-WT (a gift from Ted Dawson, Addgene plasmid # 17608), Ub-K48R (a gift from Ted Dawson, Addgene plasmid # 17604) and Ub-K63R (a gift from Cecile Pickart, Addgene plasmid # 18898) were cloned into pEGFP-N1 vector (Clontech).

Depletion of USP9X was carried out with siRNAs pools targeting human (L-006099-00-0005, Dharmacon) and mouse USP9X (L-046869-01-0005, Dharmacon) in mouse fibroblasts, RPE-1, Hela and MDA-MB-231 cells. The transduced cells were detached, 48 hours later, washed twice with PBS, seeded on PLL-coated 12-well plates in DMEM supplemented with 10% FBS or in FN-coated 12-well plates in serum replacement medium (Benito-Jardon *et al*, 2017) containing 46.5% AIM-V medium (#12055, Gibco), 5% RPMI-1640 medium (#61870, Gibco), 1% Non-essential amino acid (NEAA,#11140, Gibco) and 47.5% DMEM medium (Nr.9007.1, Carl Roth) and cultured overnight at 37 ºC. The surface levels of Itgb1 were assessed by flow cytometry and the total levels by Western blot.

To disrupt the ESCRT function, a co-depletion was performed using siRNAs targeting HGS (L-055516-01-0005, Dharmacon) and TSG101 (L-049922-01-0005, Dharmacon) (Lobert *et al*, 2010). A non-targeting siRNA (D-001810-10-05, Dharmacon) was used as control.

Transient transfection and viral transduction

Cells were transfected with plasmids using Lipofectamine 2000 or with siRNA using Lipofectamine RNAiMAX following the manufacturer's protocol (Invitrogen). Viral transduction of expression constructs to generate stable cell lines was carried out as described previously (Theodosiou *et al*, 2016).

Antibodies and reagents

The following antibodies were used for Western blot: α5 integrin (#4705, Cell Signaling Technology, 1:1,000), human β1 integrin (Clone 18, BD biosciences, 1:1,000), mouse β1 integrin (homemade, 1: 10,000) (Azimifar *et al*, 2012), GAPDH (CB1001, Calbiochem, 5,000), Flag (clone M2, Sigma, 1:1,000), GFP (A10262, Invitrogen, 1:1,000), SNX17 (10275-1-AP, Proteintech, 1:1,000), haemagglutin (HA)-tag (clone 3F10, Roche, 1:1,000), WDR48 (sc-514473, Santa Cruz Biotechnology, 1:500), WD20 (sc-100900, Santa Cruz Biotechnology, 1:500), HGS (10390-1-AP, Proteintech, 1:1,000), TSG101 (sc-7964, Santa Cruz Biotechnology, 1:1,000), ubiquitin (clone P4D1, Cell Signaling Technology, 1:1,000), RFP (PM005, MBL Life Science, 1:1,000).

The following antibodies were used for flow cytometry analysis: mouse β_1 integrin (HMbeta1-1, Biolegend, 1:400), mouse α_5 integrin (5H10-27, BD Pharmingen, 1:400), human β_1 integrin (Ha2/5, BD Pharmingen, 1:400), human α_5 integrin (IIA1, BD Pharmingen, 1:400).

The following antibodies were used for immunofluorescence (IF): mouse β_1 integrin (homemade, 1:5,000) (Azimifar *et al.*, 2012), human α_5 integrin (VC5, BD biosciences, 1:400), mouse lamp1 (1D4B, DSHB, 1:400), ubiquitin (UBCJ2, Enzo Life Sciences, 1:200). Fluorophore-conjugated secondary antibodies: donkey anti-rat Alexa 488 (A21208, Invitrogen, 1:400), goat anti-rabbit Alexa 568 (A11036, Invitrogen, 1:400), donkey anti-mouse Alexa 568 (A10037, Invitrogen, 1:400), donkey anti-mouse Alexa 647 (A31571, Invitrogen, 1:400).

The following chemicals were used: TRITC-conjugated phalloidin (P1591, Sigma, 1:4,000 for staining); Hoechst 33342 (#H1399, ThermoFischer), N-ethylmaleimide (E-3876, Sigma); protease inhibitor cocktail (4693159001, Roche); DMSO (042780.AK, ThermoFisher); MG132 (474787, Sigma); bafilomycin A1 (BVT-0252, Adipogen); cycloheximide (sc-3508A, Santa Cruz); mytomycin C (M4287, Sigma); Poly-L-lysine solution (PLL, P4707, Sigma).

Proximity-dependent biotin identification

To perform proximity-dependent biotin identification, Itgb1 floxed and Itgb1-KO cells stably expressing miniTurbo-tagged Itga5 were cultured in three 15-cm dishes, grown to 80% confluence, incubated with 50 µM biotin in PBS solution for 30 minutes at 37 ºC, washed twice with PBS and then incubated with DMEM for a further 10 minutes. After cells were washed twice with PBS, lysates were generated with lysis buffer (0.1% SDS, 0.1% SDC, 1% Triton, 150 mM NaCl, 50 mM Tris, pH=8) containing protease inhibitor cocktail, then incubated with streptavidin magnetic beads (Cytiva) for 2.5 hours at 4 ºC. The beads were washed three times with lysis buffer, once with PBS to remove detergent and then incubated in SDC buffer comprising of 1% sodium deoxycholate (SDC, Sigma), 40 mM 2-chloroacetamide (CAA, Sigma), 10 mM tris (2-carboxyethyl) phosphine (TCEP; ThermoFisher), and 100 mM Tris, pH 8.0 at 37 °C. After a 20-minute incubation at 37 °C, the samples were diluted at a 1:2 ratio with MS grade water (VWR), the proteins digested overnight at 37 °C with 0.5 µg of trypsin (Promega) and the resulting supernatant containing the peptide mixture harvested using a magnetic rack, acidified with trifluoroacetic acid (TFA; Merck) to achieve a final concentration of 1% and desalted using SCX StageTips. The samples were eluted, vacuum-dried and reconstituted in LC-MS grade water containing 0.1% formic acid before being loaded onto Evotips (Evotip Pure, Evosep).

A LC-MS/MS system coupled to a timsTOF Pro mass spectrometer (Bruker) was used to analyze the peptides. Evotips eluates were applied onto a 15-cm column (PepSep C18 15cmx15cm, 1.5 µm, Bruker Daltonics) utilizing the Evosep One HPLC system. The column temperature was set to 50 °C, peptide separation was achieved with the 30 SPD (samples per day) method, eluted and directly introduced into the timsTOF Pro mass spectrometer (Bruker Daltonics) via the nanoelectrospray interface. Data acquisition on the timsTOF Pro instrument was performed via the timsControl software. The MS functioned in data-dependent PASEF mode, performing one survey TIMS-MS scan and ten PASEF MS/MS scans per acquisition cycle. Analysis spanned a mass scan range of 100-1700 m/z and an ion mobility range from 1/K0 = 0.85 Vs cm-2 to 1.35 Vs cm-2, with uniform ion accumulation and ramp time of 100 milliseconds each in the dual TIMS analyzer, achieving a spectra rate of 9.43 Hz. Precursor ions suitable for MS/MS analysis were isolated within a 2 Th window for m/z < 700 and 3 Th for m/z > 700 by promptly adjusting the quadrupole position as precursors eluted from the TIMS device. Collision energy was adapted based on ion mobility, commencing at 45 eV for 1/K0 = 1.3 Vs cm-2 and decreasing to 27 eV for 0.85 Vs cm-2. Collision energies were

interpolated linearly between these thresholds and remained constant above or below them. Uniquely charged precursor ions were filtered out employing a polygon filter mask, and supplementary m/z and ion mobility details were harnessed for 'dynamic exclusion' to avert the re-evaluation of precursors once they attained a 'target value' of 14500 a.u.

The MaxQuant computational platform (version 2.2.0.0) (Cox & Mann, 2008) was used to analyze the raw data with typical configurations tailored for Orbitrap or ion mobility data. Essentially, the peak list was cross-referenced against the Uniprot database of mus musculus (downloaded in 2023). Cysteine carbamidomethylation was designated as a fixed modification, while methionine oxidation and N-terminal acetylation were considered variable modifications. Protein quantification across runs was performed utilizing the MaxLFQ algorithm.

Flow cytometry

To assess surface integrin levels, cells were trypsinized, washed with cold PBS, incubated with FACS antibodies diluted 1:400 in PBS supplemented with 1% BSA for 30 minutes on ice in the dark, washed with cold PBS and analyzed using the BD LSRFortessa^{TM} X-20 Cell Analyzer. The geometric mean fluorescence intensity of each sample was then evaluated using the FlowJo software version 10.10.

Cell surface proteome

Cells were cultured in three independent 6-cm dishes at approximately 80% confluence. Cells were surface biotinylated with 0.2 mg/ml EZ-Link™ Sulfo-NHS-SS-Biotin (21217, ThermoFisher) in cold PBS for 30 minutes at 4 ºC. Cell lysates were generated by incubating cells in lysis buffer (0.1% SDS, 0.1% SDC, 1% Triton, 150 mM NaCl, 50 mM Tris, pH=8) with protease inhibitor cocktail. The cell lysate was then incubated with Streptavidin Mag Sepharose beads (Cytiva#28985799) for 2.5 hours at 4 ºC. The beads were washed three times with lysis buffer and once with PBS to remove detergent. Proteins on beads were digested by trypsin and the peptides were prepared as described above for proximity-dependent biotin identification. MDA-MB-231 samples were analyzed on the Brucker TimsTOF Pro with procedures and parameters as described above. Mouse fibroblast samples were analysed on an ThermoFisher QExactive HF mass spectrometer. Peptides were chromatographically separated using a 30-cm analytical column (inner diameter: 75 microns), packed in-house with ReproSil-Pur C18-AQ 1.9-micron beads from Dr. Maisch GmbH. This separation was achieved through a 60-minute gradient ranging from 8% to 30% buffer composed of 80% acetonitrile and 0.1% formic acid. The mass spectrometer operated in a data-dependent mode, with survey scans

spanning from 300 to 1650 m/z at a resolution of 60,000 (at m/z = 200). It selectively picked up to 10 of the top precursors for fragmentation using higher energy collisional dissociation (HCD) with a normalized collision energy of 28. MS2 spectra were acquired at a resolution of 30,000 (at m/z = 200). Automatic gain control (AGC) targets for both MS and MS2 scans were set to 3E6 and 1E5, respectively, with maximum injection times of 100 ms for MS scans and 60 ms for MS2 scans. The raw data was analyzed as described above in proximity-dependent biotin identification.

Quantitative PCR

Total RNA was extracted from fibroblasts using TRIzol™ Reagent (15596026, Invitrogen) following the manufacturer's instructions. cDNA was synthesized using iScript™ cDNA Synthesis Kit (1708896, Bio-Rad), followed with real-time PCR using iQ SYBR Green Supermix (#1708880, Bio-Rad) on LightCycler® 480 (Roche). Primers for GAPDH: forward 5'-AGGTCGGTGTGAACGGATTTG-3', reverse 5'- TGTAGACCATGTAGTTGAGGTCA-3'. Primers for Itgb1: forward 5'- ATGCCAAATCTTGCGGAGAAT-3', reverse 5'-TTTGCTGCGATTGGTGACATT-3'.

Western blot

Cells were lysed in RIPA buffer (0.1% SDS, 0.1% SDC, 1% Triton, 150 mM NaCl, 50 mM Tris, pH=8) containing protease inhibitor cocktail. Protein concentrations were determined using the BCA assay kit (#23225, ThermoFisher), lysates were boiled at 95 °C for 5 minutes in 1x Laemmli buffer, resolved on SDS-PAGE gels and transferred to 0.45 um PVDF membranes (IPVH00010, Millipore). After transfer, the membranes were briefly washed with PBS containing 0.1% Tween-20 (PBST) for 5 minutes before incubation with 5% BSA in PBST for 1 hour at RT, incubated with primary antibodies overnight at 4 ºC , washed in PBST and then incubated with HRP-conjugated secondary antibodies for 1 hour at RT. A GE Amersham AI600 imager was used to detect the chemiluminescence generated upon addition of Immobilon Western Chemiluminescent HRP substrate (Millipore#WBKLS0500) to the membranes and Image Lab version 6.1 was used to quantify densitometries.

Integrin degradation, internalization and recycling assays

These assays were carried out as previously described (Böttcher *et al.,* 2012).

Immunoprecipitation

The GFP-based immunoprecipitation (GFP IP) was carried out as previously described with slight modifications (Chen *et al*, 2022). In brief, cells were lysed in lysis buffer (50 mM Tris-HCl, 150 mM NaCl, 1 mM EDTA, 1% Triton, protease inhibitor cocktail) and the supernatant was incubated with GFP nano-trap beads (gta, Chromotek) for 2 hours at 4 °C. The beads were washed three times with the lysis buffer, then boiled in 2x Laemmli buffer, separated onto SDS–PAGE followed by WB for detecting the indicated proteins.

Itgb1 *in vivo* crosslinking co-IP

Fibroblasts grown 15-cm dish to 80% confluence were siRNA-treated for 48 hours, washed with PBS twice, incubated on ice, then incubated with cross-linker (DSP, 0.1 mg/ml in PBS) solution or PBS for 30 minutes on ice, washed and quenched with quenching solution (50 mM Tris, pH 7.4, 150 mM NaCl, 1 mM $MgCl_2$, 1 mM $CaCl_2$). Cells were lysed in lysis buffer (50 mM Tris-HCl, 150 mM NaCl, 1 mM EDTA, and 1% Triton), the lysates were sonicated and cleared by centrifugation. The supernatant was incubated with anti-β1 integrin antibody (homemade) and protein A/G agarose beads (sc-2003, Santa Cruz) for 3 hours at 4 °C. The beads were washed with lysis buffer three times and one more time with PBS to remove the detergent. Peptides were prepared and processed on the MS as described above for proximity-dependent biotin identification. Raw data were analyzed using the Spectronaut 18.0 in directDIA+ (library-free) mode with the peak list was cross-referenced against the Uniprot database of mus musculus (downloaded in 2023). Cysteine carbamidomethylation was designated as a fixed modification, while methionine oxidation and N-terminal acetylation were considered variable modifications. Protein quantification across samples was achieved via label-free quantification (MaxLFQ) at the MS2 level.

Ubiquitination assay

To measure endogenous ubiquitinated Itgb1, fibroblasts cultured in a 15-cm dish at approximately 80% confluence in the presence of 10% FBS were treated with non-targeting siRNA or siRNA simultaneously targeting mouse HGS and TSG101 (ESCRT-KD) for 48 hours. Cells were collected by scraping with PBS supplemented with 20 mM N-ethylmaleimide. Cell pellets were then lysed with 100 ul of 1% SDS in PBS and immediately boiled for 10 minutes to denature the proteins. The lysate was then diluted with 900 ul lysis buffer (1% Triton, 150 mM NaCl, 50 mM Tris, pH=8, 1 mM EDTA, 20 mM N-ethylmaleimide) supplemented with the protease inhibitor cocktail. The diluted lysate was further sonicated and cleared by centrifugation. The supernatant was then incubated with anti-β1 integrin antibody (homemade)

and protein A/G agarose beads for 3 hours at 4 °C. The beads were then boiled in 2x Laemmli buffer, eluted and the elute was Western blotted for ubiquitin and Itgb1. Alternatively, cells were lysed in RIPA buffer (0.1% SDS, 0.1% SDC, 1% Triton, 150 mM NaCl, 50 mM Tris, 20 mM N-ethylmaleimide, pH=8) with protease inhibitor cocktail. The cell lysate was then incubated with the ubiquitin selector beads (N2510, NanoTag) for 3 hours at 4 °C to enrich for ubiquitinated proteins. Then the beads were boiled in 2x Laemmli buffer and the elute was subjected to SDS–PAGE followed by WB for Itgb1.

To assess the ubiquitination sites on Itgb1 cytoplasmic tail, the ubiquitin selector beads samples were prepared as above and peptides on the beads were prepared and analyzed by MS as described above for proximity-dependent biotin identification.

To determine the ubiquitin linkage specificity of Itgb1, fibroblasts were cultured in 15-cm dish to 80% confluence, transfected with constructs expressing HA tagged Ub^{WT}, Ub^{K48R} or Ub^{K63R} in the presence or absence of ESCRT-KD siRNA for 48 hours, harvested, followed by Itgb1 immunoprecipitation as described above. The beads were boiled in 2x Laemmli buffer, eluted and the elute was subjected to SDS–PAGE followed by WB for HA and Itgb1.

For the *in vitro* deubiquitination assay, USP12/46 dKO fibroblasts cultured in a 15-cm dish 80% confluence were treated with or without ESCRT-KD siRNA for 48 hours. Cells were harvested, Itgb1 was immunoprecipitated using the anti-β1 integrin antibody (homemade) coupled protein A/G agarose beads. The agarose beads were incubated with 100 nM recombinant USP12-WDRs complexes (generated as described below), recombinant UCHL5 (NBP1-72315, Novus Biologicals) or USP7 (E-519-025, Novus Biologicals) in a reaction buffer containing 40 mM Tris, 0.5 mM EDTA, 100 mM Nacl. 0.1% BSA, 1 mM TCEP (PH=7.4) for 30 minutes at 37 °C with constant shaking at 900 rpm in a thermal mixer. The beads were washed three times with washing buffer (1% Triton, 150 mM NaCl, 50 mM Tris, 1 mM EDTA, pH=8), boiled in 2x Laemmli buffer, eluted and the elute was subjected to SDS–PAGE followed by WB for ubiquitin and Itgb1.

Expression and purification of recombinant proteins

Full-length recombinant WDR20 (1-569aa) N-terminally tagged with His6 was expressed in *E.coli.*, and WDR48 (1-580 aa) N-terminally tagged with Strep-tag II together with untagged $USP12^{WT}$ and $USP12^{C48S}$ (both 40-370aa) were expressed in insect cells as reported previously (Li *et al*, 2016) using the pCoofy expression vectors (a gift from Sabine Suppmann, Addgene plasmid # 43974) and purified to approximately 80% purity followed previously published protocols (Aretz *et al*, 2023). The purified USP12-WDR48 complex was incubated with

WDR20 overnight to form the ternary DUB complex that was purified by size-exclusion chromatography. The purity of the recombinant proteins was verified by SDS-PAGE followed with Coomassie staining and MS.

Immunofluorescence microscopy

Cells were grown overnight on FN-coated (5 µg/ml) coverslips that were kept in a 12-well plate ($1x10^5$ per well), fixed with 4% PFA for 15 minutes at RT, and permeabilized with 0.1% Triton X-100 for 10 minutes at RT. Cells were blocked with 5% BSA for 1 hour at RT, incubated with primary antibodies overnight at 4 ℃, then with secondary antibodies (1:400 dilution) for 1 hour at RT and finally mounted in Elvanol No-Fade™ Mounting Medium.

Images were captured by the Zeiss LSM780 confocal laser scanning microscope or by the Zeiss Elyra PS.1 structured illumination microscope using ZEN software (Black version). Pearson correlation coefficient (PCC) analysis was performed using Fiji ImageJ software with the EzColocalization plug-in (Stauffer *et al*, 2018).

Adhesion, spreading and wound healing assays

The adhesion and spreading assays were performed as previously described (Theodosiou *et al.*, 2016) with slight modifications. Briefly, fibroblasts were starved for 4 hours in DMEM without FBS. Then the cells were trypsinized and incubated for a further 1 hour at 37 °C in DMEM supplemented with 3% BSA. The starved cells were then seeded on 96-well plates (40,000 per well) coated with either Poly-L-Lysine (PLL, P4707, sigma, 1:10 dilution) or fibronectin (5 µg/ml) or 3% BSA and incubated for 5, 10, 20 and 30 minutes at 37 °C, vigorously washed with PBS, fixed in 4% PFA, stained with 0.1% Crystal Violet solution and then dissolved in 2% SDS. The OD value of each well was acquired by a plate reader at 595 nm. Adhesion capacity was normalized using the equation: Normalized OD_{595}= (OD_{FN}-OD_{BSA})/ OD_{PLL}.

For the spreading assay, the starved cells were seeded on FN-coated (5 µg/ml) glass coverslips and incubated at 37 °C for indicated time. Cells were then fixed in 4% PFA and stained with TRITC-conjugated phalloidin (1:4,000, 2 hours at RT) and Hoechst 33342 (1:10,000, 10 minutes at RT). Images were captured by the LSM780 confocal microscope and at least 45 cells per time point were analyzed for cell spreading area using Fiji ImageJ software.

For the wound healing assay, cells were seeded on FN-coated (5 µg/ml) 24-well plate containing a 2-well silicone insert (81176, ibidi) with a cell-free gap of approximately 500 µm overnight ($1x10^4$ cells per well). Then the insert was removed, cells were briefly washed with PBS to remove cell debris and allowed to migrate for 12 hours at 37 ºC with 5% CO_2 in DMEM

supplemented with mytomycin C (5 µg/ml) to inhibit cell proliferation. The wound healing area was imaged using an EVOS FL Auto2 microscope (ThermoFisher) and measured using Fiji ImageJ software.

Transwell migration and invasion assays

Transwell chambers with 8-µm pore sized membranes (353097, Corning) and Matrigel invasion chambers with 8-µm pore sized membranes (354483, Corning) were used for migration and invasion assays, respectively. Briefly, $5x10^4$ cells in DMEM without FBS were added to the upper chamber of the inserts, while DMEM supplemented with 10% FBS was added to the lower compartment. Cells were incubated for 16 hours. Cells on the upper side of the membrane were gently scraped and washed off with PBS before the inserts were immersed in ice-cold methanol for 20 minutes at RT to fix the cells on the lower side of the membrane. The cells were then stained with 0.1% Crystal Violet solution for 20 minutes at RT, washed three times with distilled water, and then imaged using a Leica DM IL LED microscope. Cell numbers were quantified in 5 random fields using Fiji ImageJ software.

Statistics

Statistical analyses were performed using GraphPad Prism v.10 (GraphPad Software). Tests used, multi-comparison correction methods, and significance cutoff were indicated in the figure legends for each quantification. The calculated *P*-values were shown in each graph.

References

Aretz J, Aziz M, Strohmeyer N, Sattler M, Fassler R (2023) Talin and kindlin use integrin tail allostery and direct binding to activate integrins. *Nat Struct Mol Biol* 30: 1913-1924

Azimifar SB, Bottcher RT, Zanivan S, Grashoff C, Kruger M, Legate KR, Mann M, Fassler R (2012) Induction of membrane circular dorsal ruffles requires co-signalling of integrin-ILK-complex and EGF receptor. *J Cell Sci* 125: 435-448

Benito-Jardon M, Klapproth S, Gimeno LI, Petzold T, Bharadwaj M, Muller DJ, Zuchtriegel G, Reichel CA, Costell M (2017) The fibronectin synergy site re-enforces cell adhesion and mediates a crosstalk between integrin classes. *Elife* 6

Böttcher RT, Stremmel C, Meves A, Meyer H, Widmaier M, Tseng HY, Fässler R (2012) Sorting nexin 17 prevents lysosomal degradation of beta1 integrins by binding to the beta1-integrin tail. *Nat Cell Biol* 14: 584-592

Chen NP, Aretz J, Fassler R (2022) CDK1-cyclin-B1-induced kindlin degradation drives focal adhesion disassembly at mitotic entry. *Nat Cell Biol* 24: 723-736

Cox J, Mann M (2008) MaxQuant enables high peptide identification rates, individualized p.p.b.-range mass accuracies and proteome-wide protein quantification. *Nat Biotechnol* 26: 1367-1372

Galaxy C (2022) The Galaxy platform for accessible, reproducible and collaborative biomedical analyses: 2022 update. *Nucleic Acids Res* 50: W345-W351

Li H, Lim KS, Kim H, Hinds TR, Jo U, Mao H, Weller CE, Sun J, Chatterjee C, D'Andrea AD *et al* (2016) Allosteric Activation of Ubiquitin-Specific Proteases by beta-Propeller Proteins UAF1 and WDR20. *Mol Cell* 63: 249-260

Lobert VH, Brech A, Pedersen NM, Wesche J, Oppelt A, Malerod L, Stenmark H (2010) Ubiquitination of alpha 5 beta 1 integrin controls fibroblast migration through lysosomal degradation of fibronectin-integrin complexes. *Dev Cell* 19: 148-159

Paulmann C, Spallek R, Karpiuk O, Heider M, Schaffer I, Zecha J, Klaeger S, Walzik M, Ollinger R, Engleitner T *et al* (2022) The OTUD6B-LIN28B-MYC axis determines the proliferative state in multiple myeloma. *EMBO J* 41: e110871

Ran FA, Hsu PD, Wright J, Agarwala V, Scott DA, Zhang F (2013) Genome engineering using the CRISPR-Cas9 system. *Nat Protoc* 8: 2281-2308

Sanjana NE, Shalem O, Zhang F (2014) Improved vectors and genome-wide libraries for CRISPR screening. *Nature Methods* 11: 783-784

Stauffer W, Sheng H, Lim HN (2018) EzColocalization: An ImageJ plugin for visualizing and measuring colocalization in cells and organisms. *Sci Rep* 8: 15764

Theodosiou M, Widmaier M, Bottcher RT, Rognoni E, Veelders M, Bharadwaj M, Lambacher A, Austen K, Muller DJ, Zent R *et al* (2016) Kindlin-2 cooperates with talin to activate integrins and induces cell spreading by directly binding paxillin. *Elife* 5: e10130

Figure 1. The USP12/46-WDRs complex stabilizes Itgb1 protein levels.

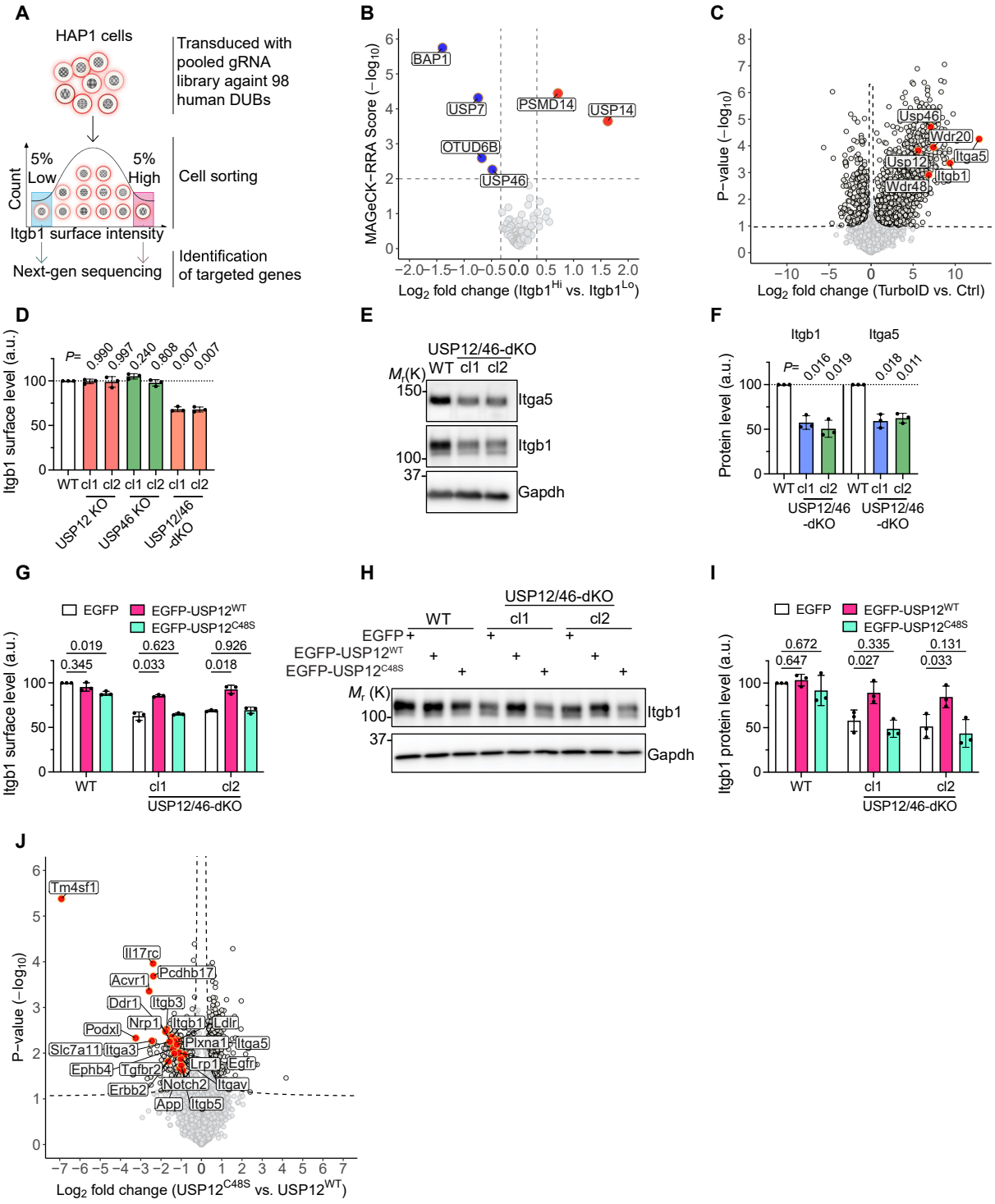

Figure EV1. The effect of USP9X-KD on integrin levels.

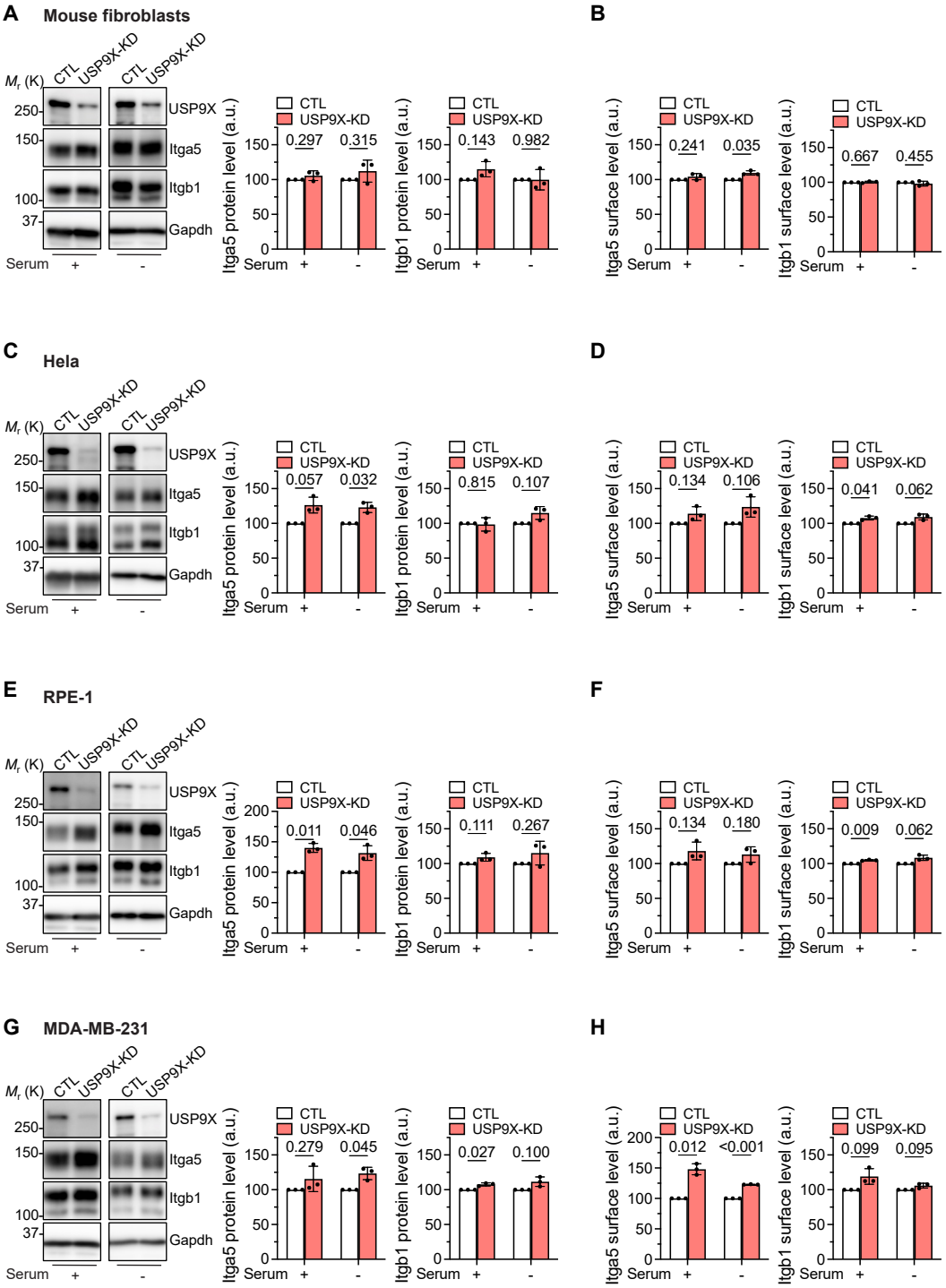

Figure EV2. Validation of KO clones.

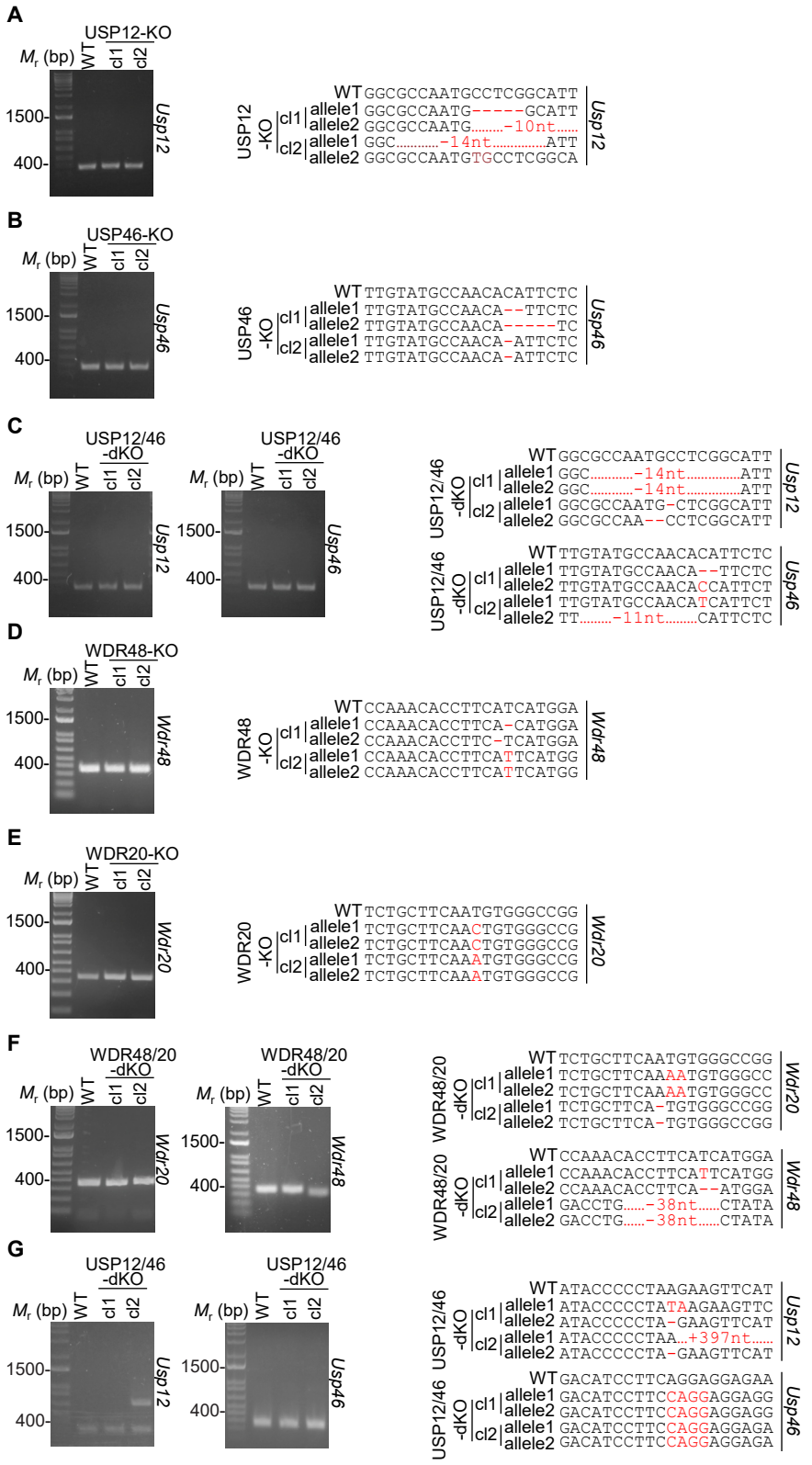

Figure EV3. The USP12/46-WDRs complex stabilizes Itgb1 protein levels.

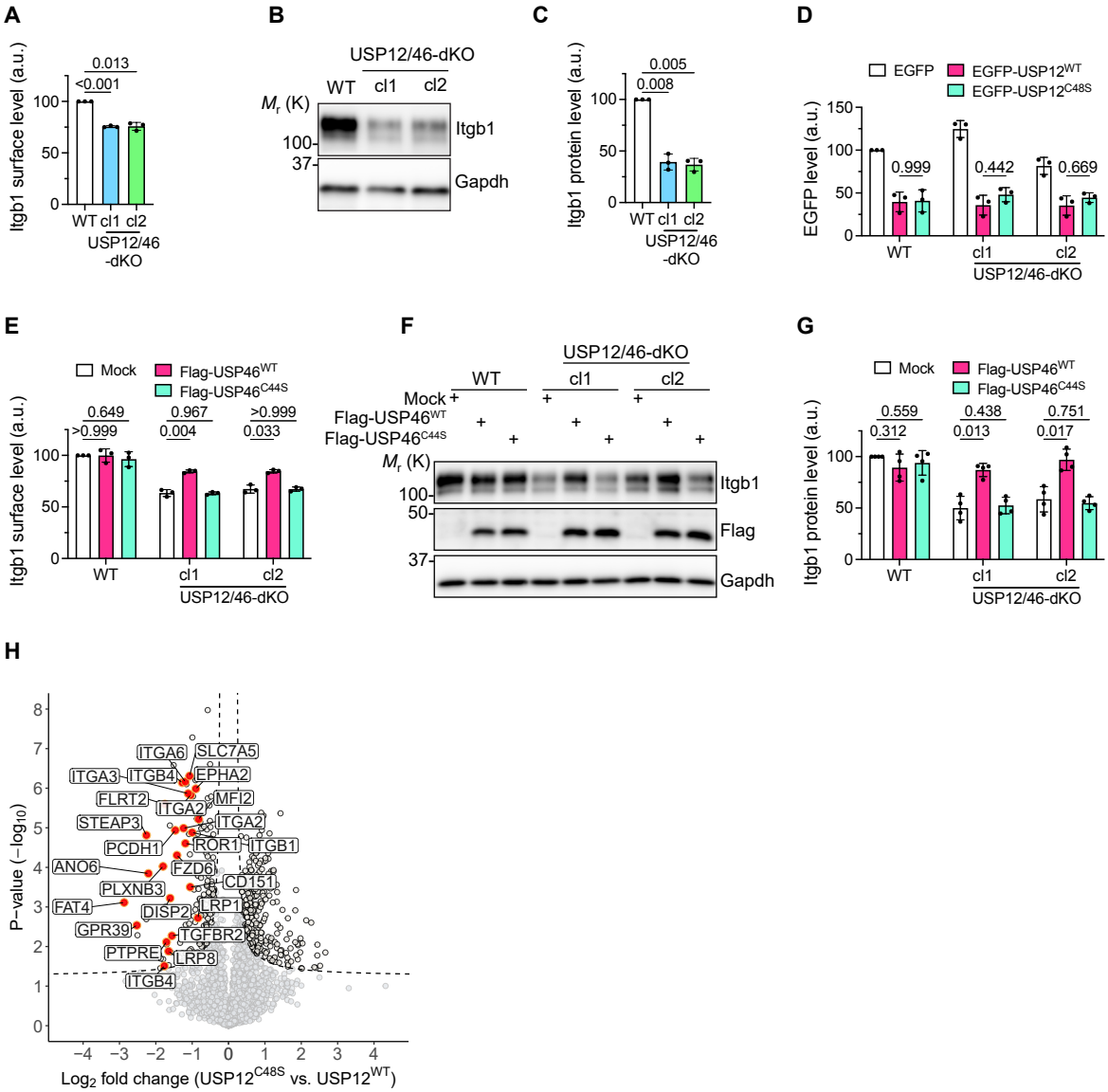

Figure 2. The integrity of the USP12/48-WDR20-WDR48 complex is required to stabilize Itgb1 protein levels.

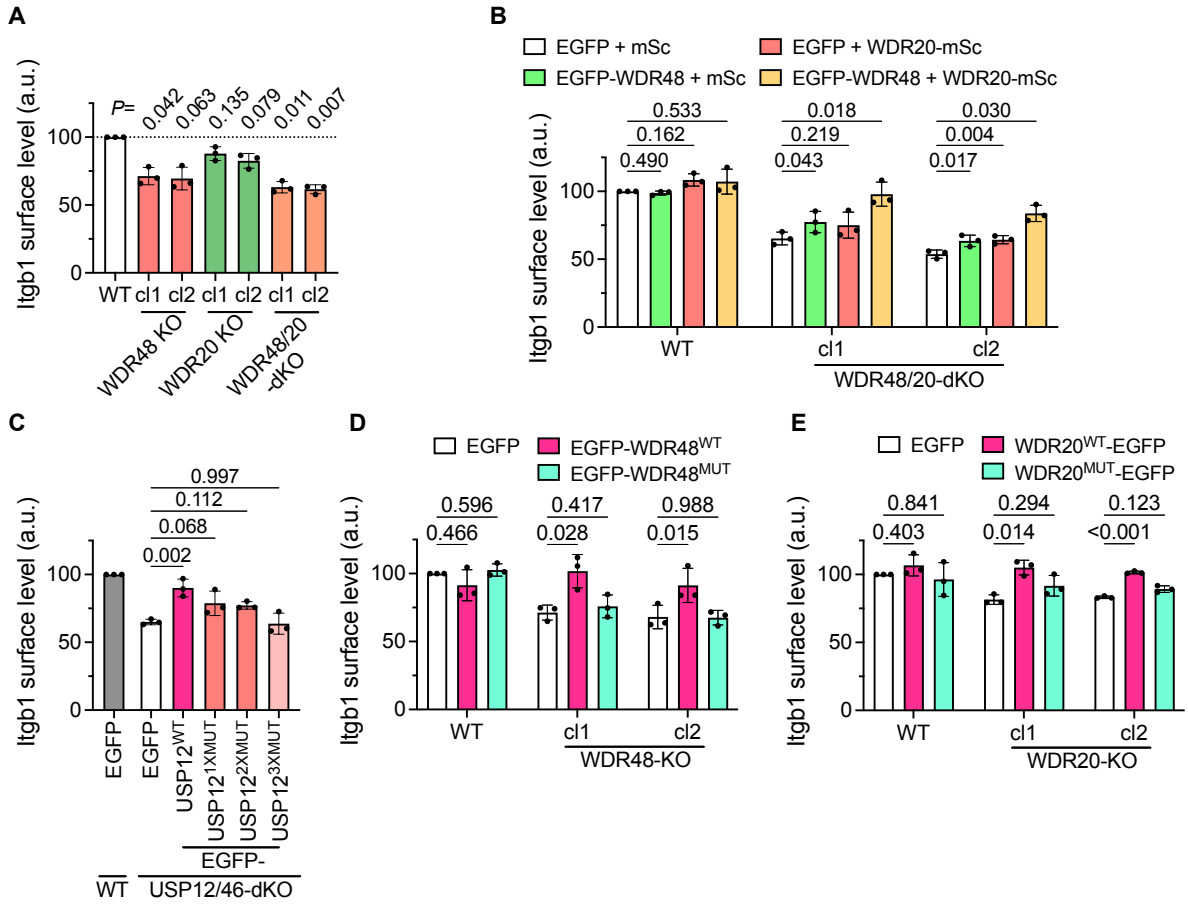

Figure EV4. Characterization of binding-deficient USP12, WDR48 and WDR20 mutants.

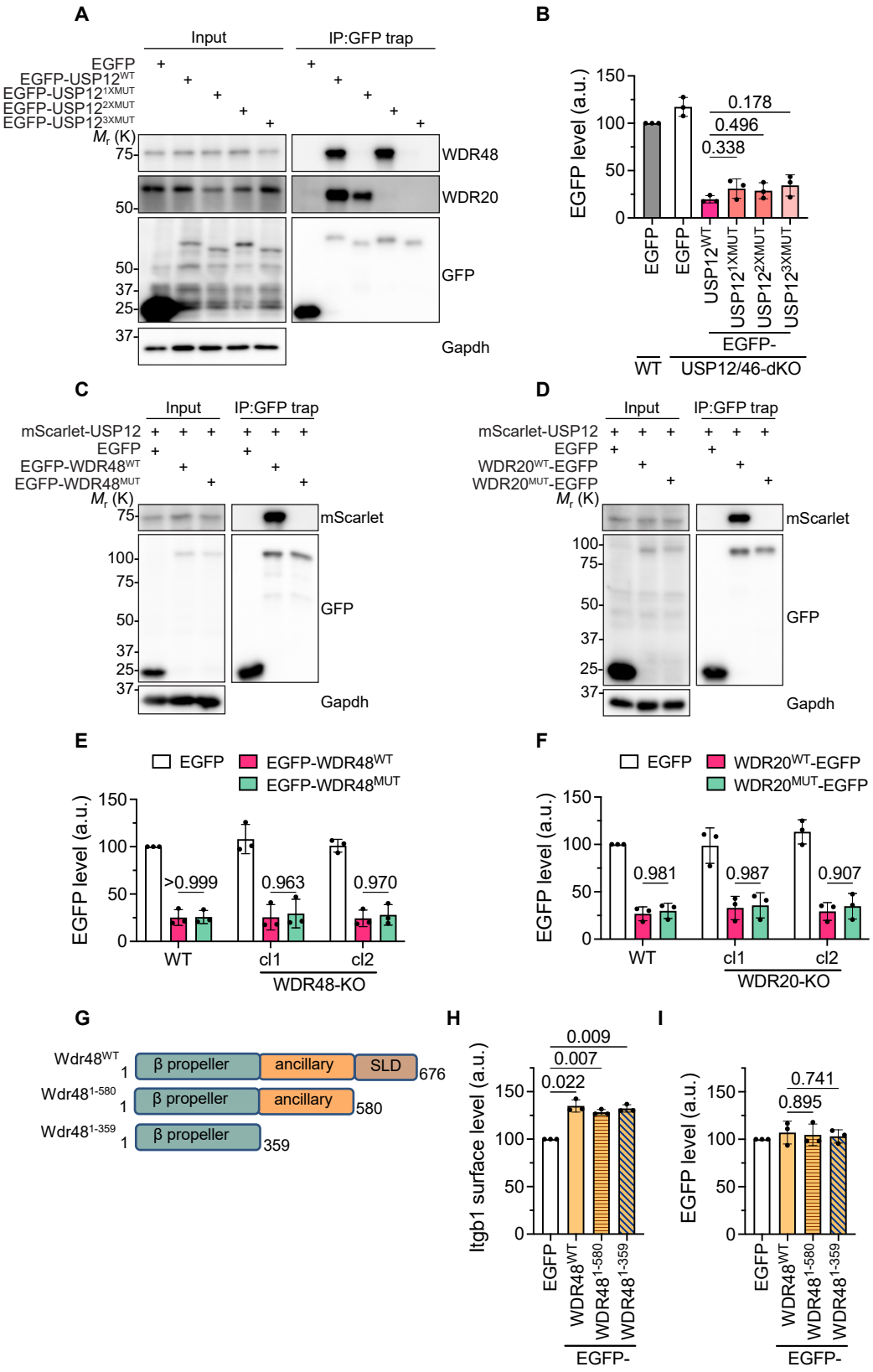

Figure 3. The USP12/46-WDRs complex stabilizes Itgb1 in a SNX17-independent manner.

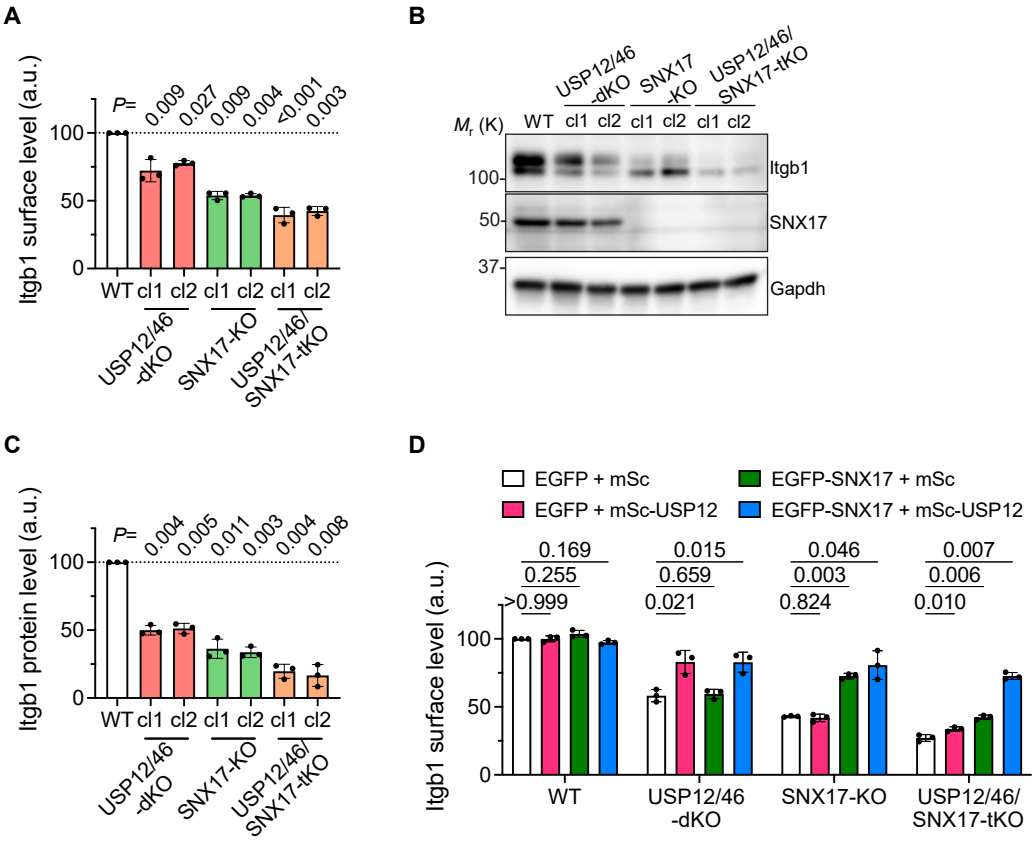

Figure 4. USP12/46-WDRs complex prevents lysosomal degradation of Itgb1.

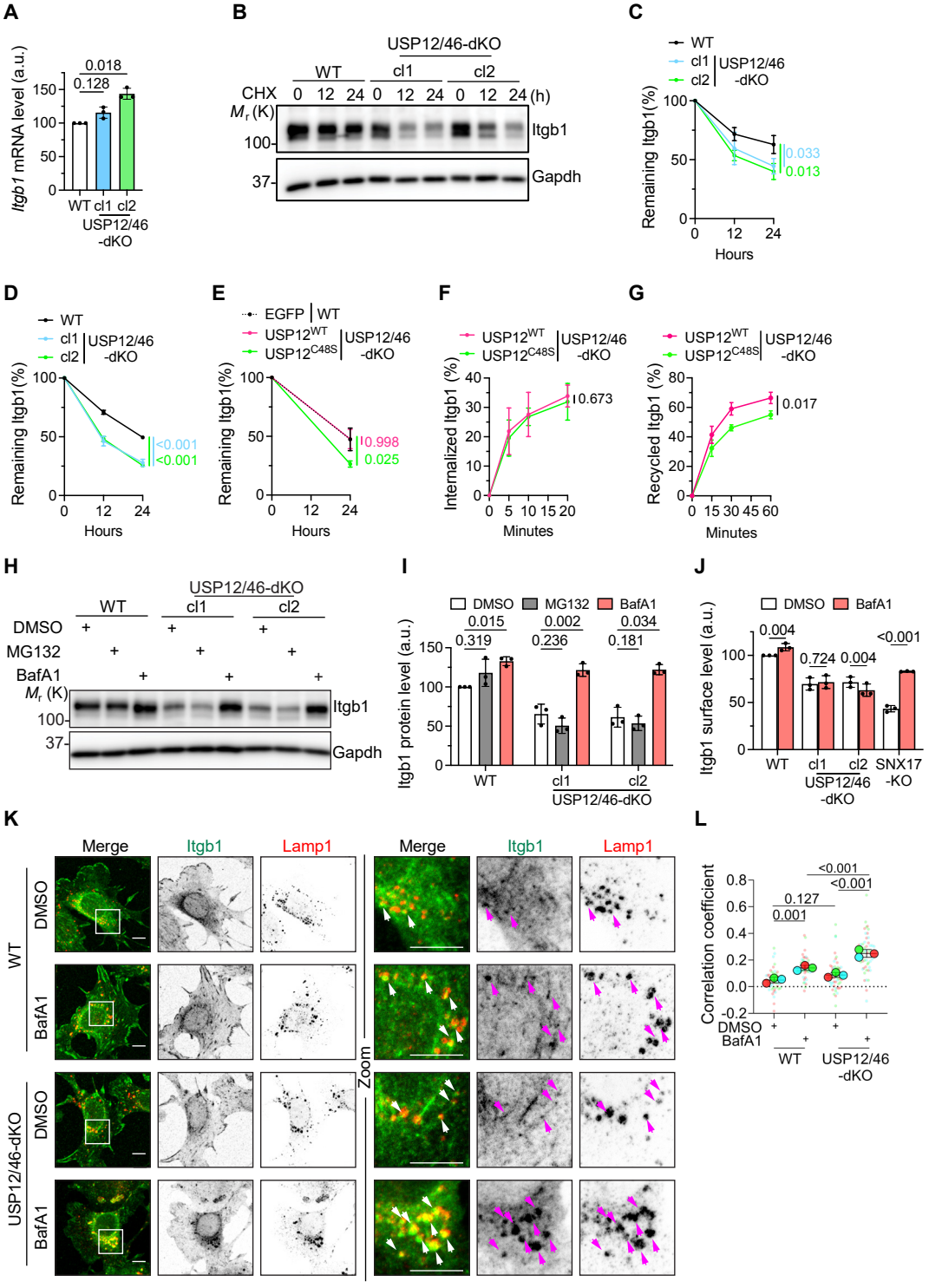

Figure 5. The USP12/46-WDRs complex deubiquitinates Itgb1 and prevents Itgb1 degradation via the ESCRT pathway.

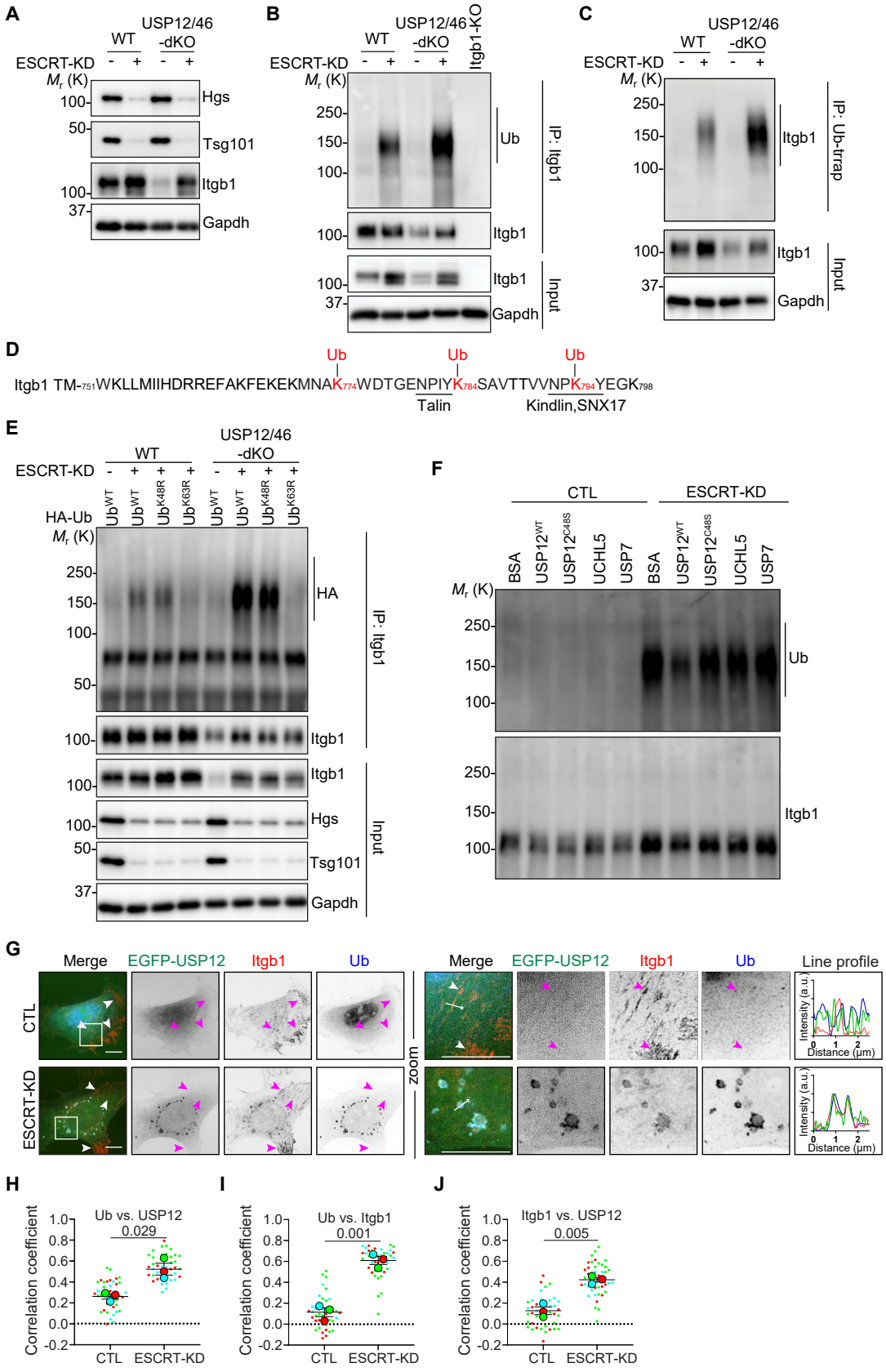

Figure EV5. The ubiquitin-ESCRT pathway mediates Itgb1 degradation.

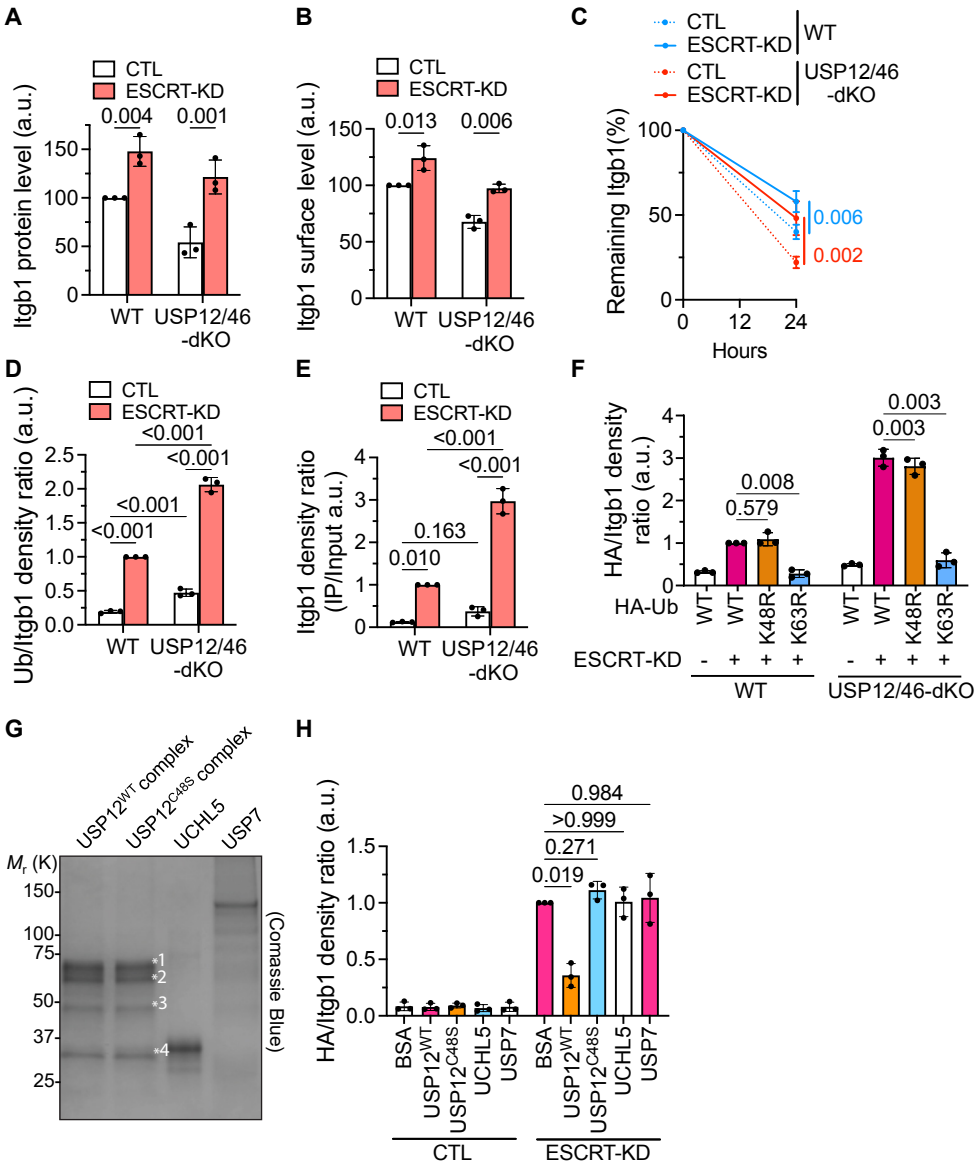

Figure 6. Itgb1 ubiquitination is required for Itgb1 sorting into the endosomal lumen.

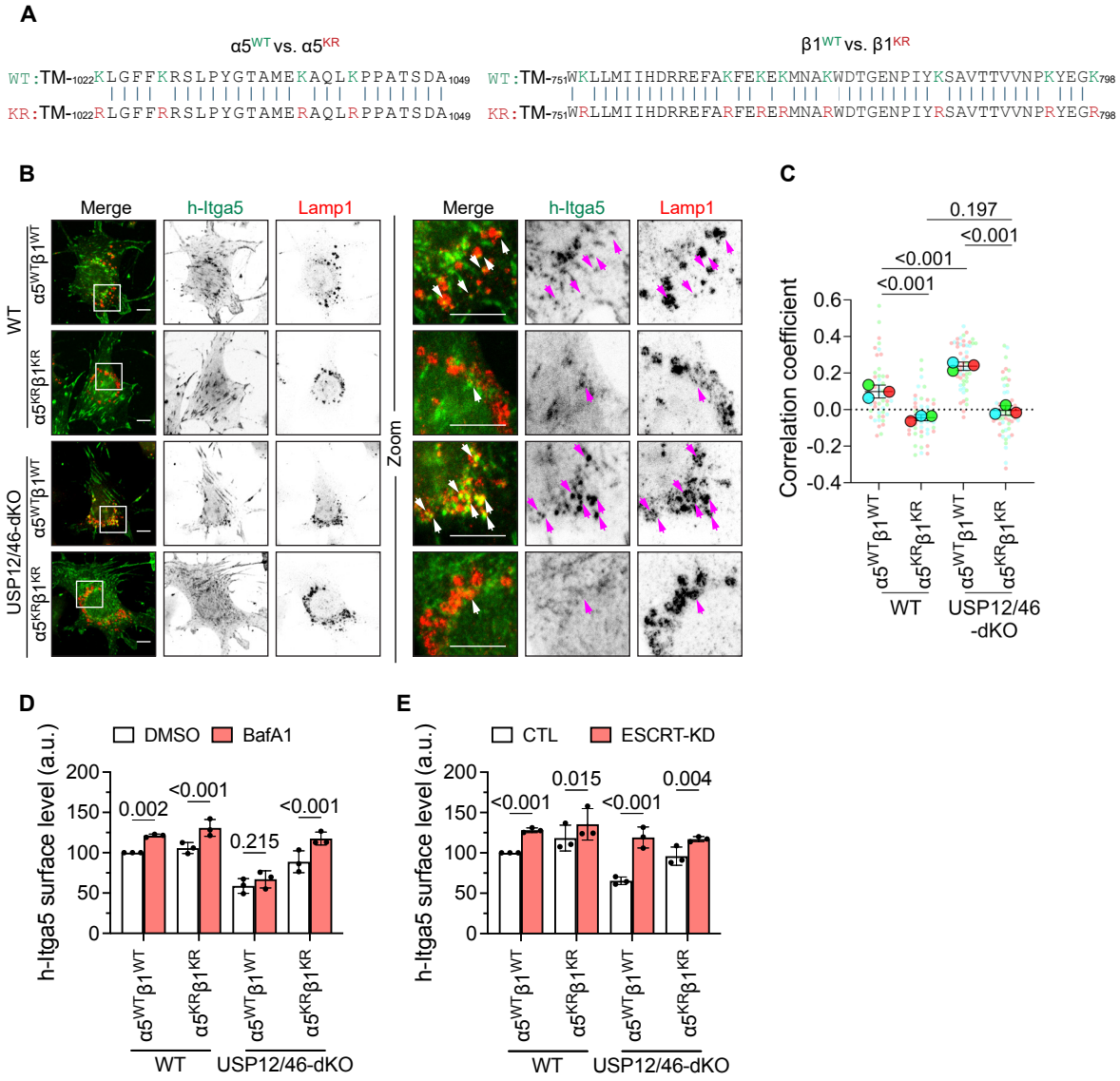

Figure 7. The USP12/46-WDRs complex promotes cancer cell migration and invasion.

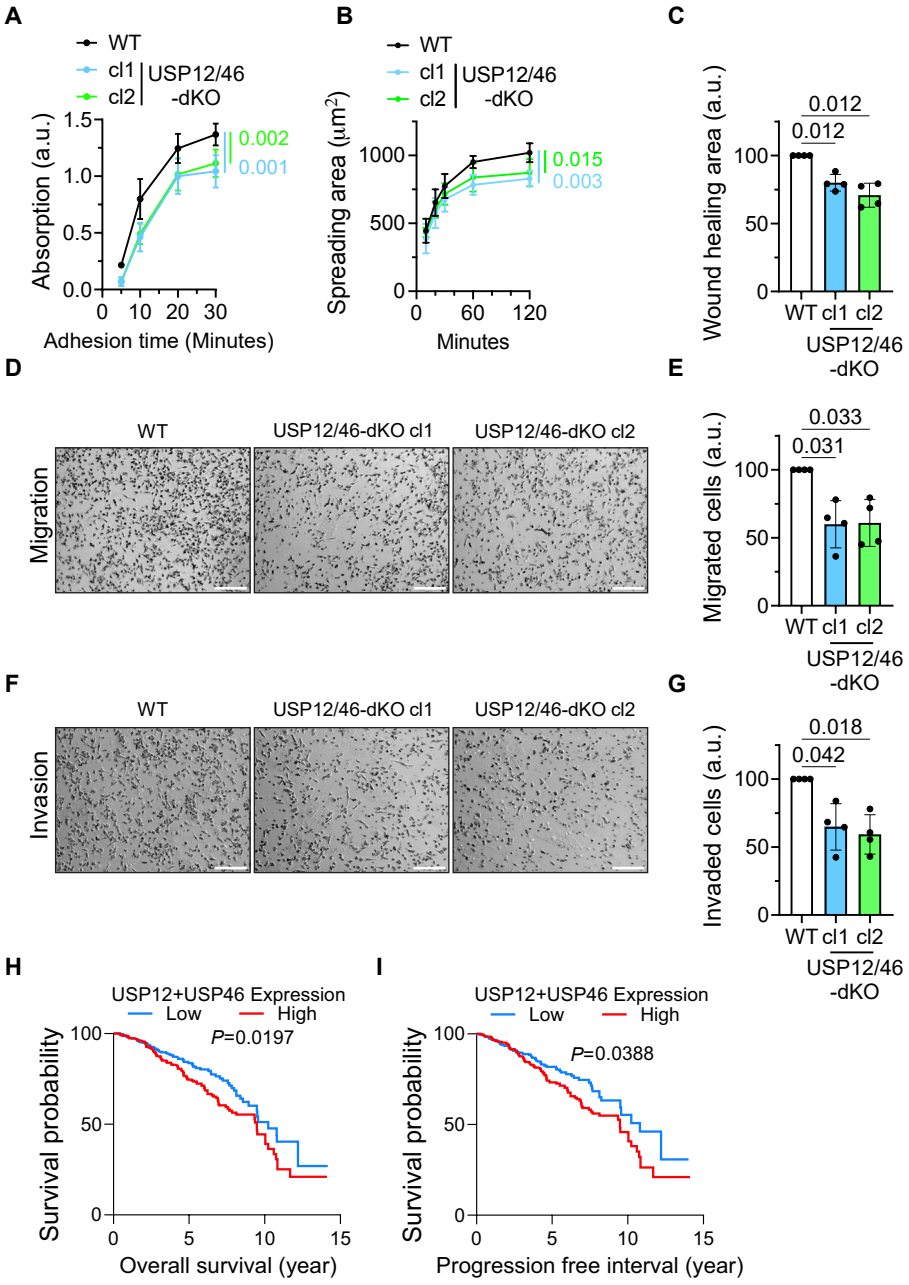

Figure EV6. USP12 and USP46 are not favorable for prognosis in cancer patients.

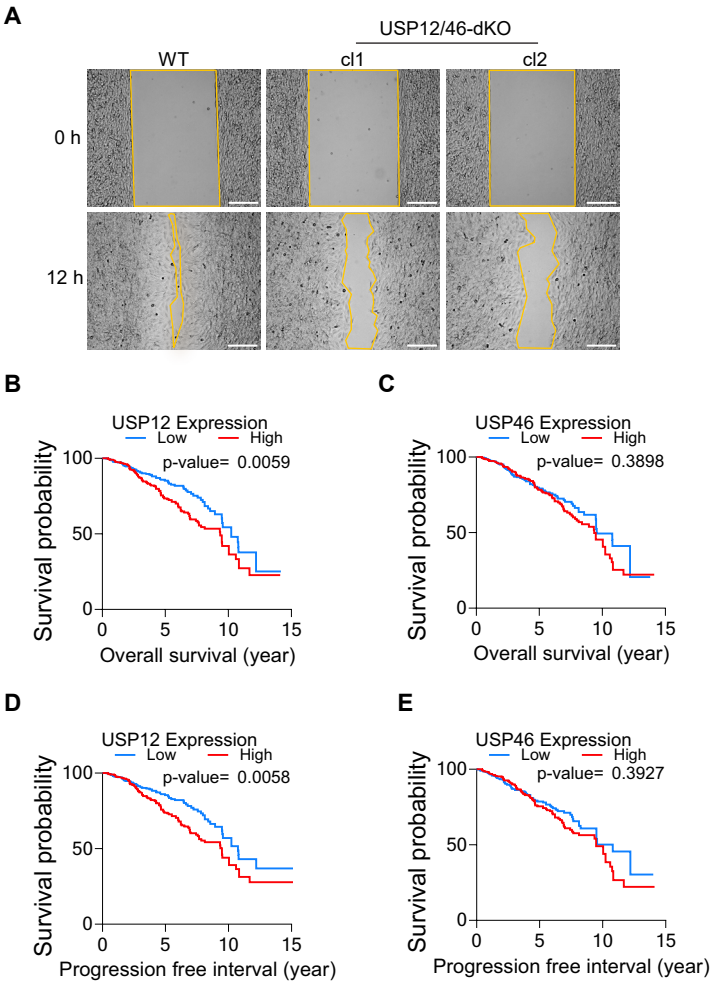

Rab7 deficiency induces lysosome formation from recycling endosomes leading to an increased degradation of cell surface proteins

Guan M. Wang[1,*], Peng Xu[2], Kaikai Yu[1], Shiny Shengzhen Guo[1] and Reinhard Fässler[1,*]

[1]Department of Molecular Medicine, Max Planck Institute of Biochemistry, Martinsried, Germany

[2]Molecular Structural Biology Group, Max Planck Institute of Biochemistry, Martinsried, Germany

[*] Correspondence: gwang@biochem.mpg.de (GW); faessler@biochem.mpg.de (RF)

Abstract

Cell surface receptors such as integrins are repeatedly internalized from and recycled back to the plasma membrane before routed to lysosomes for degradation. In search for modulators of β1 integrin surface stability, we identified the Rab7 small GTPase, believed to be required for lysosome biogenesis, as integrin stabilizer. We show that Rab7 deficiency produces late endosomes and lysosomes with acidic pH, lysosome-specific proteins and membrane architectures that are functional in protein degradation and organelle fusion. Furthermore, Rab7-deficient lysosomes form from Rab4- and transferrin receptor-positive recycling endosomes, resulting in the degradation of proteins designated for recycling. Finally, we also found that overexpression of Rab4 can direct lysosome formation from recycling endosomes in absence as well as presence of Rab7, however, the latter to a much lesser extent. Our findings reveal a lysosome biogenesis and lysosomal protein degradation pathway that becomes dominant in absence of Rab7 or when Rab4 is highly abundant.

Introduction

Eukaryotic cells have a highly dynamic endomembrane system that compartmentalizes biochemical reactions and exchanges a multitude of molecules with the extracellular environment by means of endo- and exocytosis. The organization of the endomembrane system depends on an accurately regulated trafficking of membranes, which is orchestrated by the evolutionarily conserved superfamily of small Rab GTPases[1-3] that cycle between an active, GTP-bound state and an inactive, GDP-bound state. The activity state of Rab proteins dictates their localization to specific endomembranes such as ER, Golgi, endosomes and lysosomes, and the recruitment of effector proteins that regulate membrane trafficking resulting in the biogenesis, transport, tethering and fusion of vesicles and organelles.

Integrins are ubiquitously expressed, mediate cell-extracellular matrix (ECM) and cell-cell adhesion and are α/β heterodimeric type I transmembrane receptors[4] that, once synthesized and exocytosed to the cell surface, are recycled numerous times from and back to the plasma membrane by the endosomal system before being eventually degraded by lysosomes. Integrin trafficking is controlled by several Rab GTPases family members including but not limited to Rab5, Rab4, Rab11 and Rab7[5, 6]. Rab5 governs the fusion of endocytic vesicles with the early endosomes as well as homotypic fusion of early endosome, leading to the delivery of internalized integrins and numerous other proteins to the intracellular sorting center[7, 8]. Rab4, which is also present on early endosomes, mediates cargo recycling either directly from early endosomes back to the plasma membrane or via dedicated protein recycling organelles, including the recycling endosomes ($Rab4^+$ and $Rab11^+$) and the $Rab11^+$ perinuclear recycling compartment (PNRC)[5, 9]. Transmembrane proteins destined for degradation are sorted from the endosomal limiting membrane into the endosomal lumen via the budding of intraluminal vesicles (ILVs)[10]. Endosomes with gradually accumulating ILVs are known as multivesicular bodies (MVBs) or late endosomes. The transition from early endosome to late endosomes is accompanied by the exchange of Rab5 by Rab7, acidification of the lumen, and changes in lipid and protein composition of the endosomal membrane[11-13]. Under the control of Rab7, late endosomes mature into endolysosomes by acquiring lysosomal proteins from transport carriers and finally into lysosomes, where transmembrane proteins including integrins are degraded[13, 14].

Whereas the three Rab5 isoforms (Rab5A, Rab5B, and Rab5C) or the two Rab4 isoforms (Rab4A and Rab4B) share similar subcellular localizations and functions[1, 15-17], only Rab7A is referred to as Rab7, because Rab7B shares limited similarity and no functional overlap with the evolutionarily conserved Rab7A[18-20]. Rab7A (from now on called Rab7) is ubiquitously expressed, controls the membrane protein and lipid composition of the endo-lysosomal system, and is therefore considered as the master regulator of lysosome biogenesis[13, 14], whereas Rab7B is expressed in few tissues and controls endosome-to-Golgi transport[18, 19]. Although the *Rab7* gene deletion results in embryonic lethality in mice[21, 22], frogs[23], flies[24], worms[25], as well as protozoan parasites[26], Rab7 deficiency does not impair viability of mammalian cell lines cultured *in vitro*. The grave consequences of Rab7 loss *in vivo* opposed to the normal cell viability *in vitro* points to unapparent but severe cellular dysfunction(s). So far, lack of Rab7 has been associated

58 in mammalian cells with impaired autophagy[22, 27, 28] and loss of the Rab7 ortholog Ypt7 in yeast with
59 impaired vacuole (yeast lysosome) biogenesis and impaired degradation[29, 30].
60 In the present study, we carried out an unbiased whole genome screen in the human haploid cell line
61 HAP1 to identify novel genes that regulate the stability of integrin cell surface levels. We found that
62 Rab7 loss massively decreased rather than increased total and cell surface levels of integrins as well as
63 other cell membrane proteins. In search for a mechanistic explanation for this striking finding, we found
64 a Rab7-independent pathway that becomes activated in the absence of Rab7 expression and generates
65 lysosomes from Rab4- and transferrin receptor-containing recycling endosomes.

Results

RAB7A gene stabilizes Itgb1 levels

To identify novel regulators of β1 integrin (Itgb1, encoded by the *ITGB1* gene in human and the *Itgb1* gene in mouse) trafficking we performed an unbiased genome-wide insertional mutagenesis screen in the human haploid cell line HAP1 using gene-trapping retroviruses carrying a splice acceptor site followed by the cDNA encoding the green fluorescent protein (GFP)[31, 32]. We generated 2.5 x 10^9 mutagenized HAP1 cells, which were fixed, stained with monoclonal anti-Itgb1 antibody and sorted by flow cytometry to obtain the 5% cells with the lowest and the 5% cells with the highest Itgb1 surface levels (Fig. 1a). Next, we determined the sites of gene-trap insertions by next-generation sequencing (NGS) and counted the total number of gene mutations in the Itgb1-low and -high cell populations, which revealed a high number of disruptive mutations in both cell populations. In the Itgb1-low population, we found known regulators of Itgb1 surface levels, such as *SNX17* and the SNX17-associated retriever complex consisting of *VPS26C*, *VPS29*, and *VPS35L* (Fig. 1b,c; indicated with orange dots). Expectedly, we also identified mutations in genes coding for binding partners of the retriever complex including the CCC, WASH and Arp2/3 complexes (Fig. 1b,c; indicated with blue dots), and genes required for Itgb1 maturation including the α integrin subunits that heterodimerize with Itgb1 (*ITGA2*, *ITGA4*, *ITGA6*, and *ITGAE*), proteins of the ER translocation machinery (*SEC62*), enzymes responsible for Itgb1 glycosylation (*GANAB*, *SRD5A3*, and *OSTC*) and chaperones (*HSP90B1*) (Fig. 1b,c; indicated with green dots). Against all expectations, however, we also identified *RAB7A* as a potent stabilizer of Itgb1 surface levels (Fig. 1b,c; indicated with red dot), which is in stark contrast to Rab7's established role as master regulator of lysosome biogenesis/maturation and protein degradation. We decided to investigate how loss of Rab7 expression decreases Itgb1 surface levels.

Rab7KO destabilizes the cell surface proteome including Itgb1

To confirm that an inactivating mutation of Rab7 indeed decreases rather than increases Itgb1 surface levels, we disrupted the *Rab7a* gene (Rab7KO) in mouse kidney fibroblasts and the *RAB7A* gene in several human cell lines including HAP1 (myeloid), HEK (kidney), MCF7 (breast) and U2OS (bone) using the Crispr/Cas9 technology. Loss of Rab7 expression decreased total Itgb1 levels in lysates as well as on the cell surface (Fig. 1d,e, Extended Data Fig. 1a-c) of these cells, suggesting that stabilization of Itgb1 by Rab7 is a general principle of mammalian cells. The internalization kinetics of Itgb1 was unaffected by the loss of Rab7 expression in mouse fibroblasts (Extended Data Fig. 1d), whereas the degradation kinetics of the surface Itgb1 (Extended Data Fig. 1e) and the total Itgb1 (Extended Data Fig. 1f) was enhanced in Rab7KO cells. In line with the reduced Itgb1 surface levels, adhesion, spreading and proliferation were impaired in Rab7KO cells (Extended Data Fig. 1g-i).

The decreased Itgb1 levels in Rab7KO cells were efficiently rescued upon retrovirus-mediated re-expression of the EGFP-tagged Rab7 (Fig. 1d-f). Furthermore, cells treated with Bafilomycin A1 (BafA1), which inhibits lysosomal protein degradation stabilized Itgb1, whereas MG132, which blocks

proteasomal protein degradation was without effect (Fig. 1g-i), which suggests that Itgb1 is degraded by lysosomes or lysosome-like organelles upon loss of Rab7 expression.

To investigate whether cell surface proteins other than Itgb1 are also downregulated on Rab7KO cells, we biotinylated the cell surface proteome of parental wild-type (WT) and Rab7KO mouse fibroblasts, precipitated the biotinylated proteins and compared their abundance by quantitative mass spectrometry (MS). The experiments revealed that Rab7KO cells displayed diminished surface levels of integrin family members (Itgb3, Itgb5, Itga2, Itga3, Itga5, Itga6 and Itgav) and numerous, integrin-unrelated proteins with different transmembrane topologies such as: amyloid-beta precursor protein (App), epidermal growth factor receptor (Egfr), low density lipoprotein receptor-related protein 1 (Lrp1), which are type I single-pass transmembrane proteins; transferrin receptor (Tfrc), a type II transmembrane protein and a classical marker of recycling endosomes; Piezo-type mechanosensitive ion channel component 1 (Piezo1), a multipass ion channel receptor; and Glypican-6 (Gpc6), a glycosylphosphatidylinositol(GPI)-anchored protein (Fig. 1j). These results indicate that Rab7 loss impairs a general and not integrin-specific trafficking route.

Rab7KO cells generate late endosomes and lysosomes

Our findings so far indicate that Itgb1 and numerous additional transmembrane proteins are decreased in the absence of Rab7 expression. This decrease requires functional lysosomes or lysosome-like organelles that express the integral proteins lysosomal-associated membrane protein 1 and 2 (Lamp1 and Lamp2), contain luminal lysosomal proteases such as the cathepsins that degrade substrates, establish an acidic luminal pH required for the function of lysosomal proteases, deliver substrates into the lumen for degradation and adopt a characteristic fingerprint-shaped ultrastructural morphology observed in the electron microscope (EM) as electron-dense membrane whorls[11, 12].

First, we immuno-stained Itgb1 and different lysosomal markers to reveal the subcellular localization in WT and Rab7KO fibroblasts (Fig. 2a, Extended Data Fig. 2a-c). In WT cells, Itgb1 was mainly observed in focal adhesions (FAs), ER and rarely in lysosomes. In Rab7KO cells, however, Itgb1 massively accumulated in lysosome-like structures that colocalized with Lamp1, Lamp2 and cathepsins such as cathepsin D (Ctsd), cathepsin B (Ctsb) and cathepsin L (Ctsl). An increased Pearson's correlation coefficient (PCC) of Itgb1 with Ctsd (Fig. 2b) and Itgb1 with Lamp1 (Extended Data Fig. 2d) confirmed their significant colocalization in Rab7KO fibroblasts.

To determine whether the Itgb1 remains at the limiting membrane or is delivered into the lumen of $Ctsd^{+}$ lysosomes, we tagged the cytoplasmic domain of the Itga5 subunit with the EGFP, whose fluorescent signal is pH-sensitive and quenched by ~50% when the α5β1 integrin heterodimer is present in an acidified environment that is below pKa ~5.5-6 (Fig. 2c). We chose to EGFP-tag Itga5 to avoid modification of the cytosolic tail of Itgb1, which is important for integrin activation and trafficking[33-35]. Itga5-EGFP signals were found on the cell surface and in a few endosomes of both, WT and Rab7KO cells, but were almost absent from lysosomes labeled with the Ctsd sensor Sir-Lysosome (Fig. 2d).

Since quenched EGFP can be recovered by neutralizing the pH of cells and lysosomes with NH_4Cl, we treated WT and Rab7KO cells with NH_4Cl. Whereas only marginal changes in Itga5-EGFP fluorescence intensity were observed in NH_4Cl-treated WT cells, numerous bright Itga5-EGFP puncta were recovered in Rab7KO cells, with some being labelled with and some without Sir-Lysosome (Fig. 2d, Extended Data Fig. 2e-g). This finding indicates that acidified Sir-Lysosome$^-$ late endosomes and acidified Sir-Lysosome$^+$ lysosomes are present in Rab7KO cells and contain α5β1 integrin in their acidic lumen. Consistent with our immunofluorescence (IF) data, the dramatically increased amounts of luminal Itga5-contaning late endosomes and lysosomes suggest an increased lysosome targeting of integrins in Rab7KO cells, in comparison to WT cells (Extended Data Fig. 2f,g).

Finally, we used transmission EM to delineate the morphology of the Itgb1-containing endosomes in Rab7KO cells. To this end, we labeled cell surface Itgb1 with immunogold-coupled anti-Itgb1 antibodies and allowed the integrin-antibody complex to internalize for 2 hours. In both, WT as well as Rab7KO cells, the integrin-antibody complex localized to MVBs/late endosomes structures containing multiple small single membrane vesicles in their lumen, mature lysosomes filled with membrane whorls, and hybrid organelles formed upon fusion of lysosomes with MVBs/late endosomes (resulting in endolysosomes) and autophagosomes (resulting in autolysosomes), respectively (Fig. 2e and Extended Data Fig.3a). Correlative light microscopy and cryo-electron tomography, which allow visualizing the morphology of endosomes and lysosomes in their native state, also revealed the presence of comparable endosomal and lysosomal morphologies in WT and Rab7KO cells (Fig. 2f, Extended Data Fig. 3b, Supplementary Video 1). These findings indicate that the biogenesis of lysosomes and the intraluminal delivery of substrates takes place in the absence of Rab7.

The Rab7KO lysosomes exhibit normal functions

Next, we tested whether the Rab7KO lysosomes exhibit genuine functions such as the degradation of autophagic materials and the exocytosis of the lysosomal content upon fusion with the plasma membrane. Functional lysosomes play a crucial role in macroautophagy (hereafter autophagy), a process that collects cytoplasmic materials and then delivers them to lysosomes for degradation[36, 37]. Autophagosomes, which are unable to mature into lysosomes on their own, were shown to fuse with pre-existing late-endosomes or lysosomes in a Rab7-dependent manner[36]. Interestingly, recent studies challenged these findings and suggested that Rab7 is dispensable for autophagosome-lysosome fusion but required for the degradation of the autophagosome contents under fed, however, not under starved conditions[27]. To examine whether autophagosomes fuse with Rab7KO lysosomes in our cell model, we performed the LC3-II flux assay[38]. The cytosolic LC3-I (abbreviated for microtubule-associated protein 1A/1B-light chain 3; MAP1LC3), which serves as specific marker of autophagosome formation, is lipidated to LC3-II, incorporated into the inner and outer membrane of autophagosomes and eventually degraded upon fusion with lysosomes. Hence, the LC3-II levels report the LC3-I to LC3-II transition and the LC3-II degradation, of which the latter can be blocked by BafA1. Using our cell model, we

found that in serum-cultured WT as well as Rab7KO fibroblasts, BafA1 treatment increased the LC3-II levels (Fig. 3a,b), indicating that Rab7 is dispensable for basal autophagy, autophagosome-lysosome fusion, and degradation of autophagosomal proteins. Nutrient starvation further increased LC3-II levels in BafA1-treated WT and Rab7KO cells, which suggests that the response to an autophagic signal proceeds normally in the absence of Rab7, irrespective whether cells are fed or starved (Fig. 3a,b).

In addition to degrading transmembrane proteins intracellularly, lysosomes and late endosomes also fuse with the plasma membrane and exocytose their luminal contents[39-41]. To investigate whether Rab7KO lysosomes secrete their elevated cell surface proteome content, we measured the total secretome of serum-starved WT and Rab7KO mouse fibroblasts by MS. The experiment revealed that peptides from numerous cell surface proteins including integrins (Fig. 3c; redish dots) and lysosomal enzymes such as Ctsb, Ctsd, Ctsl, Gaa, Grn, Pld3 were elevated in the Rab7KO secretome (Fig. 3c; blue dots). To obtain a general overview of molecular functions affected by the activities of the secretome components, we performed a gene ontology (GO) enrichment analysis which revealed a significant over-representation of plasma membrane proteins with GO terms “membrane raft”, “membrane microdomain”, “cell leading edge”, “myelin sheath” and “apical part of cell” (Fig. 3d). These data confirm an increased targeting of transmembrane proteins to lysosomes, and moreover, indicate that Rab7KO cells generate mature, functional lysosomes that secure protein degradation, autophagy progression and secretion of lysosomal contents.

Rab7KO lysosomes are generated from recycling endosomes

Although our findings demonstrate that Rab7KO cells generate lysosomes with genuine lysosomal properties, our experiments so far do not answer as to why cell surface proteins are increasingly targeted to lysosomes in Rab7KO cells. The identification of the membrane source for Rab7KO lysosomes and the mechanism of Itgb1 delivery to Rab7KO lysosomes is key to understand the difference between the canonical, Rab7-dependent and the Rab7-independent lysosome biogenesis pathway. A first clue to these questions came from the cell surface proteome analysis of Rab7KO cells, which revealed in addition to the decreased Itgb1 levels, a dramatic reduction of Tfrc (Fig. 1j), which is generally used as marker for recycling endosomes in WT cells. The decreased Tfrc surface levels were confirmed by flow cytometry and restored upon Rab7 expression (Extended Data Fig. 4a). Since in WT cells, Tfrc is barely sorted into late endosomes and lysosomes[42], the reduced Tfrc surface levels in Rab7KO cells pointed to a malfunction of the recycling endosome pathway and increased degradation. This hypothesis was supported by immunostaining, which demonstrated co-staining of Tfrc and Itgb1 in $Ctsd^{+}$ lysosomes and an increased PCC of Tfrc with Ctsd in Rab7KO compared to WT cells (Fig. 4a,b).

The increased lysosomal targeting of Tfrc suggests that recycling endosomes play a role in the formation of Rab7KO lysosomes. To test this hypothesis, we expressed EGFP-tagged forms of the three major Rab proteins orchestrating Tfrc recycling[9]: Rab4, which is associated with (classical) recycling endosomes; Rab5, which is associated with endocytic vesicles and early endosomes that can, to a low

extent, directly recycle surface proteins back to the plasma membrane; and Rab11, which is associated with recycling endosomes and the PNRC.

Our immunostaining revealed that Tfrc colocalized with Rab4, Rab5 and Rab11 on endosomal vesicles in WT as well as Rab7KO cells (Fig. 4c-e), indicating that Tfrc is present in all three trafficking routes irrespective whether Rab7 is expressed or not. Since the overexpressed Rab5 and Rab11 resulted in the colocalization of Tfrc with Rab5 or Rab11, however, not with Ctsd in WT as well as Rab7KO cells (Fig. 4c,d), we conclude that $Tfrc^+/Ctsd^+$ lysosomes are neither directly generated from $Rab5^+$ nor from $Rab11^+$ endosomes.

Overexpression of Rab4 resulted in colocalization of Tfrc and Rab4 on $Ctsd^-$ and $Ctsd^+$ structures of different sizes, ranging from puncta at the limit of optical resolution to large vesicular structures with a diameter up to 1µm in WT and Rab7KO cells (Fig. 4e). A thorough examination of the vesicular structures revealed that four different classes of organelles could be distinguished both, in WT and Rab7KO cells, which differed in size, in Rab4 and Ctsd signals and in the localization of Tfrc on the limiting membrane or in the lumen (Fig. 4e, box 1-4). One class of small structures showed colocalization of Tfrc and Rab4 and absence of Ctsd, which points to classical recycling endosomes (see box 1). A second class of large vesicles showed Rab4 and Tfrc colocalizing at the limiting membrane and Ctsd in the lumen both, in WT and Rab7KO cells, indicating that these structures originate upon fusion of $Rab4^+$ recycling endosomes with $Ctsd^+$ carriers (see box 2). A third class also of large vesicles showed Rab4 at the limiting membrane and Tfrc as well as Ctsd in the lumen indicating endosomal maturation with internalized, luminal Tfrc (see box 3). Finally, a fourth of small structures lacked Rab4 but was positive for Tfrc and Ctsd signals, indicating that Rab4 dissociated from the endosomal membrane during lysosome conversion (see box 4). The unconventional $Tfrc^+/Rab4^+/Ctsd^+$ endo/lysosomal organelles (class 2 and 3) resemble late endosomes/endolysosomes that are likely formed by the fusion of recycling endosomes with carriers containing lysosomal enzymes.

$Rab4^+$ late endosomes and $Rab4^+$ endolysosomes generate lysosomes

Although $Rab4^+$ late endosomes and $Rab4^+$ endolysosomes were apparent to a much lesser extent in WT compared to Rab7KO cells (Fig. 4e), we asked how we can most accurately determine their numbers in WT and Rab7 cells. The question could be addressed by determining the census of the four vesicular structures in WT and Rab7KO cells. The census determined by immunostaining, however, would produce inaccurate numbers as the transition of recycling endosomes to late endosomes and finally lysosomes is a continuous, highly dynamic process with intermediate structures in which immunosignals will be low and therefore difficult to flawlessly detect and assign to a specific class of vesicular structures. For example, Tfrc can be present at the limiting membrane as well as in the lumen at the same time, or Ctsd may initially be present at a low level that is difficult to distinguish from background noise and gradually increase during the transition to late endosomes and lysosomes.

To overcome this hurdle, we developed an image-based flux-like assay focusing on the large class 2 and class 3 donut-like structures whose limiting membrane and lumen can be optically resolved (Extended Data Fig. 4b). The measurement of Rab4, Tfrc and Ctsd immunosignals in these structures was used to deduce a quantitative transition from $Tfrc^{+}/Rab4^{+}/Ctsd^{-}$ recycling endosomes to $Tfrc^{+}/Rab4^{+}/Ctsd^{+}$ endo/lysosomal organelles. In our assay we compared the full width of a fluorescence line profile at half maximum (FWHM), which is a statistical parameter used to describe the width of a function. In our case, the function described by FWHM is a Gaussian-like distribution of fluorescence signals and represents the distance between points on the Gaussian curve (width) at half of the maximum value. Fluorescence signals emitted from the endosome lumen generate a function of a single Gaussian-like distribution (SGD), whereas fluorescence emitted at the limiting membrane generate a function of a double Gaussian-like distribution (DGD). The FWHM measurements of Tfrc and Ctsd on hundreds of class 2 and class 3 structures allows to accurately measure their size (which differs if the signal is emitted at the limiting membrane or in the lumen), the flux of membrane proteins such as Tfrc from the limiting membrane into the lumen, and the gradual accumulation of lysosomal proteases occurring in the lumen during lysosome maturation.

To obtain the quantitative FWHM assessment of Tfrc, we normalized the intensity and isotropicity of the Tfrc signal of donut-like endosomes in WT and Rab7KO cells, respectively, and then made an average projection to create a model endosome (Extended Data Fig. 4b). Since Rab4 should localize to the outer leaflet of the limiting membrane, the Rab4 signal should produce DGD profiles and the dimension of the FWHM should reflect the size of the endosome. The Ctsd signal, on the other hand, should produce SGD profiles and only be emitted from inside the lumen. Accordingly, Rab4 produced a DGD profile and an average FWHM of about 1μm and Ctsd SGD profiles and a FWHM of 0.6μm in WT as well as Rab7KO cells (Fig. 4f,g), indicating that the size of the large, donut-like endosomes is similar in both cell lines. The Tfrc also produced DGD profiles in WT cells with a FWHM, similarly like for Rab4, of around 1μm, indicating that in WT cells the majority of Tfrc colocalizes with Rab4 at the limiting membrane. In sharp contrast, in Rab7KO cells Tfrc produced SGD profiles with a dramatically decreased FWHM, indicating that the majority of Tfrc was internalized from the limiting membrane into the lumen. We also observed that the accumulation of Ctsd in donut-like endosomes, calculated as ratio of Ctsd intensity in endosomes versus Ctsd intensity in whole cells, was increased in Rab7KO compared to WT cells (Extended Data Fig. 4c). In line with this finding, also the PCC revealed that the correlation of Tfrc and Ctsd immunosignal in co-staining experiments was significantly higher in Rab7KO compared to WT cells (Extended Data Fig. 4d). The underlying reason for the very low Tfrc and Ctsd flux in WT compared to Rab7KO cells is very likely due to a diminished ability of recycling endosomes to mature into late endosomes and lysosomes when the Rab7-mediated conventional lysosomal maturation pathway prevails.

Finally, we measured the ratio of the FWHM of Tfrc versus Rab4 in individual endosomes with either high or low Ctsd levels to obtain a semiquantitative measure of the endo/lysosome maturation. A high Tfrc-over-Rab4 ratio indicates less internalization and thus low luminal Tfrc, whereas a low Tfrc-over-Rab4 ratio indicates more internalization and thus high luminal Tfrc in $Ctsd^{high}$ and $Ctsd^{low}$ endosomes. Hence, (1) low luminal Tfrc and Ctsd indicate classical recycling endosomes, (2) either high luminal Tfrc or high Ctsd indicates maturing intermediates between recycling endosomes and endolysosomes, and (3) high luminal Tfrc as well as high luminal Ctsd indicate endolysosomes. The experiment revealed that in WT cells, 44.7% of $Rab4^+$ endosomes showed low luminal levels of Tfrc and Ctsd and were classified as classical recycling endosomes, 38.6% displayed high levels of either Tfrc or Ctsd and were classified as maturing endosomes and 16.7% showed high luminal levels of Tfrc as well as Ctsd and were classified as endolysosomes (Fig. 4h, Extended Data Fig. 4e,f). In Rab7KO cells, the distribution of the three classes of particles shifts from classical recycling endosomes to endolysosomes: 14.4% exhibited low luminal levels of Tfrc and Ctsd, 38.5% displayed high luminal signals of either Tfrc or Ctsd, and 47.2% showed high luminal levels of Tfrc as well as Ctsd. Altogether, these results imply that the generation and size control of $Rab4^+$ enlarged endosomes are Rab7 independent and that loss of Rab7 promotes the maturation of $Rab4^+$ recycling endosomes towards lysosomes.

Biochemistry confirms systematic shift of lysosome biogenesis pathway

The cell imaging studies suggest that in Rab7KO cells the cell surface proteins are routed from recycling endosomes via $Rab4^+$ late endosomes to lysosomes, which results in the massively decreased their surface levels. To confirm this finding biochemically, we expressed GFP-tagged Rab4 or Rab5 in WT and Rab7KO fibroblasts, immuno-isolated intact $Rab4^+$ or $Rab5^+$ endosomes using anti-GFP antibody-coupled beads and compared their protein contents using quantitative MS (Fig. 5a). In WT cells, $Rab5^+/Rab7^+$ endosomes are the source of lysosome biogenesis and therefore lysosomal protein should be detected in $Rab5^+$ endosomes but not in $Rab4^+$ recycling endosomes. Indeed, we found that lysosomal proteins, including lysosomal membrane-associated proteins (e.g. the Lamtors/Regulator complex), transmembrane proteins (e.g. Lamp1 and Lamp2) and lysosomal luminal proteins (e.g. cathepsins) were enriched in $Rab5^+$ but not $Rab4^+$ endosomes of WT cells (Fig. 5b). In sharp contrast, in Rab7KO cells these proteins were enriched in $Rab4^+$ and not in $Rab5^+$ endosomes (Fig. 5c,d). This finding together with the GO ontology analysis showing specific enrichment of proteins from the classical late-endosome/lysosome pathway (GO term “late endosome”, “vacuolar membrane”, “lytic vacuole membrane” and “lysosomal membrane”; Fig. 5e) for $Rab4^+$ endosomes in Rab7KO cells independently confirms that lysosomes are primarily generated from $Rab4^+$ rather than $Rab5^+/Rab7^-$ endosomes in Rab7KO cells (Fig. 6).

Rab4 overexpression generates endo/lysosomes and decreases protein surface levels in WT cells

Since expression of EGFP-Rab4 leads to the appearance of $Rab4^+$ endo/lysosomal organelles in WT cells, although to a much lesser extent than in Rab7KO cells, we assessed Itgb1 and Tfrc surface levels

in Rab4-overexpressed WT cells. The experiment revealed decreased Tfrc surface levels (that were similarly low like in EGFP-transfected Rab7KO cells) and only slightly decreased Itgb1 surface levels (Extended Data Fig. 4g,h). Interestingly, the Tfrc surface levels further decreased when Rab4 is overexpressed in Rab7KO cells, whereas Itgb1 levels did not significantly differ between Rab4- and EGFP-expressed Rab7KO cells (Extended Data Fig. 4g,h). These findings indicate that Rab4 overexpression generates late endosomes in WT cells, which receive large amounts of Tfrc and less Itgb1 from $Rab4^+$ recycling endosomes.

Similarly like in mouse fibroblasts, the human MCF7 breast cancer cell line and the human U2OS sarcoma cell line also increased lysosomal targeting of Tfrc and Itgb1 upon deleting the *RAB7A* gene (Extended Data Fig. 5a-d and Extended Data Fig. 6a-d), indicating the Rab4-mediated lysosomal pathway is also activated in these cells upon Rab7 loss. The WT and Rab7KO U2OS cells contained, in contrast to mouse fibroblasts and human MCF7 cells, particularly large $Tfrc^+$ structures with the Tfrc signals enriched on the limiting membrane and Ctsd signals enriched in the lumen (Extended Data Fig. 6c), suggesting that $Rab4^+$ recycling endosomes fused in WT and Rab7KO U2OS cells with Ctsd carriers without the need to manipulate the endogenous Rab4 levels. The overexpression of EGFP-Rab4 further increased the formation of $Rab4^+/Tfrc^+/Ctsd^+$ structures in Rab7KO UO2S cells, induced these structures in Rab7KO MCF7 cells and to a lesser extent in WT MCF7 and U2OS cells (Extended Data Fig. 5e and 6e), which altogether demonstrates that the Rab4-mediated lysosome biogenesis pathway operates in mouse and human cells.

Discussion

Our whole genome screen in HAP1 cells for regulators of Itgb1 surface stability identified Rab7 as unexpected candidate as stabilizer of Itgb1 and many additional cell surface proteins including Tfrc. Whereas genetic loss-of-function studies of Rab7 lead to embryonic lethality in all animal models tested[21-25], deficiency of Rab7 in mammalian cells[22, 27, 43] produced viable and apparently normally appearing cells *ex vivo*, indicating that the developmental arrest *in vivo* must underlie severe defect(s) that are not obvious *ex vivo*. Since the massive degradation of surface proteins likely accounts for the embryonic lethality *in vivo*, we decided to investigate the mechanism that underlies this unexpected finding.

In search for a mechanistic explanation, we identified a novel lysosome maturation pathway, in which $Rab4^+/Tfrc^+$ recycling endosomes generate endo/lysosomal organelles (Fig. 6). The $Rab4^+$ late endosomes/endolysosomes, in the style of the canonical $Rab7^+$ late endosomes/endolysosomes, acquire membrane proteins such as Lamp1 and Lamp2, contain hydrolytic enzymes such as the cathepsins, an acidic environment in their lumen, and further mature into lysosomes filled with characteristic membrane whorls[11, 12]. In support of these findings, an orthogonal, biochemistry-based assay with Rab7KO cells also revealed that $Rab4^+$ and not $Rab5^+$ endosomes were enriched with late endosome- and lysosome-specific proteins including membrane associated proteins such as the LAMTOR/Ragulator complex[44], transmembrane proteins such as Lamp1 and 2, and hydrolytic enzymes. Expectedly, in WT cells these proteins were enriched on $Rab5^+$ and not $Rab4^+$ endosomes. Furthermore, the Rab4-induced lysosomal pathway described and characterized here for Rab7-null mouse fibroblasts is also activated upon loss of Rab7 in all cell types that were analyzed in this study.

Our immunostainings showed that $Tfrc^+/Ctsd^+$ lysosomes are readily detected in several Rab7-deficient cell lines and only sporadically in WT cell lines. Upon expression of EGFP-Rab4, the abundance of $Rab4^+/Tfrc^+/Ctsd^+$ endo/lysosomal organelles increased in Rab7KO and also became more obvious in the WT cell lines that we analyzed. Since the maturation of lysosomes from recycling endosomes is a fluent process with intermediate organelles that cannot be unequivocally assigned to either recycling endosomes, late endosomes or endolysosomes, it is difficult to accurately determine their census and compare the abundance of $Rab4^+$ endo/lysosomal organelles between WT and Rab7KO cells. To overcome this obstacle, we determined size and sub-organelle localization of Rab4, Tfrc and Ctsd by measuring the full width at half maximum (FWHM) of their fluorescence signals. These measurements revealed a clear bias of endo/lysosome maturation characterized by an elevated accumulation of luminal Tfrc and Ctsd in Rab7KO compared to WT cells, while their size was similar between WT and Rab7KO cells. In light of the presence of $Rab4^+$ endo/lysosomal organelles also in WT cells, it is conceivable that the Rab7- and the Rab4-induced protein degradation pathways can principally act in parallel, and that the latter may become relevant in cells which contain low Rab7 and/or high Rab4 levels. It will be important in future to experimentally define condition(s) in which the Rab4-induced protein degradation

pathway is activated and outweighs the Rab7 pathway and degrades cell surface proteins that are actually designated to recycle back to the plasma membrane.

It is well known that Rab7 promotes the formation of late endosomes and their subsequent maturation into endolysosomes and further into lysosomes to ensure that proteins designated for degradation are degraded, and proteins designated for recycling to the plasma membrane are routed by the activity of Rab4 from early endosomes into recycling endosomes and are not degraded. The ability of $Rab4^+$ recycling endosomes to principally route cargo to lysosomes for degradation, although to a very small scale, suggests that in WT cells Rab7 outcompetes Rab4 enabling lysosome fusion on the acceptor membrane. The competition between Rab7 and Rab4 might be based on the higher affinity of the Rab7 for recruiting proteins that regulate membrane fusion such as tethering complexes, SNAREs, SNARE regulators and additional small GTPases via Rab7 effectors or via the microenvironment of Rab7 microdomains[13, 14, 45].

Our immunostaining also demonstrated that, in contrast to Rab4, neither overexpressed Rab5 nor Rab11 colocalized with lysosomal markers. Given that Rab4, Rab5 and Rab11 can be present on the same endosomes but in distinct microdomains[9], it remains to be shown whether $Rab4^+$ endo/lysosomal organelles originate from endosomes solely decorated with Rab4 or from endosomes that also harbor Rab5 and Rab11 which become rapidly lost during maturation. The mechanism and timing of Rab4 dissociation from maturing lysosomes and the involvement of other small GTPases are important questions that need to be addressed in future studies.

We also found that autophagosome-lysosome fusion or plasma membrane-lysosome fusion are unaffected by the loss of Rab7 in our fibroblast model. The LC3-flux assay showed that LC3-II is delivered to both, WT and Rab7KO lysosomes for degradation irrespective whether cells are serum starved or serum treated, indicating that autophagosome-lysosome fusion does not require the activity of Rab7. These findings contradict the previous studies reporting that Rab7KO compromises autophagy[22, 27]. In both studies, however, serum starvation failed to increase LC3-II levels, *i.e.* induce autophagy which could be caused by the specific cell handling or the cell models used in these studies.

Interestingly, the quantitative and qualitative measurements of the secretome also indicate that fusion of late endosomes and lysosomes with the plasma membrane proceeds in a Rab7-independent manner. Quantitatively, the Rab7KO cells released more cargo such as luminal enzymes and cell surface receptors than WT cells, which, however, is expected from the massive 'misrouting' of proteins normally destined to recycle into the lysosomal degradation pathway. Given the involvement of the lysosomal secretome in various physiological and pathological conditions[39, 46, 47], switching the canonical, Rab7-directed or non-canonical, Rab4-directed protein degradation pathway, e.g. by decreasing Rab7 and/or increasing Rab4 levels, can have significant consequences not only due to the decrease of the surface proteome but also due to the abundant secretion of lysosomal contents.

Acknowledgment

We thank the sequencing, mass spectrometry and imaging facilities of the Max Planck Institute of Biochemistry and the EM-Histo Lab of the Max Planck Institute for Biological Intelligence for the invaluable support. This work was supported by the European Research Council (ERC) under the European Union's Horizon 2020 research and innovation program (grant agreement No. 810104 – Point) and the Max Planck Society.

Author contribution

Conceptualization and writing: GW and RF; Investigation: GW, XP, KY and SG; Supervision and Funding Acquisition: RF.

Declaration of interests

The authors declare no competing interests.

Reference

1. Homma, Y., Hiragi, S. & Fukuda, M. Rab family of small GTPases: an updated view on their regulation and functions. *The FEBS Journal* **288**, 36-55 (2021).
2. Stenmark, H. The Rabs: a family at the root of metazoan evolution. *BMC Biol* **10**, 68 (2012).
3. Wandinger-Ness, A. & Zerial, M. Rab proteins and the compartmentalization of the endosomal system. *Cold Spring Harb Perspect Biol* **6**, a022616 (2014).
4. Hynes, R.O. Integrins: bidirectional, allosteric signaling machines. *Cell* **110**, 673-687 (2002).
5. Moreno-Layseca, P., Icha, J., Hamidi, H. & Ivaska, J. Integrin trafficking in cells and tissues. *Nat Cell Biol* **21**, 122-132 (2019).
6. Paul, N.R., Jacquemet, G. & Caswell, P.T. Endocytic Trafficking of Integrins in Cell Migration. *Curr Biol* **25**, R1092-1105 (2015).
7. Zeigerer, A. *et al.* Rab5 is necessary for the biogenesis of the endolysosomal system in vivo. *Nature* **485**, 465-470 (2012).
8. Zerial, M. & McBride, H. Rab proteins as membrane organizers. *Nature Reviews Molecular Cell Biology* **2**, 107-117 (2001).
9. Sonnichsen, B., De Renzis, S., Nielsen, E., Rietdorf, J. & Zerial, M. Distinct membrane domains on endosomes in the recycling pathway visualized by multicolor imaging of Rab4, Rab5, and Rab11. *J Cell Biol* **149**, 901-914 (2000).
10. Babst, M. MVB vesicle formation: ESCRT-dependent, ESCRT-independent and everything in between. *Curr Opin Cell Biol* **23**, 452-457 (2011).
11. Huotari, J. & Helenius, A. Endosome maturation. *EMBO J* **30**, 3481-3500 (2011).
12. Saftig, P. & Klumperman, J. Lysosome biogenesis and lysosomal membrane proteins: trafficking meets function. *Nat Rev Mol Cell Biol* **10**, 623-635 (2009).
13. Langemeyer, L., Frohlich, F. & Ungermann, C. Rab GTPase Function in Endosome and Lysosome Biogenesis. *Trends Cell Biol* **28**, 957-970 (2018).
14. Guerra, F. & Bucci, C. Multiple Roles of the Small GTPase Rab7. *Cells* **5**, 34 (2016).
15. Bucci, C. *et al.* Co-operative regulation of endocytosis by three Rab5 isoforms. *FEBS Lett* **366**, 65-71 (1995).

16. Homma, Y. *et al.* Comprehensive knockout analysis of the Rab family GTPases in epithelial cells. *J Cell Biol* **218**, 2035-2050 (2019).
17. Perrin, L. *et al.* Rab4b controls an early endosome sorting event by interacting with the γ subunit of the clathrin adaptor complex 1. *Journal of Cell Science* **126**, 4950-4962 (2013).
18. Yang, M. *et al.* Rab7b, a novel lysosome-associated small GTPase, is involved in monocytic differentiation of human acute promyelocytic leukemia cells. *Biochem Biophys Res Commun* **318**, 792-799 (2004).
19. Progida, C. *et al.* Rab7b controls trafficking from endosomes to the TGN. *J Cell Sci* **123**, 1480-1491 (2010).
20. Mackiewicz, P. & Wyroba, E. Phylogeny and evolution of Rab7 and Rab9 proteins. *BMC Evol Biol* **9**, 101 (2009).
21. Kawamura, N. *et al.* Delivery of endosomes to lysosomes via microautophagy in the visceral endoderm of mouse embryos. *Nat Commun* **3**, 1071 (2012).
22. Roy, S.G., Stevens, M.W., So, L. & Edinger, A.L. Reciprocal effects of rab7 deletion in activated and neglected T cells. *Autophagy* **9**, 1009-1023 (2013).
23. Kreis, J., Wielath, F.M. & Vick, P. Rab7 is required for mesoderm patterning and gastrulation in Xenopus. *Biology Open* **10** (2021).
24. Cherry, S. *et al.* Charcot-Marie-Tooth 2B mutations in rab7 cause dosage-dependent neurodegeneration due to partial loss of function. *eLife* **2**, e01064 (2013).
25. Skorobogata, O. & Rocheleau, C.E. RAB-7 antagonizes LET-23 EGFR signaling during vulva development in Caenorhabditis elegans. *PLOS ONE* **7**, e36489 (2012).
26. Silverman, J.S., Schwartz, K.J., Hajduk, S.L. & Bangs, J.D. Late endosomal Rab7 regulates lysosomal trafficking of endocytic but not biosynthetic cargo in Trypanosoma brucei. *Molecular Microbiology* **82**, 664-678 (2011).
27. Kuchitsu, Y., Homma, Y., Fujita, N. & Fukuda, M. Rab7 knockout unveils regulated autolysosome maturation induced by glutamine starvation. *J Cell Sci* **131**, jcs215442 (2018).
28. Kuchitsu, Y. & Fukuda, M. Revisiting Rab7 Functions in Mammalian Autophagy: Rab7 Knockout Studies. *Cells* **7**, 215 (2018).
29. Wichmann, H., Hengst, L. & Gallwitz, D. Endocytosis in yeast: evidence for the involvement of a small GTP-binding protein (Ypt7p). *Cell* **71**, 1131-1142 (1992).
30. Haas, A., Scheglmann, D., Lazar, T., Gallwitz, D. & Wickner, W. The GTPase Ypt7p of Saccharomyces cerevisiae is required on both partner vacuoles for the homotypic fusion step of vacuole inheritance. *The EMBO Journal* **14**, 5258-5270 (1995).
31. Carette, J.E. *et al.* Haploid genetic screens in human cells identify host factors used by pathogens. *Science* **326**, 1231-1235 (2009).
32. Jae, L.T. *et al.* Deciphering the glycosylome of dystroglycanopathies using haploid screens for lassa virus entry. *Science* **340**, 479-483 (2013).
33. Bottcher, R.T. *et al.* Sorting nexin 17 prevents lysosomal degradation of beta1 integrins by binding to the beta1-integrin tail. *Nat Cell Biol* **14**, 584-592 (2012).
34. Steinberg, F., Heesom, K.J., Bass, M.D. & Cullen, P.J. SNX17 protects integrins from degradation by sorting between lysosomal and recycling pathways. *J Cell Biol* **197**, 219-230 (2012).
35. Rognoni, E., Ruppert, R. & Fassler, R. The kindlin family: functions, signaling properties and implications for human disease. *J Cell Sci* **129**, 17-27 (2016).
36. Yim, W.W.-Y. & Mizushima, N. Lysosome biology in autophagy. *Cell Discovery* **6** (2020).
37. Mizushima, N. A brief history of autophagy from cell biology to physiology and disease. *Nature Cell Biology* **20**, 521-527 (2018).
38. Klionsky, D.J. *et al.* Guidelines for the use and interpretation of assays for monitoring autophagy (4th edition)¹. *Autophagy* **17**, 1-382 (2021).
39. Blott, E.J. & Griffiths, G.M. Secretory lysosomes. *Nat Rev Mol Cell Biol* **3**, 122-131 (2002).
40. Samie, M.A. & Xu, H. Lysosomal exocytosis and lipid storage disorders. *Journal of Lipid Research* **55**, 995-1009 (2014).
41. Machado, E.R., Annunziata, I., van de Vlekkert, D., Grosveld, G.C. & d'Azzo, A. Lysosomes and Cancer Progression: A Malignant Liaison. *Front Cell Dev Biol* **9**, 642494 (2021).

42. Maxfield, F.R. & McGraw, T.E. Endocytic recycling. *Nature Reviews Molecular Cell Biology* **5**, 121-132 (2004).
43. Schleinitz, A. *et al.* Consecutive functions of small GTPases guide HOPS-mediated tethering of late endosomes and lysosomes. *Cell Reports* **42**, 111969 (2023).
44. Laplante, M. & Sabatini, D.M. mTOR signaling at a glance. *Journal of Cell Science* **122**, 3589-3594 (2009).
45. de Araujo, M.E.G., Liebscher, G., Hess, M.W. & Huber, L.A. Lysosomal size matters. *Traffic* **21**, 60-75 (2020).
46. Buratta, S. *et al.* Lysosomal Exocytosis, Exosome Release and Secretory Autophagy: The Autophagic- and Endo-Lysosomal Systems Go Extracellular. *International Journal of Molecular Sciences* **21**, 2576 (2020).
47. Lee, J. & Ye, Y. The Roles of Endo-Lysosomes in Unconventional Protein Secretion. *Cells* **7**, 198 (2018).

Figure legends

Fig. 1 | Rab7 deficiency decreases β1 integrin protein levels

a, Schematic overview of the haploid genetic screen. The 5% lowest ($Itgb1^{LO}$) and the 5% highest Itgb1 ($Itgb1^{HI}$) surface levels were FACS-sorted and analyzed for gene trap insertion.

b, Haploid genetic screen for $Itgb1^{HI}$ and $Itgb1^{LO}$ surface levels. In the fishtail plot, genes enriched in the Itgb1 high and low populations are colored in blue and apricot, respectively. Dots represent individual genes and dot size corresponds to false discovery rate (FDR)-adjusted p-values (P_{adj}) calculated with the Chi-square test. The y-axis indicates the number of disruptive insertions per gene and the x-axis indicates the mutation index (MI), which describes the frequency of independent insertions in $Itgb1^{HI}$ channel over the frequency of insertions in the $Itgb1^{LO}$ channel for each gene. Dark grey dots indicate genes with significant enrichment of insertions ($P_{adj}<10^{-10}$) and light grey dots with insignificant enrichment ($P_{adj}>10^{-10}$). Blue dots indicate genes coding for components of the retriever complex, orange dots indicate genes coding for components of the CCC, WASH and Arp2/3 complex, red dot indicate the Rab7 gene.

c, Close-up of highlighted region in **b**.

d,e, WB (d) and densitometric quantification (e) of Itgb1 in WT and Rab7KO fibroblasts, and Rab7KO fibroblasts stably re-expressing EGFP-Rab7. Gapdh served as loading control. Rab7KO cl.1 and cl.2 are independently generated cell clones. In WB (d) Itgb1 appears as 100 kDa immature and 125 kDa mature protein due to different glycosylation. The latter was quantified (e). Statistics was analyzed by two-sided multiple paired *t*-test with Holm-Šidák correction. Data are shown as Mean±SD, n=3 independent experiments.

f, Cell surface levels of Itgb1 on indicated cell lines determined by flow cytometry. Statistical tests were carried out as in **e**. Data are shown as Mean±SD, n=3 independent experiments.

g,h, WB (g) and densitometric quantification (h) of Itgb1 in WT and Rab7KO fibroblasts treated with DMSO (0.1% v/v), the lysosome inhibitor Bafilomycin A1 (BafA1, 10nM) or the proteasome inhibitor MG132 (100nM). Gapdh served as loading control. Statistics was analyzed by ordinary one-way ANOVA with Šidák's post hoc tests. Data are shown as Mean±SD, n=3 independent experiments.

i, Cell surface levels of Itgb1 on indicted cell lines treated with DMSO, BafA1 or MG132 determined by flow cytometry. Statistical tests were carried out as in H. Data re shown as Mean±SD, n=3 independent experiments.

j, Volcano plot of the cell surface proteome of WT versus Rab7KO mouse fibroblasts identified by label-free MS. P-values are determined using two-sided permuted *t*-test with 250 randomizations. The

549 black dotted line indicates the significance cutoff (FDR:0.05, S0:0.1) estimated by the Perseus software.
550 n=3 biological replicates. Arbitrarily selected cell surface receptors are highlighted in red.

551

Fig. 2 | Itgb1 is delivered to *bona fide* lysosomes in Rab7KO cells.

a, Representative IF images of Itgb1, Lamp1 and Cathepsin D (Ctsd) in mouse fibroblasts. Arrowheads indicate Itgb1 accumulation in Lamp1- and Ctsd-positive lysosomes. Boxes indicate cell areas shown magnified in the Zoom panel. Sum intensity projections of confocal stacks are shown. Scale bar, 10µm.

b, Superplots showing Pearson correlation coefficient (PCC) between Itgb1 Ctsd in WT and Rab7KO mouse fibroblast. "P" indicates the p-value obtained by two-sided Welch's *t*-test from the mean values of each independent experiment, N=3. "p" indicated the p-value obtained by two-sided Welch's *t*-test from all individual values collected, WT n=82, KO n=103 cells. Bars represent Mean±SD of the mean values.

c, Schematic overview of EGFP-tagged Itga5 on the limiting membrane and in the lumen of lysosomes. The fluorophore signal is quenched by the intraluminal acidic pH and recovered upon neutralization with NH_4Cl.

d, Representative widefield live-cell images of EGFP-tagged Itga5 and Sir^+ lysosomes in mouse fibroblast before and after neutralization by NH4Cl. Boxes indicate cell areas shown in Zoom. Denoised images without and with (labeled as "processed") background subtraction are shown. Arrowheads indicate Itga5-Itgb1 heterodimers in the acidic lumen of late endosomes (white arrowheads) and lysosomes (magenta arrowheads). Scale bar, 10µm. n≥3 independent experiments for each cell line.

e, Representative TEM images showing immunogold-labelled Itgb1 (arrowheads) in MVBs/late endosomes and lysosomes (LY). Scale bar, 0.2 µm. n=2 independent experiments with at least 2 EM grids imaged for each experiment.

f, Representative cryo-ET images showing morphology of MVBs/late endosomes and lysosomes (LY) in vitrified mouse fibroblast. Images show one slice of an electron tomography stack. Cells were stained with LysoTracker before vitrification to localize acidic organelles in cryo-fluorescence microscopy. Lamellae with a thickness around 100 nm were milled in the LysoTracker signal-rich area using focused ion beam (FIB). Scale bar, 0.2 µm. n=2 independent experiments with at least 2 different EM grids imaged for each experiment.

Fig. 3 | Rab7KO lysosomes function normally

a,b, WB (a) and quantification (b) of LC3 in WT and Rab7KO mouse fibroblasts treated with and without BafA1. Tubulin served as loading control. Statistics was carried out by one-way ANOVA with Šidák's post hoc tests. Data are shown as Mean±SD, n=3 independent experiments.

c, Volcano plot of the secretome of WT versus Rab7KO mouse fibroblast. The black dotted line indicates the significance cutoff (FDR:0.05, S0:0.1) estimated by the Perseus software. n=3 biological replicates. The arbitrarily highlighted cell surface receptors are indicated in red and representative lysosomal proteins in blue.

d, Gene ontology (GO) enrichment analysis of proteins showing a significant increase in the Rab7KO secretome. The top 10 GO terms regarding cellular components are displayed. P-values are show for each GO term and adjusted by the Benjamini-Hochberg (BH) method for controlling the FDR. Counts represent the number of genes found in the GO term. GeneRatio represents the ratio between the number of genes found in the GO term over total number of genes subjected to analysis.

Fig. 4 | Rab7KO cells generate lysosomes from Rab4$^+$ recycling endosomes

a, Representative IF images of Transferrin receptor (Tfrc), Itgb1 and Ctsd in WT and Rab7KO mouse fibroblasts. Arrowheads indicate intracellular accumulation of Tfrc and Itgb1 in Ctsd-positive lysosomes. Boxes indicate cytoplasmic areas shown in Zoom. Sum intensity projections of confocal stacks are shown. Scale bar, 10μm.

b, Superplots showing PCC between Tfrc and Ctsd in WT and Rab7KO mouse fibroblast. "P" indicated the p-value obtained by two-sided Welch's *t*-test from the mean values of each independent experiment, N=3. "p" indicated the p-value obtained by two-sided Welch's *t*-test from all individual values collected, WT n=100, KO n=120 cells. Bars represent Mean±SD of the mean values.

c,d, Representative IF images of Tfrc and Ctsd in WT and Rab7KO mouse fibroblasts expressing EGFP-Rab5 (c) and EGFP-Rab11 (d), respectively. Arrowheads indicate colocalization of Rabs and Tfrc. Boxes indicate cytoplasmic areas shown at in Zoom. Sum intensity projections of confocal stacks are shown. Scale bar, 10μm.

e, Representative IF images of Tfrc and Ctsd in WT and Rab7KO mouse fibroblasts expressing EGFP-Rab4. Arrowheads indicate colocalization of Rab4 and Tfrc. Yellow boxes indicate cytoplasmic areas shown in Zoom. Numbered white boxes indicate endosomes of different classes. Arrows indicate the direction of line profiles of EGFP-Rab4 (green), Tfrc (red) and Ctsd (blue). The upper panels show sum intensity projections of confocal stacks. The lower panels show a single confocal slice. Each line profile was produced from a single slice. Scale bar: upper, 10μm; lower, 1μm

f, Image of modelled Rab4$^+$ endosomes in WT and Rab7KO cells. Rab4$^+$ endosomes with a donut-like shape (n=516 from WT and n=505 from Rab7KO cells) were collected and normalized in intensity and isotropicity from three independent experiments and in total of 62 WT and 58 Rab7KO cells expressing EGFP-Rab4. Arrows indicate the direction of the line profiles. Dashed lines show the line profiles of each independent experiment. The line profile generated from the input of all cells is shown as solid lines in the right panel.

g, Quantification of the full width at half maximum (FWHM) of Rab4, Tfrc and Ctsd line profiles generated in the independent experiments. Statistics was calculated by the Two-sided Welch's *t*-test. Data are shown as Mean±SD, n=3 independent experiments.

h, Classification of Rab4$^+$ endosomes based on the degree of luminal levels of Tfrc (Tfrc-Lu) and Ctsd (Ctsd), categorized into high (Hi) or low (Lo) levels. P-value for the contingency test is determined using Chi-squared test. See also Extended Data Fig. 4e,f.

Fig. 5 | Rab4$^+$ endosomes outcompete Rab5$^+$ endosomes for lysosome biogenesis in Rab7KO cells

a, Schematic representation showing the immunoisolation of intact EGFP-Rab4$^+$ and EGFP-Rab5$^+$ endosomes for proteomic profiling.

b,c, Volcano plot of proteins in Rab4$^+$ versus Rab5$^+$ endosomes of WT (b) and Rab7KO (c) cells. Representative lysosomal proteins are highlighted in blue. Out-of-range values (outside the x-axis range of -5 to 5) are plotted on the border.

d, Volcano plot showing the relative difference in proteins localization in Rab4$^+$ endosomes in Rab7KO vs. WT cells. P-values are determined using two-sided permuted t-test with 250 randomizations. The black dotted line indicates the significance cutoff (FDR:0.05, S0:0.1) estimated by the Perseus software. n=3 biological replicates.

e, Gene ontology enrichment analysis of proteins with significant shifts from Rab5$^+$ to Rab4$^+$ endosomes. The top 10 GO terms are displayed. P-values are show for each GO term and adjusted by the Benjamini-Hochberg (BH) method for controlling the FDR. Count represents number of genes found in the GO term. GeneRatio represents ratio between number of genes found in the GO term over total number of genes subjected to analysis.

Fig. 6 | Schematic representation of integrin and Tfrc degradation via the Rab7- or Rab4-mediated lysosome biogenesis pathway

In the canonical Rab7-mediated lysosome biogenesis pathway, late endosomes mature into lysosomes by fusing with carriers containing lysosomal enzymes. In the Rab4-mediated non-canonical lysosome biogenesis pathway operating upon Rab7 loss, lysosomes are generated from $Rab4^{+}$ recycling endosomes, resulting in the degradation of proteins originally routed to the recycling pathway.

Extended Data Fig. 1 | Rab7 deficiency decreases protein levels and stability of Itgb1, related to Fig. 1.

a,b, WB (a) and quantification (b) of Itgb1 in WT and Rab7-null clones derived from HAP1, HEK, MCF7 and U2OS cells. HAP1 cl.1 and cl.2 are independently generated Rab7KO clones. HEK, MCF7 and U2OS cell lines indicated as KO1 and KO2 are expanded pools derived from 100 flow cytometry sorted cells. The matured form of Itgb1 (upper band) was quantified in (b). Statistics was analyzed by two-sided multiple paired *t*-test with Holm-Šidák correction. Data are shown as Mean±SD, n=3.

c, Itgb1 surface levels on indicated cell lines determined by flow cytometry. Statistical tests were carried out as in **b**. Data are shown as Mean±SD, n=3 independent experiments.

d, Quantification of Itgb1 internalization kinetics in WT and Rab7KO mouse fibroblasts. Biotinylated proteins were pulled down by streptavidin beads and the amount of Itgb1 were measured by capture-ELISA. Statistics was analyzed by two-way ANOVA with Šidák's post hoc tests. Mean±SD, n=4 independent experiments.

e, Quantification of surface Itgb1 degradation kinetics in WT and Rab7KO mouse fibroblasts. The amount of Itgb1 remaining over indicated times were measured by capture-ELISA. Statistics was analyzed by two-way ANOVA with Šidák's post hoc tests. Data are shown as Mean±SD, n=4 independent experiments.

f, Quantification of total Itgb1 degradation kinetics in WT and Rab7KO mouse fibroblasts using the cycloheximide chase assay. Cells were lysed at indicated times and Itgb1 levels were measured by WB. Statistics was analyzed by two-way ANOVA with Šidák's post hoc tests. Data is shown as Mean±SD, n=4 independent experiments.

g, Numbers of adherent WT and Rab7KO mouse fibroblasts at indicated time points after seeding on FN-coated glass. Symbols represent mean values of independent experiments; lines sigmoidal curve fit and numbers indicate p-values determined by two-way ANOVA with Šidák's post hoc tests, n=4 independent experiments.

h, Cell spreading area of WT and Rab7KO mouse fibroblasts on FN-coated glass surface at indicated time points after seeding. Colored symbols represent mean values of independent experiment; lines represent sigmoidal curve fit; numbers p-values determined by two-way ANOVA with Šidák's post hoc tests, n=4 independent experiments.

i, Superplots showing cell doubling time of WT and Rab7KO mouse fibroblasts. "P" indicated the p-value obtained by two-sided Welch's *t*-test from the mean values of each independent experiment, N=3. "p" indicated the p-value obtained by two-sided Welch's *t*-test from all individual data points collected, n=24 imaged areas. Bars represent the Mean±SD of the mean values.

Extended Data Fig. 2 | Rab7KO leads to the colocalization of Itgb1 with lysosome markers, related to Fig. 2.

a-c, Representative confocal image sections of WT and Rab7KO mouse fibroblasts. Cells were immunostained for Itgb1, Lamp2 and Ctsd in **a**; Itgb1, Lamp1 and Cathepsin B (Ctsb) in **b**; and Itgb1, Lamp1 and Cathepsin L (Ctsl) in **c**. Arrowheads indicate triple colocalization of Itgb1, Lamp and Cathepsin. Boxes indicate cytoplasmic areas shown in Zoom. Sum intensity projections of confocal stacks are shown. Scale bar, 10μm.

d, Superplots showing PCC between Itgb1 and Lamp1 in WT and Rab7KO mouse fibroblast. "P" indicated the p-value obtained by two-sided Welch's *t*-test from the mean values of independent experiments, N=3. "p" indicated the p-value obtained by two-sided Welch's *t*-test from all individual values collected, WT n=82, KO n=103 cells. Bars represent the Mean±SD of the mean values.

e, Quantification of EGFP intensity differences before and after NH_4Cl treatment in individual WT and Rab7KO mouse fibroblast. Values were measured on cell bodies in processed images and normalized to the pretreatment condition. P-value was analyzed by two-sided Welch's *t*-test. WT n=34, KO n=35 cells from 4 independent experiments. Bars represent Mean±SD.

f,g, Quantification of EGFP-positive (f) and EGFP/Sir-Lysosome (SirLyso) double positive (g) structures in WT and Rab7KO mouse fibroblasts following the NH_4Cl treatment. Statistics was analyzed by two-sided Welch's *t*-test. WT n=34, KO n=35 cells from 4 independent experiments. Bars represent Mean±SD.

Extended Data Fig. 3 | Rab7KO cells have comparable endosomal and lysosomal morphologies to WT cells, related to Fig. 2.

a, TEM images of Itgb1 containing endosomes and lysosomes in the WT and Rab7KO mouse fibroblast. EE, early endosome, MVB, multi-vesicular body; HY, hybrid endosome (endolysosome or autolysosome); LY, lysosome. Arrowheads indicate immunogold-labelled Itgb1. Scale bar, 0.2 μm. n=2 independent experiments with at least 2 different EM grids analyzed. Boxes indicate area shown in Fig. 2e.

b, Cryo-EM images of acidic endosomes and lysosomes in WT and Rab7KO mouse fibroblast. EE, early endosome, MVB, multi-vesicular body; AP, autophagosome; HY, hybrid endosome (endolysosome or autolysosome); LY, lysosome; MT, mitochondria. Scale bar, 0.2 μm. WT n=3, KO n=2 independent experiments with at least 2 different EM grids analyzed. Boxes indicate area shown in Fig. 2f, corresponding tomographs are shown in Supplementary Video 1.

Extended Data Fig. 4 | Rab7KO promotes maturation of Rab4$^+$ recycling endosomes to lysosomes, related to Fig. 4.

a, Cell surface levels of Tfrc in WT and Rab7KO fibroblasts, and Rab7KO fibroblasts stably re-expressing EGFP-Rab7 determined by flow cytometry. Statistics was analyzed by one sample *t*-test when compared to WT or by two-sided Welch's *t*-test. Data are shown as Mean±SD, n=4 independent experiments.

b, Schematic of the workflow for quantitative analysis of recylolysosomes. Enlarged Rab4$^+$ endosomes with a donut-like appearance were collected from sum-projected confocal stacks. To measure the relative accumulation of fluorescence signal on endosome, the pixel values were transformed from grey level to the percentage of intensity in each endosome compared to the whole cell. To assess the full width at half maximum (FWHM) of the fluorescent signals, endosomes were normalized for intensity and isotropy and averaged to obtain a model endosome, on which a line profile could be generated.

c, Quantification of the Ctsd intensity of individual endosomes. The integrated intensity was measured in a round area with a diameter of 1.4μm in the center of the image. On top of box-and whisker plot with all individual values shown, dots with solid outline show the geometric means of each independent experiment, red dashed lines show the mean value of 3 geometric means. Values higher than 3 were plotted on the border. "P" indicated the p-value obtained by two-sided Welch's *t*-test from the geometric means of each independent experiment, N=3. "p" indicated the p-value obtained by Mann-Whitney test from all individual values collected, WT n=516, KO n=505 endosomes.

d, Superplots showing PCC between Tfrc and Ctsd in WT and Rab7KO mouse fibroblast expressing EGFP-Rab4. "P" indicated the p-value obtained by two-sided Welch's *t*-test from the mean values of each independent experiment, N=3. "p" indicated the p-value obtained by two-sided Welch's *t*-test from all individual values collected, WT n=62, KO n=58 cells. Bars represent the Mean±SD of the mean values.

e,f, Quantification of Tfrc internalization and Ctsd accumulation in individual enlarged Rab4$^+$ endosomes of WT (e) and Rab7KO (f) fibroblasts expressing EGFP-Rab4. The y-axis indicates the ratio between FWHM of Tfrc signals and Rab4 signals in individual endosomes. The x-axis indicates the -$\log_2$ transformed Ctsd intensity of individual endosomes. The red lines indicate the cutoffs between the high and low groups, arbitrarily set at x=-1 and y=0.95. Numbers indicate the percentage of endosomes classified in each group. Endosomes with erroneous FWHM values (negative, extremely large) due to the presence of interfering signals from a second structure were omitted from the analysis. Points with x-values less than 5 were plotted along the border. Y-axis is capped at y=2. WT n=490, KO n=494 endosomes.

g,h, Cell surface levels of Tfrc (g) and Itgb1 (h) determined by flow cytometry in WT and Rab7KO fibroblasts transiently expressing EGFP or EGFP-Rab4. Statistics was analyzed by two-sided multiple paired *t*-test with Holm-Šidák correction. Data are shown as Mean±SD, n=4 independent experiments.

Extended Data Fig. 5 | Rab7KO promotes the lysosomal targeting of Tfrc and Itgb1 in MCF7 cells, related to Fig. 4.

a, Representative IF images of Itgb1 and Ctsd in WT and Rab7KO MCF7 cells. Boxes indicate cytoplasmic areas shown in Zoom. Sum intensity projections of confocal stacks are shown. Arrowheads indicate Itgb1 accumulation in Ctsd-positive lysosomes. Scale bar, 10μm.

b, Superplots showing PCC between Itgb1 and Ctsd in WT and Rab7KO MCF7 cells. "P" indicated the p-value obtained by two-sided Welch's *t*-test from the mean values of each independent experiment, N=3. "p" indicated the p-value obtained by two-sided Welch's *t*-test from all individual values collected, WT n=67, KO n=71 cells. Bars represent the Mean±SD of the mean values.

c, Representative IF images of Tfrc and Ctsd in WT and Rab7KO MCF7 cells. Boxes indicate cytoplasmic areas shown in Zoom. Sum intensity projections of confocal stacks are shown. Arrowheads indicate Tfrc accumulation in Ctsd-positive lysosomes. Scale bar, 10μm.

d, Superplots showing PCC between Tfrc and Ctsd in WT and Rab7KO MCF7 cells. "P" indicated the p-value obtained by two-sided Welch's *t*-test from the mean values of each independent experiment, N=3. "p" indicated the p-value obtained by two-sided Welch's *t*-test from all individual values collected, WT n=67, KO n=74 cells. Bars represent the Mean±SD of the mean values.

e, Representative IF images of Tfrc and Ctsd in WT and Rab7KO MCF7cells expressing EGFP-Rab4. Boxes indicate cytoplasmic areas shown at in Zoom. Sum intensity projections of confocal stacks are shown. Arrowheads indicate colocalization of Rab4 and Ctsd. Scale bar, 10μm.

Extended Data Fig. 6 | Rab7KO promotes the lysosomal targeting of Tfrc and Itgb1 in U2OS cells Related to Fig. 4.

a, Representative IF images of Itgb1 and Ctsd in WT and Rab7KO U2OS cells. Boxes indicate cytoplasmic areas shown in Zoom. Sum intensity projections of confocal stacks are shown. Arrowheads indicate Itgb1 accumulation in Ctsd-positive lysosomes. Scale bar, 10μm.

b, Superplots showing PCC between Itgb1 and Ctsd in WT and Rab7KO U2OS cells. "P" indicated the p-value obtained by two-sided Welch's *t*-test from the mean values of each independent experiment, N=3. "p" indicated the p-value obtained by two-sided Welch's *t*-test from all individual values collected, WT n=65, KO n=57 cells. Bars represent the Mean±SD of the mean values.

c, Representative IF images of Tfrc and Ctsd in WT and Rab7KO U2OS cells. Boxes indicate cytoplasmic areas shown in Zoom. Sum intensity projections of confocal stacks are shown. Arrowheads indicate Tfrc accumulation in Ctsd-positive lysosomes. Arrows in single confocal slice indicate direction of line profiles of Tfrc (green) and Ctsd (red). Scale bar: left and middle panel 10μm, right panel 1μm.

d, Superplots showing PCC between Tfrc and Ctsd in WT and Rab7KO U2OS cells. "P" indicated the p-value obtained by two-sided Welch's *t*-test from the mean values of each independent experiment, N=3. "p" indicated the p-value obtained by two-sided Welch's *t*-test from all individual values collected, WT n=61, KO n=66 cells. Bars represent the Mean±SD of the mean values.

e, Representative IF images of Tfrc and Ctsd in WT and Rab7KO MCF7cells expressing EGFP-Rab4. Boxes indicate cytoplasmic areas shown in Zoom. Sum intensity projections of confocal stacks are shown. Arrowheads indicate colocalization of Rab4 and Ctsd. Scale bar, 10μm.

Supplementary Video 1.

Cryo-tomography of endosomal organelles in WT and Rab7KO mouse fibroblast. Scale bar, 0.2μm.

Fig. 1

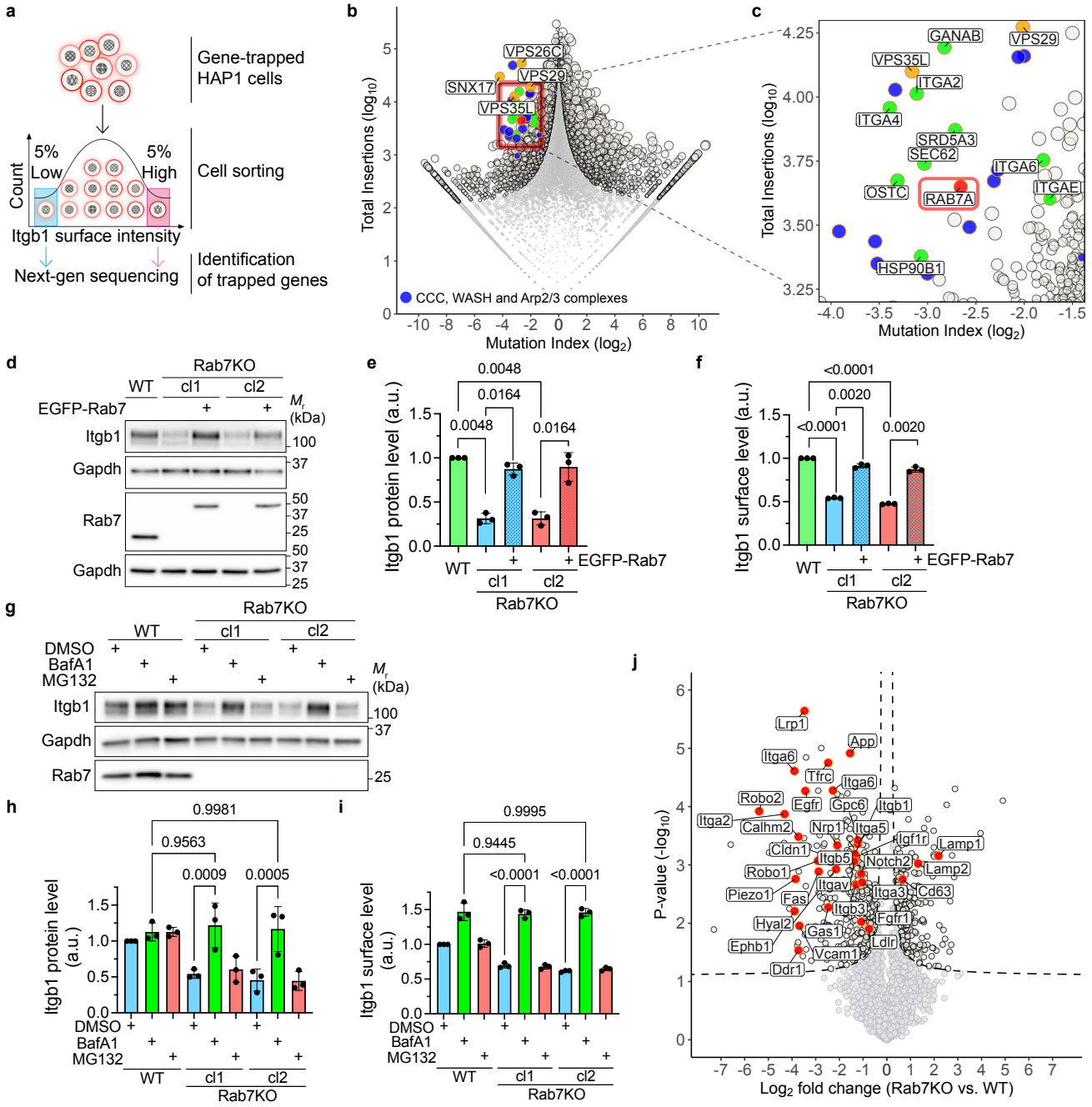
a
Gene-trapped HAP1 cells
Cell sorting
Identification of trapped genes
Count
5% Low
5% High
Itgb1 surface intensity
Next-gen sequencing
b
Total Insertions (log10)
Mutation Index (log2)
VPS26C
VPS29
SNX17
VPS35L
CCC, WASH and Arp2/3 complexes
c
GANAB
VPS29
VPS35L
ITGA2
ITGA4
SRD5A3
SEC62
ITGA6
ITGAE
OSTC
RAB7A
HSP90B1
d
Rab7KO
WT
cl1
cl2
EGFP-Rab7
Mr (kDa)
Itgb1
Gapdh
Rab7
e
Itgb1 protein level (a.u.)
0.0048
0.0164
0.0048
0.0164
WT
cl1
cl2
Rab7KO
+ EGFP-Rab7
f
Itgb1 surface level (a.u.)
<0.0001
0.0020
<0.0001
0.0020
g
DMSO
BafA1
MG132
h
Itgb1 protein level (a.u.)
0.9981
0.9563
0.0009
0.0005
i
Itgb1 surface level (a.u.)
0.9995
0.9445
<0.0001
<0.0001
j
P-value (-log10)
Log2 fold change (Rab7KO vs. WT)
Lrp1
App
Itga6
Tfrc
Itga6
Robo2
Egfr
Gpc6
Itgb1
Itga2
Calhm2
Nrp1
Itga5
Igf1r
Lamp1
Cldn1
Itgb5
Notch2
Lamp2
Robo1
Itgav
Piezo1
Itga3
Cd63
Fas
Itgb3
Fgfr1
Hyal2
Gas1
Ephb1
Ldlr
Vcam1
Ddr1

Fig. 2

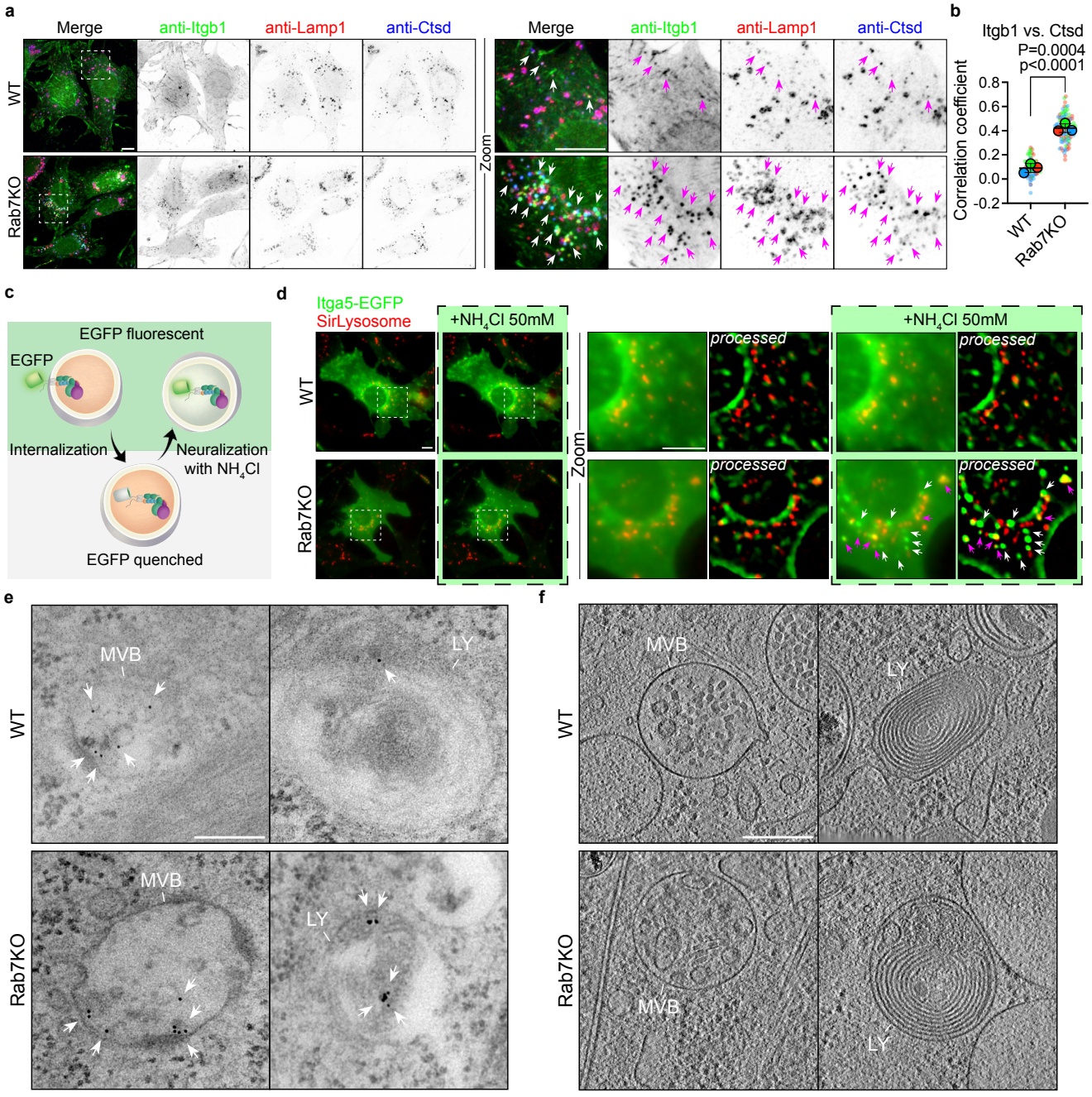
a
Merge
anti-Itgb1
anti-Lamp1
anti-Ctsd
WT
Rab7KO
Zoom
b
Itgb1 vs. Ctsd
P=0.0004
p<0.0001
Correlation coefficient
0.8
0.6
0.4
0.2
0.0
-0.2
WT
Rab7KO
c
EGFP fluorescent
EGFP
Internalization
Neuralization with NH4Cl
EGFP quenched
d
Itga5-EGFP
SirLysosome
+NH4Cl 50mM
processed
WT
Rab7KO
Zoom
e
MVB
LY
WT
Rab7KO
f
MVB
LY
WT
Rab7KO

Fig. 3

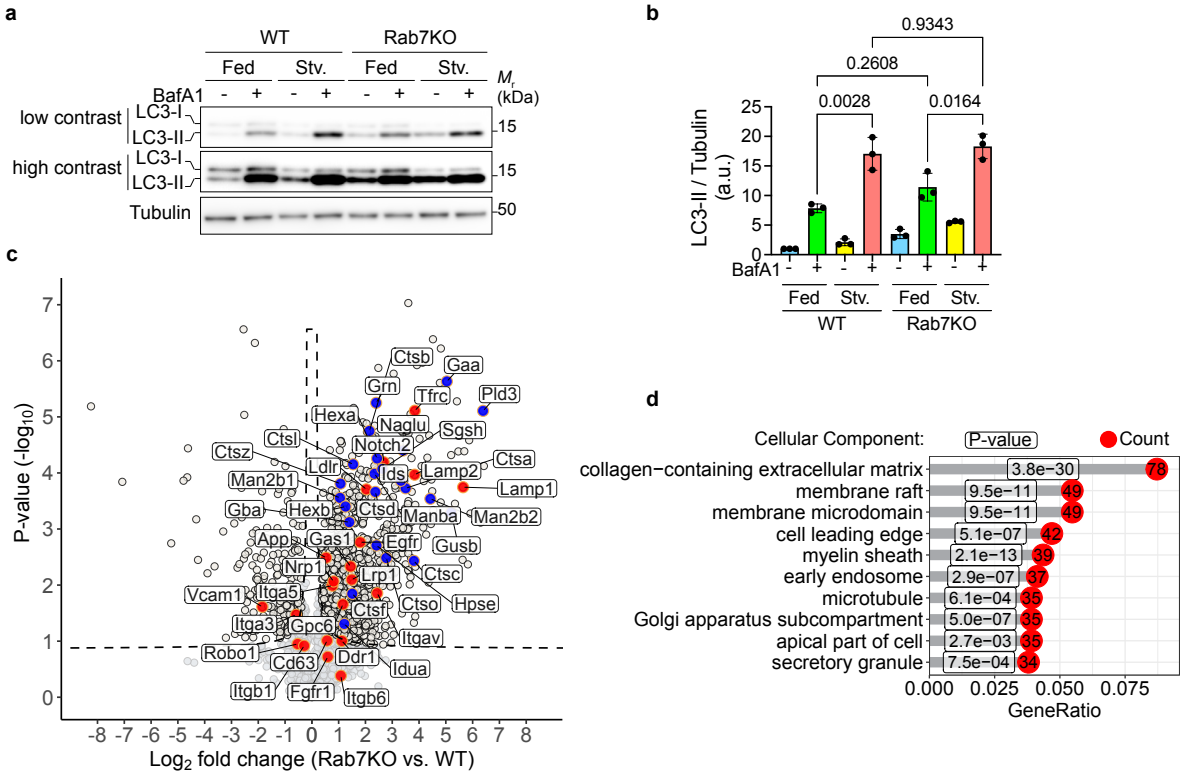
a
WT
Rab7KO
Fed
Stv.
Fed
Stv.
BafA1
- + - + - + - +
M_r (kDa)
low contrast
LC3-I
LC3-II
15
high contrast
LC3-I
LC3-II
15
Tubulin
50
b
0.9343
0.2608
0.0028
0.0164
LC3-II / Tubulin (a.u.)
25
20
15
10
5
0
BafA1
- + - + - + - +
Fed
Stv.
Fed
Stv.
WT
Rab7KO
c
P-value (-log10)
7
6
5
4
3
2
1
0
Ctsb
Gaa
Grn
Tfrc
Pld3
Hexa
Naglu
Sgsh
Ctsl
Notch2
Ctsz
Ctsa
Ldlr
Ids
Lamp2
Lamp1
Man2b1
Gba
Hexb
Ctsd
Manba
Man2b2
Appb
Gas1
Egfr
Gusb
Nrp1
Lrp1
Ctsc
Vcam1
Itga5
Ctsf
Ctso
Hpse
Itga3
Gpc6
Itgav
Robo1
Cd63
Ddr1
Idua
Itgb1
Fgfr1
Itgb6
-8 -7 -6 -5 -4 -3 -2 -1 0 1 2 3 4 5 6 7 8
Log2 fold change (Rab7KO vs. WT)
d
Cellular Component:
P-value
Count
collagen−containing extracellular matrix
3.8e−30
78
membrane raft
9.5e−11
49
membrane microdomain
9.5e−11
49
cell leading edge
5.1e−07
42
myelin sheath
2.1e−13
39
early endosome
2.9e−07
37
microtubule
6.1e−04
35
Golgi apparatus subcompartment
5.0e−07
35
apical part of cell
2.7e−03
35
secretory granule
7.5e−04
34
0.000
0.025
0.050
0.075
GeneRatio

Fig. 4

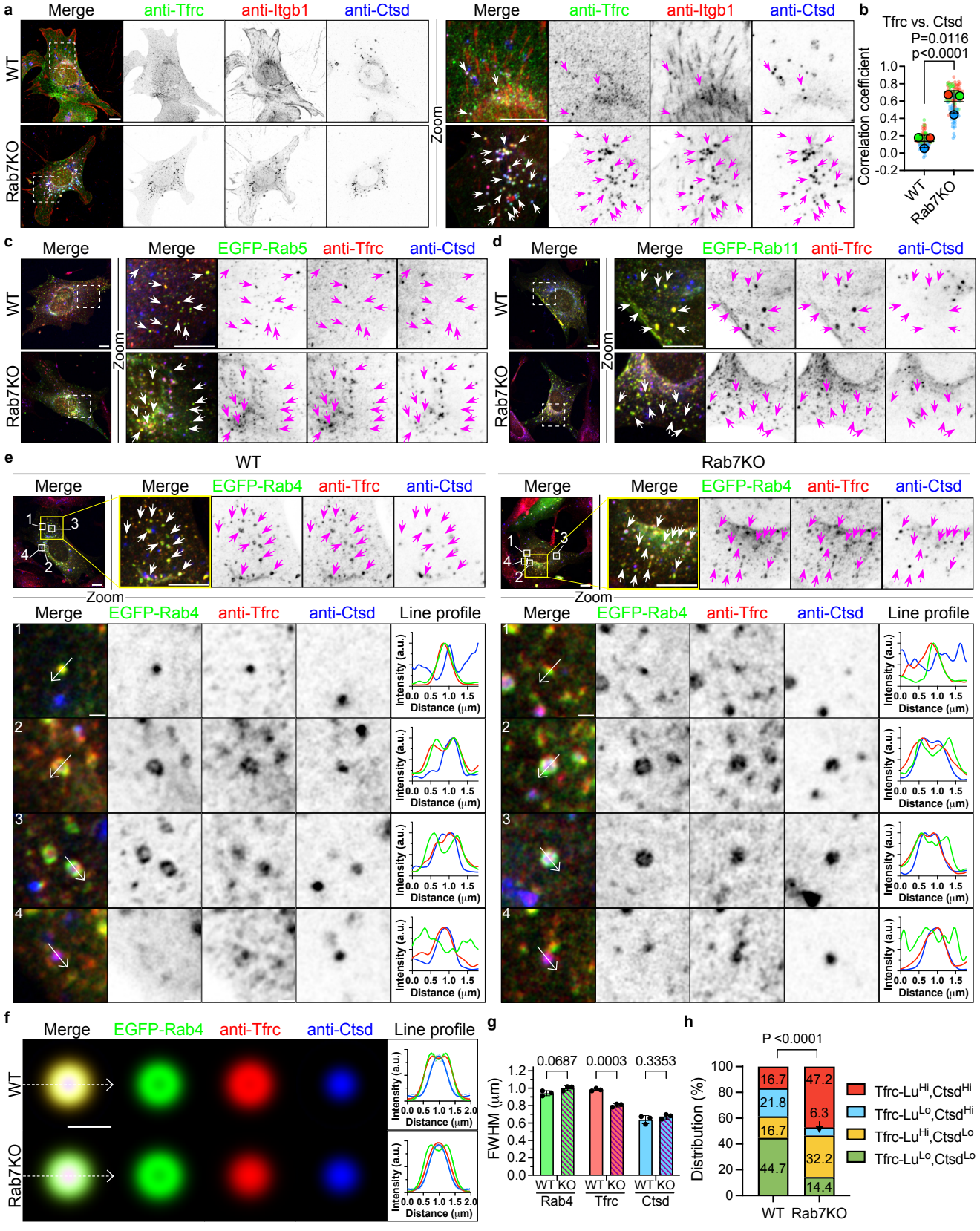
a
Merge
anti-Tfrc
anti-Itgb1
anti-Ctsd
WT
Rab7KO
Zoom
b
Tfrc vs. Ctsd
P=0.0116
p<0.0001
Correlation coefficient
WT
Rab7KO
c
Merge
EGFP-Rab5
d
EGFP-Rab11
e
WT
Rab7KO
EGFP-Rab4
Line profile
Intensity (a.u.)
Distance (μm)
f
g
FWHM (μm)
0.0687
0.0003
0.3353
Rab4
Tfrc
Ctsd
h
P <0.0001
Distribution (%)
Tfrc-Lu^Hi,Ctsd^Hi
Tfrc-Lu^Lo,Ctsd^Hi
Tfrc-Lu^Hi,Ctsd^Lo
Tfrc-Lu^Lo,Ctsd^Lo

Fig. 5

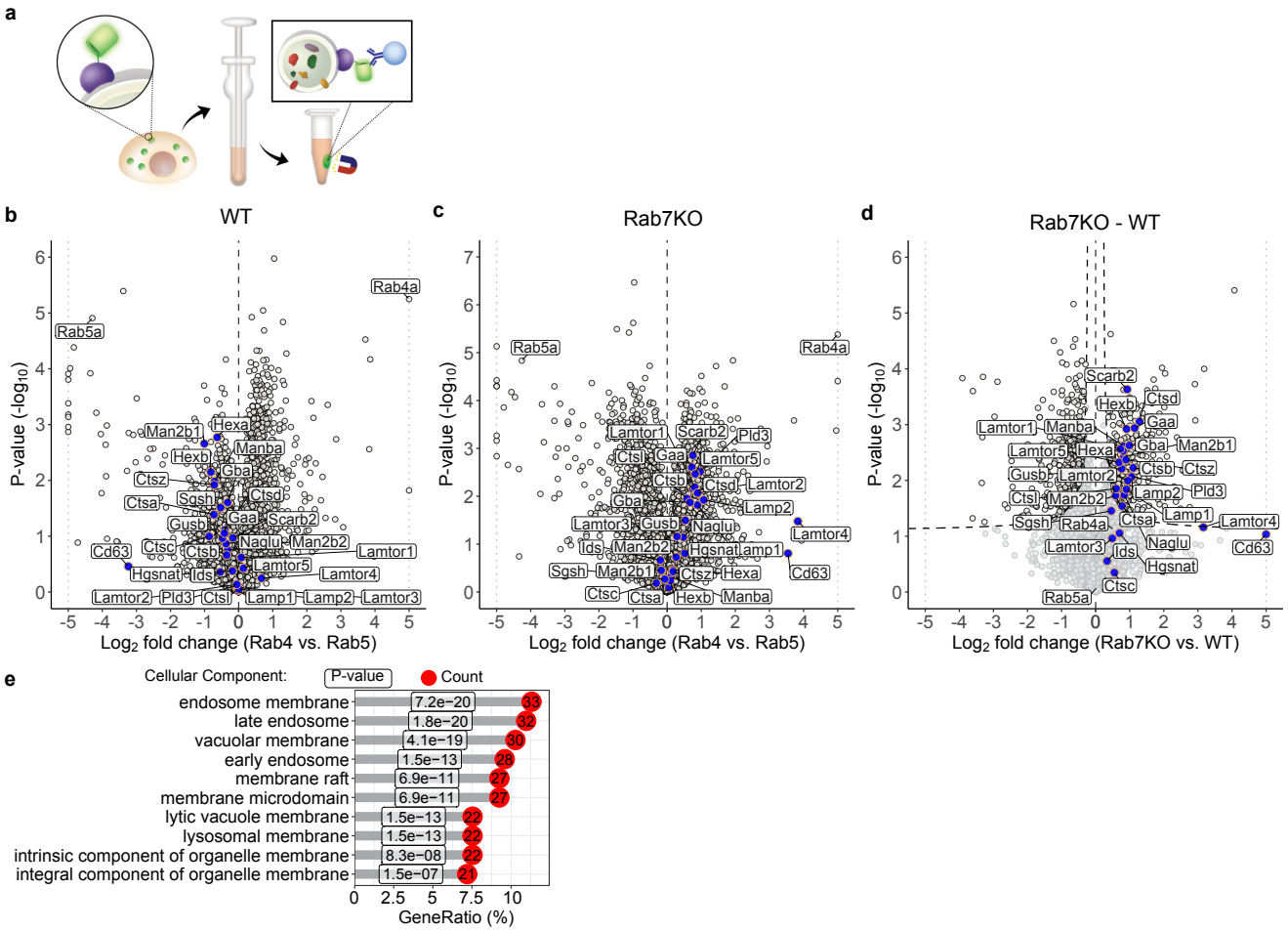
a
b
WT
c
Rab7KO
d
Rab7KO - WT
P-value (-log10)
Log2 fold change (Rab4 vs. Rab5)
Log2 fold change (Rab4 vs. Rab5)
Log2 fold change (Rab7KO vs. WT)
Rab4a
Rab5a
e
Cellular Component:
P-value
Count
endosome membrane
late endosome
vacuolar membrane
early endosome
membrane raft
membrane microdomain
lytic vacuole membrane
lysosomal membrane
intrinsic component of organelle membrane
integral component of organelle membrane
7.2e−20
1.8e−20
4.1e−19
1.5e−13
6.9e−11
6.9e−11
1.5e−13
1.5e−13
8.3e−08
1.5e−07
33
32
30
28
27
27
22
22
22
21
GeneRatio (%)

Fig. 6

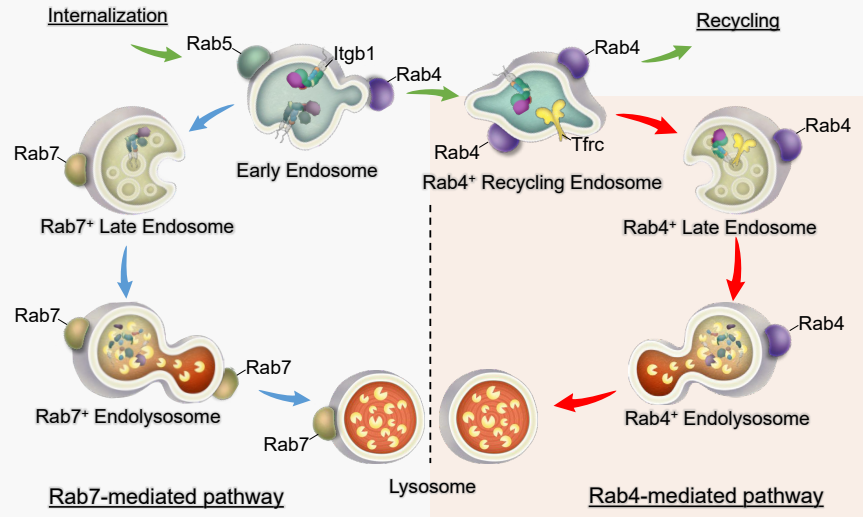
Internalization
Rab5
Itgb1
Rab4
Early Endosome
Rab7
Rab7⁺ Late Endosome
Rab7
Rab7⁺ Endolysosome
Rab7
Rab7-mediated pathway
Lysosome
Recycling
Rab4
Rab4
Tfrc
Rab4⁺ Recycling Endosome
Rab4
Rab4⁺ Late Endosome
Rab4
Rab4⁺ Endolysosome
Rab4-mediated pathway

Extended Data Fig. 1, related to Fig. 1

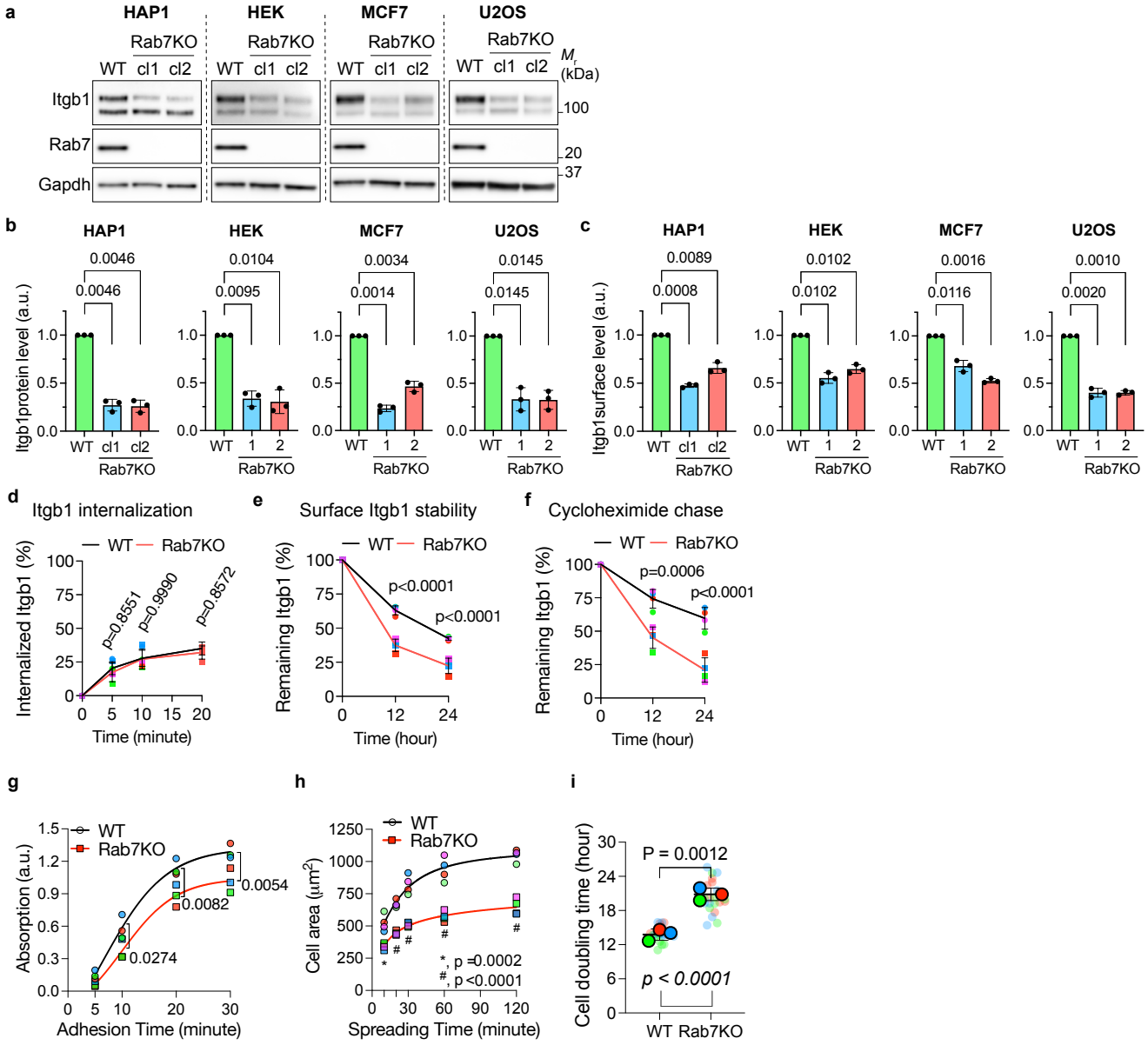

Extended Data Fig. 2, related to Fig. 2

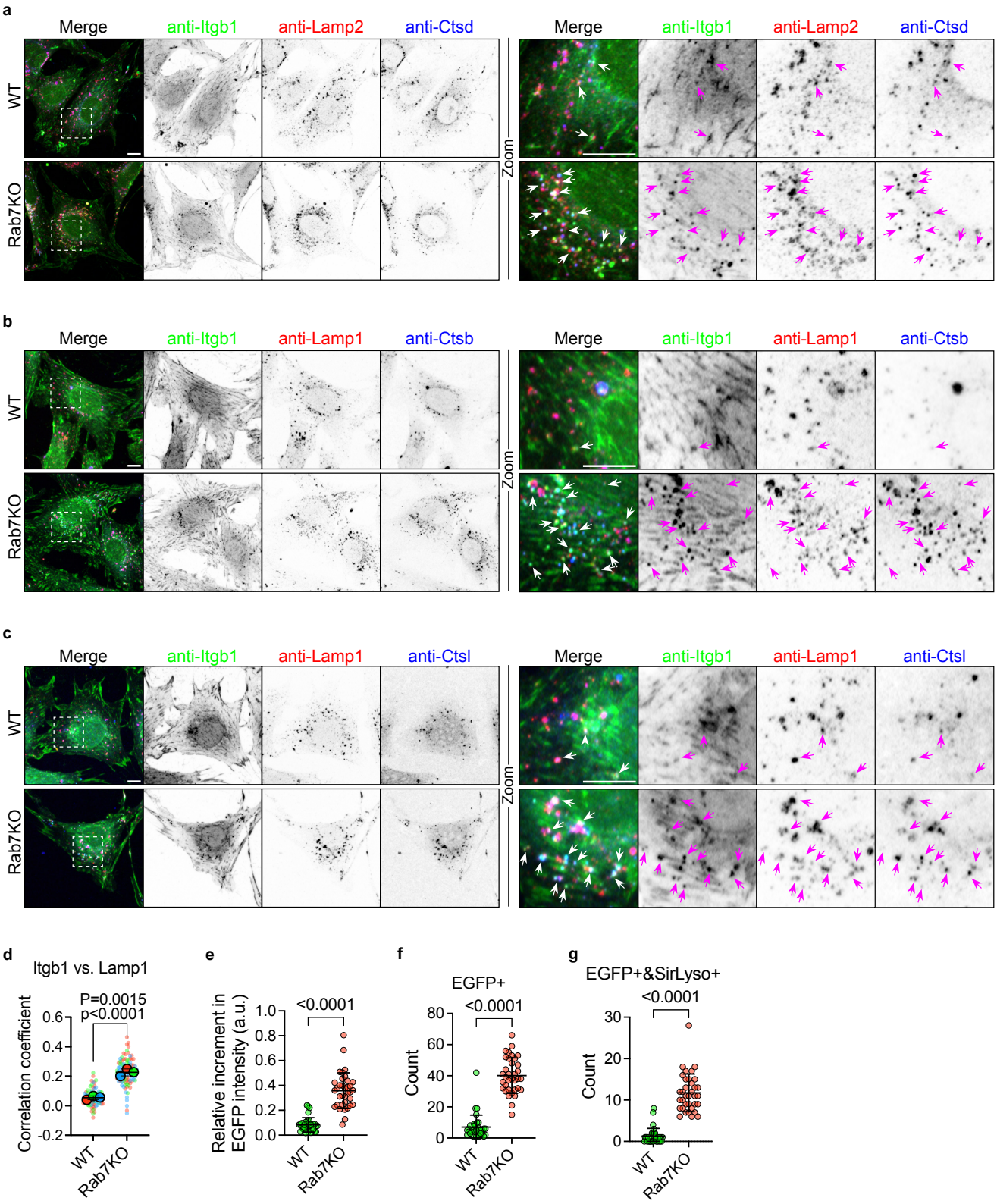

Extended Data Fig. 3, related to Fig. 2

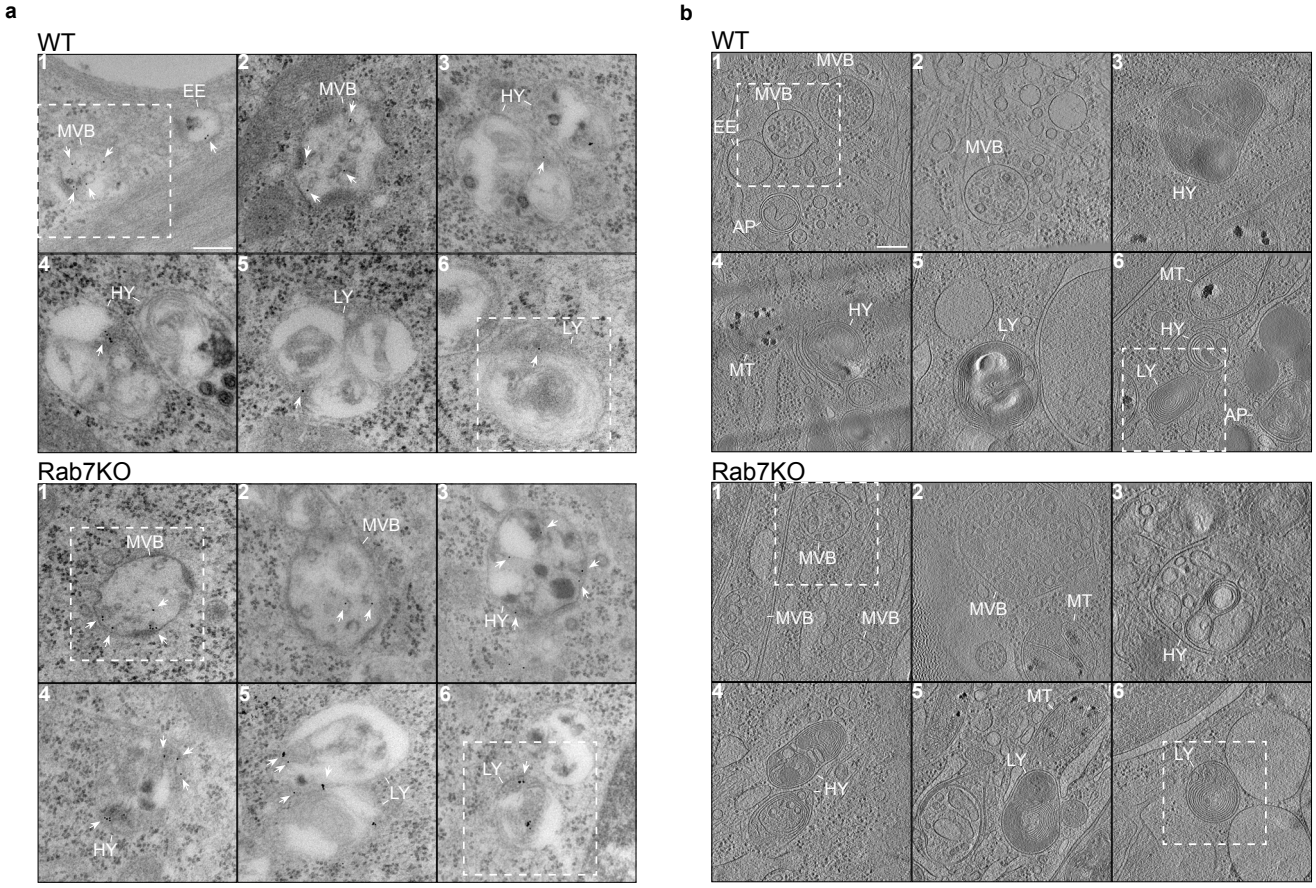

Extended Data Fig. 4, related to Fig. 4

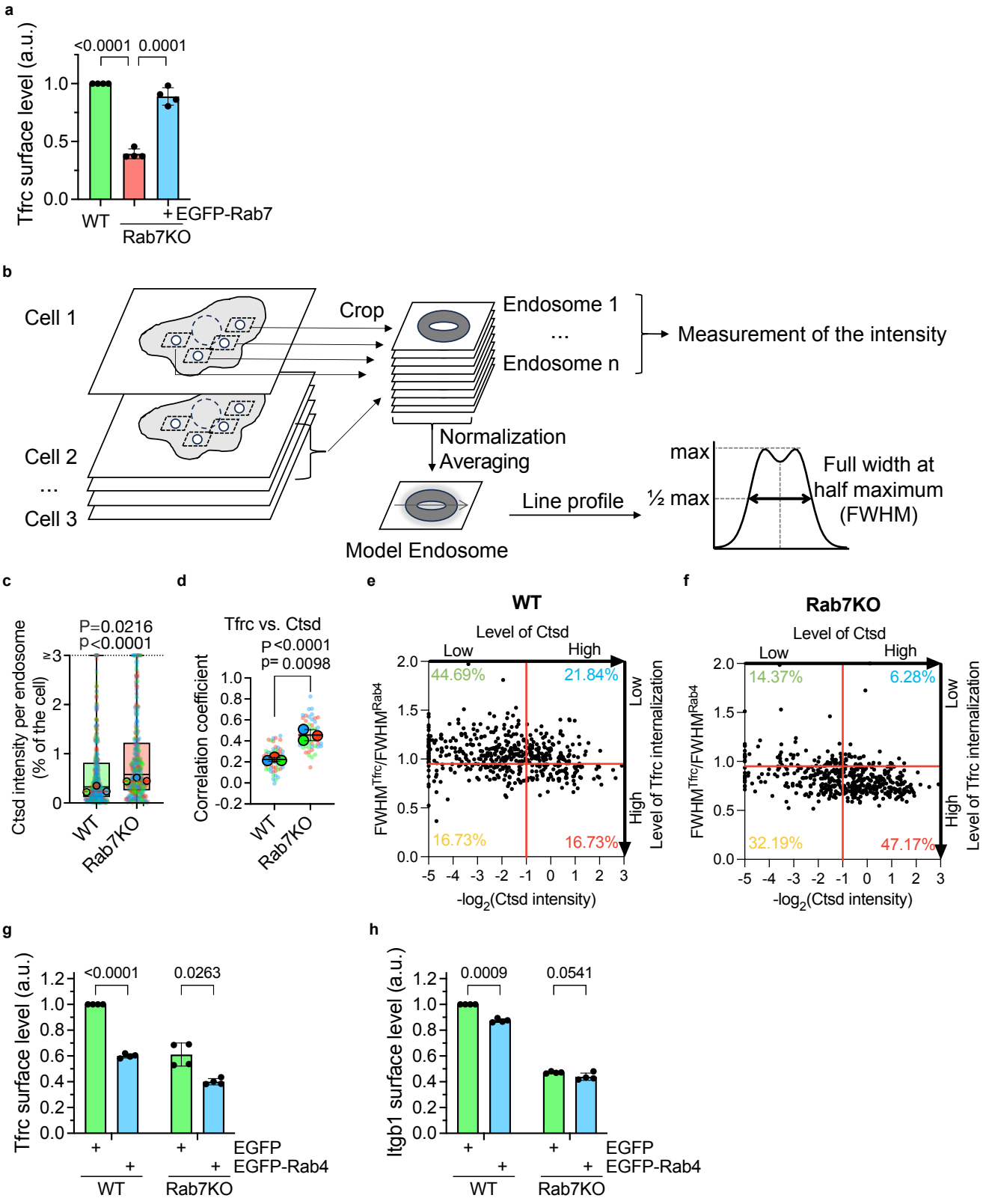

Extended Data Fig. 5, related to Fig. 4

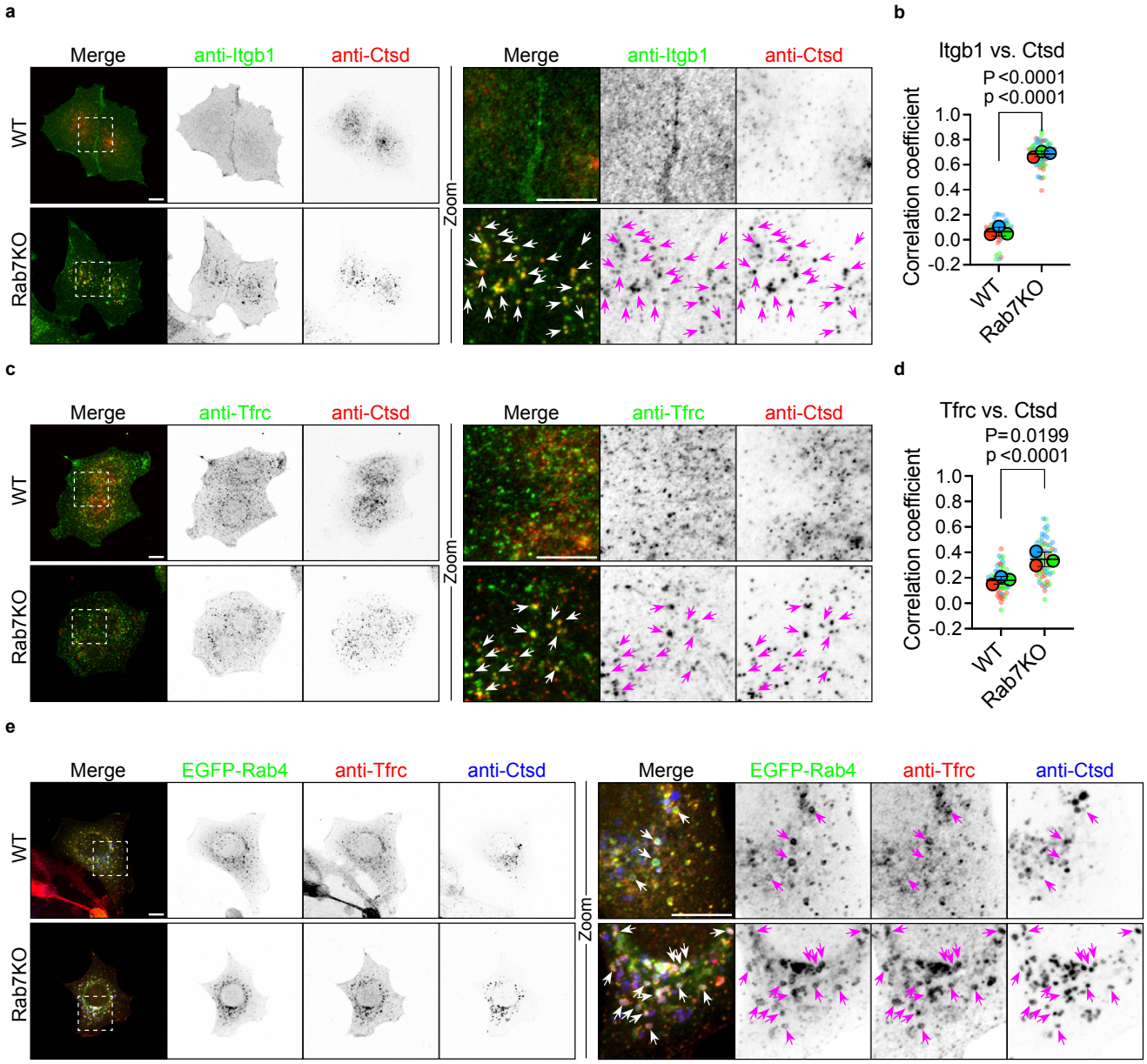

Extended Data Fig. 6, related to Fig. 4

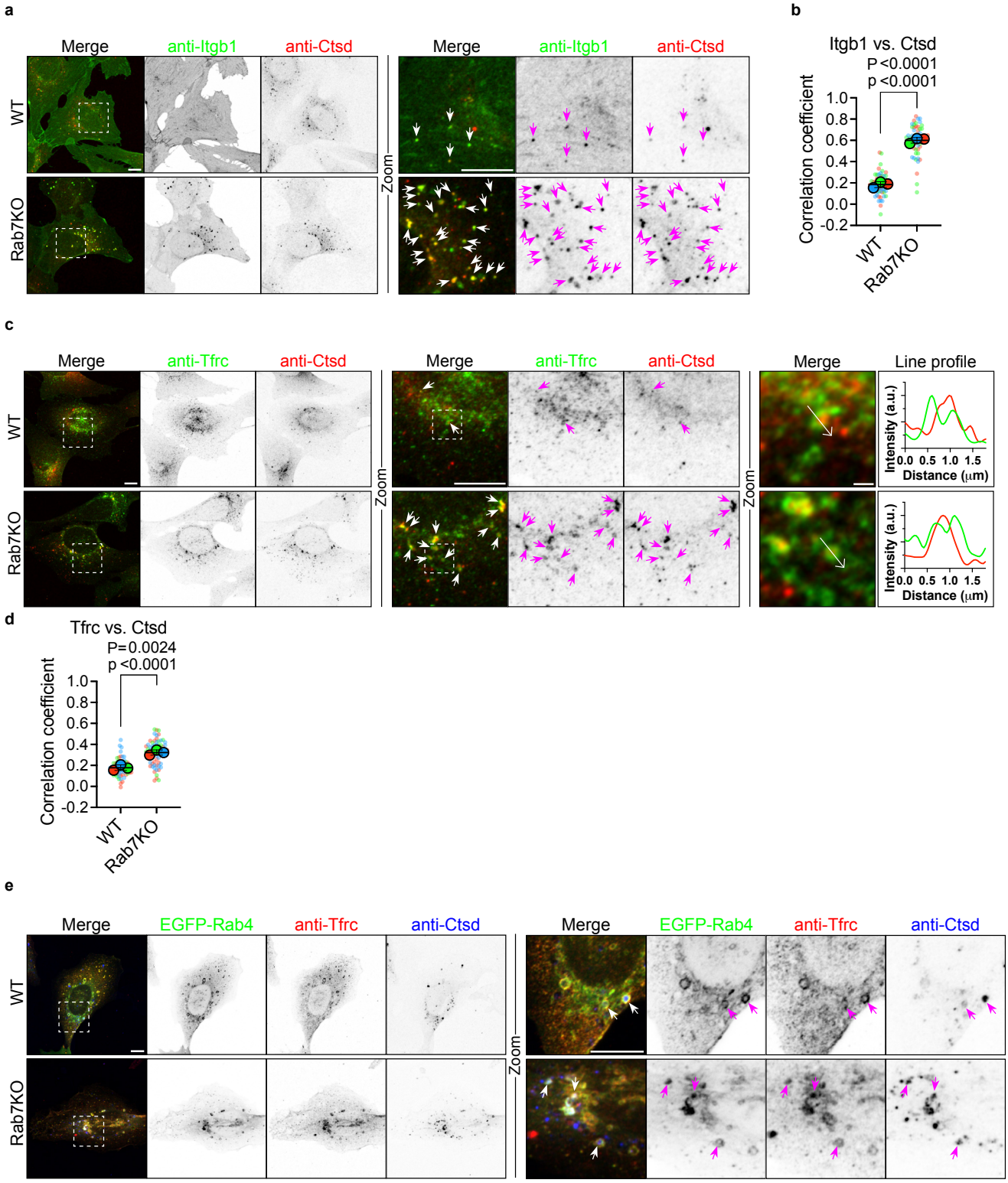

Email

Manuscript #	EMBOR-2024-59594-T
Title	The USP12/46 deubiquitinases protect integrins from ESCRT-mediated lysosomal degradation
Corresponding Author	Dr. Guan Wang (Max Planck Institute of Biochemistry)
Date:	24th Jun 24 09:52:08
Last Sent:	24th Jun 24 09:52:08
Created By:	Redacted
From:	contact@emboreports.org
To:	gwang@biochem.mpg.de
BCC:	Redacted
Subject:	EMBOR-2024-59594-T Decision Letter
Email	Dear Dr. Wang Thank you for the submission of your research manuscript to our journal. We have now received the full set of referee reports that is copied below. As you will see, all referees acknowledge that the findings are interesting and that the conclusions are overall supported by the data presented but they also raise a number of concerns and have suggestions how to further strengthen the data, which should be addressed in a revision. Please also note that all Methods must be part of the main manuscript text. Along these lines, I noted that the section on "Integrin degradation, internalization and recycling assays" refers to a previous study without giving any more details. Please carefully check whether you indeed followed exactly this protocol and I recommend adding at least a minimal set of experimental details. Given the constructive comments and support from the referees, we would like to invite you to revise your manuscript with the understanding that the referee concerns (as detailed above and in their reports) must be fully addressed and their suggestions taken on board. Please address all referee concerns in a complete point-by-point response. Acceptance of the manuscript will depend on a positive outcome of a second round of review. It is EMBO Reports policy to allow a single round of revision only and acceptance or rejection of the manuscript will therefore depend on the completeness of your responses included in the next, final version of the manuscript. We realize that it is difficult to revise to a specific deadline. In the interest of protecting the conceptual advance provided by the work, we recommend a revision within 3 months (September 24). Please discuss the revision progress ahead of this time with the editor if you require more time to complete the revisions. I am also happy to discuss the revision further via e-mail or a video call, if you wish. You can either publish the study as a short report or as a full article. For short reports, the revised manuscript should not exceed 27,000 characters (including spaces but

excluding materials & methods and references) and 5 main plus 5 expanded view figures. The results and discussion sections must further be combined, which will help to shorten the manuscript text by eliminating some redundancy that is inevitable when discussing the same experiments twice. For a normal article there are no length limitations, but it should have more than 5 main figures and the results and discussion sections must be separate. In both cases, the entire materials and methods must be included in the main manuscript file.

*****IMPORTANT NOTE:
We perform an initial quality control of all revised manuscripts before re-review. Your manuscript will FAIL this control and the handling will be delayed IN CASE the following APPLIES:

1) A data availability section providing access to data deposited in public databases is missing. If you have not deposited any data, please add a sentence to the data availability section that explains that.

2) Your manuscript contains statistics and error bars based on n=2. Please use scatter blots in these cases. No statistics should be calculated if n=2.

When submitting your revised manuscript, please carefully review the instructions that follow below. Failure to include requested items will delay the evaluation of your revision.*****

When submitting your revised manuscript, we will require:

1) a .docx formatted version of the manuscript text (including legends for main figures, EV figures and tables). Please make sure that the changes are highlighted to be clearly visible.

2) individual production quality figure files as .eps, .tif, .jpg (one file per figure). Please download our Figure Preparation Guidelines (figure preparation pdf) from our Author Guidelines pages https://www.embopress.org/page/journal/14693178/authorguide for more info on how to prepare your figures.

3) a .docx formatted letter INCLUDING the reviewers' reports and your detailed point-by-point responses to their comments. As part of the EMBO Press transparent editorial process, the point-by-point response is part of the Review Process File (RPF), which will be published alongside your paper.

4) a complete author checklist, which you can download from our author guidelines (<https://www.embopress.org/page/journal/14693178/authorguide>). Please insert information in the checklist that is also reflected in the manuscript. The completed author checklist will also be part of the RPF.

5) Please note that all corresponding authors are required to supply an ORCID ID for their name upon submission of a revised manuscript (<https://orcid.org/>). Please

find instructions on how to link your ORCID ID to your account in our manuscript tracking system in our Author guidelines (<https://www.embopress.org/page/journal/14693178/authorguide#authorshipguidelines>)

6) We replaced Supplementary Information with Expanded View (EV) Figures and Tables that are collapsible/expandable online. A maximum of 5 EV Figures can be typeset. EV Figures should be cited as 'Figure EV1, Figure EV2" etc... in the text and their respective legends should be included in the main text after the legends of regular figures.

- For the figures that you do NOT wish to display as Expanded View figures, they should be bundled together with their legends in a single PDF file called *Appendix*, which should start with a short Table of Content. Appendix figures should be referred to in the main text as: "Appendix Figure S1, Appendix Figure S2" etc. See detailed instructions regarding expanded view here: <https://www.embopress.org/page/journal/14693178/authorguide#expandedview>

- Additional Tables/Datasets should be labeled and referred to as Table EV1, Dataset EV1, etc. Legends have to be provided in a separate tab in case of .xls files. Alternatively, the legend can be supplied as a separate text file (README) and zipped together with the Table/Dataset file.

7) Before submitting your revision, primary datasets (and computer code, where appropriate) produced in this study need to be deposited in an appropriate public database (see < https://www.embopress.org/page/journal/14693178/authorguide#dataavailability>). Specifically, we would kindly ask you to provide public access to the mass spectrometry dataset.

Please remember to provide a reviewer password if the datasets are not yet public.

The accession numbers and database should be listed in a formal "Data Availability " section (placed after Materials & Method) that follows the model below (see also < https://www.embopress.org/page/journal/14693178/authorguide#dataavailability>). Please note that the Data Availability Section is restricted to new primary data that are part of this study.

Data availability

The datasets (and computer code) produced in this study are available in the following databases:

- RNA-Seq data: Gene Expression Omnibus GSE46843 (https://www.ncbi.nlm.nih.gov/geo/query/acc.cgi?acc=GSE46843)
- [data type]: [name of the resource] [accession number/identifier/doi] ([URL or identifiers.org/DATABASE:ACCESSION])

*** Note - All links should resolve to a page where the data can be accessed. ***

8) At EMBO Press we ask authors to provide source data for the main figures. Our source data coordinator will contact you to discuss which figure panels we would need source data for and will also provide you with helpful tips on how to upload and organize the files.

Additional information on source data and instruction on how to label the files are available
<https://www.embopress.org/page/journal/14693178/authorguide#sourcedata>.

9) The journal requires a statement specifying whether or not authors have competing interests (defined as all potential or actual interests that could be perceived to influence the presentation or interpretation of an article). In case of competing interests, this must be specified in your disclosure statement. Further information: https://www.embopress.org/competing-interests

10) Figure legends and data quantification:
The following points must be specified in each figure legend:

- the name of the statistical test used to generate error bars and P values,
- the number (n) of independent experiments (please specify technical or biological replicates) underlying each data point,
- the nature of the bars and error bars (s.d., s.e.m.)

- If the data are obtained from n {less than or equal to} 5, show the individual data points in addition to the SD or SEM.
- If the data are obtained from n {less than or equal to} 2, use scatter blots showing the individual data points.

Discussion of statistical methodology can be reported in the materials and methods section, but figure legends should contain a basic description of n, P and the test applied.

See also the guidelines for figure legend preparation:
https://www.embopress.org/page/journal/14693178/authorguide#figureformat

- Please also include scale bars in all microscopy images and define their size in the legend, not the image.

11) Our journal encourages inclusion of *data citations in the reference list* to directly cite datasets that were re-used and obtained from public databases. Data citations in the article text are distinct from normal bibliographical citations and should directly link to the database records from which the data can be accessed. In the main text, data citations are formatted as follows: "Data ref: Smith et al, 2001" or "Data ref: NCBI Sequence Read Archive PRJNA342805, 2017". In the Reference list, data citations must be labeled with "[DATASET]". A data reference must provide the database name, accession number/identifiers and a resolvable link to the landing page from which the data can be accessed at the end of the reference. Further instructions are available at

<https://www.embopress.org/page/journal/14693178/authorguide#referencesformat>.

12) All Materials and Methods need to be described in the main text. We would encourage you to use 'Structured Methods', our new Methods format. According to this format, the Methods section should include a Reagents and Tools Table (listing key reagents, experimental models, software and relevant equipment and including their sources and relevant identifiers) followed by a Methods and Protocols section in which we encourage the authors to describe their methods using a step-by-step protocol format with bullet points, to facilitate the adoption of the methodologies across labs. More information on how to adhere to this format as well as downloadable templates (.docx) for the Reagents and Tools Table can be found in our author guidelines: <
https://www.embopress.org/page/journal/14693178/authorguide#manuscriptpreparation>.

An example of a Method paper with Structured Methods can be found here: <https://www.embopress.org/doi/full/10.1038/s44320-024-00037-6#sec-4>.

13) As part of the EMBO publication's Transparent Editorial Process, EMBO Reports publishes online a Review Process File to accompany accepted manuscripts. This File will be published in conjunction with your paper and will include the referee reports, your point-by-point response and all pertinent correspondence relating to the manuscript.

You are able to opt out of this by letting the editorial office know (emboreports@embo.org). If you do opt out, the Review Process File link will point to the following statement: "No Review Process File is available with this article, as the authors have chosen not to make the review process public in this case."

We would also welcome the submission of cover suggestions, or motifs to be used by our Graphics Illustrator in designing a cover.

I look forward to seeing a revised form of your manuscript when it is ready and please let me know if you have questions or comments regarding the revision.

You can use this link to submit your revision: https://embor.msubmit.net/cgi-bin/main.plex

Yours sincerely,

Martina Rembold, PhD
Senior Editor
EMBO reports

****

Referee #1:

In their manuscript, Yu and colleagues, by combining genetic screening in haploid Cas9-expressing HAP1 cells and a BioID-based proximitome of integrin β1 (Itgb1) identify USP46, USP12, WDR48 and WDR2 as the components of the major deubiquitinating complex (DUB) of Itgb1 under steady-state culture conditions. Through an extremely robust series of knockdown (KO) and rescue experiments with wild type (WT) or mutant constructs in at least two different clones of murine fibroblasts and MDA-MB-231 human breast carcinoma cells, the Authors clearly demonstrate how the DUB USP12/46-WDR48-WDR20 complex is critical in enabling the post-endocytic recycling and rescue from polyubiquitin K63-dependent and ESCRT-dependent lysosomal degradation of Itgb1, and the α5β1 heterodimer in particular. The Authors conclude by demonstrating how expression levels of USP12/46, in addition to controlling adhesion, migration and invasion of MDA-MB-231 cells, are related to the overall survival and progression-free interval of breast cancer patients.

The study is clearly and thoroughly developed, identifying a novel and crucial complex that, by allowing the recycling of endocytosed Itgb1, controls Itgb1 half-life and function with important (also pathological) implications. The overall picture could still be completed by two integrations.

1. In a series of experiments, such as those shown in Figure 4H-j, the Authors give evidence that deubiquitylation is necessary for the recycling of endocytosed Itgb1. Indeed, lysosomal inhibition with Bafilomycin A1 restores total Itgb1 levels, but does not recover its physiological levels on the surface of USP12/46-dKO fibroblasts. On the other hand, ESCRT silencing increases the surface levels of α5WTβ1WT, but little of α5KRβ1KR in Itgb1-KO/USP12/46-dKO fibroblasts. It would complete the overall picture of the manuscript if the Authors could offer support for a mechanistic hypothesis of the reason why deubiquitylation is required for subsequent surface recycling of endocytosed Itgb1. Could the ubiquitination of the cytosolic tail of Itgb1 (e.g., at the K794 level of the NPK794Y motif) impair the PTB-domain-mediated interaction with SNX17, while favoring its association with the ESCRT complex? Would this be experimentally testable, e.g., by using the approach described in Böttcher et al., Nat Cell Biol, 2012?

2. It would be helpful if the Authors could comment in the Discussion about whether or not USP12 and USP46 might represent potential targets of a hypothetical pharmacological approach aimed at their inhibition, for example in the context of breast cancer.

Referee #2:

Review of Yu et al (USP46/USP12 and ITGB1 manuscript)

I very much enjoyed reading this very interesting, well-crafted manuscript, which uses a DUB focussed CRISPR based screen in conjunction with proximity biotinylation

proteomics to identify the two paralogous DUBs, USP12 and USP46 as direct regulators of lysosomal trafficking of integrins.

Both DUBs form functional ternary complexes with two WD40-proteins WDR48 and WDR20, and the authors provide compelling evidence in form of KO and rescue experiments, for a requirement not just of catalytic activity of the DUBs but also of the presence of and association with these two cofactors. In the absence of both The authors go on to implicate the ESCRT machinery (using an ESCRT-0 and ESCRTI double knock down) and K63-linked ubiquitin chains as mediators of ubiquitin dependent downregulation of ITGB1 and ITGA5. A final set of figures relates the effects of USP12 and 46 KO on integrin expression levels and integrin surface lecvels to functional adhesion read-outs. The biochemical approaches are supplemented by very informative quantitated immunofluorescence imaging approaches. The manuscript is well written and well argued. Overall this manuscript provides important new mechanistic insights into the trafficking routes and ubiquitin dependent turnover of integrins and informs on the biology of two hitherto poorly characterised DUBs.

I have listed a few minor data-specific comments below:

With regards to Figure 1 and the discussion: The authors do not comment on why they think it was possible for them to identify USP46 in their CRISPR screen, if there is clear redundancy between USP46 and USP12. It may also be useful to point to USP12 in Figure 1B? Is it possible that USP12 expression levels are particularly low in the HAP1 cells?
Figure EV2G cl1 allele 1 and 2 usp46 - should the last base be an A rather than a G or should the G be labelled in red?
Figure 3A and C : in these graphs and associated legend it is unclear what the P-values are related to. If as the figure implies the comparison is made with the WT then the key stats are missing. The text states that the KO of SNX17 on top of USP12/46 has a stronger effect that either 12/46 alone or SNX17 alone.
Figure 4: Please clarify on the x-axis of the graphs in this figure whether the time is refering to a CHX chase and on the Y-axis whether the data refer to total or cell surface levels. This will help the reader. In Figure 4H please state clearly in the text that the treatment was for 9 hours.
General comment on the CHX chases - such long chases are difficult to interprete, and with such few datapoints I would suggest refraining from deducing values for halflifes in the text.
Figure 4J - That BAF does not rescue cell surface levels was not surprising to this reader, but what is more surprising and not remarked on is that it does rescue the SNX17 KO associated decrease in ITGB1 cell surface levels. This may be worthwhile mentioning and exploring in the discussion.
Figure 5 - It would be really helpful if ideally all quantitations that have been relegated to EV5 could be shown in Figure 5. I think that EV5 is essential and should be incorporated in the main figures.
Figure 5D - it is currently very unclear from the text and legends, which cells these mass spec data have been derived from. Is this from a comparison of USP12/46 dKO vs WT lines in each case with ESCRT KD? I also could not find a section for this in the methods. Later on the authors generate Knull mutants of ITGB1 and elect to mutate all Ks. Do the autrhors have evidence that suggests the three identified Ks in Figure

	5D are not the only ones that are ubiquitylated? This choice (of generating a complete Knull) may just be worth rationalising in the result section. Figure 5G - this is very nice and could become its own figure if space is needed for the quantifications for the blots above. It does look like USP12 and ITGB1 colocalise on enlarged endosomes, but the authors have not provided a colocalisation of either with an endosomal marker. An additional set of panels showing the colocalisation of ITGB1 and USP12 with endosomes would be very helpful - an EEA1 antibody would be appropriate here. Aligned with this: have the authors assessed the localisation of endogenous USP12 or USP46 under these conditions? It is odd to find no parts of the Methods in the main part of the manuscript. Line 205-207: "cells. A role for Itgb1 mRNA transcript stability in regulating Itgb1 protein levels could be excluded as no difference in Itgb1 mRNA levels were found between USP12/46-dKO and WT fibroblasts (Fig. 4A). - the p-value for cl2 actually suggests an increase - so suggest replacing "no difference" with "no decrease". Line 2019-202: "the USP12/46-WDRs complex stabilizes the surface as well as total Itgb1 protein levels" - suggest replacing "stabilizes" with "maintains". Line 291: "ubiquitinable" - typo Line 331 - 332 - consider rephrasing. Line 335 - consider replacing "we fund that" with "we hypothesised that" Referee #3: The manuscript by Yu et al describes a robust approach combining a Crispr/Cas9 screen with proximity labelling proteomics to identify DUBs that regulate ITGB1 levels in cells at steady state. The authors convincingly show that USP12 and its paralogue USP46 are DUBs that maintain integrin levels at steady state by removing K63-linked ubiquitin modifications. The USP12/46 associated adaptor proteins WDR48 and WDR20 are also required for maintenance of steady-state integrin levels. Functionally, low levels of USP12/46 decrease cell adhesion and motility, and high levels of USP12 correlate with poor outcomes in breast cancer. This is a very convincing and detailed study that identifies new players in regulation of integrins, and is close to the level and quality required for publication. I have three queries that the authors should address however: 1. The authors state that "SNX17 and USP12/46-WDR complex stabilise ITGB1 independently". Could it not be sequential, whereby USP12/46-WDRs remove ubiquitin to allow SNX17 binding and recycling? Perhaps this doesn't need to be addressed experimentally but warrants discussion. For figure 3 perhaps further statistical analysis of differences between USP versus SNX17 knockdown would reveal significant differences. 2. Figure 5 western blots would benefit from quantification, particularly panels panel A, E and F 3. Previous studies have identified USP9X and USP10 (Gillespie 2017 JCS) as DUBs targeting ubiquitin-modified integrins. The former is addressed, although some differences between the two studies can be observed, but the latter is not. This could easily be remedied with a brief addition to the discussion section, highlighting differences between the studies perhaps.

Email

Manuscript #	EMBOJ-2024-117710-T
Title	Rab7 deficiency induces lysosome formation from recycling endosomes leading to an increased degradation of cell surface proteins
Corresponding Author	Reinhard Fässler (Max Planck Institute of Biochemistry)
Date:	30th May 24 07:57:04
Last Sent:	30th May 24 07:57:04
Created By:	Redacted
From:	w.teale@embojournal.org
To:	faessler@biochem.mpg.de
BCC:	Redacted
Subject:	Manuscript EMBOJ-2024-117710-T - Decision
Email	Dear Dr. Fässler, Thank you again for the submission of your manuscript entitled "Rab7 deficiency induces lysosome formation from recycling endosomes leading to an increased degradation of cell surface proteins" (EMBOJ-2024-117710) and for your patience during the review process. We have now received the reports from the referees, which I copy below. As you can see from their comments, although referee #2 raises a range of technical concerns that will require your attention, there is a concensus that the work is novel and timely. Based on the overall interest expressed in the reports, I would like to invite you to address the comments of all referees in a revised version of the manuscript. I should add that it is The EMBO Journal policy to allow only a single major round of revision and that it is therefore important to resolve the main concerns at this stage. I believe the concerns of the referees are reasonable and addressable, but please contact me if you have any questions, need further input on the referee comments or if you anticipate any problems in addressing any of their points. I suggest we discuss referee #2's report by Zoom next week, once you have had the opportunity to go through it. Please, follow the instructions below when preparing your manuscript for resubmission. I would also like to point out that as a matter of policy, competing manuscripts published during this period will not be taken into consideration in our assessment of the novelty presented by your study ("scooping" protection). We have extended this 'scooping protection policy' beyond the usual 3 month revision timeline to cover the period required for a full revision to address the essential experimental issues. Please contact me if you see a paper with related content published elsewhere to discuss the appropriate course of action. When preparing your letter of response to the referees' comments, please bear in

mind that this will form part of the Review Process File, and will therefore be available online to the community. For more details on our Transparent Editorial Process, please visit our website: https://www.embopress.org/page/journal/14602075/authorguide#transparentprocess

Again, please contact me at any time during revision if you need any help or have further questions.

Thank you very much again for the opportunity to consider your work for publication. I look forward to your revision.

Best regards,

William

William Teale, Ph.D.
Editor
The EMBO Journal

When submitting your revised manuscript, please carefully review the instructions below and include the following items:

1) a .docx formatted version of the manuscript text (including legends for main figures, EV figures and tables). Please make sure that the changes are highlighted to be clearly visible.

2) individual production quality figure files as .eps, .tif, .jpg (one file per figure).

3) a .docx formatted letter INCLUDING the reviewers' reports and your detailed point-by-point response to their comments. As part of the EMBO Press transparent editorial process, the point-by-point response is part of the Review Process File (RPF), which will be published alongside your paper.

4) a complete author checklist, which you can download from our author guidelines (https://wol-prod-cdn.literatumonline.com/pb-assets/embo-site/Author Checklist%20-%20EMBO%20J-1561436015657.xlsx). Please insert information in the checklist that is also reflected in the manuscript. The completed author checklist will also be part of the RPF.

5) Please note that all corresponding authors are required to supply an ORCID ID for their name upon submission of a revised manuscript.

6) We require a 'Data Availability' section after the Materials and Methods. Before submitting your revision, primary datasets produced in this study need to be deposited in an appropriate public database, and the accession numbers and database listed under 'Data Availability'. Please remember to provide a reviewer

password if the datasets are not yet public (see https://www.embopress.org/page/journal/14602075/authorguide#datadeposition). If no data deposition in external databases is needed for this paper, please then state in this section: This study includes no data deposited in external repositories. Note that the Data Availability Section is restricted to new primary data that are part of this study.

Note - All links should resolve to a page where the data can be accessed.

7) When assembling figures, please refer to our figure preparation guideline in order to ensure proper formatting and readability in print as well as on screen: http://bit.ly/EMBOPressFigurePreparationGuideline

Please remember: Digital image enhancement is acceptable practice, as long as it accurately represents the original data and conforms to community standards. If a figure has been subjected to significant electronic manipulation, this must be noted in the figure legend or in the 'Materials and Methods' section. The editors reserve the right to request original versions of figures and the original images that were used to assemble the figure.

8) For data quantification: please specify the name of the statistical test used to generate error bars and P values, the number (n) of independent experiments (specify technical or biological replicates) underlying each data point and the test used to calculate p-values in each figure legend. The figure legends should contain a basic description of n, P and the test applied. Graphs must include a description of the bars and the error bars (s.d., s.e.m.).

9) We would also encourage you to include the source data for figure panels that show essential data. Numerical data can be provided as individual .xls or .csv files (including a tab describing the data). For 'blots' or microscopy, uncropped images should be submitted (using a zip archive or a single pdf per main figure if multiple images need to be supplied for one panel). Additional information on source data and instruction on how to label the files are available at <https://www.embopress.org/page/journal/14602075/authorguide#sourcedata >.

10) We replaced Supplementary Information with Expanded View (EV) Figures and Tables that are collapsible/expandable online (see examples in https://www.embopress.org/doi/10.15252/embj.201695874). A maximum of 5 EV Figures can be typeset. EV Figures should be cited as 'Figure EV1, Figure EV2" etc. in the text and their respective legends should be included in the main text after the legends of regular figures.

- For the figures that you do NOT wish to display as Expanded View figures, they should be bundled together with their legends in a single PDF file called *Appendix*, which should start with a short Table of Content. Appendix figures should be referred to in the main text as: "Appendix Figure S1, Appendix Figure S2" etc. See detailed instructions regarding expanded view here: <https://www.embopress.org/page/journal/14602075/authorguide#expandedview >.

- Additional Tables/Datasets should be labelled and referred to as Table EV1, Dataset EV1, etc. Legends have to be provided in a separate tab in case of .xls files. Alternatively, the legend can be supplied as a separate text file (README) and zipped together with the Table/Dataset file.

11) At EMBO Press we ask authors to provide source data for the main manuscript figures. Our source data coordinator will contact you to discuss which figure panels we would need source data for and will also provide you with helpful tips on how to upload and organize the files.

12) Our journal encourages inclusion of *data citations in the reference list* to directly cite datasets that were re-used and obtained from public databases. Data citations in the article text are distinct from normal bibliographical citations and should directly link to the database records from which the data can be accessed. In the main text, data citations are formatted as follows: "Data ref: Smith et al, 2001" or "Data ref: NCBI Sequence Read Archive PRJNA342805, 2017". In the Reference list, data citations must be labeled with "[DATASET]". A data reference must provide the database name, accession number/identifiers and a resolvable link to the landing page from which the data can be accessed at the end of the reference. Further instructions are available at <https://www.embopress.org/page/journal/14602075/authorguide#referencesformat >.

Instructions for preparing your revised manuscript:

Please make sure you upload a letter of response to the referees' comments together with the revised manuscript.

Please also check that the title and abstract of the manuscript are brief, yet explicit, even to non-specialists.

When assembling figures, please refer to our figure preparation guideline in order to ensure proper formatting and readability in print as well as on screen:
https://bit.ly/EMBOPressFigurePreparationGuideline
See also guidelines for figure legends:
https://www.embopress.org/page/journal/14602075/authorguide#figureformat

At EMBO Press we ask authors to provide source data for the main manuscript figures. Our source data coordinator will contact you to discuss which figure panels we would need source data for and will also provide you with helpful tips on how to upload and organize the files.

IMPORTANT: When you send the revision we will require
- a point-by-point response to the referees' comments, with a detailed description of the changes made (as a word file).
- a word file of the manuscript text.

- individual production quality figure files (one file per figure)
- a complete author checklist, which you can download from our author guidelines (https://www.embopress.org/page/journal/14602075/authorguide).
- Expanded View files (replacing Supplementary Information)
Please see out instructions to authors
https://www.embopress.org/page/journal/14602075/authorguide#expandedview

Please remember: Digital image enhancement is acceptable practice, as long as it accurately represents the original data and conforms to community standards. If a figure has been subjected to significant electronic manipulation, this must be noted in the figure legend or in the 'Materials and Methods' section. The editors reserve the right to request original versions of figures and the original images that were used to assemble the figure.

Further information is available in our Guide For Authors:
https://www.embopress.org/page/journal/14602075/authorguide

We realize that it is difficult to revise to a specific deadline. In the interest of protecting the conceptual advance provided by the work, we recommend a revision within 3 months (28th Aug 2024). Please discuss the revision progress ahead of this time with the editor if you require more time to complete the revisions. Use the link below to submit your revision:

https://emboj.msubmit.net/cgi-bin/main.plex

Referee #1:

In this manuscript, the authors report that loss of RAB7A, a RAB GTPase predominantly associated with late endosomes and lysosomes, results in the decrease of the expression of many surface proteins. The starting point of this study was an unbiased genome-wide insertional mutagenesis screen performed in the human haploid cell line HAP1 that identified RAB7A as a stabilizer of integrin beta-1 (Itgb1) surface level. They show that RAB7A loss produces functional lysosomes and that these lysosomes originate from RAB4A positive endosomes, which results in the degradation of proteins that are normally recycled to the cell surface.
This is an intriguing and somewhat unexpected finding as, to my knowledge, RAB4A has not been found so far to be associated with lysosome biogenesis. Most of the described experiments are generally convincing. However, some key experiments need to be strengthened or clarified.

Main points:

1. It is shown that Itgb1 accumulates in Lamp1 and cathepsin D (Ctsd) positive structures in RAB7A KO cells (Fig. 2a), which likely explains why loss of RAB7A reduces Igtb1 surface levels and consequently cell adhesion, spreading and

proliferation (Extended data Fig. 1g-i). A more direct experiment would be to investigate the kinetics of recycling of internalized Igtb1 in WT and RAB7A KO cells.
2. The same holds true for transferrin receptor (TfnR). In the early publications on RAB4A, its overexpression increases the level of cell surface associated TfnR (van der Sluijs et al, Cell 1992). In addition, RAB4A overexpression induces its accumulation in non-acidic compartments, presumably in fast recycling vesicles. The authors found the opposite, even in WT cells (Fig. 4, extended data Figs 4 and 5). To clarify this point, TfnR recycling experiments should be performed.
3. RAB4 positive lysosomes were identified under conditions of RAB4A overexpression (Fig. 4 e-f). A key missing experiment is to investigate what is happening when RAB4A is depleted in RAB7A KO cells.
4. The authors propose (Fig. 6) the existence of two separate pathways involved in lysosome biogenesis. They suggest that RAB5 and RAB11 do not participate in the biogenesis of RAB4 positive endosomes based on the experiments shown in Fig. 4c (overexpressed RAB5 and RAB11 do not colocalize with Ctsd+ lysosomes). This argument is rather weak and should be strengthened by investigating whether RAB4+/TfR+/Ctsd+ lysosomes are positive (or not) for RAB5 or RAB11.

Other points:

- Fig. 5: A mass spec analysis was performed on RAB4+ and RAB5+ endosomes isolated from RAB7A KO cells. The results show a clear difference in the protein content of the two populations. It is difficult however to appreciate the pertinence of this experiment in the absence of experimental details (yield and purity of the two samples).
- Fig. 4 c, e: The extent of colocalization between RAB4/RAB5 and TfR/Ctsd should be quantified.
- Introduction: "whether the three Rab5 isoforms share similar localization and functions". This is not true. Several publications suggest that it is not the case (see for instance Chen et al, PLoS One 2014, e90384).

Referee #2:

In "Rab7 deficiency induces lysosome formation from recycling endosomes leading to an increased degradation of cell surface proteins," Wang et al began by performing a genetic screen in haploid HAP1 cells to identify genes that regulate surface levels of integrin beta 1. They found that, surprisingly, both in the initial gene trap screen and after follow-up CRISPR-Cas9 editing in several cell lines, Rab7 deficiency led to the loss of surface and total cellular Itgb1 (integrin beta 1) as a result of increased BafA1-inhibitable (lysosomal) degradation. The authors demonstrate that autophagy (LC3-II +/-BafA1 and nutrients) and lysosomal exocytosis (LC-MS/MS of the secretome) still occur in Rab7 deficient cells. They then evaluate endosomal marker localization in Rab7 WT and deficient MEFs by microscopy, employing quantitative strategies in some cases; Itgb1, Lamp1, EGFP-Rab4, transferrin receptor, and cathepsin D localization were followed. A claim is made that lysosomes are "generated" from Rab4+ endosomes, but the data in Figs 4-

	5 does not strongly support this statement. Major concerns 1. The findings are significant in that, based on the literature, Rab7 loss might have been expected to decrease, rather than enhance, the lysosomal degradation of integrins by promoting recycling. However, beyond this initial point, there is not a clear story or message in this manuscript. Mechanisms are not definitively explored, and experiments are not clearly connected to each other. Moreover, the authors seem to confound lysosomal biogenesis with trafficking of surface proteins to lysosomes. Figs 4-5 do not provide sufficient evidence for the authors to conclude that Rab4 is now supporting "lysosomal biogenesis" in the absence of Rab7. Critical "necessary and sufficient" type experiments are not performed. The physiological relevance of the findings is also not clearly defined. 2. Concerns about data reporting and replication. Some examples: a. CRISPR approach does not include critical controls - two different guides and rescue by reconstitution across critical experiments. One rescue experiment is performed in fibroblasts for Itgb1 expression only. None of the proteomics or microscopy includes a reconstitution control. Moreover, vector (Cas9 only) or non-targeting sgRNA control is not performed anywhere in the paper. It appears that Cas9 is constitutively expressed (retroviral transduction of Cas9 in many cell lines, no clear explanation of CRISPR strategy used in fibroblasts; transfection was used to introduce editing constructs in HAP1 cells). Cells constitutively expressing Cas9 were passaged for an indeterminate amount of time prior to experiments without a non-targeting control for the effects of long-term Cas9 expression. The methods are unclear, but it seems only one sgRNA was used in many cases, and it is difficult to determine when clones were used, which particular clone was utilized, and which sgRNA was used. Taken together, these issues represent a significant experimental design problem that negatively impacts rigor. Controls are particularly important given that at least some of the results are unexpected based on the literature. b.Information about replication is not always consistent with what is shown in figures and with expectations for data variability. The authors routinely state that 3 replicates were performed, but the spread of the data and inconsistencies between figures suggest that technical replicates are presented in many of the graphs and that statistical analysis was performed on technical rather than true biological replicates performed on different days. For example, in Fig 1f/i there is not enough variation to be realistic biological replicates. Moreover, the same Rab7 KO clones produce variable results in Fig 1f and i (both surface Itgb1 levels in Rab7 deficient cells by flow), yet each individual graph shows replicates that are almost identical. It seems highly unlikely that the measurements made in Fig 4g would have the limited variability shown. Similarly, for the endosomal proteomics in Fig 5, what does "n=3 biological replicates" mean? This uncertainty about replication is an issue throughout the figures. c. No histograms are shown to support flow cytometry. It is unclear how well the Ab used in flow detects Itgb1 relative to background (a non-specific antibody) or whether the shape of these histograms changes +/-Rab7; histogram shape is a critical variable determining whether the MFI is an accurate representation of the

	data. d. The microscopy data is inconsistently quantitative and many of the analyses could be subject to bias and would best have been performed in a blinded manner. In Fig 4, it is not clear how many or which subset of endosomes were evaluated. In Fig 2a/b the zoom is confusing. The quantitation does not seem to reflect the data as the vast majority of Itgb1 (lots of green signal) is not colocalized with catB even in the Rab7 KO. It also appears that max projections were used to follow colocalization which is inappropriate; colocalization should be evaluated in a single confocal slice. e. Proteomics data is not provided in a format that would allow independent analysis, only as processed data in randomly labeled plots. f. While it can be hard to detect surface proteins by IF, there is not a clear decrease in surface or total Itgb1 in Fig 2a as would be expected from Fig 1. Moreover, microscopy analysis should have included an image showing that Rab7 is not present in these cells (the antibody works well for IF) and Itgb1 levels should have been quantified. There also seems to be a strong nuclear signal for Itgb1 which seems unexpected and is not explained - the Itgb1 antibody is not validated as specific, and it is unclear if Itgb1 is nuclear. 3. Autophagy data is mischaracterized and misrepresented; statements on lines 390-395 are not consistent with the data shown. In addition to normalized LC3-II intensity, flux analysis should be presented: the ratio of normalized LC3-II +Baf/-Baf. If this were done, the flux in the cells +/-Rab7 could be compared. From the data shown, it looks like flux is blocked in the Rab7 KO just as was previously reported - the change +/- BafA1 is reduced in Rab deficient cells and LC3-II is accumulating even without Baf (due to reduced degradation) when Rab7 is lost. The levels of Rab7 should also have been shown by WB in these same cells. Conditions for "starvation" and [BafA1] in Fig 3a/b should be defined in the legend. 4. Secretome data could include EVs, not just lysosome exocytosis and it is not clear what this or autophagy has to do with integrin surface levels which is where the paper started. 5. Line 341 - "the massive degradation of surface proteins likely accounts for the embryonic lethality in vivo" - there is no evidence supporting this statement. Minor concerns 1. line 324 refers to "deleting" the Rab7 gene. With traditional CRISPR editing, the gene is still there and may have only a single nucleotide added or lost. Traditional CRISPR editing lowers proteins levels when it causes a frameshift mutation that leads to nonsense mediated decay of the mRNA. The gene is not deleted. Accurate language should be employed. 2. In Fig 1 b,c the colors don't make sense with the legend, color coding is confusing. 3. GFP-Rab7 can mislocalize in cells (localization does not match endogenous Rab7). It would have been preferrable to use untagged Rab7 to reconstitute as there is an excellent antibody available and no need here for GFP tagging. 4. Fig 2c obscures the mechanism by which a TM protein moves into the lumen.

5. ED Fig 2e-g legend is incomplete.
6. The main text does not adequately explain methods or why certain reagents were chosen/used.
7. In the transfection section of the Methods section, transduction is instead described. Methods for internalization assay are not clear.

Referee #3:

This is a very high quality and interesting study characterizing the unexpected finding that RAB7 knockout destabilizes a recycling integrin (and other cell surface cycling cargoes) and appears to reveal a new pathway for lysosome organelle biogenesis. The authors may not know that Bernard Hoflack many years ago showed that newly synthesized lysosomal enzymes are delivered by mannose 6-phosphate receptors from the Golgi, first to early, transferrin receptor-positive endocytic compartments [PMID 12529433]. This would set up the existence of a Rab4 and/or Rab 5 positive structure that contains proton pumps and hydrolases and could even accumulate LAMP proteins. Without Rab7 it cannot mature but would none-the-less appear to be what they are observing-a TfR positive, lysosome-like compartment. Rab5 appears to able to cycle out-perhaps by membrane fission? And cargoes might be more rapidly degraded under these conditions due to premature exposure to hydrolases that don't get sorted into later structures? Also, in the absence of Rab7, motors may have better chances to interact with the other endocytic Rabs. And I would predict that autophagy of these structures would be increased.

The story is interesting, timely, and suitable for EMBO J. after the authors address the following points to provide suitable background for the readers in the context of prior work.

1. I strongly encourage the authors to consider and discuss the implications of the scenario described above. Also, the original characterization of Rab7 function by Wandinger-Ness and colleagues (PMID: 8522602) should be cited and described in detail in terms of what they reported.

2. I would guess that Rab7 KO cells induce expression of lysosomal hydrolases via TFEB. Is this true? If so this would enhance the scenario describing above.

-Suzanne Pfeffer (signed review)